Fabrication and Characterization of Stretchable Supercapacitors for Energy Systems Applications

Hafeez ur Rehman

Registration No. 103-FET-PHDEE-F15

Supervised By: Prof. Dr. Ahmed Shuja Syed

Co-Supervisor: Dr. Imran Murtaza

A dissertation submitted to IIUI in partial fulfillment of the requirements for the degree of

DOCTOR OF PHILOSOPHY (Ph.D)

Department of Electrical Engineering
Faculty of Engineering and Technology
INTERNATIONAL ISLAMIC UNIVERSITY
ISLAMABAD

2021

1. Electrical batteries -- Design
2. Fabrications -- Supercapacitors

Certificate of Approval

Title of Thesis: Fabrication and Characterization of Stretchable Supercapacitors for Energy Systems Applications

Name of Student: Hafeez-ur-Rehman

Registration No: 103-FET-PhDEE-F15

Accepted by the Department of Electrical Engineering, Faculty of Engineering and Technology at International Islamic University Islamabad, Pakistan in partial fulfillment of the requirement for the degree of the Ph.D Electronics Engineering.

Viva Voce Committee

Supervisor

Dr. Ahmed Shuja Syed
Executive Director
Center for Advanced Electronics and Photovoltaic Engineering, (CAEPE)
International Islamic University Islamabad

Co-Supervisor

Dr. Imran Murtaza
Associate Professor
Department of Physics
International Islamic University Islamabad

Internal Examiner

Dr. Muhammad Amir
Department of Electrical Engineering
International Islamic University Islamabad

External Examiner

Dr. M. M. Talha
Principle Scientist
KRL

External Examiner

Dr. Ehsan ullah Khan
Professor
Namal Institute Mianwali

Chairman

Dr. Suheel Abdullah Malik
Department of Electrical Engineering
International Islamic University Islamabad

Dean

Prof. Dr. Nadeem Ahmed Sheikh
Faculty of Engineering and Technology
International Islamic University Islamabad

DEDICATED TO

I, dedicate this Thesis to Almighty ALLAH for guidance, strength and power of mind, skills and healthy life. Then to my Commander in-Chief, The Prophet (Piece and blessings be upon him), Ehle-Bait, his Companions and his followers, whole Muslim Ummah, My Mother, My Father, My teachers, my beloved sister, Brothers, family members, friends, the Children of Bajoor Attack, APS attacks and to all those shuhada of Islam.

.

ABSTRACT

Since the energy storage and power demand for the consumer market is in the ever-increasing trend, global electronics industry is looking for generic structures that are equally powerful in storing energy and are equally reliable and flexible for universal integration into the systems. The longer life time and higher power density of the supercapacitors make them better than the conventionally used lithium-based batteries particularly for miniaturized devices and systems. As compared to batteries, supercapacitors are preferable and more suitable for diverse applications. Moreover, they can also extend the battery's life time. In this systematic Study; we have focused three set of different kinds of conducting polymer based supercapacitors i.e. PEDOT:PSS, Polyurethane and PVA+KOH to study the electronics of such devices for technology exploitation. PEDOT: PSS electrodes have readily been used as a prominent research candidate as the supercapacitor's active electrode. The benefits of PEDOT based super-capacitors as a charge storage material are wide i.e. high conductivity, prominent stability, suitable conjugated porous backbone, wider working range, fast redox reaction, optical transparency, and easy processability. While the drawback of PEDOT: PSS shows inhomogeneous electrical and morphological properties that result in poor long term stability and causes the limitation in its shelf-life. This work proposes a significant cause of its degradation (during active and standby modes) and provides the transient charge level analysis for the very first time. PEDOT: PSS based supercapacitor are fabricated and subsequently characterized with a special focus to evaluate the post-aging (~120 days) charging and discharging nature of the devices. The defects present within the PEDOT:PSS interface are also studied to address the less-evaluated problematic area in order to better understand the inhomogeneities in view of basic charge, for improved system-level applications. From this study, two distinct defect centers are measured and calculated i.e. E_{T1} = Ec-0.0305 eV with capture cross section of 2.05×10^{-25} cm^{-2} and E_{T2} = Ev+0.0896 eV with capture cross section of 9.13×10^{-24} cm^{-2}. In Polyurethane based supercapacitor, Kirchhoff's, Ohm's, and Thevenin's circuit laws are solved with specific focus on foldable supercapacitors. In view of frequency and time domain, the comparative nurture of Alternating and Direct current (AC-DC) analysis are also presented from EIS and potentiostatic techniques. The defect analysis is also carried out to predict the trap energy level near the conduction band that is localized at ~Ec-78.7meV with a capture cross-section of 8.29×10^{-27} cm^2. This level is thought to be responsible for the charge leakage at internal self-discharge resistance (Rp) and reduces the charge collection especially in a standby mode of supercapacitor's operation. In PVA based supercapacitor the

electrolyte has been synthesized with Potassium Hydro-Oxide (KOH) as ionic migration agent, which may enhance the Electronic Double-Layers Capacitance (EDLC) activity. In order to mechanically strengthen the active material with in the device matrix; graphene based activated carbon enclosed within the larger pore fabric/textile is utilized in one of the experiments performed. After successful fabrication, the PVA based super capacitor is charged for 60 second at a potential of 1 Volt and took ~30 minutes to completely discharge it's self at "full load operation. Findings presented in this thesis are important and have ramifications for design, device and process engineers.

LIST OF PUBLICATIONS AND PATENT OUT OF THE WORK

Published

- **Rehman, H. U.,** Shuja, A., Ali, M., Murtaza, I., and Meng, H. (2020). Evaluation of defects and current kinetics for aging analysis of PEDOT: PSS based supercapacitors. ***Journal of Energy Storage***, *28*, 101243. **(Impact Factor: 6.583)** DOI: 10.1016/j.est.2020.101243

- **Rehman, H. U.,** Shuja, A., Ali, M., S. Khan, Murtaza, I., and Meng, H. (2022). Investigation of Charge and Current Dynamics in PVA-KOH Gel Electrolyte Based Supercapacitor **(Journal of Materials Science: Materials in Electronics) (Impact Factor: 2.478)** DOI: 10.1007/s10854-021-07432-x

PATENT

- A novel method for the performance evaulation of strechable and foldable supercapacitor for energy storage application. **(Filled: Intlectual Property Organization, Govt. of Pakistan)**
  (Patent Application No. **846/2021**) (Patent Receipt No. **2103044450**)

  Inventor_1: Hafeez ur Rehman
  Inventor_2: Prof. Dr. Ahmed Shuja Syed
  Inventor_3: Engr. Muhammad Ali

ACKNOWLEDGEMENTS

In the name of Allah (SubhanahuWaTa'ala), who is the most gracious and the merciful. I would like to thank Allah for giving me strength and patience to complete this research work. Peace and blessings of Allah be upon His last Prophet Muhammad (Sallulah-o-Alaihihe-Wassalam) and all his Sahaba (Razi-Allah-o-Anhu) who dedicated their lives for Dawah and spread of Knowledge.

I am truly grateful to my supervisor Prof. Dr. Ahmed Shuja Syed, whose inspiration, ideas and efforts make it possible for me to complete my higher studies. He has been a role model for me and many others in teaching, research, and other aspects of life. I offer my sincere thanks to Research Associates Muhammad Ali, Shoaib Alam, Shah Fahad and all the supporting staff of Centre of Advanced Electronics and Photovoltaics Engineering for their never-ending support and for their useful discussions during last few years. I would like to acknowledge the support of International Islamic University Islamabad Pakistan for providing me half fee waiver during the PhD studies.

I am really grateful to my Mother and father for their prayers, love and support throughout my life. I have no words to describe the unprecedented care and support of my immediate family which made it realize the dream of pursuing a PhD degree.

Engr. Hafeez-ur-Rehman

TABLE OF CONTENTS

Abstract ---- iii
LIST OF PUBLICATIONS AND PATENT OUT OF THE WORK ---- v
Acknowledgements ---- vi
Table of Contents ---- vii
List of Figures ---- ix
List of Tables ---- xii
List of Abbreviations ---- xiii
List of Symbols ---- xv
Chapter 1: Introduction ---- 1
1.1 Energy Demand ---- 1
1.2 Scaling in Technology ---- 2
1.3 Flexible Devices ---- 3
1.4 Energy Storage Devices ---- 5
1.5 Supercapacitors ---- 7
1.5.1 Application of supercapacitor ---- 9
1.5.2 Demand ---- 10
1.5.3 Industry ---- 10
1.6 Gap Analysis and Issues ---- 11
1.6.1 Solving the Problem ---- 12
1.7 Problem Statement ---- 13
1.8 Objectives of the Research ---- 14
1.9 Structure of the Thesis ---- 15
1.10 Summary ---- 15
Chapter 2: Background Theory ---- 17
2.1 Introduction ---- 17
2.1.1 Electrochemical Energy Conversion and Storage Systems ---- 17
2.2 Energy Storage Mechanism ---- 18
2.2.1 Electrostatic Double Layer Capacitor (EDLC) ---- 19
2.2.2 Electrochemical Pseudocapacitor ---- 21
2.2.3 Hybrid Supercapacitor ---- 22
2.3 Stretchable Supercapacitor ---- 24
2.4 Electrode ---- 25
2.4.1 Carbon Materials ---- 26
2.4.2 Metal Oxides ---- 27
2.4.3 Conducting Polymers ---- 28
2.5 Electrolyte ---- 32
2.6 Supercapacitor Systems ---- 34
2.6.1 Symmetric Supercapcitor ---- 34
2.6.2 ASymmetric Supercapcitor ---- 34
2.7 Equivalent Circuit Model (Randless Cell) of the supercapacitor ---- 34
2.8 Defects in Crystals ---- 35
2.9 Summary ---- 37
Chapter 3: Literature Review ---- 39
3.1 Energy Density ---- 39
3.2 Stretchable Supercapacitors ---- 40
3.3 Choice of electrode materials for stretchable supercapacitors ---- 42
3.4 Design strategy for stretchable supercapacitors ---- 49
3.4.1 Linear supercapacitors (One Dimensional design) ---- 50
3.4.2 Planar supercapacitors (Two Dimensional design) ---- 52
3.4.3 Stereo supercapacitors (Three Dimensional design) ---- 54
3.5 Electrolyte for supercapacitor ---- 56
3.6 Summary ---- 59
Chapter 4: Experimental Techniques ---- 61
4.1 Device Fabrication ---- 61
4.1.1 Spin Coating ---- 61
4.1.2 Spray Coating ---- 62
4.2 Testing and Characterization of Fabricated device Design ---- 63

4.2.1 Nano Chip Reliability grade Hall Effect System ---- 63
4.2.2 ASMEC Electro-physical Characterization System ---- 65
4.2.2.1 Current-Voltage Analysis ---- 66
4.2.2.2 Charge Deep Level Transient Spectroscopy (QDLTS) ---- 67
4.2.3 Arrhenius Analysis ---- 70
4.2.4 Electrochemical Impedance Spectroscopy (EIS) Analysis ---- 71
4.2.5 Photo-Luminance System ---- 74
4.2.6 Hot Plate and Magnetic Stirrer ---- 75
4.2.7 Scanning Electron Microscopy (SEM) ---- 76
4.2.8 Energy Dispersive Spectroscopy (EDS) ---- 77
4.2.9 Atomic force Microscopy (AFM) ---- 78
4.3 Precautions in Experimentation ---- 80
4.4 Summary ---- 81
Chapter 5: Experiments, Results & Discussion ---- 82
5.1 PEDOT:PSS based supercapacitor ---- 82
5.1.1 Experimental ---- 82
5.1.2 Characterization ---- 84
5.1.2.1 Current Voltage (I-V) Analysis ---- 86
5.1.2.2 Q-DLTS: Defect Analysis of PEDOT:PSS based Supercapacitor ---- 88
5.1.2.3 EIS Analysis of PEDOT:PSS based Supercapacitor ---- 93
5.1.2.3.1 Nyquist Plot ---- 93
5.1.2.3.2 Bode Plot ---- 95
5.1.2.4 Kinetics of electric current under charging voltage and temperature ---- 98
5.2 Stretchable and Foldable Polyurethane Based Supercapacitors ---- 102
5.2.1 Experimental ---- 103
5.2.2 Characterization ---- 104
5.2.2.1 Current Voltage (I-V) Analysis ---- 105
5.2.2.2 Q-DLTS: Defect Analysis of Stretchable and foldable Supercapacitor ---- 106
5.2.2.3 EIS Analysis Polyurethane Based Supercapacitors ---- 109
5.2.2.4 Kinetics of electric current under charging voltage and temperature ---- 111
5.3 Alternating and Direct Current Analysis of said Supercapacitors ---- 115
5.3.1 Characterization ---- 116
5.3.2 Alternating and Direct Current Analysis ---- 116
5.4 PVA-KOH Gel Electrolyte Based Supercapacitor ---- 135
5.4.1 Experimental ---- 136
5.4.2 Characterization ---- 137
5.4.2 Comparison with the reported Devices ---- 150
Chapter 6: Conclusion & Future Work ---- 165
6.1 Conclusion ---- 165
6.1.1 PEDOT:PSS Based Super-capacitor ---- 165
6.1.2 Alternating and Direct Current (AC/DC) analysis of Polyurethane Based Supercapacitor -- 168
6.1.3 PVA-KOH Based Super-capacitor ---- 167
6.2 Future Work ---- 169
References ---- 173

LIST OF FIGURES

Fig. 1.1: More than Moore's approach ---------- 3
Fig. 1.2: Road map of flexible products and flexible substrates---------- 4
Fig. 1.3. Illustration of flexible Devices attached to humans through textile channel for stretchable-flexible electronic strip to measure the temperature and accelerometer to measure the respiration and heart beat---------- 5
Fig 1.4 Ragone plot for different types of energyy-storage devices---------- 6
Fig 1.5. Comparison between the Properties of Batteries and Supercapacitor---------- 7
Fig 1.6 Overview of the types and classification of supercapacitors ---------- 8
Fig. 1.7: Application of supercapacitors ---------- 11
Fig. 2.1 Historic timeline for the development of supercapacitors---------- 18
Fig. 2.2 Schematic illustrations of supercapacitor---------- 19
Fig 2.3 Charge Storage mechanism of EDLC Supercapacitor---------- 20
Fig 2.4 Charge Storage mechanism of Pseducapacitor---------- 22
Fig 2.5 Charge Storage mechanism of hybrid supercapacitor ---------- 23
Fig 2.6 Four design strategies for stretchable supercapacitors (a) wrinkled and wavy design (b)Serpentine bridge-island design (c) Origami design (d) Fractal inspired bridge-island design-------- 31
Fig 2.7: Comparison of specific capacitance of different electrode materials for supercapacitors------- 33
Fig 2.8: Role of electrolyte on the properties of Electrochemical Supercapacitor (ES) ---------- 33
Fig 2.9: Electrolyte Classifications---------- 34
Fig 2.10: Schematic illustration of **(a)** Symmetric supercapacitors **(b)** Asymmetric---------- 35
Fig 2.11: Equivalent Circuit Model (Randles Cell) of the Supercapacitor---------- 36
Fig 2.12: Classification of defects in crystalline solid---------- 37
Fig. 2.13: Crystal defects, a) impurity interstitial, b) dislocation, c) self-interstitial, d) cluster of impurity atoms, e) extrinsic dislocation loop, f) small substitutional impurity, g) vacancy, h) intrinsic dislocation loop, i) large substitutional impurity. ---------- 44
Fig. 3.1: (a) fabrication of buckled SWCNT film on PDMS (b) Buckled SWCNT film (c) Crumbled CNT/PANI composite (d) Stretchable wire shaped supercapacitor fabrication procedures ---------- 46
Fig. 3.2: (a) SEM image of MoS2 nanosheets. (b) Fabrication of the stretchable supercapacitor based on composite films of graphene/MoS_2 (c) asymmetric stretchable supercapacitor based on the wrinkled negative Fe_2O_3/CNT hybrid film electrode and positive MnO_2/CNT hybrid film electrode. (d and e) wrinkled Fe_2O_3/CNT and MnO_2/CNT hybrid films SEM images---------- 47
Fig. 3.3: Stretchable supercapacitors based on polyaniline ---------- 48
Fig 3.4: Highly Stretchable and Self-Healable Supercapacitor ---------- 49
Fig 3.5: Design strategies for stretchable supercapacitors---------- 51
Fig 3.6: One dimensional Supercapacitor (a) Representation of a twisted sandwich fiber, (b) Commercial glove on 20 cm long sandwich fiber is woven---------- 53
Fig 3.7: (a) Fabrication of all solid state planar two dimensional stretchable Supercapacitor (b) printed planar flexible supercapacitor on a PET substrate---------- 54
Fig 3.8: Fabrication of microsupercapacitor using Tripod structure PDMS---------- 55
Fig 3.9: Powering electronic Watch (a) (b) structure and schematic of electronic watch along with "watch strap" as stretchable supercapacitor. (c)Watch strap" at different places of arm i.e. wrist, middle and upper arm (d) powering the watch at different places of arm i.e. wrist, middle and upper arm------ 59
Fig 3.10: PVA based Supercapacitors (a) Schematic of a supercapacitor prepared by two different gel electrolytes (b) Schematic of a typical symmetric supercapacitor based on the graphene electrodes and PVA/H2SO4 gel electrolytes. (c) Schematic of a typical symmetric flexible paper supercapacitor based on the carbon nanomaterials electrodes and PVA/H3PO4 gel electrolytes (d) A typical micro-supercapacitor based on the carbon nanomaterials electrode and PVA/H2SO4 gel electrolyte---------- 62
Fig 4.1: Four stages of spin coating---------- 63
Fig 4.2: Schematic of the spray coating of CNT onto glass fiber fabrics and fabrication process-------- 64
Fig 4.3: Hall Effect Measurement Setup---------- 65
Fig 4.4: Halls Effect Measurement Setup in CAEPE, IIUI. ---------- 66
Fig 4.5: ASMEC Setup in CAEPE, IIUI---------- 67
Fig 4.6: I-V characteristic of (a) Symmetric, (b) asymmetric and (c) hybrid supercapacitor---------- 70
Fig 4.7: Charge based transient analysis of Ag/PTCDA 28 nm/ n-GaAs sample---------- 73
Fig 4.8: EIS analysis of flexible grapheme based supercapacitor (a) Nyquist plot (b) Bode Plot--------- 73
Fig 4.9: EIS setup in CAEPE, IIUI---------- 75
Fig 4.10: Principle of Photoluminescence Spectroscopy---------- 76
Fig 4.11. Hot plate and magnetic stirrer----------

Fig 4.12: SEM layout---------- 77
Fig 4.13: **(a)** Energy dispersive X-ray spectroscopy (b) Elemental Composition mapping of sample analyzed via EDS---------- 79
Fig 4.14: Schematic of basic AFM operation (left), real micro-cantilever and components (right)---------- 79
Fig 5.1: Fabrication of ITO Coated PEDOT: PSS based Supercapacitor:(a) ITO coated glass substrate, (b) Spin coated PEDOT:PSS onto the substrate , (c) drop casting of gel-electrolyte (d) U-V exposure to solidify the gel electrolyte. ---------- 83
Fig 5.2: General schematic of PEDOT: PSS based Supercapacitor (a) layer-wise structure, (b) Energy band structure. ---------- 84
Fig 5.3: Current-Voltage characteristic of PEDOT:PSS based supercapacitor at variable temperatures--- 87
Fig 5.4: Charge based transient analysis of PEDOT:PSS based supercapacitor---------- 89
Fig 5.5: Arrhenius analysis of PEDOT:PSS based supercapacitor---------- 91
Fig 5.6: Visualized Trap levels within the energy band of PEDOT:PSS based supercapacitor---------- 92
Fig 5.7: Logarithmic scaled Nyquist plot---------- 94
Fig 5.8: Normalize scaled Nyquist plot---------- 95
Fig 5.9: Impedance based Bode plot at multiple charging voltages---------- 96
Fig 5.10: Phase based Bode plot at multiple charging voltages---------- 98
Fig 5.11: Kinetics of electric current under subject charging voltages i.e. 0.1-1V (a) At 26 °C ambient temperature, (b) At 86 °C ambient temperature. ---------- 99
Fig 5.12: Overall charging behavior of subject supercapacitor under 1V charging voltage (a) At 26°C, (b) At 86°C ambient temperatures---------- 101
Fig 5.13: Capacitance of the PEDOT:PSS supercapacitor at varying temperature---------- 102
Fig 5.14: Fabrication of stretchable and foldable Supercapacitor:(a) stretchable and foldable Polyurethane substrate, (b) dense metal net, c) substrate/metal net stack, (d) drop casting of gel-electrolyte (e) U-V exposure and layer vise stack of stretchable supercapacitor. ---------- 104
Fig 5.15: Current-Voltage characteristic stretchable and foldable polyurethane based based supercapacitor at variable temperatures. ---------- 106
Fig 5.16: Charge-Discharge events of supercapacitor in Q-DLTS measurements (a) charging through R_{ESR} (b) discharging through R_P---------- 107
Fig 5.17: Q-DLTS spectra of stretchable/foldable supercapacitor. ---------- 108
Fig 5.18: EIS based Nyquist plot---------- 111
Fig 5.19. Current-time spectra's at multi-charging voltage pulses, (a) I(t) at 300K, (b) I(t) at 310K, (c) I(t) at 320K, (d) I(t) at 330K, (e) I(t) at 340K, (f) I(t) at 350K. ---------- 114
Fig 5.20. Reverse polarity in current magnitude---------- 115
Fig 5.21. Thevenin's Equivalent circuit of stretchable Supercapacitor. ---------- 117
Fig 5.22: Thevenin's Equivalent impedance model (a), Thevenin's Equivalent impedance (b) Thevenin's Equivalent impedance with DC source. ---------- 120
Fig 5.23: Charging Circuit of stretchable supercapacitor, (a) supercapacitor charging along with positive and negative series wires. (b) Charging circuit diagram (practical), (c) equivalent circuit diagram during charging phase, (d) Equivalent circuit diagram during charged phase. ---------- 121
Fig 5.24-I: Circuit Diagram of Precise R_{ESR} determination. ---------- 122
Fig 5.24-II: Effect of the ambient temperature on stretchable supercapacitor performance parameters. (a) Effect of the DC voltage on effective capacitance at multi temperature. (b) Effect of the DC voltage on Parallel resistance at multiple temperatures. ---------- 126
Fig 5.25: AC-induced power source for measuring stretchable super-capacitor: Proposed Assembly. -- 128
Fig 5.26: Spectral response of individual and combine voltages for charging of super-capacitor, (a) DC-voltage spectral response. (b) AC- Voltage spectral response. (c) Spectral response of off-setted AC combined voltage and red colored part shows the DC-level clipping due to negative half of AC. (d) Equivalent voltage source for charging super-capacitors---------- 129
Fig 5.27: Supercapacitor's Equivalent Circuit coupled with Equivalent Voltage Source. ----------
Fig 5.28: Comparative analysis of AC and DC technique for supercapacitors evaluation characteristic parameters, (a) comparative analysis of 'R_P' (b) Comparative analysis of 'C'. 135
Fig 5.29 : Fabrication steps of PVA based Super-capacitor, (1) Polymer sheets for encapsulation, (2) larger pore fabric for active material encapsulation, (3) Activated Carbon dropped with Graphene Ink, (4) Interconnection of Anode and Cathode with Copper wire, (5-6) PVA based Electrolyte, (7-8) Super-capacitor ready for charge/discharge activity---------- 137
Fig 5.30: SEM imaging of PVA based super-capacitor's elements, (a) Activated carbon mixed with graphene ink, (b) dense metal net, (c) standalone activated carbon and (d) PVA electrolyte---------- 138

Fig 5.31: EDS analysis of PVA based super-capacitor's elements, (a) Activated carbon mixed with graphene ink, (b) dense metal net, (c) standalone activated carbon and (d) PVA electrolyte---------- 138
Fig 5.32: AFM image of PVA electrolyte---------- 139
Fig 5.33: Schematic diagram of PVA + KOH based SC, (a) Layer wise structure of SC, (b) Full load equivalent circuit of SC, (c) No Load equivalent circuit---------- 140
Fig 5.34: Discharge characteristics at Full and No Load conditions---------- 141
Fig 5.35: Electrical schematic overview of the super-capacitor's equivalent circuit and the test bench-- 142
Fig 5.36: Ionic charge state for PVA and KOH based Electrolyte---------- 143
Fig 5.37: Nyquist Plot against each discharge DC potentials---------- 144
Fig 5.38: Direction of Current Flow with respect to geographical planes---------- 145
Fig 5.39: Current-Voltage analysis of PVA based Electrolyte at variable temperatures---------- 146
Fig 5.40: Voltage-Charge (V-Q) analysis of PVA based Electrolyte---------- 147
Fig 5.41: Q-DLTS scans of PVA based Electrolyte---------- 148
Fig 5.42: Arrhenius analysis of Current-voltage and Q-DLTS scans---------- 148
Fig 5.43: Photo-Luminescence (PL) scans of PVA based Super-Capacitor Electrolyte---------- 149
Fig 5.44: Energy band picture of PVA based Electrolyte. ---------- 150
Fig 5.45. Schematic representation of flexible electrode fabrication
Fig 5.46. Nyquist plots for pure PEDOT–PSS and EG doped PEDOT–PSS:rGO Composites ---------- 153
Fig 5.47: a) Fabrication Process of PEDOT:PSS-based electrodes on cloth. b) Cloth before coating (c) cloth after PEDOT: PSS coating---------- 153
Fig 5.48: Performance of the sweat-based SC in real application. a) SC attached to clothes of a person who is partly wet due to sweat. b) The CV (inset EIS) and c) GCD analysis d) SC attached to clothes of a person who is fully wet due to sweat e,f) GCD and CV analysis of the fully wet SC. h–j) The textile SC on a polar pro strap for conformal contact and k) SC performance with sweat during workout. ----- 154
Fig 5.49: Imaginary impedance vs real impedance recorded on the supercapacitor cells having as active electrodes composites (a) 90 wt % activated carbon and 10 wt % SWCNT (b) 30 wt % activated carbon 70 wt % SWCNT---------- 157
Fig 5.50: Charge/discharge curve of supercapacitor at 20 mA with 55 wt % of active carbon and 45 wt% SWCNT. ---------- 158
Fig 5.51: Schematic design of the hybrid supercapacitor---------- 161
Fig 5.52: Specific capacitance comparison of different Gel eletrolytes. ---------- 162

LIST OF TABLES

Table 1.1 Comparison of physicochemical properties of the various supercapacitor materials ---------- 09
Table 2.1: Carbon based electrode materials with specific capacitance ---------- 26
Table 2.2: Metal oxide and hydroxides based electrode materials with specific capacitance ---------- 27
Table 2.3: Conducting Polymer based electrode materials with specific capacitance---------- 29
Table 2.4: Comparison of different properties of electrode materials---------- 30
Table 3.1: Electrolytes with voltage window---------- 57
Table 4.1: Precautions in Experimentation ---------- 80
Table 5.1: Surface Trap Densities of PEDOT: PSS based supercapacitor at multiple temperatures------ 90
Table 5.2: Trap parameters of stretchable/foldable supercapacitors---------- 109
Table 5.3: Parallel Resistance magnitudes measured from potentiostatic DC Analysis---------- 125
Table 5.4: Conductivity and Properties of common conductive polymers---------- 151

LIST OF ABBREVIATIONS

A	Contact Area
AC	Alternating current
ADC	Analog to Digital Converters
AFM	Atomic Force microscopy
AgNW	Silver nanowire
C	Capacitance
C_{eff}	Effective capacitance
CNTs	carbon nanotubes
CPs	conducting polymers
DC	Direct current
DQ	Dihydroxyanthra-quinone
DMM	Digital Multi-Meter
DMPAP	2-dimethoxy-2-phentlacetophenone
DUT	Device under Test.
Ec	Lower edge of Conduction Band
EDLCs	Electrochemical Double-Layer Capacitors
EDOT	3, 4-Ethylenedioxythiophene
EDS	Energy Dispersive X-ray Spectroscopy
EG	Ehtylne glycol
EIS	Electrochemical Impedance Spectroscopy
ES	Electrochemical supercapacitor
E_T	Trap energy
FWHM	Full Width and Half Maxima
GNPs	Graphenenano-platelets
GPE	Gel Polymer Electrolyte
HQ	hydroquinone
H_2SO_4	Sulfuric acid
I	Current
IC	Integrated Circuit
IoT	Internet of things
ITRS	International Technology Roadmap of semiconductors
ITO	Indium Tin Oxide
I-V	Current-Voltage
$j_s(t)$	Current Density
K	Boltzmann's constant
KOH	Potassium Hydroxide
MnO_2	manganese dioxide
MoS_2	Molybdenum disulfide
N_T	Interface Trap states
N_T	Trap concentration
PPy	Polypyrrole
PEDOT	Poly (3,4- ethylenedioxythiophene)
PTh	Polythiophene
PANI	Polyaniline
PEDOT: PSS	Poly (3, 4-ethylene dioxythiophene) polystyrene sulfonate
PFPT	Poly(4-flourophenyl-3-thiophene)
PMT	Poly(3-methyl thiophene)
PU	Polyurethane
PDMS	Polydimethylsiloxane
PVA	Poly- vinyl alcohol
PMMA	Polymethylmethacrylate
PAN	polyacrylonitrile
PEO	Polyethylene oxide
PC	Propylene carbonate
PUA	Polyurethane acrylate
PVDF	Polyvinylidene fluoride
PIFTS	Photo-stimulated internal field transient spectroscopy
PGC	Polypyrrole-graphene quantum dots composites

PZT	Piezoelectric
QDLTS	Charge deep level transient spectroscopy
RKE	Remote keyless entry
Rct	charge-transfer resistance
R_{ESR}	Equivalent Series Resistance
R_P	Parallel Resistance
R_P	Self Discharge Resistance
R_s	series resistance
RMS	Root Mean Square
rGO	Reduced Graphene oxide
SCs	Supercapacitors
SN	Succinonitrile
SWNT	Single-walled carbon nanotube
SEBS	styrene–(ethylene–butylene)–styrene
SEM	Scanning electron Microscopy
SMPS	Switch Mode Power Supply
TENG	Tribo-electrical nano-generator
$TEABF_4$	Tetraethylammonium tetrafluoroborate
t_1	Time initially
t_2	Final charge/discharge time
V	Voltage
V_H	Hall voltage
V_{eq}	Equivalent voltage
V-Q	Voltage-Charge
Z	Impedance

LIST OF SYMBOLS

τ	Rate window
$\psi s(t)$	Electric potential
σ	Capture cross-sections
ΔQ	Charge magnitude

Chapter 1

Introduction

This section clarifies a portion of basic introduction which is critical to comprehend the foundation of fabrication and characterization of stretchable supercapacitors for energy system applications.

1.1 Energy Demand

Electrical energy is common consumer good and in mosst cases is an unseen, ubiquitous commodity and is readily available at lowest possible cost [1]. Environmental, social and economic aspects are dependent on energy for all developing and developed countries as they need energy for the functioning of all the activities. Energy is depleting exponentially all over the world in the past decade as its demand is increases day by day [2]. Quality of life, population, education, health, industrial production, access to water, etc. all are linked to energy, as the environmental security and future economic prosperity depends on energy management and storage [3]. The environmental issues and huge prices of fossil fuels created concerns among countries to shift to other energy sources. With depleting resources and global warming also increases the concerns over fossil fuel usage, resulting use of renewable energy sources like photovoltaic and wind [4]. Renewable energy sources are fluctuating and variable sources and are different in so many aspects form conventional sources like they are smaller in size, unpredictable, location-constrained, and have low short-run cost [5]. The introduction of fluctuating and variable energy sources (renewable energy sources: wind, turbines, solar, etc.) to power network and delocalized electricity production increases issues and difficulties in stabilizing the power system due to the imbalance of demand- supply. Thus creating challenges in prevailing power systems [6]. To progress for better solution energy storage demand is the biggest challenge. Although renewable energy is free and environment

friendly source of electricity, a storage element is required as an energy buffer in wind and photovoltaic systems to bridge the gap between available and required energy. Due to high cost and bulky equipment, it is difficult to store energy. With depleting fossil resources and growing energy demands discovering reliable, environmental friendly, low cost, and sustainable energy adaptation and storage systems stays a key challenge across the globe. Thus Energy needs to be produced, transmit, and store it as its huge amount is required by today's society and most importantly this energy need to be delivered at any time. A lot of research is going on in the field of energy management, power electronics, and energy storage devices, etc., in terms of lower cost, high reliability, longer lifetime, and high efficiency for developing energy storage systems [7].

1.2 Scaling in Technology

The growth of electronic industry as compared to other industry sectors, is unmatched after the invention of Integrated Circuit (IC). Semiconductor industry has kept on progressing and has been instrumental in the advancement of numerous different businesses since 1970s. The semiconductor business has been a spine of the current day technology as a rule and customer electronics specifically. The accomplishment of this industry is the normally contracting device feature size [8]. Which overall contributed to the high performance and at financially conceivable expense. To make an impact on consumer application, the devices need both flexibility and scalability for the semiconductor industry. In the past, we have witnessed that the scalability was addressed using new and improved technologies and techniques [9]. The "More than Moore's" approach is the idea behind this industry shift as shown in Fig 1.1. In real world the use of these devices becomes more targeted and application specific as with the passage of time the devices become miniaturized. As the semiconductors market is expending it requires more advancements requiring devices to be portable, flexible, bendable, and compact for medical, civilian and military applications [10]. This is also desirable to

meet up with the International Technology Roadmap of semiconductors (ITRS) node requirements [11].

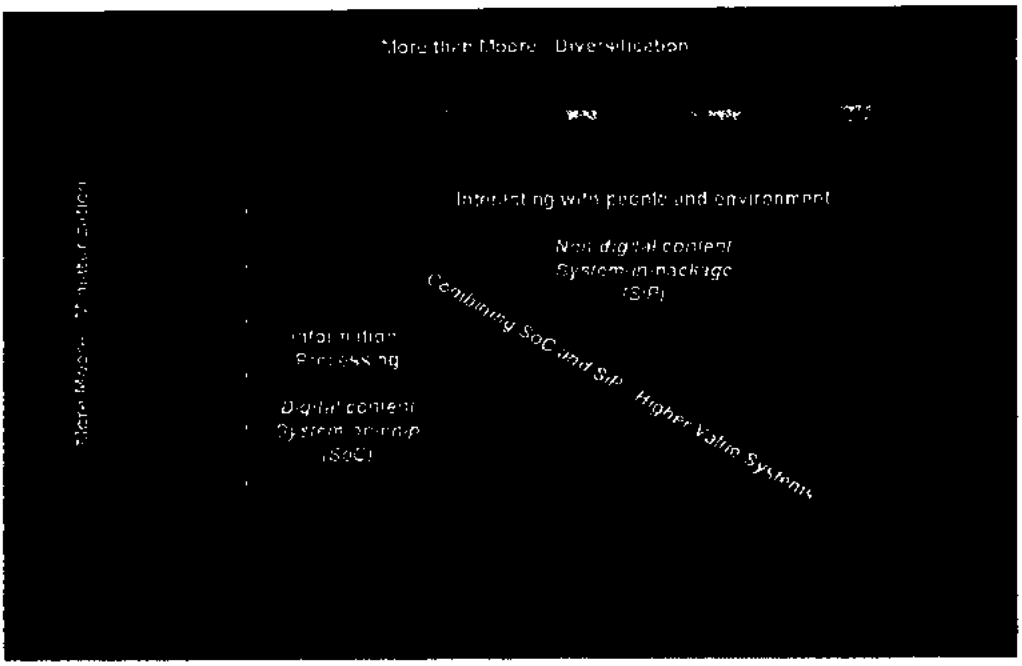

Fig 1.1: More than Moore's approach [11]

Internet of things is a trendy concept in which the portable and small devices are used as sensors and can be remotely controlled and accessed. These devices are connected with each other to exchange data providing an opportunity to design accurate, maintenance free, self-powered and efficient systems. Due to heavy demand in market on board energy is required for Wearable electronics, internet of things and wireless sensor networks [12].

1.3 Flexible devices

In recent years the requirement for flexible and wearable electronics is very much in the market. Fig 1.2 shows a road map for flexible substrates and products [13]. Consumer portable Electronics devices are becoming lightweight, wearable and flexible [14, 15]. Recently a lot of work is going on stretchable and flexible substrates for applications in electronics [16], organic and inorganic transistors [17,18], CMOS [19, 20], memory [21,22], antennas [23,24] and triboelectric nanogenartors [25], etc.

The other aspect of this technology advancement is the requirement of such structures that

can "store charge" and "drive" such flexible and stretchable devices with lightweight, thin and conformable properties [26,27]. On the other hand the demands for the storage of high energy that can be used at once will be the major source of inspiration that needs to be researched [28].

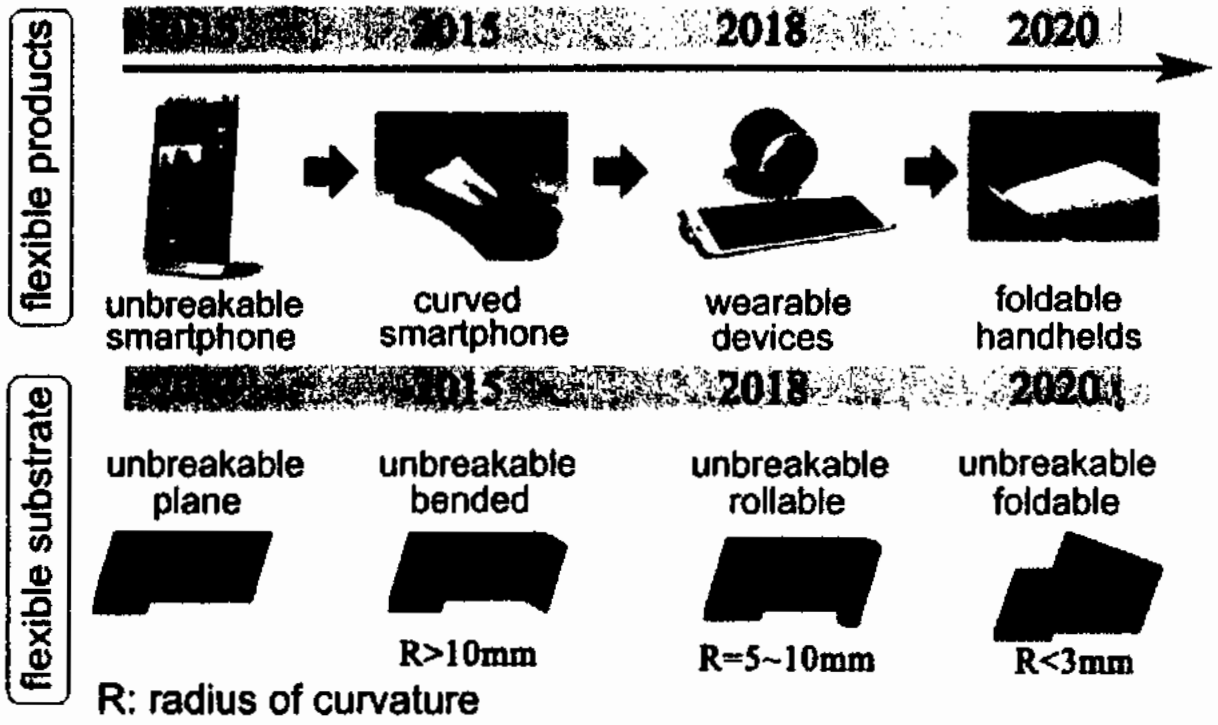

Fig 1.2: Road map of flexible products and flexible substrates [13]

Wearable and flexible electronics brings a revolution even in medical field while away from hospital. Healthcare has two major classes as textile electronics and on-skin. Fig 1.3 shows explains the concept of wearable and flexible electronics in which an electronic textile suit is attached to human body for wireless sensing that monitors the temperature of skin surface, respiration and heart rate. Electronic strips are made by customized fabric to make it stretchable and flexible and can be connected to sensor ICs and interconnects. Double layer Flexible printed circuit boards are developed by using the interconnects and sensor ICs with washable encapsulant and passive component assembly. The Fig also represents the

prototype of electronic textile suit [29].

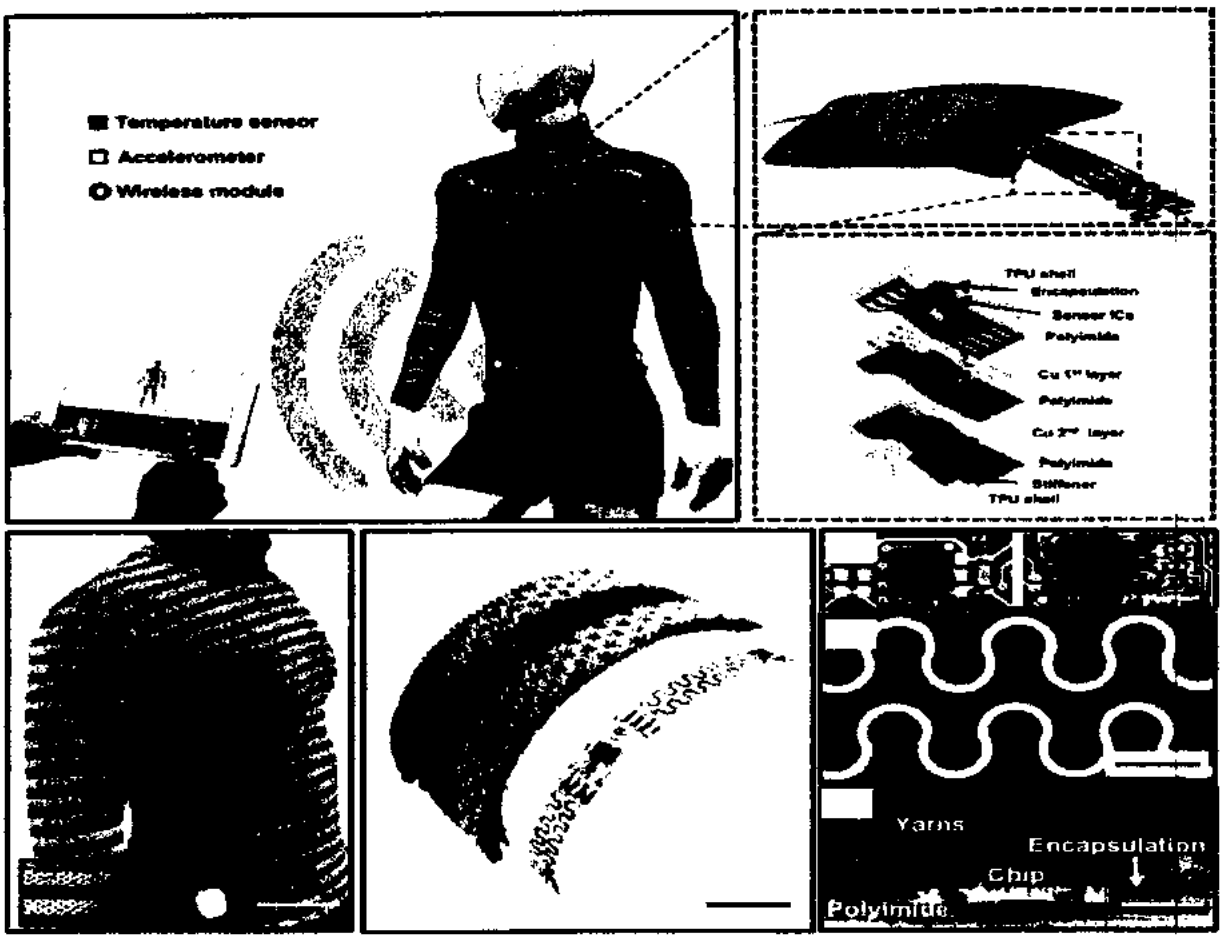

Fig 1.3: Illustration of flexible Devices attached to humans through textile channel for stretchable-flexible electronic strip to measure the temperature and accelerometer to measure the respiration and heart beat [29]

1.4 Energy Storage Devices

The widely known energy storage devices are batteries and capacitors which are the most common as well. Batteries provide long duration of energy storage with higher energy densities but low power densities while capacitors provide very high power densities but very low energy densities.

The application of secondary batteries also called rechargeable batteries are from medical implants to toys. The issues with batteries are that they are not safe for environment, lower lifecycle, taking more time to charge, lower power densities and having heating problem. They also have large internal resistance, higher volume, poor transient response and weight

[30]. Fig 1.4 shows Ragone plot for different types of energy-storage devices with respect to power densities and energy densities [31].

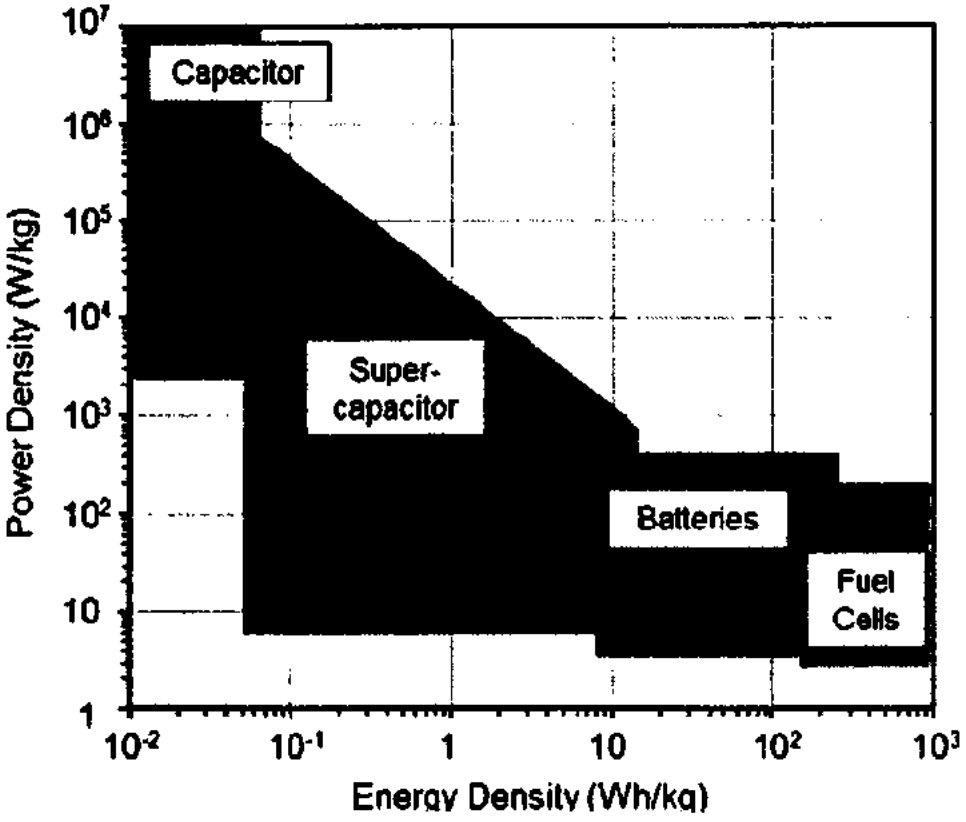

Fig 1.4: Ragone plot for different types of energy-storage devices [31]

A lot of work is done on the development of rechargeable batteries in past few years. But the power density of batteries are low as compared to supercapacitors, because of limited cations diffusion of electrodes [32]. For reliable and continuous operations on a chip, energy storage components plays a vital role by providing power. Hence, increasing a strong demand of compact energy storage device having small size and still providing high energy for operation. Supercapaciator including pseudo capacitors and Electrochemical Double-Layer Capacitors (EDLCs) provide fast surface reaction of electrodes, higher power density and fast delivery of energy [33]. Fig 1.5 Show the comparison between the properties of batteries and supercapacitor [34].

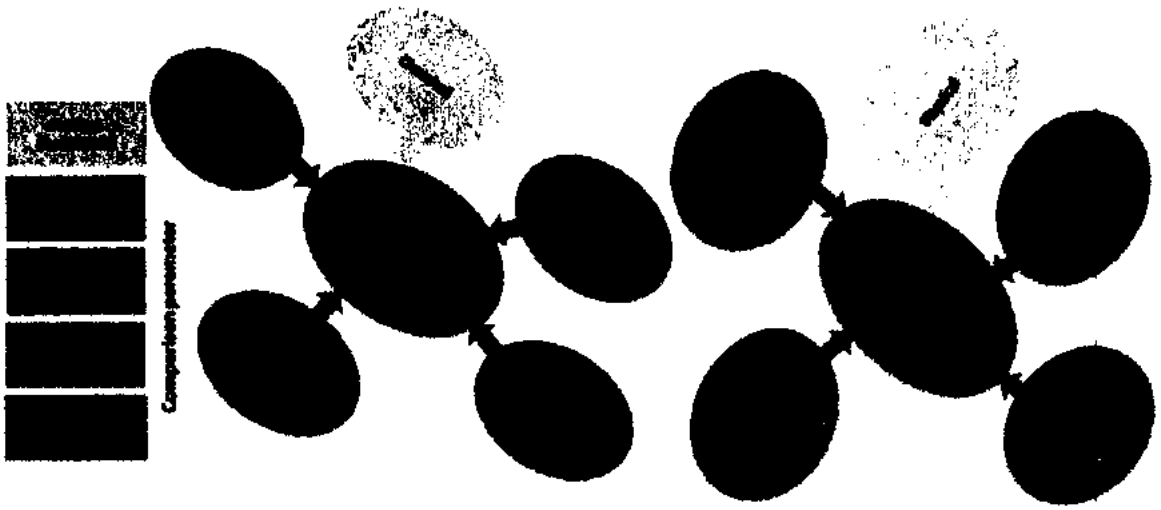

Fig 1.5: Comparison between the Properties of Batteries and Supercapacitor [34]

1.5 Supercapacitors

Capacitors and batteries are not providing enough power densities and energy densities to applications which require high power and energy density. This lead scientists to investigate a new energy storage device which will provide high energy and power density called as supercapacitors (SCs). It provides high specific capacitance, economic friendly characteristics, fast charge discharge capabilities and extremely high storage capabilities. A lot of research is going on supercapacitors making it closer and alternate to conventional batteries [35-37].

Development of nanostructured electrode material is the promising approach for the progress in technology of supercapacitor. One, two, and three dimensional nanosturctures are developed for designing electrode materials for better performance. Supercapacitors are divided into three categories electrochemical double layer capacitors (EDLCs), Pseudosupercapacitors and hybrid supercapacitors. The overview of supercapacitor types is shown in Fig 1.6 [38]. Power and energy density debate is rate-determining step for the development of SCs.

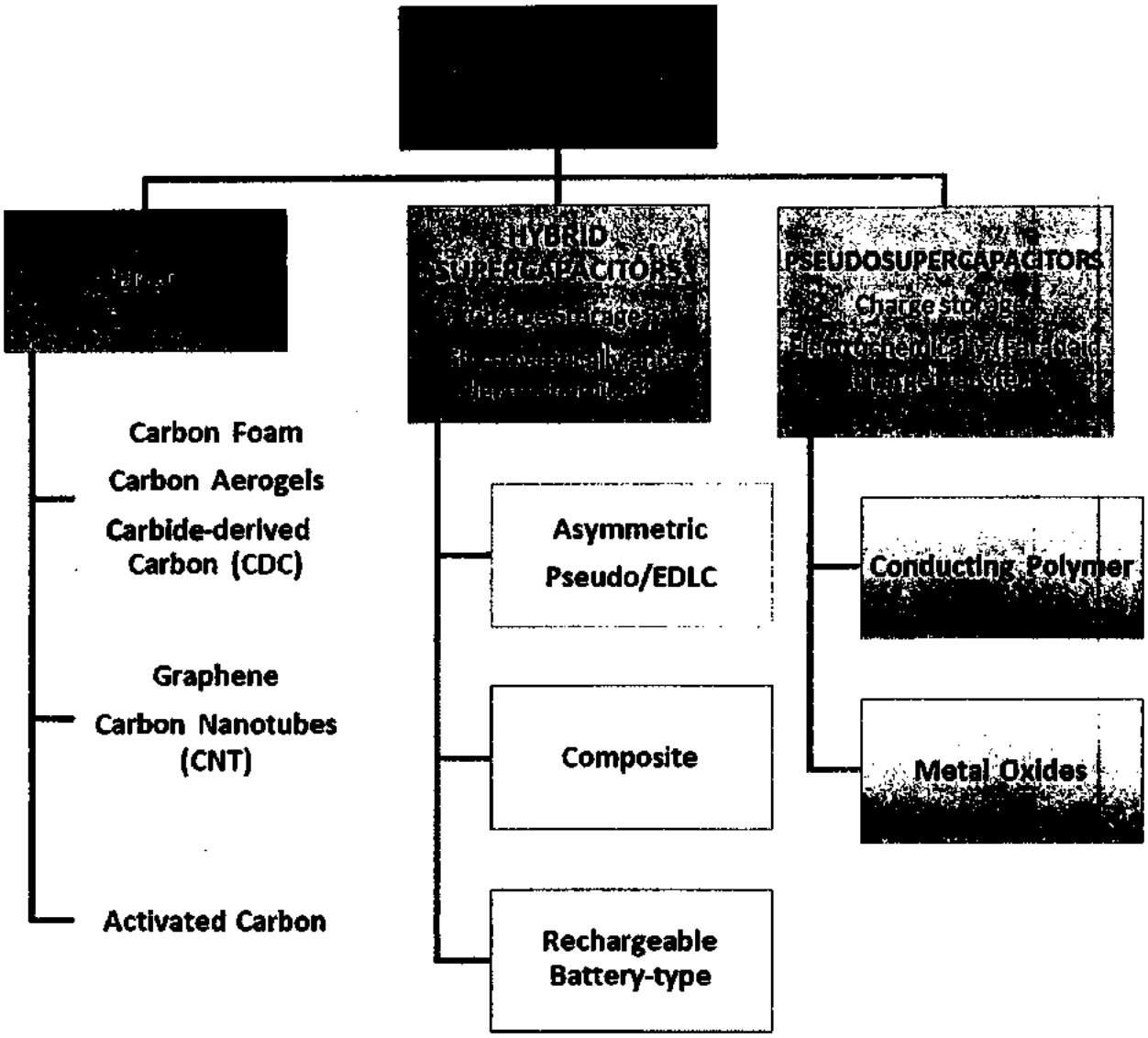

Fig 1.6: Overview of the types and classification of supercapacitors [38]

As per literature no material is "ideal" for fabrication of supercapacitor as every material has its own pros and cons as shown in Table 1.1. Carbon based supercapacitors, show high stability and high power density, but they are not suitable for applications requiring high energy density. Carbon material shows higher life time as compared to metal oxides and Conducting Polymers (CPs). While the conductivity of carbon and CPs is also very high as compared to metal oxides, these carbon materials show high chemical stability. CPs show high energy density as compared to carbon based materials. The efficiency of carbon based materials is greater than CPs due to their high stability. CPs are preferred due to its high flexibility and can be used in flexible applications [39].

Table 1.1: Comparison of physicochemical properties of the various supercapacitor materials [39]

Physicochemical properties	Carbone materials	Metal oxides	Conducting polymers
Non faradic capacitance	○○○○	○○	○○
Faradic capacitance	●	○○○○	○○○○
Conductivity	○○○○	○	○○○○
Energy density	○	○○○	○○
Power density	○○○	○	○○
Cost	○○	○○○	○○
Chemical stability	○○○○	○	○○○
Cycle life	○○○○	○○	○○
Easy fabrication process	○○	○	○○○
Flexibility	○○	●	○○○

Very high, ○○○○; high, ○○○; medium, ○○; low, ○; very Low, ●.

So far, supercapacitors are widely applied to the fields of vehicle mobilization, energy storage and electronic products with considerable markets. Unfortunately, these markets are heavily occupied by leading manufacturers from America, Japan and Korea. It is thus greatly imperative to develop independent core technologies for the advancement of scientific research and addressing the needs of the national economy.

1.5.1 Application of Super capacitors

Supercapacitors can be fully charged/discharged in seconds or minutes as they possess inferior energy density but higher power density as compared to the batteries. Stretchable supercapacitors can be used in tablets, laptops, cameras, mobile phones and many smart and portable electronic devices as shown in Fig 1.7 [40]. Long life cycle gives supercapacitors very big advantage, which is comparable with functional devices. In large scale application high power density of supercapacitors and high energy density of the batteries can be

combined to ensure sufficient power supply.

LEDs, compact DC motor device, remote keyless entry (RKE) system, smart meters, power supply for audio equipment's, communication, security and health care devices.

1.5.2 Demand

Such supercapacitors that can deliver low ESR levels in a thin package and discharge electricity with a large output of watts. Portable devices will become more multi-functionalized scaled and light weight to fully realize the benefits of internet of things (IoT). On the other hand, when a smart device becomes multi-tasked (multi-functionalized), it tends to consume high power at peak operation. Thus we must leverage energy storage solutions that may be mountable in a limited space. Supercapacitors, which exhibit high capacitance and high output may achieve this. When these devices are used as an auxiliary power supply during peak output, they are likely to reduce the supply unit size, improve overall performance and add a higher output function.

1.5.3 Industry

IOT, WSN, are add the core of IOT, composed of nodes (few to thousands) where each node is connected to one (or sometimes several) nodes. Currently; WSN, are typically powered with a primary battery. This becomes problematic, when sensor terminal/nodes number in thousand on the network.

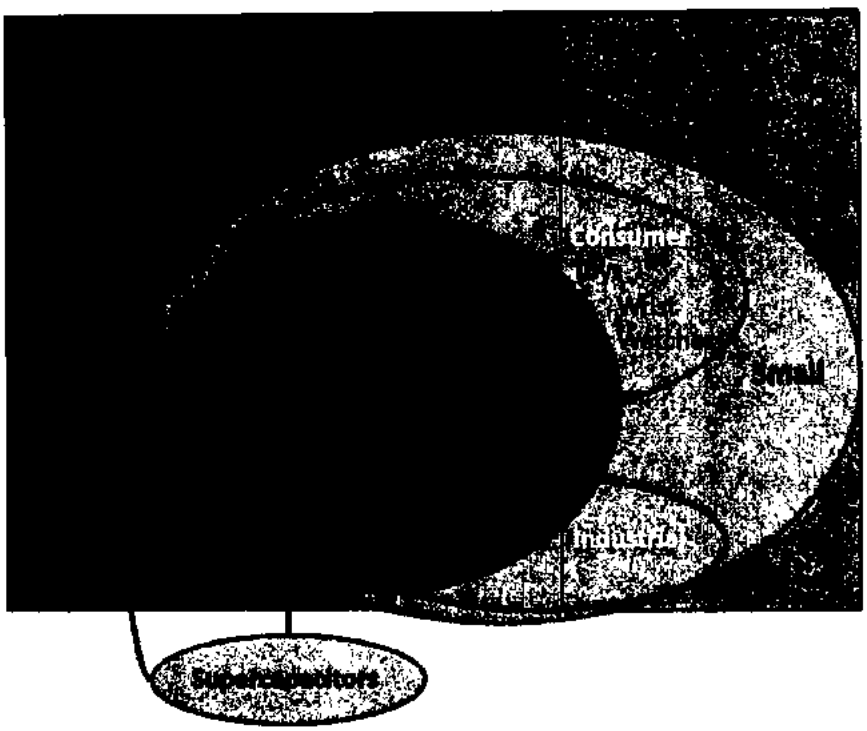

Fig 1.7: Application of supercapacitors [40]

1.6 Gap Analysis and Issues

Although the technology of supercapacitors seems like a perfect step forward that may one day replace the existing conventional battery storage devices but the term coin as supercapacitor as a storage device is not without problems.

Effect of temperature on the performance of the supercapacitors is one of the main issue that is needed to be addressed in the making of such devices. Ideally a stable performance is required over a wide operating temperature. Alongside the operating temperatures the altogether life time is also an important issue that is needed to be addressed. The supercapacitors are required to perform over longer period of time so that the cost of their purchase and maintenance can be justified. A gradual decay in the performance is expected but this can be hindered with the longer working hours. The supper capacitors are required to be stable, flexible and fast. This means that they when connected with the power system, the cycling of the device gets fast enough that out last the current Lithium-Ion batteries.

Cycling is one of the routine test that the power devices go through to access their performance.

Being a power storage device frequency response of supper capacitor is also a term that needed quantification. How quickly the capacitor is charging and what is the output characteristics of the device in the form of voltage. Since the supper capacitor charging is not a chemical reaction, this means it can charge and discharge at the same time. The idea of this exquisite feature relate to the different methods that can be used to charge the supper capacitor. The detail analysis is required to access the methodology of supper capacitor charging. The overall efficiency of the supper capacitor device and supper capacitor itself is a study of careful measurements to accurately judge the device efficiency and value. All these problems are the potential thread to any supercapacitor device that may be required to compete in the current power storage era [41-46].

1.6.1 Solving the Problems: Motivation

The overall research framework for global supercapacitor's industry can be presented in the following scheme:

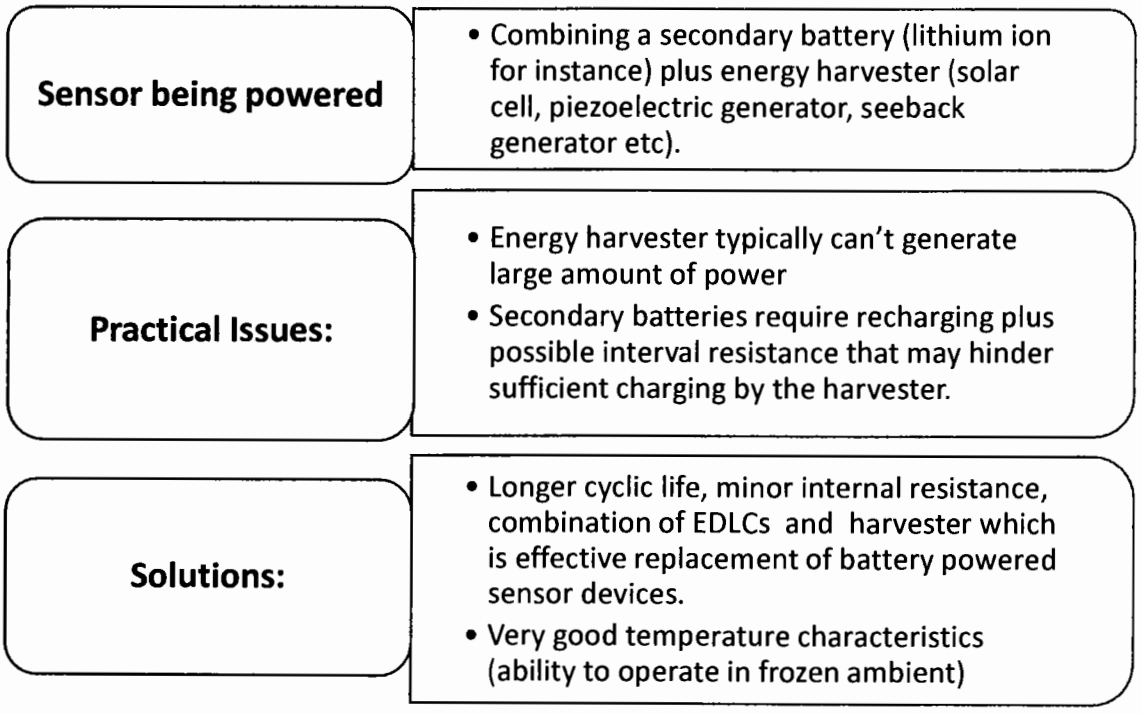

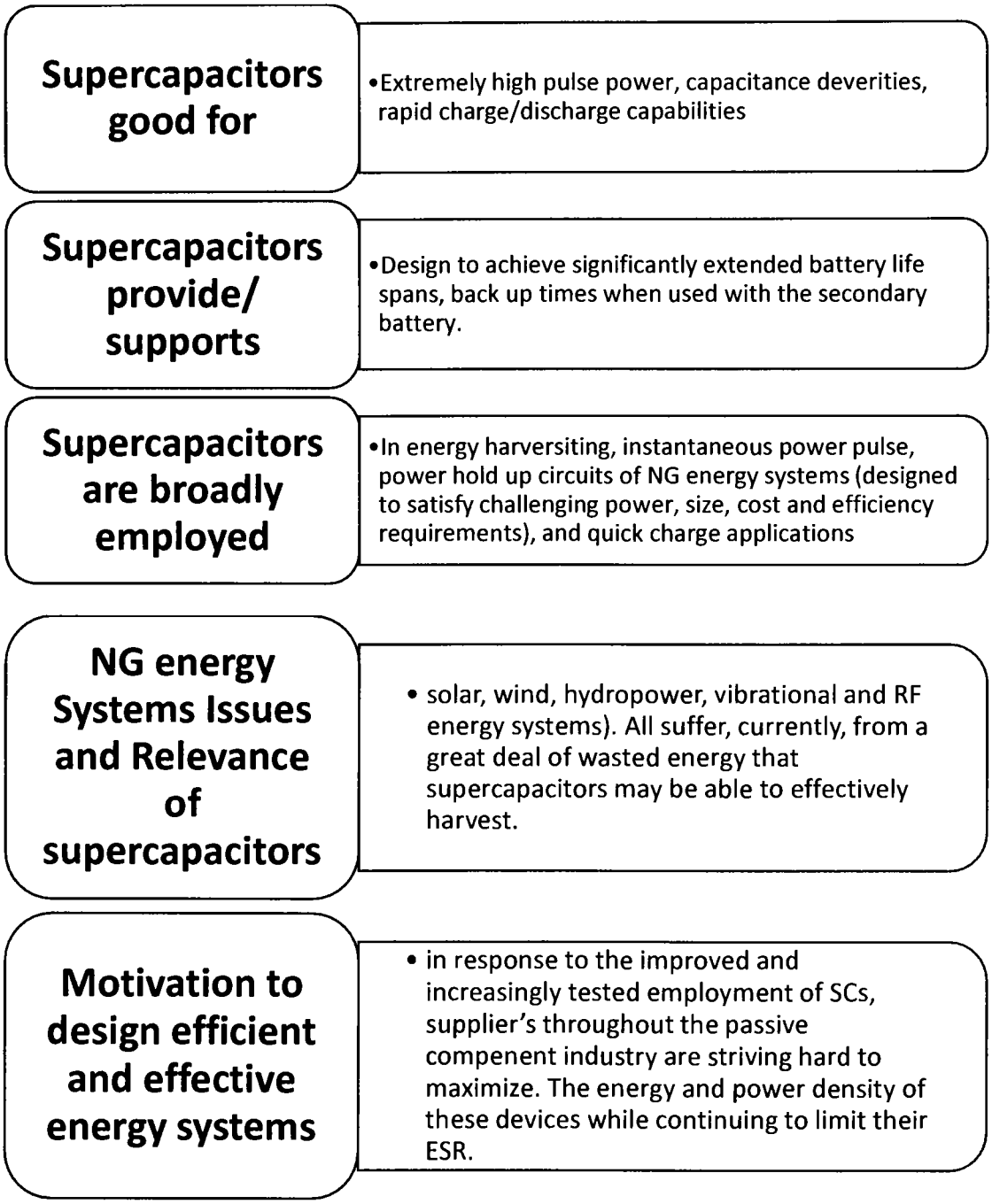

"Supercaps" have been used to fill the gap between an electrical power failure and startup of backup generator.

1.7 Problem Statement

Since the energy storage and power demand for the consumer market is in the ever increasing trend, semiconductor electronics industry is looking for generic structures that are equally

powerful in storing energy and are equally reliable and flexible for universal integration into the systems.

The problem/issues in this emerging research are the applicability of device design, process strategy, and optimization of output characteristics and integration of such device design in the energy systems in terms of flexibility, capacity and system level performance etc. The proposed problem is aimed to develop a new design and process strategy for supercapacitors based on the stretchable organic electronics for subsequent energy storage applications, relevant to the power requirements of system level IoT implementation. This is thought to be done with the help of design engineering materials exploitation, novel fabrication routines (development of prototype supercapacitors including sandwich, planar and fiber structure) and rigorous testing and evaluation in order to qualify the future requirements of energy electronics regimes.

The overall study aimed may bear important scientific meanings in furthering the development of device designs and process integration of stretchable supercapacitors that can act as a source of power and energy for future devices and systems.

1.8 Objectives of the Research

The scope of this work revolves around two main objectives:

- Detailed literature review about the variants of design and manufacturing methods for the fabrication of stretchable supercapacitors based on polymers and preparation and characterization of stretchable conducting polymers with acceptable physical properties for the subsequent development of supercapacitors.
- Device fabrication and characterization of stretchable polymer-based supercapacitors, followed by detailed analytics (*analysis of relationships between device design and performance*) inclusive of the investigation of both the Alternating a Direct current analysis in special preview of testing of such type of supercapacitors.

1.9 Structure of the Thesis

Thesis is systematically divided into six chapters. Chapter 1 provides the basic introduction, which is critical to comprehend the foundation of fabrication and characterization of stretchable supercapacitors for energy system applications. Chapter 2 clarifies a portion of the key ideas which are critical to form the theoretical basis of the problem and thesis. Chapter 3 enlists and review research and studies taken up in fabrication and characterization of stretchable supercapacitors for energy Systems applications, whereas Chapter 4 gives an insight to the experimental techniques used in this work. In Chapter 5 four distinct approaches are used to conduct a systematic study on problem. Experimental details, findings and discussion is presented in this chapter. The case wise conclusion and corresponding future work has been elaborated in Chapter 6.

1.10 Summary

With depleting fossil resources and growing energy demands discovering reliable, environmental friendly, low cost, and sustainable energy adaptation and storage systems stays a key challenge across the globe. Thus Energy needs to be produced, transmit, and store it as its huge amount is required by today's society and most importantly this energy need to be delivered at any time. Due to heavy demand in market on board energy is required for Wearable electronics, internet of things and wireless sensor networks. The other aspect of this technology advancement is the requirement of such structures that can "store charge" and "drive" such flexible and stretchable devices with lightweight, thin and conformable properties. The widely known energy storage devices are batteries and capacitors which are the most common as well. Batteries provide long duration of energy storage with higher energy densities but low power densities while capacitors provide very high power densities but very low energy densities. Supercapacitors (SCs) provides high specific capacitance, economic friendly characteristics, fast charge discharge capabilities and extremely high

storage capabilities. A lot of research is going on supercapacitors making it closer and alternate to conventional batteries. Effect of temperature, cycling and life time is one of the main issue that is needed to be addressed in the making of supercapacitors. The supper capacitors are required to be stable, flexible and fast. The proposed problem is aimed to develop a new design and process strategy for supercapacitors based on the stretchable organic electronics for subsequent energy storage applications, relevant to the power requirements of system level IoT implementation. This is thought to be done with the help of design engineering materials exploitation, novel fabrication routines (development of prototype supercapacitors including sandwich, planar and fiber structure) and rigorous testing and evaluation in order to qualify the future requirements of energy electronics regimes. The overall study aimed may bear important scientific meanings in furthering the development of device designs and process integration of stretchable supercapacitors that can act as a source of power and energy for future devices and systems.

Chapter 2

Background Theory

2.1 Introduction

This section clarifies a portion of the key ideas which are critical to comprehend the foundation of fabrication and characterization of stretchable supercapacitors for energy system applications. It will also help to study the internal structure and working principle of different types of supercapacitors specifically conducting polymer based supercapacitor. It will help us understand the electro-chemical energy conversion and storage systems along with energy storage mechanism of rechargeable battery, Electrostatic Double Layer Capacitors (EDLCs) and pseduocapactiors. An account of stretchable substrates are also explained to emphasize the stretchable and foldable supercapacitors energy system applications. The concepts of Equivalent Series Resistance (R_{ESR}) and self-discharge resistance R_P are also elucidated to understand the equivalent circuit of supercapacitors.

2.1.1 Electrochemical Energy Conversion and Storage Systems

Supercapacitors, fuel cells and batteries are major part of our life in various applications. Due to huge demand of energy in various application we need to store harvested energy. Supercapacitors are energy storage devices used for variety of energy and power requirement while bridging the gap between batteries and capacitors [47]. Supercapacitors materials don't need maintenance, making it highly stable. Supercapacitors are having small size, cost effective, long cycle life, high power density and higher energy density then conventional capacitors. High efficiency and reusability of electrochemical energy conversation has attracted a lot of attention [48]. The story behind the history of development of supercapacitor

is charge storage mechanism as illustrated in Fig 2.1, starting from Leyden jar Ewald Georg von Kleist in 1745 to the development of modern theory of EDLC between liquid electrolytes and two metal electrodes [49].

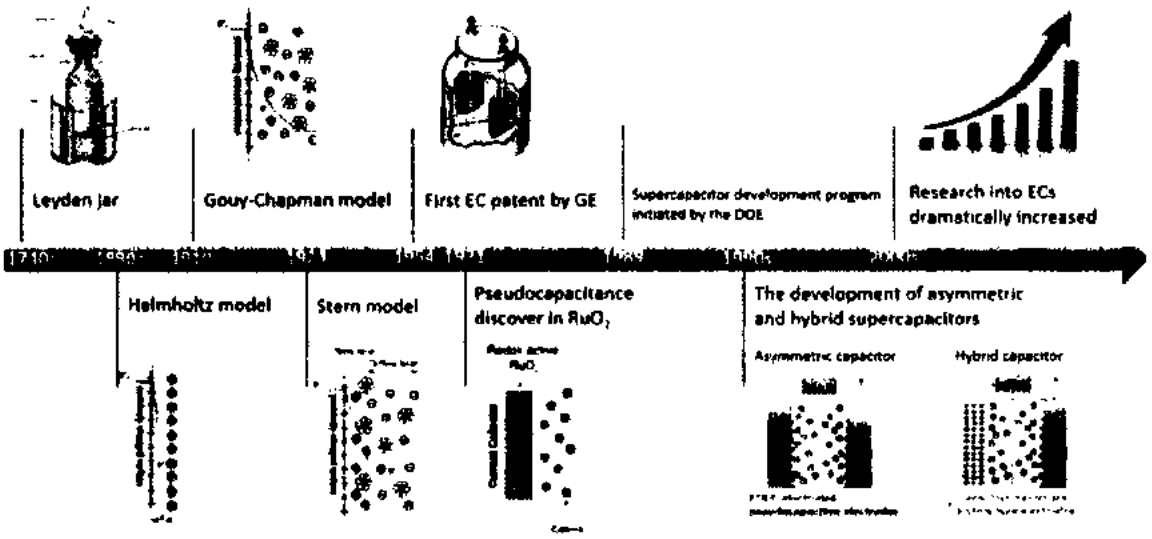

Fig 2.1: Historic timeline for the development of supercapacitors [49]

Due to developments of advance characterization methods and Nano-science, many electrochemical and physical phenomena were developed for pseudocapacitive and EDLC systems. For further study, the charge storage mechanism of pseudocapacitance and EDLC are clearly in need.

2.2 Energy Storage Mechanism

The energy density debate has gradually become the rate-determining step of developing processes in this field. Supercapacitor consists of two plates like ordinary capacitor divided by dielectric as an electrolyte inside the plates creating double layers and creating the ability to store more charge in few seconds and long life cycle as shown in Fig 2.2. Electrochemical reactions occurs by versatile, clean and efficient electrical charge which acts as oxidizing and reducing agent. Due to ion moment between the electrodes the charge storage is rapid [50].

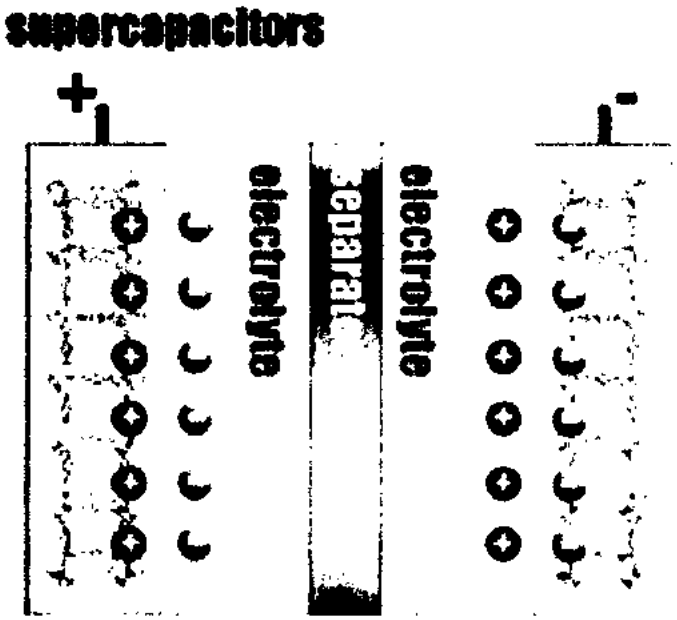

Fig 2.2: Schematic illustrations of supercapacitor [50]

2.2.1 Electrostatic Double Layer Capacitor (EDLC)

Electrostatic Double Layer Capacitor is simplest and most commercially available electrochemical capacitor, storing charge electrostatically [51]. EDLC store charge by absorbing the electrostatic charge between electrolyte and electrode interface. Electrolyte solution is ion-conductive in which the conductive electrodes are immersed making a double layer due to arrangement of charges at the interface of electrode and electrolyte [52-54]. Two opposite charges are created when we dip electrodes into the electrolyte solution and these opposite charges are responsible for double layer. One charge polarity layer (positive/negative) is formed while other layer with opposite polarity layer is formed in electrolyte solution. These layers are separated by water molecules or solvent and working as dielectric. When supply is connected to electrodes, these layers starts getting charged. The process is schematically shown in Fig 2.3 [55, 56].

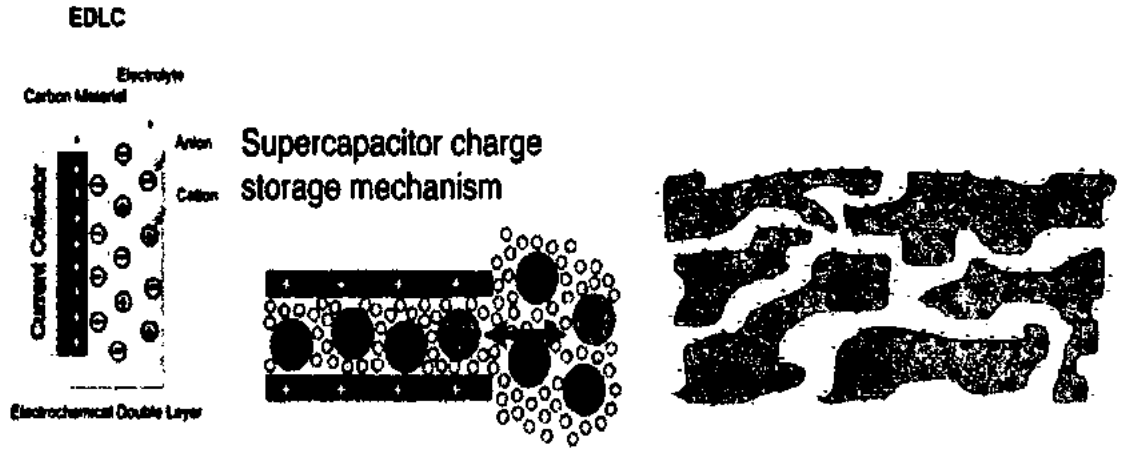

Fig 2.3: Charge Storage mechanism of EDLC Supercapacitor [55-56]

Due to higher surface area and very small charge separation distance of the magnitude of few nanometers, the EDLCS show higher storage capabilities of electrical energy as compared to conventional capacitors. EDLCS used carbon-based active materials like carbon nanomaterials [57, 58], carbon nanotubes [59, 60], activated carbons [61, 62], graphene[63-65] and carbon aerogels [66] showing desirable reliability and higher specific surface areas. The process of formation and relaxation of double layers occurs very quickly of the order of $\sim 10^{-8}$ seconds [67].

EDLC capacitance can be calculated according to Equation 2.1 [68].

$$C = \frac{\varepsilon_r \, \varepsilon_0}{d} A \qquad (2.1)$$

Where ε_0 is the permittivity of vacuum, ε_r is relative permittivity of liquid electrolyte, d is the effective charge separation distance between electrical double layers also known as debye length and A is the effective surface area of electrode materials which are available to the electrolyte ions. EDLCs charge/discharge process does not involve any Faradaic reactions as it only requires charge rearrangement, hence responding immediately to any potential change. Electrical double layers effective thickness depends on the size and concentration of

solvation shell and electrolyte ions, ranging from 5–10 Å [69]. The specific capacitance of EDLCs depends on relative permittivity of electrolyte medium and effective capacitance. Specific capacitance is considered to be from 10 to 21 μF cm^{-2} [70]. High capacitance of 300–550 F g^{-1} is achieved due to carbon materials high specific area of 1000– 3000 m^2 /g. The specific capacitance achieved practically is around ~100–250 F g^{-1} which is limited because of unavailability of surface sites and finite conductivity. In market the EDLCs can store charge in range of 3–10 Wh kg^{-1} [71].

2.2.2 Electrochemical Pseudocapacitor

As compared to preliminarily commercialized EDLCS, electrochemical pseudocapacitors show higher energy densities because of superficial redox reactions charge/ discharge mechanism. Pseudocapacitors are based on conducting polymers and/or transition metal oxides. Accumulative charge is stored rapidly and behaves like a capacitance, as a result of redox reaction in the bulk of a material [72]. EDLCs uses surface layer to store charge while pseudo capacitors redox reaction occurs at the bulk of the material. That is why pseudo-capacitors have higher per weight unit of capacitance as compared to EDLC. The redox reactions at the material bulk improves the storage of energy due to conducting polymers (CPs) and can store the charge in a superior manner which prompts high energy density [73]. On the other hand, there are many advantages of CPs in comparison to their drawbacks relating to the EDLCs and batteries because the electron transfer kinetics show faster behavior than other materials including metal oxides (Pasquier, et al., 2002) [74]. Pseudocapacitance (C) can be calculated according to Equation 2.2 [75].

$$C=\frac{d(\Delta q)}{d(\Delta V)} \qquad (2.2)$$

Where d(Δq) is derivative of charge acceptance and d(ΔV) is derivative of changing potential. Energy is stored fardacially in psuedocapacitors and depends on reversible and fast

electrochemical redox reactions same like batteries. The electronic charge is transferred between electrode and electrolyte ions. Two electric double layers by the molecules of electrolyte are formed to store the charge between the electrode and electrolyte. Absorbed and de-solvated ion is responsible for charge transfer between electrolyte and electrode. In contrast to batteries only top surface of electrode is utilize as redox reaction because there is no chemical reaction of absorbed ion with electrode because of only charge transfer making it more stable and reliable [76, 77]. Fig 2.4 shows the charge storage mechanism of psuedocapacitor.

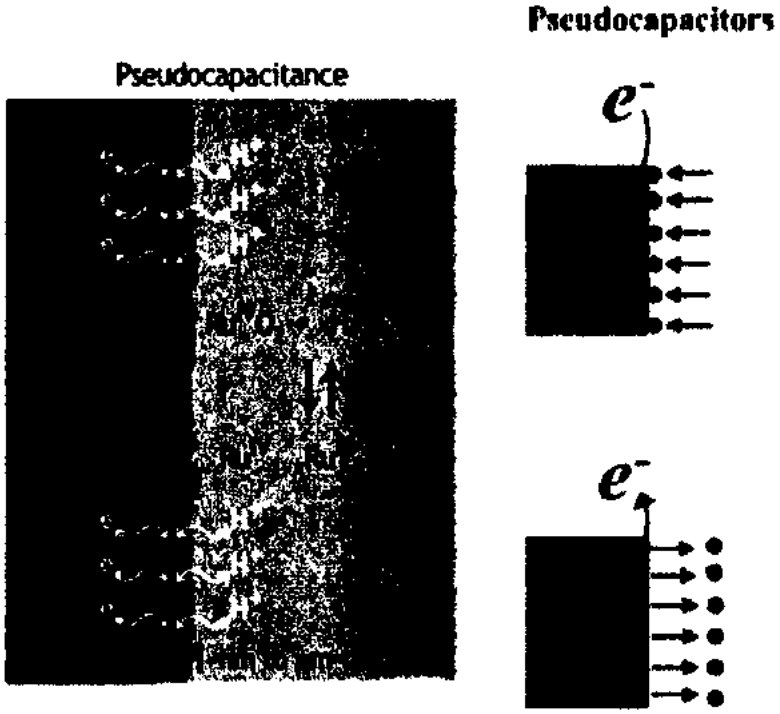

Fig 2.4: Charge Storage mechanism of Pseducapacitor [76, 77]

2.2.3 Hybrid Supercapacitor

Hybrid supercapacitors are the type of supercapacitor having more energy storing capability and high capacitance. It is basically the combination of properties of components of pseudocapacitor and EDLC, that is having fetched much attention [78]. Numerous

possibilities are available with more importance to electroactive and conducting components leading to higher energy storage [79]. Energy storage mechanism of hybrid supercapactior is constituted by the combination of two storage mechanisms EDLC and pseudocapacitor. One half part behaved like pseudocapacitor and the other half behaves like EDLC. That why hybrid supercpacitor has higher power and energy densities then normal pseudocapacitor and EDLC. Due to these properties they are favored in energy efficient systems as compared to other storage devices [80]. Fig 2.5 shows the charge storage mechanism of hybrid supercapacitor.

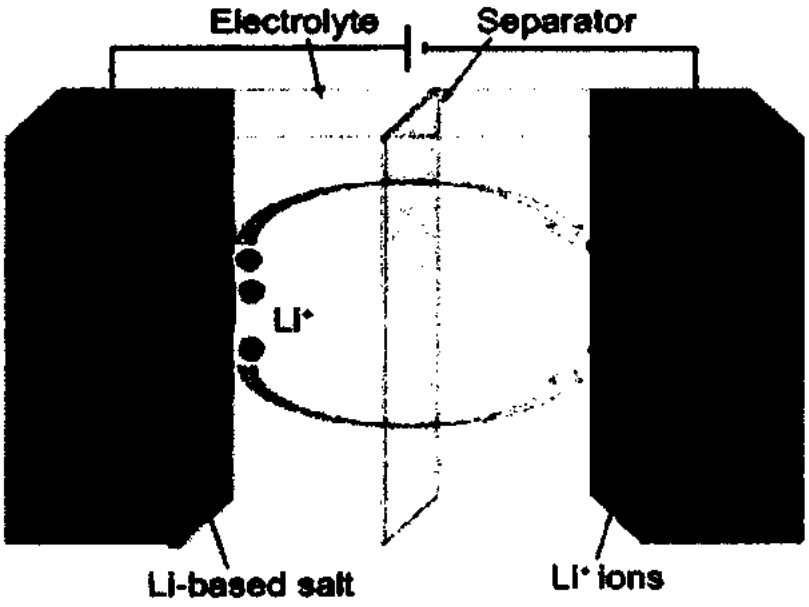

Fig 2.5: Charge Storage mechanism of hybrid supercapacitor [81]

From Fig 2.5 it can be seen that the hybrid supercapacitor is having two electrodes, one is Carbon based electrode and the other one is lithium based electrode. Hybrid supercapacitors shows better properties when two different material electrodes are combined as compared to individual one [81].

2.3 Stretchable Supercapacitor

The field of stretchable devices has been advancing quickly during the last few years, from the view point of developing basic enabling technologies, exploring device system and creating new application opportunities. Stretchable electronic devices could offer the function of established technologies, when these devices are attached with mechanical attributes like stretching, twisting and bending, and still retain its operating properties upon deformation [82, 83]. These mechanical properties leads us to a range of applications like soft surgical instruments [84], eyeball digital camera [85], health monitors [86] and sensitive robotic skins [87]. To complete the entire package of integration of stretchable devices, there is also a need for developing stretchable energy storage system. There are two methods for stretchable energy storage systems: (a) development of novel materials that can be intrinsically stretchable for electrodes and electrolytes [88-90], (b) development of novel structural design for diverse integration of soft and hard components for to stretchable device structures [91-93]. Four strategies have been exploited for structural design to achieve stretchable supercapacitor: (a) Wrinkled, wavy design using prestrain in soft elastomeric substrate [94-96], (b) serpentine bridge-island design [97], (c) origami design using crease patterns [98], and (d) fractal inspired bridge-island design using photolithography technology [99]. Fig 2.6 show these four design strategies for stretchable supercapacitors [100]. A lot of efforts have been done for the development of analytical and computational models for every individual strategy. These strategies are developed by few assumptions, and might not be able to sustain properties under extreme conditions for new applications. That is why there are still a lot many opportunities and open challenges for future research.

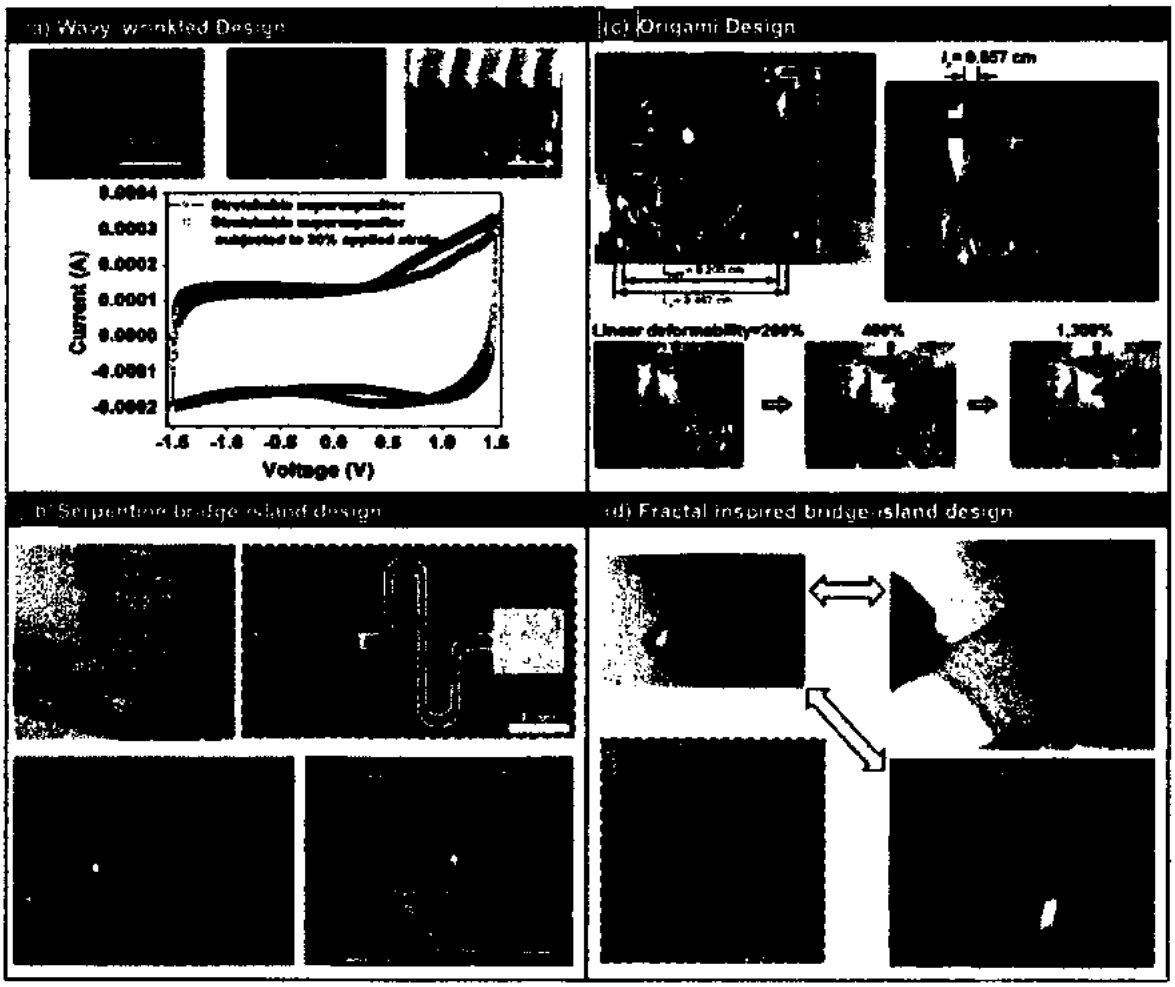

Fig 2.6: Four design strategies for stretchable supercapacitors (a) wrinkled and wavy design (b) Serpentine bridge-island design (c) Origami design (d) Fractal inspired bridge-island design [100]

2.4 Electrode

Electrode plays an important role on the performance of supercapacitor. It is the most important task to search for the best electrode material with excellent properties and performance. The properties of supercapacitor depends on the interaction of electrode material with the electrolyte, determining the thermal and electrical properties of supercapacitor [101]. The electrodes must possess high chemical stability, processability, good conductivity, temperature stability, maximum corrosion resistance, low cost, environmental friendly, and controlled pore structure [102]. Capacitance of supercapacitor can be increased by capacity of material due to faradic charge transfers [103].

2.4.1 Carbon materials

Carbon materials are widely used as electrode material due to its non-toxicity, abundance, excellent electronic conductivity, easy processing, large specific surface area, wide operating temperature range and high chemical stability [104]. Numerous carbon based materials like carbon nanotubes (CNTs), activated carbons, graphene, porous carbon, carbon black, graphite, carbon aerogels, and mesoporous carbon, have been reported in as electrode materials for EDLCS in past few years. Porous activated carbons delivers capacitance of 100 Fg^{-1} and 200 Fg^{-1}. They are used conventionally as an electrode material with huge specific area of around 2000 m^2g^{-1}. By increasing the specific surface area, charge accumulation capacity is increased at the interface of electrode and electrolyte [105]. The carbon materials used as electrode must have three properties: (a) more than 1000 $m^2\ g^{-1}$ specific surface area, (b) High conductivity of inter and intra -particle, and (c) extraordinary electrolyte convenience to intra-pore space of carbon based electrode materials [106]. Carbon nanotubes are also being considered as a candidate for electrode material due to its chemical stability and high conductivity. But lower specific area of CNTs provides lower capacitances of around of 30 F g^{-1} in organic electrolytes [107,108]. Different type of carbon and carbon based materials used as electrode materials for supercapacitors with electrolytes used and specific capacitance are summarized in Table 2.1. It shows that activated carbon provide much higher specific capacitance than all other carbon based electrodes.

Table 2.1: Carbon based electrode materials with specific capacitance

Electrode	Cap Fg^{-1}	Electrolyte	Ref.
Activated carbon	200-400	Aqueous (NaOH/KOH)	[109]
Carbide Driven Carbon	100-150	Ionic Liquids (KCl/NaCl)	[109]
Carbon black	<300	Aqueous (NaOH/KOH)	[109]

Templated Carbon	120-350	Aqueous (NaOH/KOH)	[110]
Carbon Aerogels/xerogels	40-200	Aqueous (NaOH/KOH)	[110]
Carbon Nanotube	20-180	Aqueous (NaOH/KOH)	[111]
Activated Carbon Fibers	180-210	KOH	[112]
Mesoporous Carbon	180	KOH	[113]
Graphite and Reduced Graphene oxide (rG0)	10-150	Tetraethylammonium tetrafluoroborate (Et_4NBF_4)	[114]

2.4.2 Metal oxides

Metal oxides provides much higher specific capacitance as compared to carbon based electrode materials. Metal oxides provides pseudocapacitance form adsorption and desorption of ions and also from faradic redox reaction at the interface of electrode and electrolyte [115]. After reviewing previous literature it is observed that metal oxide electrode materials development are of three types: (a) Mn-based Materials, (b) Ru-based materials, and (c) nickel or cobalt based material. During last few years various metal oxides have been widely investigagted as electrode materials like RuO_2, MnO_2, H_2O, Fe_2O_3, IrO_2, V_2O_5, Co_3O_4, SnO_2 and few hydroxides and their composites like $Ni(OH)_2$ and $Co(OH)_2$ [116]. Different type of metal oxide materials used as electrode materials for supercapacitors with electrolytes used and specific capacitance are summarized in Table 2.2.

Table 2.2: Metal oxide and hydroxides based electrode materials with specific capacitance

Electrode Materials	**Cap Fg^{-1}**	**Electrolyte**	**Ref.**
RuO_2	650-735	H_2SO_4	[117]
$Ni(OH)_2$	578	KOH	[118]
V_2O_5	262	KCL	[119]

MnO_2	261	K_2SO_4	[120]
TiN	238	KOH	[121]
$MnFeO_2$	126	PF_6	[122]

From Table 2.2, it can be seen that RuO_2 provides maximum specific capacitance and show remarkable performance. The use of RuO_2 is limited due to huge cost and harmfulness to environment, that's why these electrodes are excluded from the wide range of supercapacitor applications. The low cost of MnO_2 and high theoretical capacitance value ranging from 1100 to 1300 Fg^{-1}, make it promising alternative material [123].

2.4.3 Conducting polymers

Conducting Polymers (CPs)-based pseudocapacitors have shown remarkable achievement in flexible and portable supercapacitor applications due to high conductivity, extraordinary redox active capacitance, and intrinsic flexibility [124-126]. CPs are organic polymers with high electrical conductivity and shows higher capacitive behavior due to the fact that the redox reaction occurs throughout the bulk, along with the surface of the material. In past few years CPs are widely used due to reversible nature, higher charger density and very low cost when compared with metal oxides [127,128]. CPs includes polypyrrole (PPy) [129], poly (3,4- ethylenedioxythiophene) (PEDOT) [130,131], polythiophene (PTh)[132], and polyaniline (PANI)[133-134] as electrode materials. Poly (3, 4-ethylene dioxythiophene) polystyrene sulfonate (PEDOT: PSS) and 3, 4-Ethylenedioxythiophene (EDOT) are two major types of PEDOT. They are readily available and easy to process into 3D structures and thin films. Chemical oxidization and electrochemical polymerization of monomer 3, 4-Ethylenedioxythiophene (EDOT) are used to produce PEDOT [135-138]. PEDOT cannot be processed in water due to its hydrophobic nature. Spray coating, drop coating, ink-printing,

and spin coating are diverse methods used for processing PEDOT: PSS. The performance of PEDOT: PSS film is dependent on electrical conductivity. Film thickness and additives are major variables that affect the electrical conductivity [139]. For energy storage, redox reactions occur due to the involvement of only a few nm-thick surface layers. To achieve high energy density large surface area will promote the utilization of electrode materials. Different type of CPs used as electrode materials for supercapacitors with electrolytes used and specific capacitance are summarized in Table 2.3.

Table 2.3: Conducting Polymer based electrode materials with specific capacitance

Electrode Materials	Cap Fg^{-1}	Electrolyte	Ref.
Polypyrrole (PPy)	40–588	Aqueous	[140,141]
	20–355	Non Aqueous	
Polyanaline (PANI)	120–1530	Aqueous	[142]
	100–670	Non Aqueous	
Poly(3,4-ethylenedioxythiophene) (PEDOT)	100–250	Aqueous	[143-145]
	121	Non Aqueous	
	130	Ionic Liquid	
Polythiophene (PTh)	1.5–6	Non-aqueous	[146]
Poly(4-flourophenyl-3-thiophene) (PFPT)	10–48	Non-aqueous	[147]
Poly(3-methyl thiophene) (PMT)	20–220	Non Aqueous	[148, 149]
	15-225	Ionic Liquid	

It can be seen from Table 2.3 that PANI shows higher specific capacitance value. When PANI is preopared by chemical method it shows capacitance of 200 Fg^{-1} and when prepared by

electrochemical method it shows specific capacitance above 1500 Fg^{-1} [142]. Thickness of electrodes and morphology are the reason behind this variation [150]. Table 2.4 shows the comparison of different properties of electrode materials.

Table 2.4: Comparison of different properties of electrode materials.

Physicochemical	**Carbon based Electrode materials**	**Metal Oxide based Electrode materials**	**Conducting Polymers based Electrode materials**
Non Faradic Capacitance	×××××	×××	×××
Faradic capacitance	×	×××××	×××××
Conductivity	×××××	××	×××××
Power density	××××	××	×××
Energy density	××	××××	×××
Cost	×××	××××	×××
Chemical stability	×××××	××	××××
Cycle life	×××××	×××	×××
Ease of fabrication process	×××	××	××××
Flexibility	×××	×	××××
Very High ×××××, High ××××, Medium ×××, low ××,very Low ×			

It can be seen that non faradic capacitance is more in carbon materials, while metal oxides and conducting polymers shows faradic capacitance. Conductivity of carbon and CPs are higher as compared to metal oxides. Carbon based materials show lower energy density and higher power density, while metal oxides and CPs show higher energy density and lower power density. Cost of metal oxides is higher than carbon and CP based materials. Carbon based material shows very high stability, while CP shows high stability as compare to metal oxides as they show very low stability. Carbon Based material shows very high cycle life, while metal oxides and CPs shows lower cycle life. CPs are easy to fabricate as compared to carbon and metal oxides. CPs shows much higher properties for stretchable supercapacitor [151].

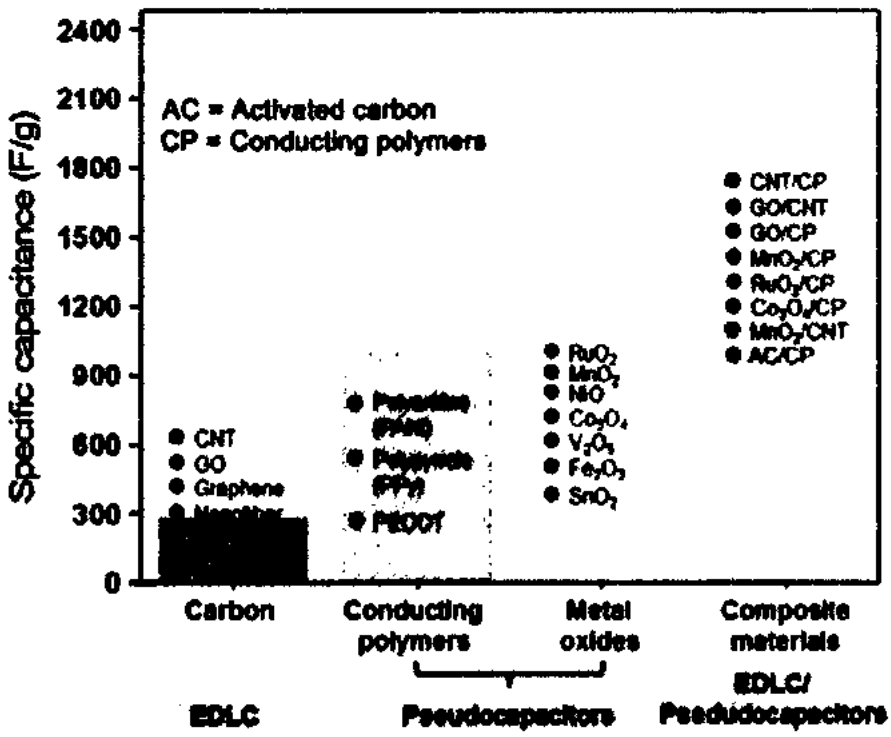

Fig 2.7: Comparison of specific capacitance of different electrode materials for supercapacitors [152]

Fig 2.7 shows comparison of specific capacitance of different electrode materials for supercapacitors. It can be seen from Fig 2.7 that Carbon based materials shows capacitance

under 300 Fg^{-1}, while CPs and metal oxides capacitance is around 1000 Fg^{-1}. Apart from these three types of materials composite materials (combination of two or more materials) shows much higher capacitance around 2000 Fg^{-1} [152].

2.5 Electrolyte

Electrolytes are considered to be the most powerful and main component of supercapacitor, performance of supercapacitors are also dependent on them. Electrolyte including salt and solvent, provide ion conductivity and charge compensation on to the electrodes of supercapacitors. Electrolyte comprises of dissolved chemicals and solvent that make positive and negative ions making it conductive. And this electrical conductivity is dependent on the number of ions present inside the electrolyte [153].Electrolytes plays an important role supercacpacitors properties like rate performance, cycle life, internal resistance, power density, energy density, toxicity and self-discharge [154]. Fig 2.8 shows the Role of electrolyte on the properties of electrochemical supercapacitor (ES). Ideal electrolyte require properties like (a) high ion conductivity,(b) wider voltage window, (c) stability, (d) internes to electrodes, (e) environment friendly, (f) low cost and (g) low volatile and (h) low flammability [155]. It's hard to achieve all these properties making a lot of opportunities for researchers.

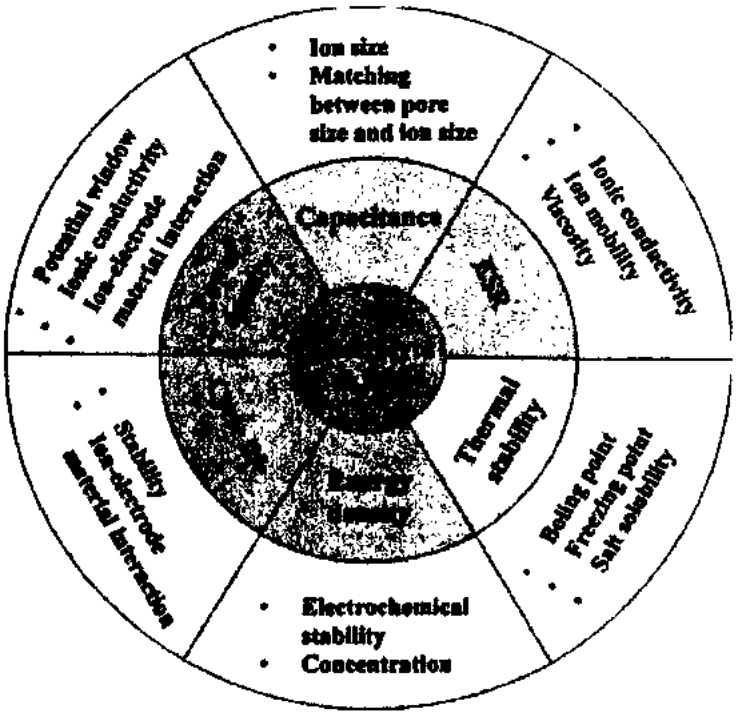

Fig 2.8: Role of electrolyte on the properties of Electrochemical Supercapacitor (ES) [155]

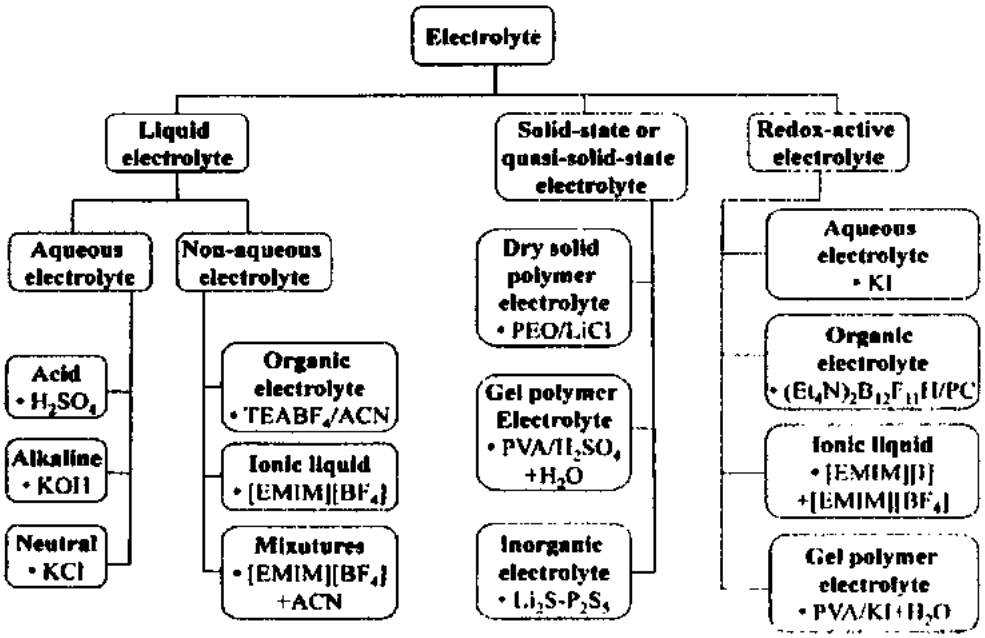

Fig 2.9: Electrolyte Classifications [155]

Electrolytes are classified into few categories organic, aqueous and non-aqueous, ionic liquids, redox electrolytes, and solid state or quasi solid state [156]. Classification of electrolytes are shown in Fig 2.9.

2.6 Supercapacitor Systems

Supercapacitor consists of two electrodes as we already studied earlier, by configuration amendment of these electrode materials, supercapacitors can be divided into two categories: Symmetric and asymmetric supercapacitors.

2.6.1 Symmetric supercapacitors

When two identical/same electrodes are used in a supercapacitor, they are known as symmetric supercapacitors. Fig 2.10(a) shows the schematic illustration of symmetric supercapacitor, in which two identical electrodes are used i.e. Mn-CuO [157].

2.6.2 Asymmetric supercapacitors

When the electrodes are of different types in supercacpacitor they are known as asymmetric supercapacitors. Fig 2.10(b) shows the schematic illustration of asymmetric supercapacitor, in which two different electrodes are used i.e. Mn-CuO and activated carbon [157].

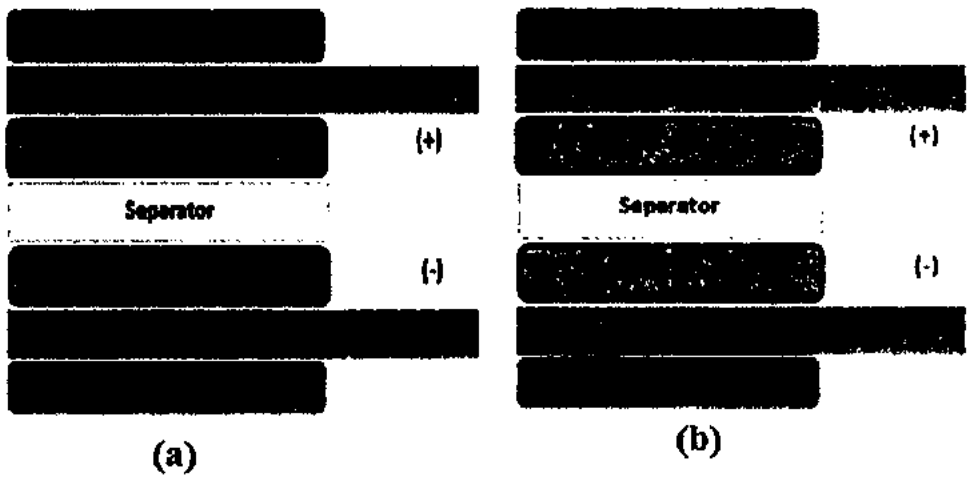

Fig 2.10: Schematic illustration of **(a)** Symmetric supercapacitors **(b)** Asymmetric supercapacitors [157]

2.7 Equivalent Circuit Model (Randles Cell) of the Supercapacitor

The complexity of charging and discharging nature of any supercapacitor has still not properly been understood due to the complex nature of electrolytic behavior of monomers

under charging and discharging mode of operation. Literature [158], has suggested that for the charge flow in supercapacitors, a Randles cell of an equivalent circuit model is very popular for the ionic behavior at the electrolytic and electrode interface levels and is shown in Fig 2.11. In Fig.2.11; 'R_{ESR}' is the equivalent series resistance, 'R_p' is the parallel resistance (also known as self-discharge resistance) and 'C' is the value of said supercapacitor.

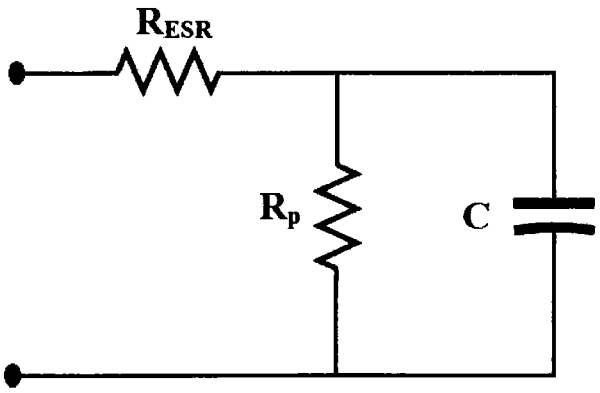

Fig 2.11: Equivalent Circuit Model (Randles Cell) of the Supercapacitor [158]

2.8 Defects in Crystals for electrical activation/deactivation of devices

Perfect crystal does not exist, they contain some defects. These defects contribute to the physical and chemical properties of the material and electronic operation of a device. They are classified into four groups, i.e. volume defect (three dimensional defects), surface defect (two dimensional defects), line defect (one dimensional defects) and point defect (zero dimensional defects) [159-160]. Volume defects are three dimensional defects, which can occur during the process of crystal growth like occurrence of cracks in crystals. During the growth, cracks are formed by small electrostatic dissimilarity between the stacking layers. Surface defects are two dimensional defects occurs between two regions of crystal and it is the region of distortion that lie about a surface. Surface defects can be classified further into four categories, i.e, twin boundaries, grain boundaries, external surfaces and staking faults. Line defects are one dimensional defects also called dislocation, it is the area where the atoms

are misaligned or out of the position in the structure. These dislocations are further classified in two categories i.e. Edge dislocations and Screw dislocations. Point defects are zero dimensional defects that occurs when an atom is at irregular place or missing in the lattice structure. They produce small strains in volume of the crystal. They are classified into four categories, i.e. vacancies, substitutional defect, interstitial defect, and electronic defects. Classification of defects are shown in Fig 2.12.

Crystal defects, impurity interstitial, dislocation, self-interstitial, d) cluster of impurity atoms, extrinsic dislocation loop, small substitutional impurity, vacancy, intrinsic dislocation loop, large substitutional impurity are shown in Fig 2.13 [161].

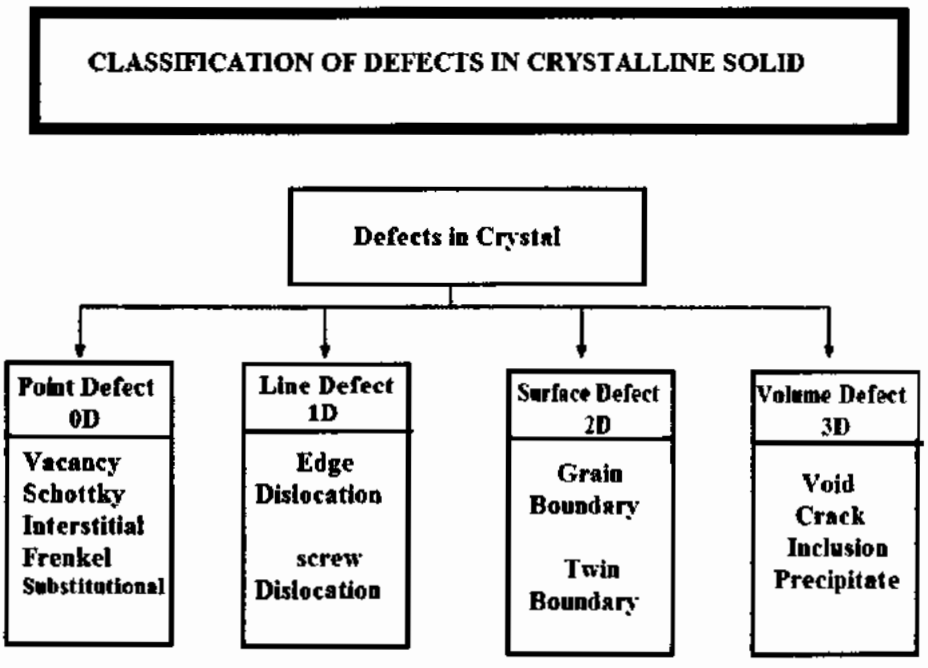

Fig 2.12. Classification of defects in a crystalline structure [161]

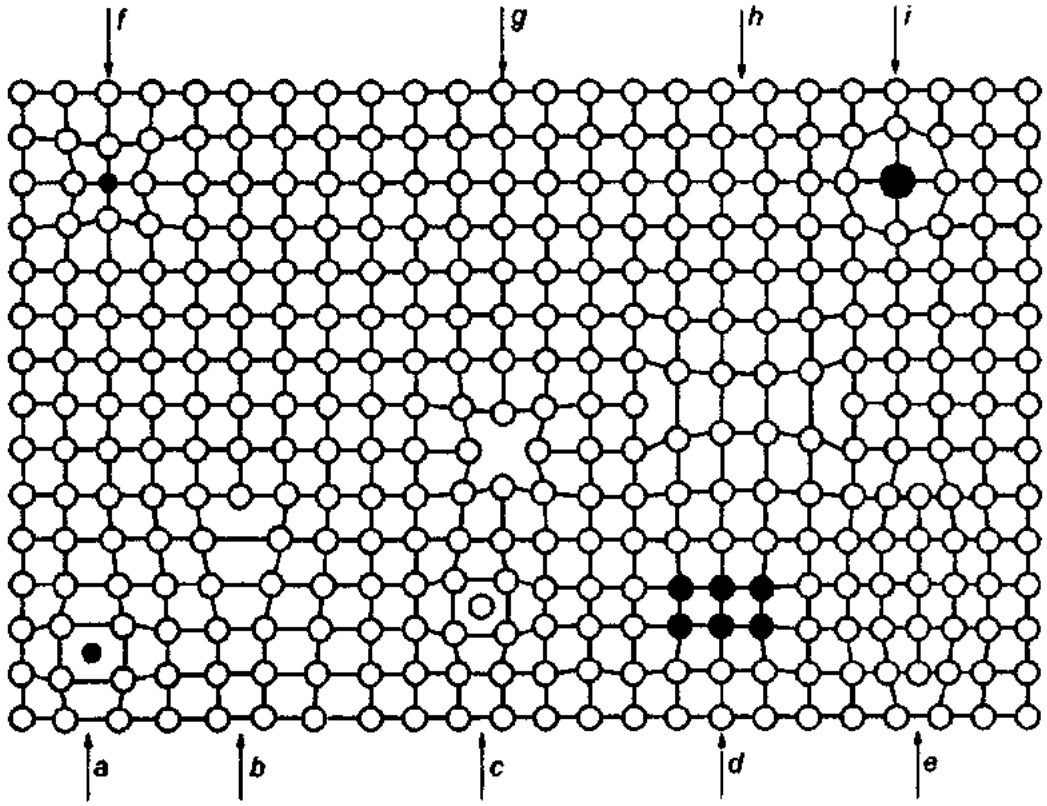

Fig 2.13: Crystal defects, a) impurity interstitial, b) dislocation, c) self-interstitial, d) cluster of impurity atoms, e) extrinsic dislocation loop, f) small substitutional impurity, g) vacancy, h) intrinsic dislocation loop, i) large substitutional impurity; [161]

2.9 Summary

Supercapacitors materials don't need maintenance, making it highly stable. Supercapacitors are having small size, cost effective, long cycle life, high power density and higher energy density then conventional capacitors. High efficiency and reusability of electrochemical energy conversation has attracted a lot of attention. Supercapacitor consists of two plates like ordinary capacitor divided by dielectric as an electrolyte inside the plates creating double layers and creating the ability to store more charge in few seconds and long life cycle. Electrostatic Double Layer Capacitor is simplest and most commercially available electrochemical capacitor, storing charge electrostatically. Electrochemical pseudocapacitors show higher energy densities because of superficial redox reactions charge/ discharge mechanism. Pseudocapacitors are based on conducting polymers and/or transition metal oxides. Hybrid supercapacitors are the type of supercapacitor having more energy storing capability and high capacitance. It is basically the combination of properties of components

of pseudocapacitor and EDLC.There are two methods for stretchable energy storage systems: (a) development of novel materials that can be intrinsically stretchable for electrodes and electrolytes (b) development of novel structural design for diverse integration of soft and hard components for to stretchable device structures. The properties of supercapacitor depends on the interaction of electrode material with the electrolyte, determining the thermal and electrical properties of supercapacitor. Carbon materials are widely used as electrode material due to its non-toxicity, abundance, excellent electronic conductivity, easy processing, large specific surface area, wide operating temperature range and high chemical stability. Metal oxides provides much higher specific capacitance as compared to carbon based electrode materials. Metal oxides provides pseudocapacitance form adsorption and desorption of ions and also from faradic redox reaction at the interface of electrode and electrolyte. Conducting Polymers (CPs)-based pseudocapacitors have shown remarkable achievement in flexible and portable supercapacitor applications due to high conductivity, extraordinary redox active capacitance, and intrinsic flexibility. Electrolyte including salt and solvent, provide ion conductivity and charge compensation on to the electrodes of supercapacitors. Electrolyte comprises of dissolved chemicals and solvent that make positive and negative ions making it conductive. Electrolytes are classified into few categories organic, aqueous and non-aqueous, ionic liquids, redox electrolytes, and solid state or quasi solid state. By configuration amendment of these electrode materials, supercapacitors can be divided into two categories: Symmetric and asymmetric supercapacitors. Perfect crystal does not exist, they contain some defects. These defects contribute to the physical and chemical properties of the material and electronic operation of a device. They are classified into four groups, i.e. volume defect (three dimensional defects), surface defect (two dimensional defects), line defect (one dimensional defects) and point defect (zero dimensional defects).

Chapter 3

Literature Review

This section of the thesis enlists the research and studies taken up in fabrication and characterization of stretchable supercapacitors for energy Systems applications. Extensive review of such studies is provided in the following subsections:

3.1 Energy Density

Energy storage devices are required for the blooming mobile electronic devices market, renewable off-grid energy sources, electric vehicles and many other such technologies. Rechargeable batteries are preferred because of high energy density. The longer life time and higher power density of the supercapacitors make them better than the batteries. As compared to batteries, supercapacitors are preferable and more suitable for many applications. Moreover, they can also extend the battery's life time. Even after a lot of effort done on energy storage devices during past few years, there are still some fundamental questions which needed to be answered to find solutions to increase specific energy density in these systems. The energy density debate has gradually become the rate-determining step of developing processes in this field.

However, due to lower energy density of supercapacitors, batteries are still more preferable for energy storage systems [162]. Energy density capacitance can be calculated according to Equation 3.1[163].

$$E = \frac{1}{2} C v^2 \qquad (3.1)$$

The energy density depends on two major factors operating voltage range (V) and capacitance (C). Energy density can be improved by enhancing the capacitance and operating potential/voltage range. For this reason, a lot of research is going on electrode materials for

enhanced energy and power density.

3.2 Stretchable Supercapacitors

The two main types of supercapacitors are electrical double layer capacitors (EDLCs) and pseudo-capacitors. Carbon materials are used to make EDLCs and they possess superior cyclic stability and mechanical strength. On the other hand, whereas pseudo-capacitors demonstrate greater capacitance but limited durability and are based on Faradaic mechanism [164, 165].

As the market is progressing, portable, wearable and flexible electronic devices, the rapid development of flexible energy storage devices has undergone a lot of work. In flexible supercapacitors, Energy is stored by the electrical charged at the interface of electrolyte and electrode materials same like traditional supercapacitors [166-168]. They possess long cycle life high power density, and fast charge/discharge capability, and they retain their properties when deformation occurs. With the passage of time the researchers are focusing on the flexible supercapacitors constructed from metal oxides, carbon Nano materials and conductive polymers [169–172]. The supercapacitor made from electrodes of hybrid carbon film gives more flexibility as compared to that provided by conventional sueprcapacitors. They can tolerate temperature and can be stretched, bend up to 180°, or form origami [173,174]. High durability is attained by the device due to which the after high deformation at high temperatures the energy storage ability remains the same. The temperature is also widen due to excellent electrochemical property device works at extreme temperatures (−40 °C to 200 °C).The fabrication of a new, high rate, symmetrical, solid state EDLC employed plastic crystal Succinonitrile (SN) based gel polymer electrolyte (GPE) and graphenenano-platelets (GNPs) as electrodes. Due to the excellent mechanical properties, the high ionic conductivity (~2 x10 $^{-3}$ S cm^{-1} at 20°C), electro-chemical stability window (~3.5

V vs. Ag), thermal stability (-30 to 80°C), it is the most sutiable candidate as electrolyte in electrical double layer capacitor (EDLC) [175].

From impedance analysis the high rate of the EDLC has been observed, in terms of low reaction time (~791 ms), high terms of knee frequency (~58 Hz), and high pulse power (~16.4 $kWkg^{-1}$). The cyclic voltametric response indicated high scan rate of 1000 mV s^{-1}capacitive performance which additionally affirms the high rate execution of the EDLC.Up to ~ 3500 cycles after ~20% decrease in capacitance, EDLC offers almost stable performance, even though low specific energy of EDLC is observed (E max ~ 8.2 Wh kg^{-1}) .High power density is absorbed (P max > 4 kW kg^{-1}), during the early charging and discharging sequences [176, 177].

Large area 2D novel carbon nano-sheets have also been produced using the $Mg(OH)_2$ powders and thiocarbanilide as carbon precursor and template. To enhance the capacitive performance of supercapacitors, based on the cooperative effect,4-dihydroxyanthraquinone (DQ) and hydroquinone (HQ), viewed as effective double redox added substances have been joined into H_2SO_4 electrolyte and electrode carbon material [178,179].

Graphene-based all-solid-state supercapacitors are also been looked at thoroughly [180]. Fabricating flexible solid-state high performance supercapacitors with high volumetric and capability to store significant energy, extreme conductivity, long term stability and robust mechanical flexibility is a huge task. Different fabrication protocols are implied to achieve such flexible all solid state supercapacitors.

Using redox/ active electrodes, advancement in supercapacitive performance [181, 182] in conducting polymers have been observed in some interesting investigations recently. The performance of rGO-PMo 12 symmetric device [183] is improvised significantly through the inclusion of redox active species (hydroquinone) in gel-electrolyte. Using PVA-H_2SO_4 gel electrolyte a symmetric cell based on rGO-PW 12 electrodes was assembled which enhanced

the cell performance. Moreover, range of potential 1.6 V providing 1.05 mWh/cm^3 energy densitywas featured. PVA- H_2SO_4 gel electrolyte is enhanced using the redox-active (hydroquinone), which was employed to get the further advancement in electrochemical performance and ultra-high energy density. The energy density is found out to be 2.38 mWh/cm^3. Consequently, the double hybrid approach is ensured and the development of hybrid electrolyte (redox-active) based supercapacitors shows high performance and is found promising [184-188].

Other studies include the use of manganese dioxide (MnO_2) for its ease of availability, low cost, good stability and tunable capability [44-46]. Based on the mentioned capabilities of MnO_2 it is investigated as a workable catalyst, oxidizing agent and electrochemical capacitor material [189–193]. The textile industry uses dyes which is a major water pollutant with severe environmental issues [194-196].

Energy storage device integration is an area in which a lot of work needs to be done. Highly conductive textiles and single-walled carbon nanotube (SWNT) ink is used for "Dipping and drying" process, with sheet resistance less than 1 Ω/sq and conductivity of 125 S cm^{-1}. Strong adhesion between the textiles of interest and the SWNTs is observed under outstanding stretchability and flexibility. High specific energy and high areal capacitance up to $0.48F/cm^2$ were obtained while using these conductive textiles as supercapacitors. 24-fold increase of the areal capacitance is achieved by loading of pseudocapacitor materials into these conductive textiles. New design opportunities can be adopted for wearable electronics and energy storage applications by using these highly conductive textiles [197].

3.3 Choice of Electrode materials for Stretchable Supercapacitors

To date, three choices are considered for constructing stretchable supercacpacitors electrode materials, i.e conducting polymers, carbon, and metal oxides based electrode materials [198]. All these materials have their own advantages and disadvantages. Metallic materials have

low capacitance but they have high intrinsic conductivity, which enhance the charge/discharge speed but usually; carbon-based materials often have limited conductivity and material processing but high capacitance due to high surface areas, conductive polymers conductivity is not ideal but they offer good mechanical flexibility [104,115,128]. Capacitance, charge discharge efficiency, power/energy density, electrochemical/mechanical stability and overall performance all depends on the electrode as it the most important part of Super capacitors [199]. If we need to build stretchable supercapaictor, so we need to build stretchable electrodes first, which requires novel structure designs and rational material selection. But while designing stretchable electrodes due to stiff nature of bulk metal materials, if we apply small deformation they lose their conductivity. Few more substrates are textiles, cellulose papers or carbon fibers which are not that much stretchable can also be used as substrate, by extrinsic structural design they can also be made stretchable[200]. Copper, gold, platinum or silver are more suitable candidates due for current collectors due to high conductivity. So keeping the context in view, metal nanostructured materials can find a way around to the restriction by making twisting structures or percolation networks that are either embedded or put into a matrix of polymers [201]. Bulk carbon materials also faces same challenges, and hence, nanocarbon materials have been investigated intensively for flexible current collectors i.e. carbon nanotubes (CNTs) and graphene [202].

For stretchable electrode designs Materials based on carbon and their composites like CNTs, graphene with different forms are mostly used. Stretchable supercapcitor system use these carbon based materials as electro-active materials and current. They have benefits like low densities, large surface area with high mechanical strength leading to high stability [203].

For stretchable designs CNTs are widely used. Fig 3.1 (a) represents a buckled structured on PDMS. By transferring CNT films on to the buckled structure PDMS films and applying strain, the strechability is attaned due to wavy or buckled structure as shown in Fig 3.1 (b)

[204]. It can bear strain of 120% with no change in electrochemical properties and achieve a capacitance of 48 F g^{-1}. Capacitance can be further increased up to 308.4 F g^{-1} and 100% strechability can be achieved by electrodepositing conductive polymer like PANI (polyaniline) on CNT film as shown in Fig 3.1 (c) [205]. CNT fibers were also used as stretchable electrodes. CNT Fibers were twisted and glued them under 100% pre-strain on a PDMS-coated spandex fiber, by releasing the strain fabricated stretchable wire-shaped supercapacitors were formed as shown in Fig 3.1(d) [206].

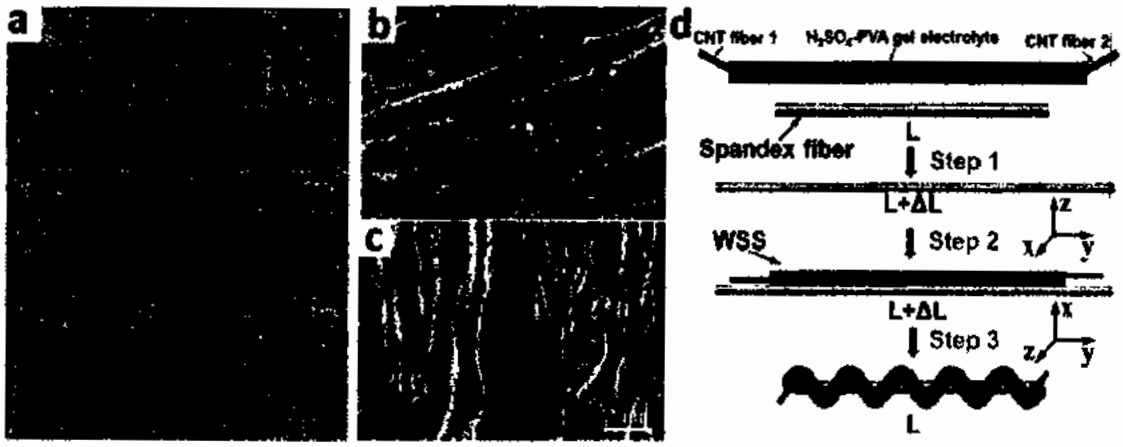

Fig. 3.1: (a) fabrication of buckled SWCNT film on PDMS (b) Buckled SWCNT film [204]. (c) Crumbled CNT/PANI composite [205]. (d) Stretchable wire shaped supercapacitor fabrication procedures [206]

For fabrication of stretchable eletrcrodes, graphene has also been widely used. High optical transparency and 40% strechability was achieved when synthesized multilayer with high stretchable sheets of graphene on copper foil having wrinkle structured and deposited onto a PDMS substrate [207]. Metal materials are widely used to their high conductivity for current collectors nowadays. Elastomeric PDMS surfaces and porous alumina oxide substrates on which self-assembled plasma treated gold nanowire membranes could be transferred to build stretchable and transparent EDLCs [208].

It was also reported that Silver nanowire (AgNW) networks are used as electrodes composed implanted in a polyurethane acrylate (PUA) matrix [209].Iron and Nickel as the negative

electrode and positive electrode were electro-coated separately on AgNWs to get a transparent Ag–Ni NWs(+)//Ag–Fe NWs(-) asymmetric supercapacitor with 35% stretchability and 1.7 V wide potential range. Strechabilty up to 40% can be achieved by using the plain weaving technique in which conductive stainless filter meshes woven from 50 mm wires. Electro-deposition of these meshes can be done easily on other active materials [210]. To fabricate a 100% stretchable asymmetric supercapacitor and having a wide voltage range, CNT films electrodeposited with MnO_2 and Fe_2O_3 respectively to pre-strained PDMS substrates [211].

Stretchable electrodes can be built, combining the CNTs with MoS_2 (molybdenum disulfide) by dip-coating on the CNT/PDMS composite film of a hydrothermally synthesized MoS_2 nanosheet solution [212]. In Fig 3.2 (a), excellent pseudo capacitance with large surface area of MoS_2 nanosheets which shows high double-layer charge storage which can be stretched to 240% and have a volumetric specific capacitance of 13.16 $F.cm^{-3}$. In Fig 3.2 (b), nickel foam is used as a template and MoS_2 was grown in situ by chemical vapor deposition, between the surface located inside graphene foam and holes [213]. 100% strechcabilty and a volumetric specific capacitance of 19.44 F cm^{-3} was achieved, when PDMS was used as a substrate on which compact graphene/MoS_2 composite films were transferred. In Fig. 3.2 c–e, 100% strechabilty and wide voltage range was achieved to build an asymmetric stretchable supercapacitor, when pre-strained PDMS is used as a substrate and CNT films electrodeposited with MnO_2 and Fe_2O_3, respectively [214].

Conducting polymers provide high conductivity of electrodes and deliver pseudo-capacitance due to redox reaction. High Conductivity, low cost, high porosity, capacitance and huge surface area are the major advantages. Polyaniline (PANi) [215], Polypyrrole (PPy) [216], polythiophene (PTh) [217] and PEDOT [218,219] have been commonly used in

supercapacitors. While using a conducting polymers as electrodes 100 to 300 $F.g^{-1}$ is recorded as the specific capacitance values.

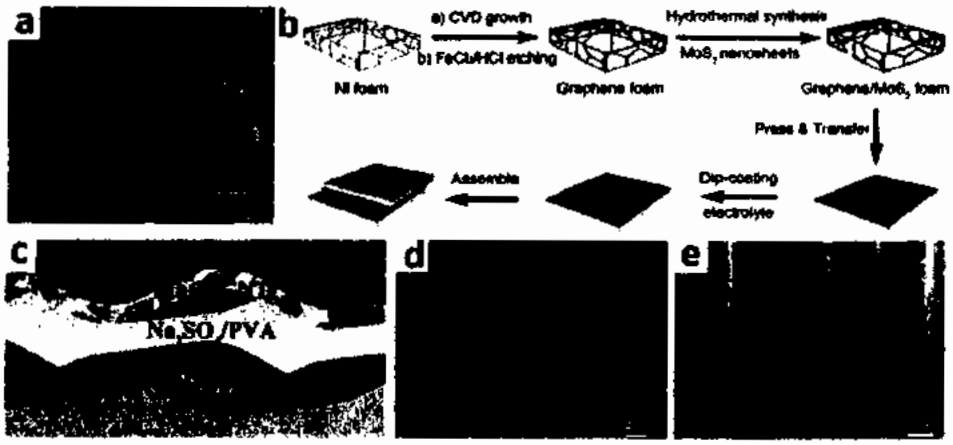

Fig. 3.2: (a) SEM image of MoS_2 nanosheets. (b) Fabrication of the stretchable supercapacitor based on composite films of graphene/MoS_2 [213] (c) asymmetric stretchable supercapacitor based on the wrinkled negative Fe_2O_3/CNT hybrid film electrode and positive MnO_2/CNT hybrid film electrode. (d and e) wrinkled Fe_2O_3/CNT and MnO_2/CNT hybrid films SEM images [214]

So far, only a few works have considered conducting polymers for stretchable supercapacitors, and only classical conducting polymers (e.g. polyaniline) have been used in some preliminary studies as shown in Fig 3.3 [220,221]. With the concept of combining conducting polymers, the design of device configuration would require new demands from novel key materials (that may even be evolved if necessary), in order to realize the development of polymer-based stretchable pseudocapacitors.

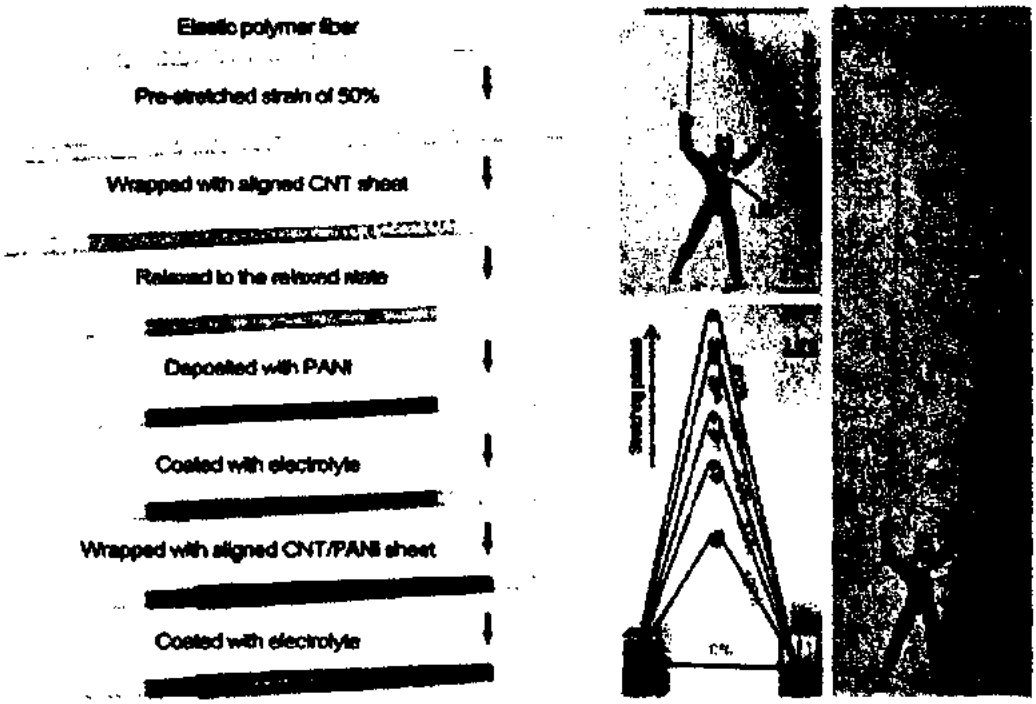

Fig. 3.3: Stretchable supercapacitors based on polyaniline [220,221]

All yarn based extremely stretchable knitting power textile with self-charging and washable property can be used for biomechanical energy harvesting. It can store energy by hybridizing supercapacitor and tribo-electrical nano-generator (TENG) into one fabric [222]. The power textile is recognized with high strechability, flexibility and elasticity due to which they can possess complex mechanical deformations, with the weft-knitting technique. Electrical energy can also be generated by using the knitting TENG fabric which can light up at least 124 light-emitting diodes with a maximum instantaneous peak power density of ~85 mW·m^{-2}. For wearable energy storage devices, due to good capacitance, excellent mechanically properties, light weight and long term stability all-solid-state symmetrical yarn SC is the best candidate. Wearable electronics can also be driving by assembled knitting power textile in which energy is formed by the movement of human body like a humidity meter or a calculator [223-226].

Mechanical deformation and unstable device structures during practical application results in less stability and reliability, thus self-heal ability and stretch ability must be considered during the fabrication of supercapacitors. Preparation of self-healable and highly stretchable electrodes is still a big challenge. For stretchable and self-healable supercapacitors, reduced graphene oxide fiber based springs can be used as electrodes. By visual inspection, the thick fiber spring having diameters of 295 μm reconnect the broken electrodes accurately. As show in Fig 3.4, a self-healable and stretchable supercapacitor is successfully realized, by wrapping self-healing polymer outer shell with fiber springs. After a large stretch (100%), the supercapacitor has about 82.4% capacitance retention and after the third heal the capacitance retention of 54.2% was achieved [227,228].

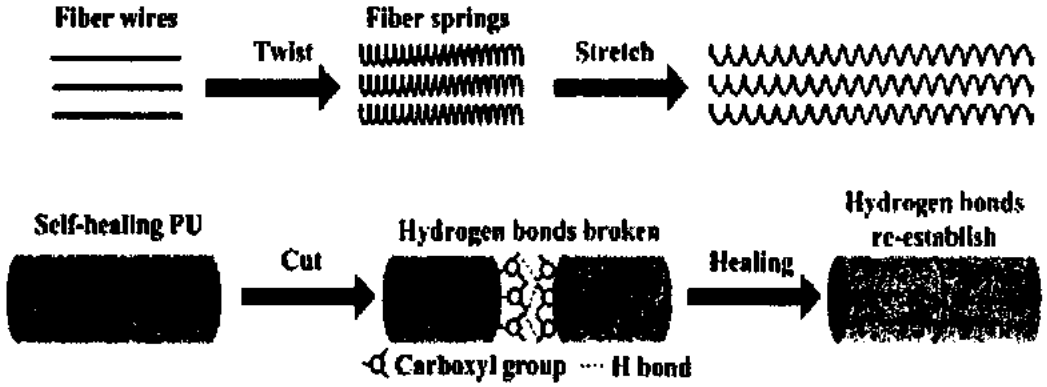

Fig 3.4: Highly Stretchable and Self-Healable Supercapacitor [228]

In general for stretchable supercapacitors, the overall electrode design is based on the electro-active material, current collectors and substrates [229]. At present for most stretchable electrodes, elastomeric polymers with intrinsic stretchability are used as a substrates [230]. Different type of stretchable electrodes can be made into thin films or fibers by PU (polyurethane), styrene–(ethylene–butylene)–styrene (SEBS) or Silicone rubber (Ecoflex), and PDMS (polydimethylsiloxane) [231].

3.4 Design strategies for stretchable supercapacitors

After considering the materials the other important parameter is the layout design of supercapacitor to achieve high flexibility. In stretchable supercapacitors the important thing to look after is the performance of electrode during charge discharge cycles, when mechanical deformation occurs [232-234]. The electrode always require high conductivity, even after deformation they need to maintain conductivity. So researchers worked on such techniques like prestraining then buckling, fiber winding and island-bridge with serpentine interconnection designs to achieve high performance of stretchable supercapacitor under mechanical deformation [235]. Layout designs can be categorized as (a) Linear Supercapacitors having one dimensional design, (b) Planar supercapcitors having two dimensional design, and (c) stereo supercapacitors having three dimensional design as shown in Fig 3.5.

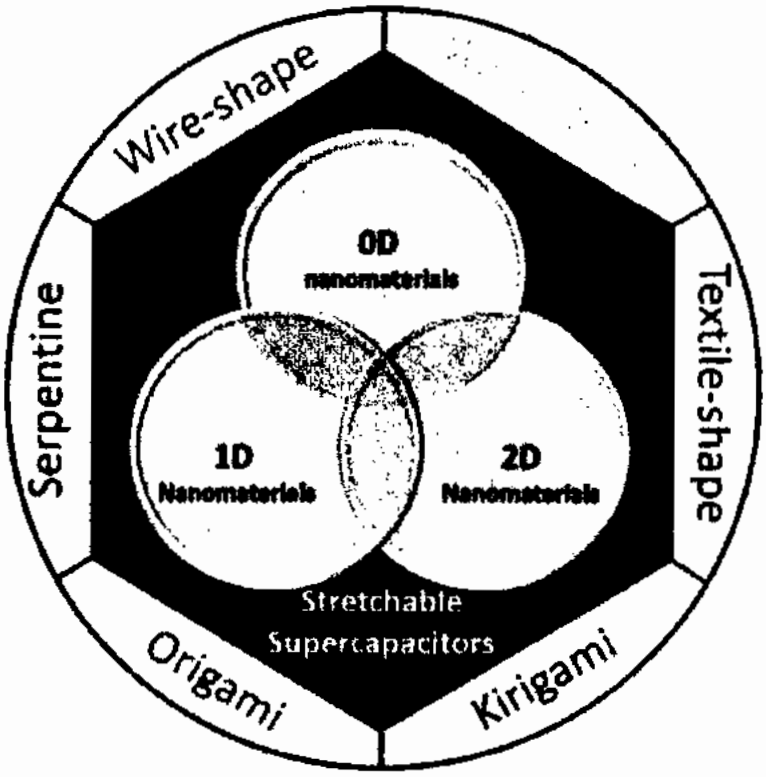

Fig 3.5: Design strategies for stretchable supercapacitors [235]

3.4.1 Linear Supercapacitors (one dimensional design)

In recent years a lot of work is done on one dimensional supercapacitor due to its excellent properties like planar supercapacitors, they can also be defined as wire, yarn shaped or fiber supercapacitor. Linear supercapacitors are used directly as electrodes or can be used as flexible substrates. They show properties like light weight, high aspect ratio and docile nature to be woven in textiles [236]. Linear supercapacitors have spinning and weaving property as compared to conventional sandwich structures, making it the best candidate for power sources for wearable electronics textiles. Extensive work is done on the development of linear fiber electrodes like polymer fibers [237-239], graphene fibers [240-241], carbon nanotube fibers [242-244] and composite fibers [245]. For enhanced functionality, nanomaterial's can be efficiently assembled into fibers, providing highly compatible technology thanks to the advances in nano-science [225].

Four types of one dimensional supercapacitors are reported in literature (a) twisted, (b) parallel (c) helix and (d) coaxial [200]. Parallel fiber structure one dimensional supercapacitors are achivied by depositing CNT sheets parallel on to ecoflex fiber(rectangular cross section and 300% pre-stained) opposite side, creating buckle structure as shown in Fig 3.6 (a). CNT fibers shows excellent mechanical stability and electrochemical properties even after applying enormous deformation including twisting, bending and stretching up to 200 % in every condition, hence can be used in application like woven gloves as shown in Fig 3.6 (b) [245,246].

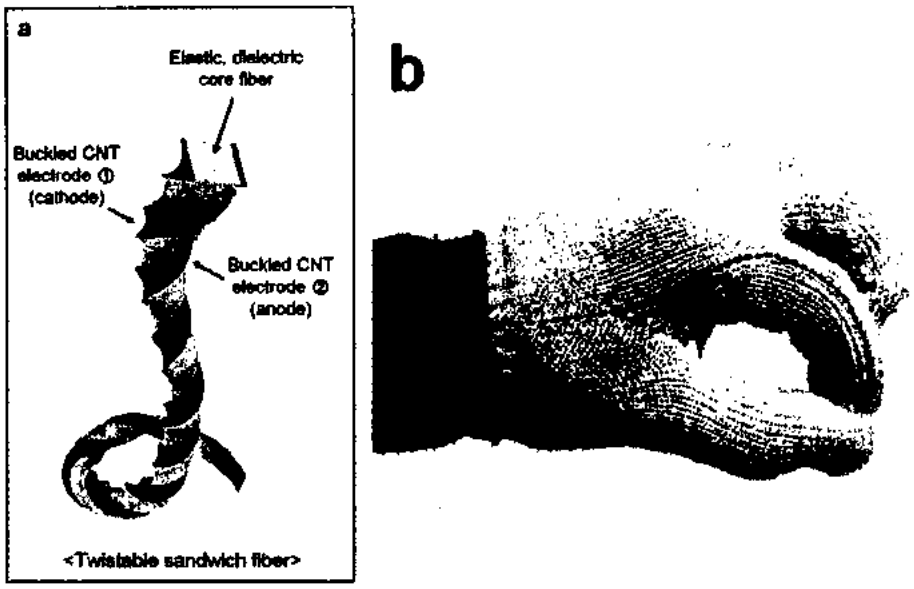

Fig 3.6: One dimensional Supercapacitor (a) Representation of a twisted sandwich fiber, (b) Commercial glove on 20 cm long sandwich fiber is woven [245]

CNT films in which conducting polymer PPy is electrodeposited can be wrapped into fibers and can be assembled on PDMS substrates and maintaining high mechanical strength with not losing properties after deformation [247]. Twisted configuration are also widely used in designing one dimensional supercapacitor. Twisted configuration can be flexible but due to their structure they cannot be stretchable [248,249]. CNT sheets can be overlapped and wrapped across elastic fibers to make twisted structure. PEDOT-PSS is coated on to that structure to enhance the performance and electrochemical properties. Two of these fibers are twisted and combined with each other with PVA/ H_3PO_4 hydrogel which is used as electrolyte to make a twisted supercapacitor. The obtained supercapacitor can retain its capacitance value of 30.7 F g^{-1} after applying a strain upto 350% [250]. The other type of one dimensional structure design is coaxial based supercapacitor. Elastic polymers fibers are used as starting substrate material. CNT sheets are rappeed around these elastic fibers and coating it with PVA/ H_3PO_4 hydrogel to make a coaxial based supercapacitor [251]. It can maintain its electrochemical properites like capacitance of 18 F.g^{-1} after 75% tensile strain. By electrodopisting PANI to this coaxial configuration can enhance the strechabilty to 400% and

capacitance to 111.6 $F.g^{-1}$ [252]. Last type of one dimensional supercapacitor is helix configuration. Helix configuration is achieved by using polymer cores on which fiber electrodes are wrapped. Many fiber electrodes are not stretchable, to make them stretchable helix configuration can be used which is basically spring like structure [253]. Twisted and helix desgnes are combined together to create ultra-stretchable supercapacitor [254]. Firstly fiber supercapacitors are constructed by twisting CNT, PANI and graphene wires. The obtained fiber supercapacitor can be coiled into spring like structure maintaining high mechanical stability and can sustain strain up to 800% and 138 F g^{-1} capacitance [255].

3.4.2 Planar Supercapacitors (Two dimensional design)

Two dimensional planar supercapacitors are widely studied for research and applications. First choice for planar supercapacitor are buckled and wavy structured electrodes over strained substrates [256]. Textiles and elastomers are used as stretchable substrate materials with deposition of carbon material and nanostructured metals. Nanoparticle of Vinyl hybrid silica and electrolyte of hydrogel are used to fabricate a planar supercapacitor with record 1500 % strechability [257]. Another planar buckle structure supercapactior was fabricated by attaching CNT film to pre-strained silicon rubber substrate to achieve 200% strechability while applying strain omnidirectional, biaxial or uniaxial. CNT and PEDOT films are also deposited on biaxially ecoflex substrates to make planar supercapacitor [258]. So many other supercapacitors are fabricated on the same design making this prestreching and buckling design most suitable for two dimensional planar supercapacitor [259-261]. Solid state flexible planar supercapactior can be fabricated by screen printing as shown in Fig 3.7(a) and it attain 80% of capacity retention after 1000 cycle and also the device can be bent up to a radius of 3.5 mm as shown in Fig 3.7 (b) [262]. Textile can be used as substrates for planar supercapacitor as it gives huge surface area and also having strechbale property. CNTs and MnO_2 nanoparticles are coated on cotton textiles for stretchable electrodes, they provide 20%

strechability [263]. Weft knitted structure of textiles are carbonized to obtained conductive textiles for planar supercapacitors. They as obtained supercapacitor can sustain strain up to 70% with high conductivity [264]. Laser induced graphene is also used for stretchable electrode and skinned off with PDMS on polyimide sheet [265]. Ultra-thin Gold nano wire is fabricated through Langmuir–Blodgett method. It is used to create a thin film and transferring that self-assembled conductive mono gold layer on to PDMS substrate to make a planar wrinkled structure of supercapacitora and it can maintain high conductivity under repeatedly stretching [211].

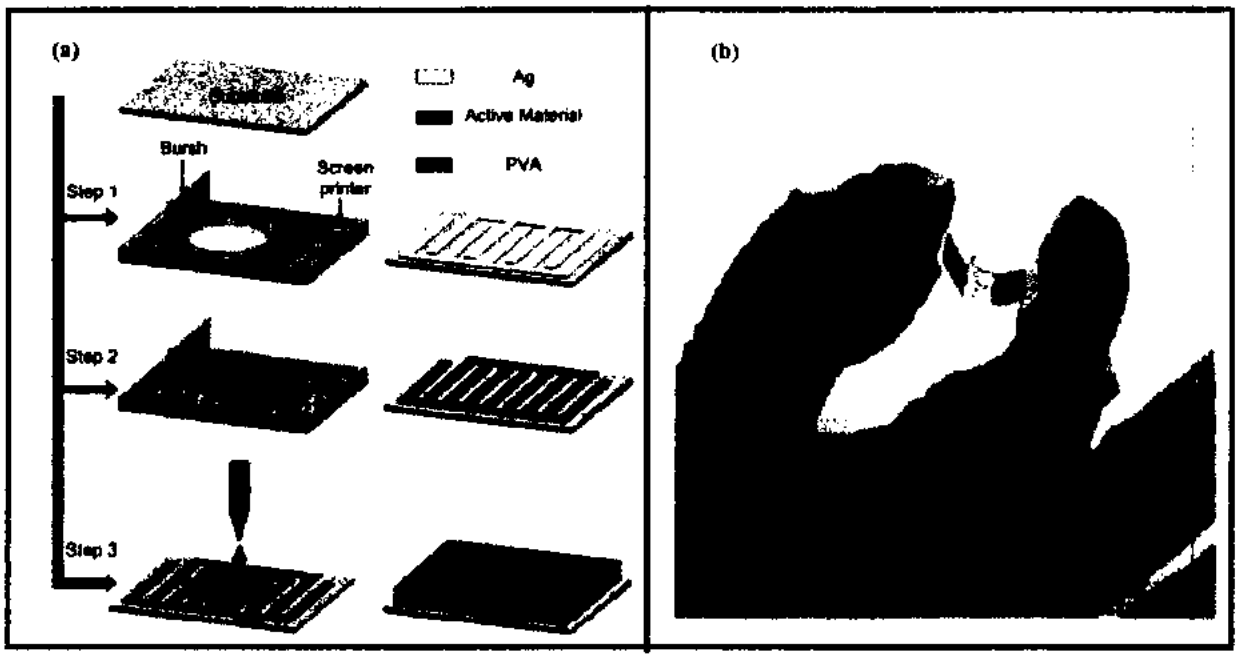

Fig 3.7: (a) Fabrication of all solid state planar two dimensional stretchable Supercapacitor (b) printed planar flexible supercapacitor on a PET substrate [262]

Micro-supercapacitors are the new type of planar supercapacitor emerged in past few years [266]. They don't need any separator, making it tiny size and thickness of system and making it best candidate for electronic units due to its ease of integration with system [267]. Island-bridge and serpentine interconnection are widely adopted for designing stretchable micro supercapacitor due to the fact that they can enhance mechanical strength and stability. Micro-supercapacitors can be isolated from the strains by placing it on to stretchable ecoflex as a

substrate and PET films implanted on them [268]. Tripod structure PDMS was also used for stretchable micro-supercapacitor configuration as a substrate. It is first stretched and then graphene oxide microribbons are transferred onto them and then released, providing suspended wavy structure as shown in Fig 3.8. This suspended wavy structure provide high mechanical strength and high stability under stretching and provide space to relive strain [269].

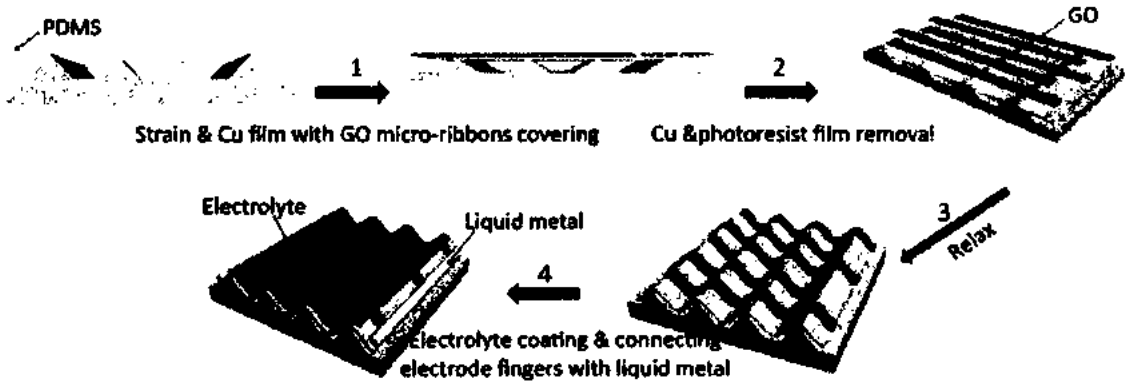

Fig 3.8: Fabrication of microsupercapacitor using Tripod structure PDMS [269]

3.4.3 Stereo Supercapacitors (Three dimensional design)

Three dimensional Stereo type supercapacitor also achieve strechability through kirigami or patterning type editable techniques. Honeycomb like stereo supercapacitor can be achieved by cutting linear patterns on fabricated planar (two dimensional) supercapacitor. The as achieved supercapacitor (made from kirigami based process) can sustain 400% strain with high conductivity and stability [270]. PANI was electrodeposited on cellular pattern CNT films which were produced by chemical vapor deposition on silica wafers with uniaxial strechability of 140% and can maintain capacitance of 42.4 $F.g^{-1}$. These cellular design stretchable supercapacitors can be connected in series or parallel to adjust current and voltage of supercapacitor. These cellular supercapacitor are used in commercial electronic watch and can be functioned as "watch strap". Fig 3.9 shows the structure and schematic of electronic

watch along with "watch strap" as stretchable supercapacitor. Watch strap" is at different places of arm i.e. wrist, middle and upper arm to power up the watch [271].

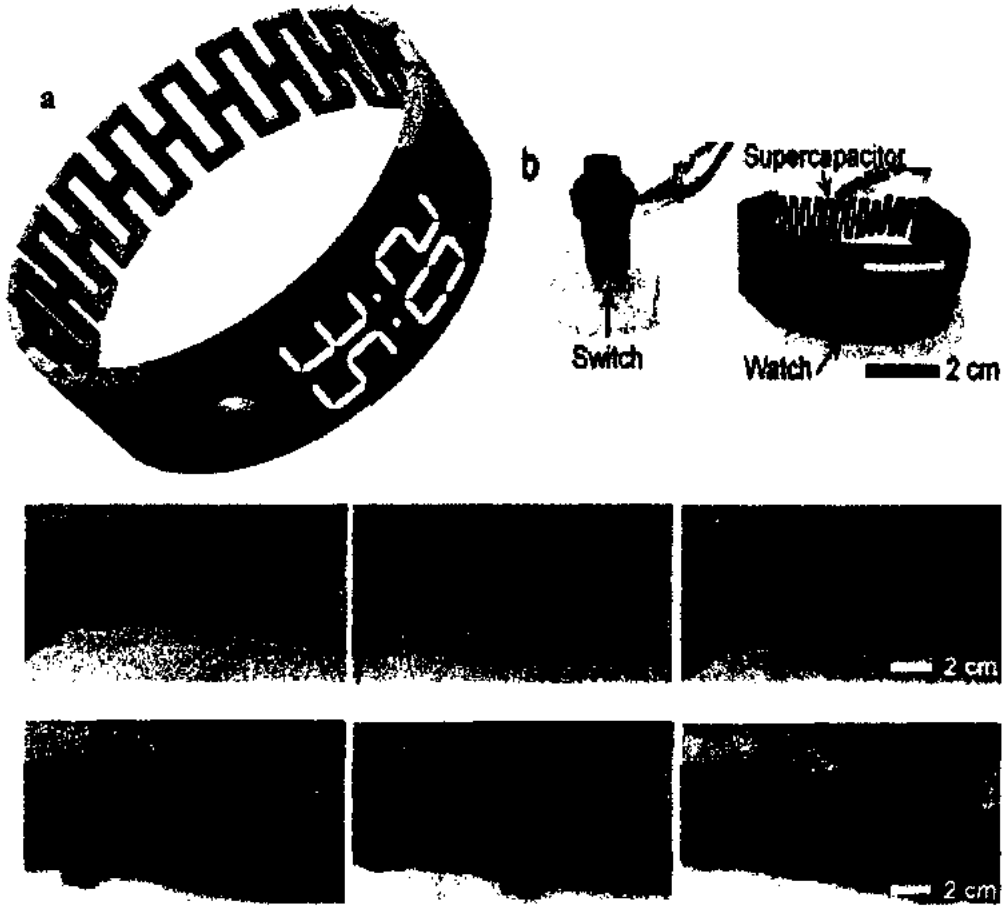

Fig 3.9: Powering electronic Watch (a) (b) structure and schematic of electronic watch along with "watch strap" as stretchable supercapacitor. (c)Watch strap" at different places of arm i.e. wrist, middle and upper arm (d) powering the watch at different places of arm i.e. wrist, middle and upper arm [271]

Origami type stretchable three dimensional supercapacitor are obtained by using graphite based isolated electrodes and are produced on a cellular paper substrate. Then sectionalized gel electrolyte was dropped on opposite side of substrate to combine electrodes and electrolyte together. This Origami type stretchable supercapacitor can have a good mechanical strength, it can withstand 30% stretch and 60% compression [272].

After the above discussion from literature on the design strategy, one can conclude that all these designs i.e. linear one dimensional design, planar two dimensional design, and stereo

three dimensional design, can achieve high strechability and can be used according to their application. Linear one dimensional supercapacitor can be sewed into textile and it can be used in daily using clothes. Planar two dimensional supercapacitor can be used for powering "tattoo like epidermal" devices, and stereo three dimensional supercapacitor are not appropriate for wearable electronics due to bulky nature [200].

3.5 Electrolytes for Supercapacitors

A lot of work is done on different type of electrolytes of supercapacitors. Electrolytes can be categorized into different types like organic electrolytes, ionic liquids, solid state polymer and aqueous electrolyte as explained in previous chapter. Organic electrolytes can be obtained by dissolving organic solvents in conducting salts which provide a voltage window of 3.5 V (as shown in Table 3.1), higher than aqueous electrolyte [273]. Organic electrolyte provides lower capacitance, high cost and less conductivity as well having few safety issues like toxicity, volatility and flammability. Tetraethylammonium tetrafluoroborate ($TEABF_4$) is salt used for organic electrolyte which is dissolved in propylene carbonate (PC) or acetonitrile solvent. PC based electrolytes are favored as compare to acetonitrile due to its environmental friendly nature and also due to having wide voltage range, good conductivity and wider working temperature [274]. As compared to organic electrolyte aqueous electrolyte provide higher conductivity of ions, low resistance and higher ionic concentration. Ionic conductivity of 1 mole of sulfuric acid (H_2SO_4) at room temperature is 0.8 S cm^{-1} and 6 mole of potassium hydroxide (KOH) conductivity is about 0.8 S cm^{-1} [275]. But these aqueous electrolyte show lower potential window (as shown in table 3.1, around 1 V) than organic electrolytes due to water decomposition. Ionic liquids are also widely used as electrolytes in recent years, due to high electrochemical and thermal stability, very low volatility and flammability, and wider voltage window of around 4.5 V. Ionic liquids which are flourine and solvent free pyrrolidinium dicyanamide are excellent to be employed as electrolytes

[276]. By adding a small amount of CNTs single wall can enhance cycling stability, capacitance and energy density [277].

Table 3.1: Electrolytes with voltage window

Electrolyte	Voltage Window	Ref.
$TEABF_4$/PC	3.5 V	[278]
Na_2SO_4	1.8 V	[279]
KOH	1.0 V	[279]
H_2SO_4	1.0 V	[279]
Li_2SO_4	2.2 V	[279]
PVA/H_3PO_4 hydrogel	0.8 V	[277]
Pyrrolidinium dicyanamide	2.6 V	[280]

Solid polymer electrolyte also shown a lot of progress in recent years due to high ion conductivity and can act as separator between the electrodes. Three most commonly used solid electrolytes are gel polymer, dry polymer and polyelectrolyte. Gel polymer electrolyte is extensively used among these three solid polymer electrolyte due to its high ion conductivity [281]. They can be used as plasticizer when water is used with gel polymer making hydrogel. They possess three dimensional network leading to many good properties like good hydrophilicity, easy preparation outstanding film-forming, low cost and non-toxic features. Widely used polymer matrix is poly- vinyl alcohol (PVA) which is mixed with water solution leading to high ionic conductivity [282-284]. Redox electrolytes are widely used to enhance the capacitance of pseudocapacitor. Extra capacitance can be added due to faradic reaction in electrolyte [285-287]. Pseudocapacitance was contributed mainly by electrodes but due to redox electrolyte they also contribute to redox reaction. Redox active

$CuCl_2$–HNO_3 electrolyte is used to enhance the capacitance up to 4700 F g^{-1}, 10 times more than conventional electrolyte [288].

Poly Vinyl Alcohol (PVA)-Electrolytes are widely used as electrolyte in various electrochemical devices due to their unique characteristics, i.e., good contact of electrolyte with electrode, lightweight, easily moldable and desirable solubility [289-291]. As compared to other polymer electrolytes, gel electrolytes have attracted more importance, due to high ionic conductivity [292-293]. Polymethylmethacrylate (PMMA), polyacrylonitrile (PAN), polyethylene oxide (PEO), and polyvinylidene fluoride (PVDF) are most favorite polymeric gel electrolytes [294-297]. PVA provides wide temperature window and good affinity to solvent holding. Gel electrolytes can be applied in solid state supercapacitors due to their excellent mechanical strength, ion migration rate, and high order of work durability due to high water retention [298]. Based on PVA matrix, aqueous form of gel electrolytes have also been used, (i.e. H_3PO_4- PVA, PVA/H_2SO_4, PVA/KOH, and PVA/LiCl), providing mechanical strength and wide range of acidity as shown in Fig 3.10 [299].

As compared to liquid electrolytes, gel electrolytes provide many advantages like flexible packaging, low internal corrosion, simple preparation techniques and being easy to handle. PVA/H_2SO_4 [300-303], PVA/H_3PO_4 [304-305], and PVA/KOH [306] have been widely studied and used as PVA based gel electrolyte for super-capacitors.

Carbon based supercapacitors, show high stability and high power density, but they are not suitable for applications requiring high energy density. Carbon material shows higher life time as compared to metal oxides and Conducting Polymers (CPs). While the conductivity of carbon and CPs is also very high as compared to metal oxides, these carbon materials show high chemical stability. CPs show high energy density as compared to carbon based materials. The efficiency of carbon based materials is greater than CPs due to their high

stability. CPs are preferred due to its high flexibility and can be used in flexible applications [39].

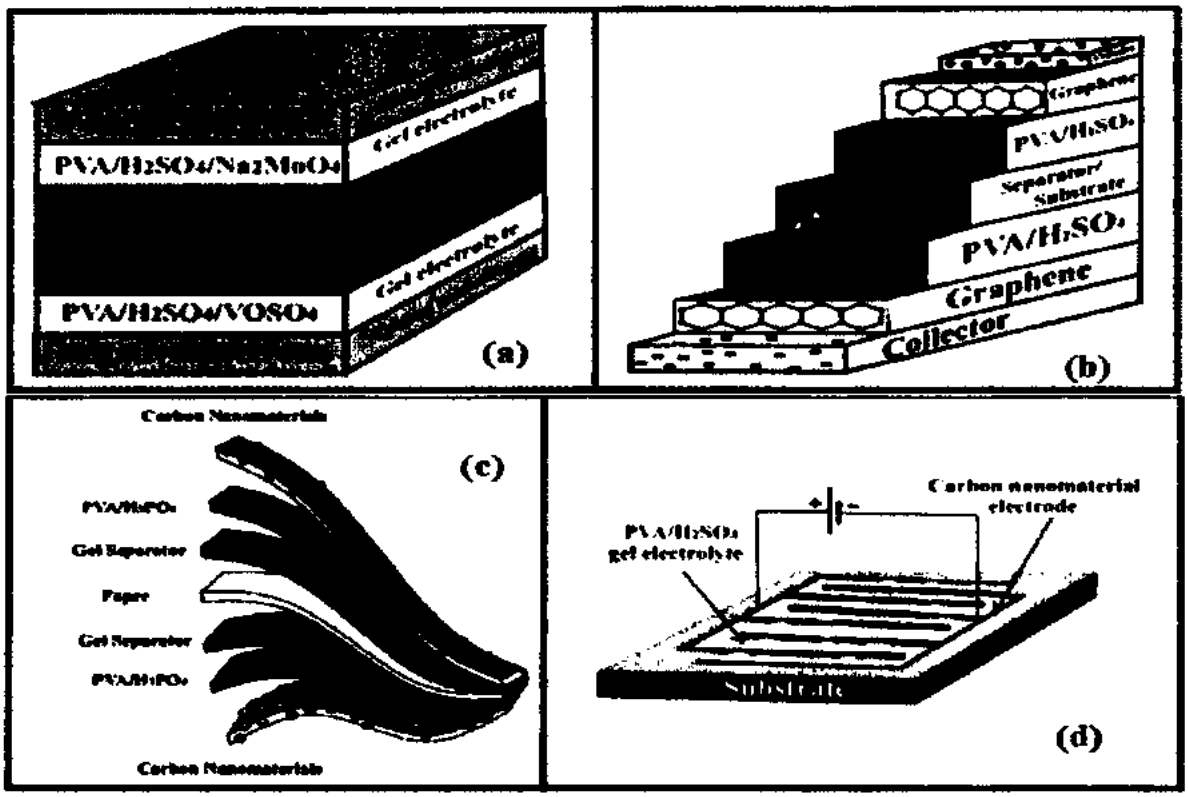

Fig 3.10: PVA based Supercapacitors (a) Schematic of a supercapacitor prepared by two different gel electrolytes (b) Schematic of a typical symmetric supercapacitor based on the graphene electrodes and PVA/H2SO4 gel electrolytes. (c) Schematic of a typical symmetric flexible paper supercapacitor based on the carbon nanomaterials electrodes and PVA/H3PO4 gel electrolytes (d) A typical micro-supercapacitor based on the carbon nanomaterials electrode and PVA/H2SO4 gel electrolyte [299]

3.6 Summary

Energy storage devices are required for the blooming mobile electronic devices market, renewable off-grid energy sources, electric vehicles and many other such technologies. Rechargeable batteries are preferred because of high energy density. The longer life time and higher power density of the supercapacitors make them better than the batteries. Even after a lot of effort done on energy storage devices during past few years, there are still some fundamental questions which needed to be answered to find solutions to increase specific energy density in these systems. The energy density debate has gradually become the rate-

determining step of developing processes in this field. As the market is progressing, portable, wearable and flexible electronic devices, the rapid development of flexible energy storage devices has undergone a lot of work. To date, three choices are considered for constructing stretchable supercacpacitors electrode materials, i.e conducting polymers, carbon, and metal oxides based electrode materials. The electrode always require high conductivity, even after deformation they need to maintain conductivity. So researchers worked on such techniques like prestraining then buckling, fiber winding and island-bridge with serpentine interconnection designs to achieve high performance of stretchable supercapacitor under mechanical deformation. Layout designs can be categorized as (a) Linear Supercapacitors having one dimensional design, (b) Planar supercapcitors having two dimensional design, and (c) stereo supercapacitors having three dimensional design. A lot of work is done on different type of electrolytes of supercapacitors. Electrolytes can be categorized into different types like organic electrolytes, ionic liquids, solid state polymer and aqueous electrolyte.

Chapter 4

Experimental Techniques

This section clarifies a portion of the key experimental techniques which are critical to investigate the scope of this work.

4.1 Device fabrication

Stretchable supercapacitors devices are fabricated by using spin coating and spray coating in our work.

4.1.1 Spin Coating

Spin coating is a technique used to uniformly deposit material onto the flat substrates [307]. The machine used to do spin coating is called as spin coater. The depositing material or coating material like in our case PEDOT: PSS is applied on to the substrate. The substrate is spin up and off at different speed by using centrifugal force to spread the coating material on to the substrate. Evaporation is done by rapid rotation, it remove high volatile components form the substrate. Spin coating is done in four steps, i.e. deposition, spin up, spin off, and evaporation as shown in Fig 4.1 [308].

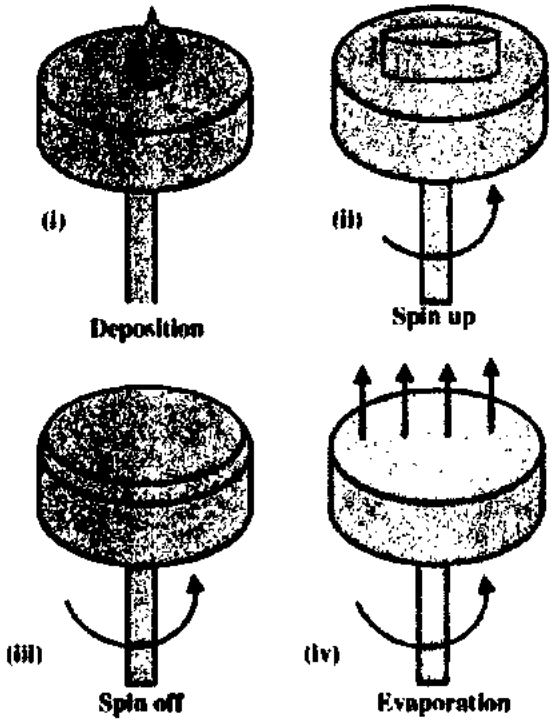

Fig 4.1: Four stages of spin coating [308]

Speed of rotation and viscosity of coating material determines the thickness of the deposited layer [309]. Spin coating has one major disadvantage as it depends on the size of the device. Spinning speed is difficult to control as the size become bigger [310]. In our case as the devices are small so uniform layers were obtained.

4.1.2 Spray Coating

Spray coating technique is used to coat the complex shaped polymeric substrates [311]. Nebulizers or atomizers are used for spray coating as they provide fine droplets. Carrier gas is given to the spray coater so that the fine droplets reach the coating chamber. These droplets are coated on to the substrate by electrostatic field or by gravity. By decreasing the atomic pressure or by increasing the viscosity of the solution can lead to higher size of the droplet. The size of the droplet determines the quality of coating. Spray coating is a fast process but it does not provide control on the uniform thickness of the layers on to the substrate [312]. Fig 4.2 shows schematic of the spray coating of CNT onto glass fiber fabrics and fabrication process [313].

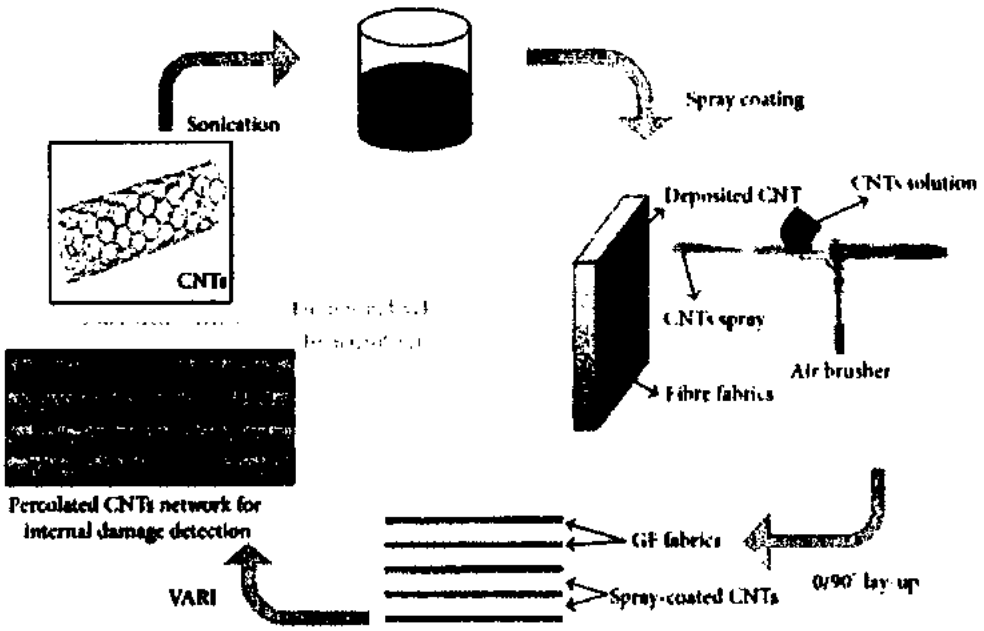

Fig 4.2: Schematic of the spray coating of CNT onto glass fiber fabrics and fabrication process [313]

4.2 Testing and Characterization of the fabricated device design

After device fabrication the testing and characterization can be done using different techniques. These techniques are explained below.

4.2.1 Nano chip reliability grade HALL effect system

Hall Effect is one of the primary and most important characterization technique used in the industry for electrical characterization for devices. The technique implies magnetic field on to a perpendicular suspended sample device placed in a calculated biased. Doing this a voltage is generated inside the device that is both perpendicular to the magnetic field and applied biased (current). Hall Effect measurement setup is shown in Fig 4.3 [314].

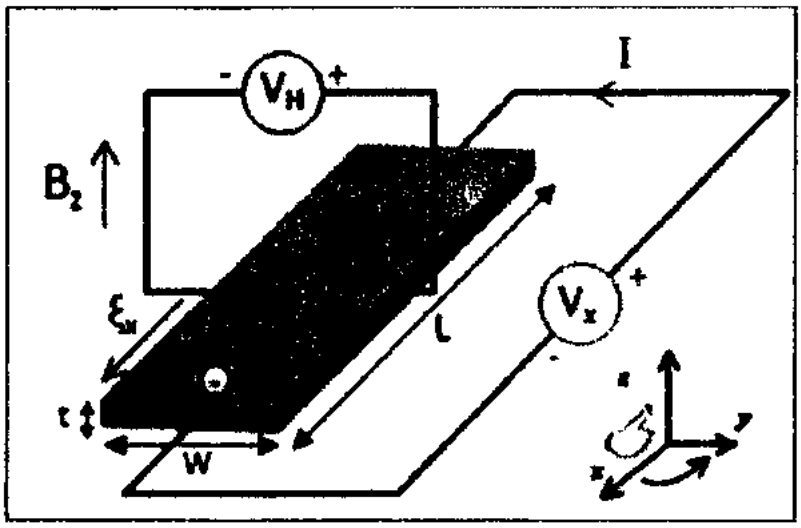

Fig 4.3: Hall Effect Measurement Setup [314]

This generating voltage is called hall voltage (V_H) is given by Equation 4.1.

$$V_H = \frac{IB}{qnd} \tag{4.1}$$

Where

d = sample thickness,

B = magnetic field strength,

q = charge on elementary particle,

n = bulk density, and I = current

Hall Effect working is based on Lorentz Principle which states that which is basically a combined effect of electric and magnetic field. Lorentz force F can be found as in equation 4.2

$$F = q\,(V \times B) \tag{4.2}$$

The technique gave us the important electrical perimeters like sheet resistance, mobility, and carrier type and carrier concentration.

Fig 4.4: Halls Effect Measurement Setup in CAEPE, IIUI.

4.2.2 ASMEC Electro-physical Characterization system

ASMEC is a powerful toll which is a consortium of many characterization techniques like Current-voltage Analysis, Charge deep level transient spectroscopy (QDLTS), and G-V Analysis. ASMEC has current sensitivity of 1pico Ampere, charge sensitivity is $5x10^{-16}$ C, voltage bias range from -13.5V to +13.5V, temperature range is from 77K to 500K and it can be extended further, and deep level concentration sensitivity of $5x10^{-7}$ cm^{-2}.

Fig 4.5: ASMEC Setup in CAEPE, IIUI.

4.2.2.1 Current-voltage Analysis

Current-voltage Analysis is done to accurately map the characterization and efficiency of the supper capacitors that helped in accessing the quality of the supper capacitor material and film. This is also important to see the impact of the contacts and the device assembly on to the performance [315]. Current voltage analysis relationship is given by equation 4.3

$$I = \frac{V}{R} \qquad (4.3)$$

Where I is current, V is voltage and R is resistance.

This technique is used to evaluate the effect of electric field with respect to the movement of charges. Different voltage levels are applied and accordingly current can be measured with respected to them, applied voltage can be either AC or DC depending on the requirement. Characterizations are performed using Current-Voltage (I-V) analysis with two probe technique using copper contacted anode-cathode. I-V tests are conducted at multiple ambient conditions to inspect the thermal stability and sustainability of the ultra-capacitor. I-V characteristics of suppercapacitor is found by connecting one probe to anode and other probe

to cathode of the supercapacitor. Applying voltage to the supercapaitor and measuring the current behavior during charging and discharging can tell us the performance of superacapaitor [316]. It also tells us how much current is flowing in supercapacitor so that we can use it for energy system application. I-V characteristics provide an indirect measure of charge-storage capability of the device. Fig 4.6 shows the I-V characteristic of Symmetric, asymmetric and hybrid supercapacitor [317].

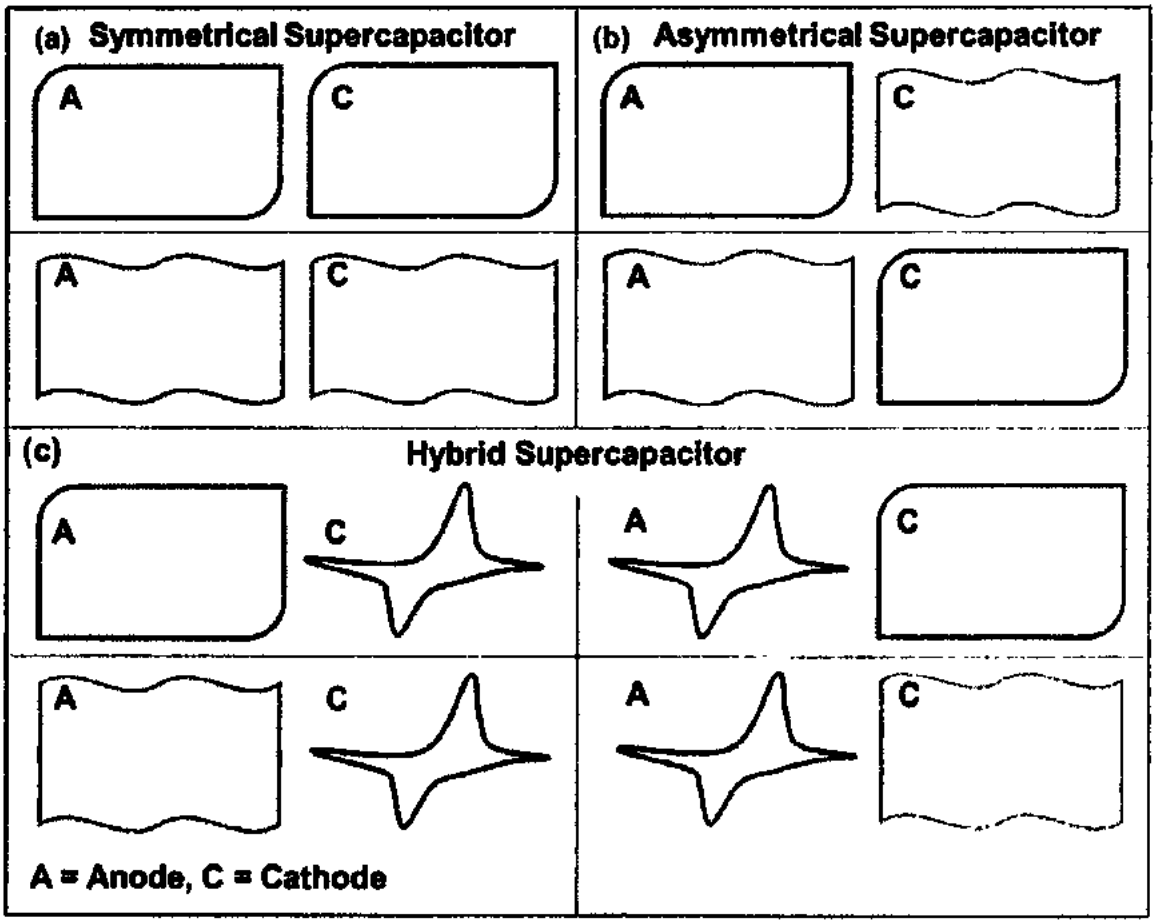

Fig 4.6: I-V characteristic of (a) Symmetric, (b) asymmetric and (c) hybrid supercapacitor [317]

4.2.2.2 Charge Deep Level Transient Spectroscopy (QDLTS)

QDLTS (Charge deep level transient spectroscopy) is used to access the performance of the device when placed in different temperatures and also the operating range at which the device

output parameters does not get too affected. Charge based Deep Level Transient Spectroscopy (Q-DLTS) technique [318] has been performed to better clarify the charging and discharging nature in the fabricated supercapacitors. Q-DLTS is used in organic materials to reduce the defect concentration. Current is applied to measure the trap defects. Q-DLTS is a charge relaxation technique based on the measurement of the transient analysis of the trapped charges produced from the interruption of given charging bias. The change in the charge magnitude (ΔQ) was recorded and plotted as a function of charge/discharge events with special expression of rate window during these interruptions. This is described as a function of times on which change in charge magnitude been recorded i.e. the charge/discharge time initially (t_1) and the final charge/discharge time (t_2). The minimizing the phase-assisted errors, times t_2 and t_1 should be perfectly matched at a certain proportion i.e. t_2/t_1=constant and this constant may further be related as 'α' i.e. $\alpha = t_2/t_1$=constant. For minimizing the errors, the discharging times would be properly proportional and the rate window (τ) for these events may be referred to as a function of these time-based events as reported [319], in Equation 4.4 as:

$$\tau = \frac{t_2 - t_1}{ln(\frac{t_2}{t_1})} = \frac{t_1(\alpha - 1)}{ln(\alpha)} \tag{4.4}$$

The charge magnitudes at these time intervals are recorded as:

$$Qt1 = Q_0 \exp(-e_n t_1) \tag{4.5}$$

$$Qt2 = Q_0 \exp(-e_n t_2) \tag{4.6}$$

And change in charge magnitude (ΔQ) will be related as:

$$\Delta Q = Q_{t2} - Q_{t1} \tag{4.7}$$

Where t_1 is charging time and t_2 is discharging times. Where $\Delta t = \Delta t_2 - \Delta t_1$ is the time window of the measurement [320].

Solving above equation i.e. Q_{t1} and Q_{t2}, the ΔQ will be related as:

$$\Delta Q = Q_0 \exp(-e_n t_2) - Q_0 exp(-e_n t_1) \quad (4.8)$$

And thus ΔQ may further related as:

$$\Delta Q = Q_0 [\exp(-e_n t_2) - exp(-e_n t_1)] \quad (4.9)$$

Electron emission rate 'e_n' is represented and related in equation 4.10 [310]:

$$e_n = \sigma T_n T^2 exp\left(-\frac{E_T}{kT}\right) \quad (4.10)$$

Where 'T' is the Temperature measured in Kelvin, 'σ' is the capture cross-section, 'K' is representing Boltzmann constant, 'E_T' is the Trap level Energy, and 'T_n' is defined as [321]:

$$T_n = 2(3)^{1/2} \left(\frac{2\pi}{h^2}\right)^{3/2} k^2 m_n \quad (4.11)$$

Where 'm_n' is effective mass of electron and 'h' is planck's constant.

Equation 4.12 is used to calculate the trap density 'N_T':

$$N_T = \frac{4\Delta Q_{max}}{qAd} \quad (4.12)$$

Where 'A' is contact area 'N_T' is Trap concentration, 'q' is absolute charge constant (i.e. =1.6x10^{-19}C), 'ΔQ' is change in charge magnitude, and the distance between two contacts is represented by 'd' The available 'space discharge states i.e. N_T' during discharge time may rise in accordance with the Equation 4.12 i.e. $N_T \, \alpha \, \Delta Q_{max}$ and $\Delta Q_{max} \alpha \, Temperature$. Fig 4.7 shows one of the graph of Charge based transient analysis of Ag/PTCDA 28 nm/ n-GaAs sample [322].

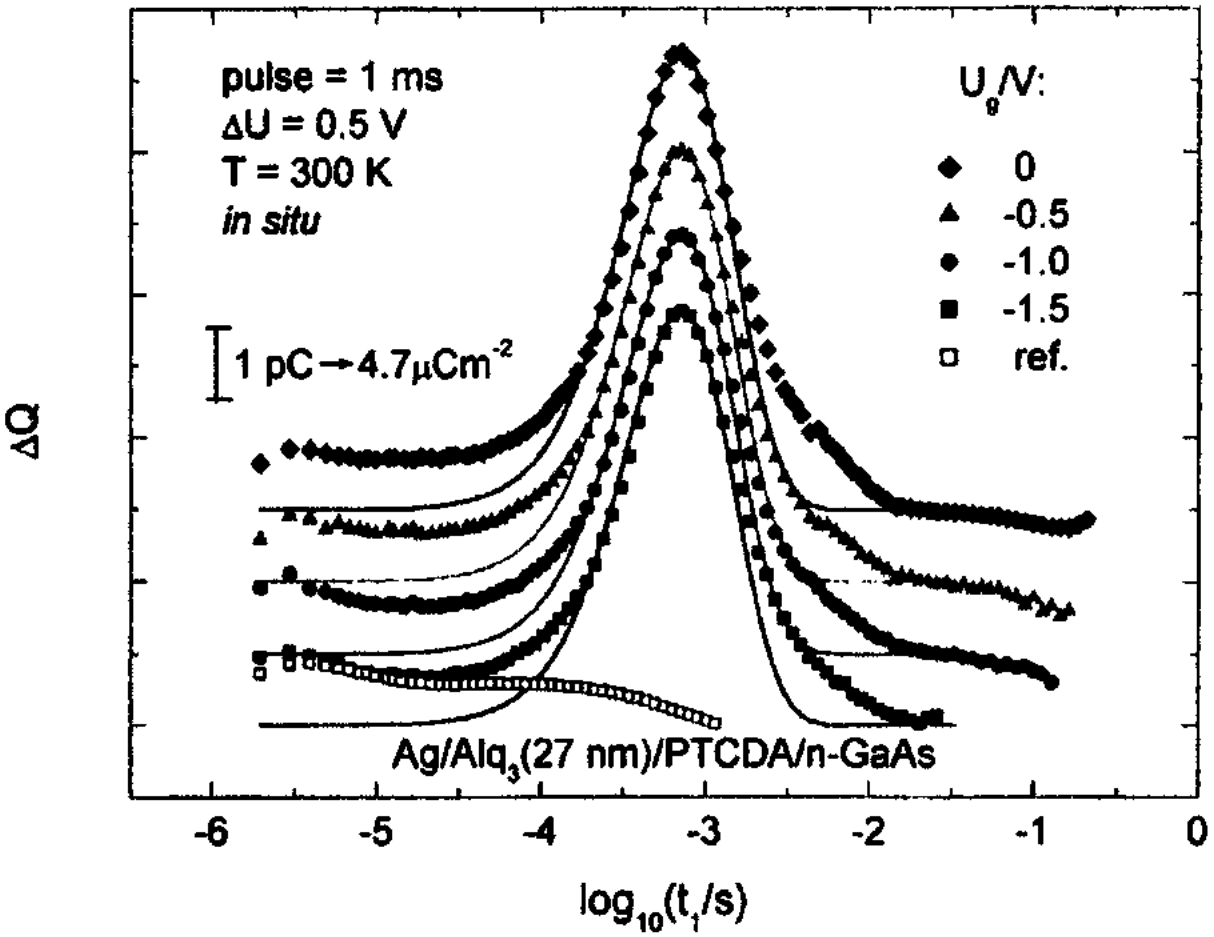

Fig 4.7: Charge based transient analysis of Ag/PTCDA 28 nm/ n-GaAs sample [322]

PIFTS (Photo-stimulated internal field transient spectroscopy) is additionally provided by ASMEC. It is used to see the impact of light on to the capacitive nature of the device. When light strikes the surface, it produces a charge that flows in the direction of the current. All of these techniques are required to accurately map the fabricated device parameters.

4.2.3 Arrhenius analysis

It is to be noted that Arrhenius equations plays a very vital role while defining the kinectics of photo current. It represents the dependency of the resistivity at specific temperature "ρ_s" of the material at wide band of temperature in terms of only two parameters i.e. resistivity at absolute temperature "ρ_0" and an exponential factor of activation energy "E_a" in electron volte by the following formula as below [319].

$$\rho S = \rho 0 \, e^{\frac{-Ea}{KT}} \qquad (4.13)$$

Where "K" is Boltzmann's constant, having value of 8.617 x 10^{-5} eV/K and "T" is the temperature in Kelvin.

As we have

$$\rho = \frac{1}{\sigma} \text{ mho/m} \tag{4.14}$$

Here σ is the conductivity of the material. Now replacing 4.14 in 4.13 we get:

$$\frac{1}{\sigma s} = \frac{1}{\sigma 0} e^{\frac{-Ea}{KT}} \tag{4.15}$$

After rearranging the equation 4.15 becomes

$$\sigma s = \sigma 0 e^{\frac{-Ea}{KT}} \tag{4.16}$$

Now taking natural log of both sides and re-arranging equation 4.16, we get

$$\text{Ln}(\sigma s) = \frac{-Ea}{KT} + \text{Ln}(\sigma 0) \tag{4.17}$$

$$\text{Ln}(\sigma s) = \frac{-Ea}{K1000}\left(\frac{1000}{T}\right) + \text{Ln}(\sigma 0) \tag{4.18}$$

As we know the equation of straight line is y = mx +c, where "m= slope" and c = y- intercept". Comparing 4.18 with equation of straight line we get

$$\text{Slop} = m = \frac{-Ea}{K1000} \quad \text{and} \quad \text{y- intercept} = \text{Ln}(\sigma 0) \tag{4.19}$$

Now we have to draw a new cartesian plane with 1000/T as x-axis and Ln (σs) as y-axis and thus calculate the Ln (σs) at multiple 1000/T i.e. x-axis. When we aligned multiple points with its linear fit. Its slope provides $\frac{-Ea}{K1000}$ value. From its slope, we can calculate the activation energy "E_a". This is the energy that is provided by the trains of incident photons whose energy/ wave length lies in the visible range of electromagnetic spectrum.

4.2.4 Electrochemical Impedance Spectroscopy (EIS) analysis

Electrochemical Impedance Spectroscopy (EIS), is used to calculate the impedance of the devices and materials used. It works on two modes i.e. potentiostatic mode and galvanostatic [323]. Current is varied and voltage is kept constant to obtain Nyquist and Bode plot. While

in galvonstatic mode the opposite happened, current is kept constant and voltage is varied to obtain the plots. Nyquist plot gives graph of real impedance with respect to negative imaginary part of impedance. Bode plot gives graph between phase-shift with respect to frequency [324]. Both modes gives almost same results depending on the application i.e. potentionstatic mode is used for high resistance materials and devices and galvanostatic mode is used for low impedance materials and devices. Electrochemical Impedance Spectroscopy (EIS), is also presented for the evaluation of supercapacitors. The EIS based Nyquist (Real Z vs Imaginary Z), and Bode (frequency-dependent impedance and phase) plot are considered to be important measure to describe the internal electrical metrology of the supercapacitors when treated under two probe analysis. Working/Sense Electrode and Counter/Reference electrode are connected in such a way that working and sense are connected together and treated as "Anode electrode", whereas, counter and Reference electrode as "Cathode electrode" [325].

EIS consists of imposing a time harmonic oscillating electric potential ψs(t) of small oscillation amplitude (e.g., less than 10 mV) around a time-independent "DC potential" at the electrode surfaces and measuring the resulting harmonic current density $j_s(t)$. Using complex notations, the imposed electric potential ψs(t) and the resulting current density $j_{s(t)}$ can be expressed as

$$\psi s = \psi dc + \psi o\, e^{i2\pi ft} \qquad (4.20)$$

$$js = jdc + jo\, e^{i[2\pi ft - \Phi(f)]} \qquad (4.21)$$

Where ψ_0 is the amplitude of the oscillating potential at frequency f, ψ_{dc} is the time-independent DC potential, j_0 is the amplitude of the oscillating current density, j_{dc} is the time-independent DC current density, and ϕ(f) is the frequency-dependent phase angle between the imposed potential ψs(t) and the measured current density js(t). Then, the electrochemical impedance Z can be defined as

$$Z = \frac{\psi s(t) - \psi dc}{js(t) - jdc} = \frac{\psi o}{jo} e^{i\Phi} = Z_{re} + I\, Z_{im} \qquad (4.22)$$

Where, Z_{re} and Z_{im} (expressed in Ω m^2) are the real and imaginary parts of the complex impedance, respectively [326-328]. Fig 4.8(a) Nyquist plot and 4.8(b) shows bode plot of flexible 3D graphane based supercapacitor [329]

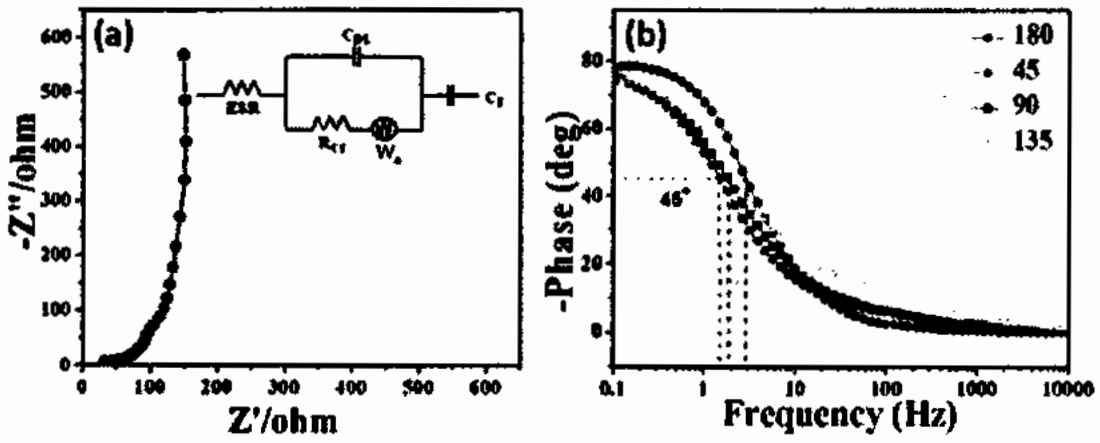

Fig 4.8: EIS analysis of flexible grapheme based supercapacitor (a) Nyquist plot (b) Bode Plot [329]

Fig 4.9: EIS setup in CAEPE, IIUI

4.2.5 Photo-Luminance System

Photoluminescence is a process in which a molecule absorbs a photon in the visible region, exciting one of its electrons to a higher electronic excited state, and then radiates a photon as the electron returns to a lower energy state. Photo luminance spectroscopy is a contact less and nondestructive method of probing the electronic structure of materials. This technique uses laser to calculate the electro-optical parameters of the device. The laser irradiate the sample surface and the resultant changes in the device dynamics are recorded. The results are coupled with the information gauged from variety of structural and microscopy techniques for material level testing for the evaluation of design parameters. Photo excitation causes electronics within the material to move into permissible excited states. When these electrons return to their equilibrium states, the excess energy is released and may include the emission of light (a radiative process) or may not (a non radiative process) as shown in Fig 4.10 [330]. The energy of the emitted light (photoluminescence) relates to the difference in energy levels between the two electron states involved in the transition between the excited state and the equilibrium state. Each Photoluminescence substance has its own excitation and emission spectra. The intensity of the Photoluminescence is proportional to its absorption, which in turn is proportional to the excitation light. The Photoluminescence emission of a substance is always at a higher wavelength than the light used to excite the substance (Stokes-shift phenomenon). The Photoluminescence of a substance is sensitive to many factors and will change or even disappear under different conditions. Photoluminescence intensity, Excitation spectra, Emission spectra, Photoluminescence lifetime, Anisotropy & Polarization, Time-based Photoluminescence intensity, and Time-based Photoluminescence lifetime are measured using photoluminace system [331].

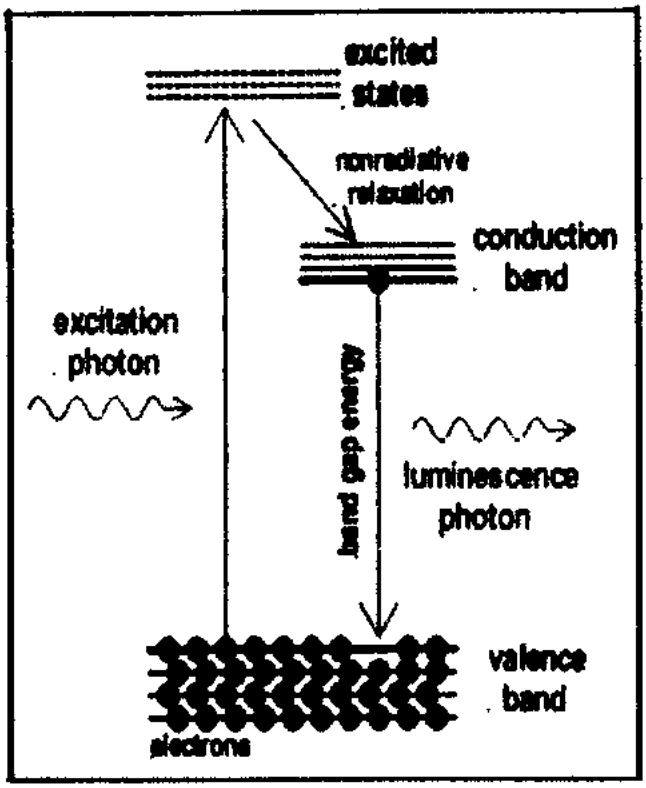

Fig 4.10: Principle of Photoluminescence Spectroscopy [330]

4.2.6 Hot Plate Magnetic Stirrer

Hot plate magnetic stirrer is used to keep the liquid circulating with heating capability to obtain homogenous mixture. It is a simple laboratory equipment and increases the speed, reliability and safety for reactions. It includes a hot plate and magnetic stirrer as shown in Fig 4.11. It has dual control which allows the users to set stirring speed and set heat output independently. The Hot plate temperature can be varied up to 550 °C. The magnetic stirrer consists of a rotating or stationary magnet whose speed can be adjusted from zero to 1500 rpm. Design of devices determines the nature and intensity of mixing. Magnetic stirring can be done with a chemical agent in closed or open system. Due to small size of stirring bar it is easily be cleaned and sterilized. They don't require any lubricants for cleaning which could contaminate the product or reaction. The devices is inserted in a liquid to spin very quickly to give homogenous mixture [332].

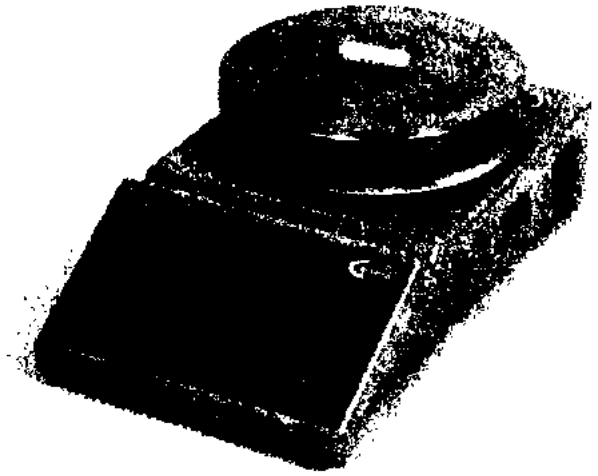

Fig 4.11: Hot plate and magnetic stirrer

4.2.7 Scanning Electron Microscopy (SEM)

Scanning electron Microscopy (SEM) is one of the most important instrument available for the investigation and analysis of the chemical composition and microstructure morphology of sample. Light microscopy has been, and continues to be, of great importance to scientific research. SEM is used to produce images of a sample using electron beams on the surface of the sample. Surface composition and topography is obtained by the interaction of electronic beams with the sample surface giving signals that contain information. It is effective for analyzing organic and inorganic materials on micrometer and nanometer scale. The magnification of SEM reaches to 300,000x and even above than that in modern models. The SEM machine use the High energy electron beam as a probe to image the surface morphology. The tungsten filament (Having diameter of 100 microns, 2700 K), acts as cathode, is used in electron gun for thermionic emission of high energy (30 keV, ~3 A) electron beam in vacuumed chamber. SEM machine has an electron gun which is a source to generate electrons, two or more electromagnetic lenses, scan coils for deflection, backscattered electron detector and secondary electron, sample chamber, Computer system along with display screens to view the scanned images and keyboard to control the electron

beam. SEM is a tool at which invisible worlds of microspace and nanospace can be seen. Details and complexity that is inaccessible by light microscopy can be revealed by SEM [333-335].

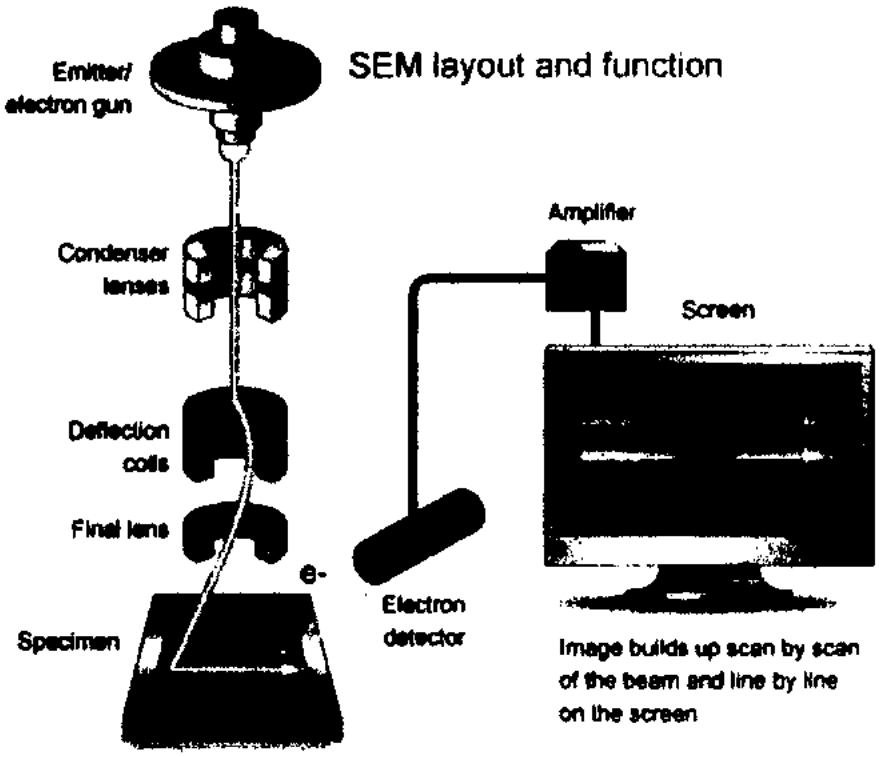

Fig 4.12: SEM layout [336]

4.2.8 Energy Dispersive Spectroscopy (EDS)

Energy Dispersive X-ray Spectroscopy (EDS) is used for the chemical and elemental analysis of a sample. Qualitative and semi quantitative results are obtained by using EDS along with SEM. X-rays are emitted when the electron beams emitted from the electron gun penetrates and interacts with volume beneath the surface of the sample, to characterize the elemental composition of the analyzed volume. It produces electromagnetic emission spectrum as each element has a different structure giving rise to unique set of peak [337]. EDS works on the principle of Moseley's law which gives direct correlation between atomic number of atom and frequency of light. At rest all electrons are unexcited and are in discrete electronic shells

bound to the nucleus. The electron beam is focused on the sample under test, that beam excite an electron in inner shell and ejecting it from that shell creating a hole. Higher energy outer electron then fills that hole of inner shell, making an energy difference leading to formation of X-ray [338].Both techniques EDS and SEM together give fundamental information on material composition which cannot be provided by any laboratory tests. Schematic diagram describing the EDS spectroscopy method is shown in Fig 4.13 [339]. The EDS detector takes the responsibility of separating the x-ray characteristic of various elements within the sample into energy spectrum. Then the spectrum will be analyzed by EDS system software to determine the amplitude of specific element (photon energy will be converted into electrical signals). Finally, the chemical composition maps of the elements can be determined both qualitatively and quantitatively.

4.2.9 Atomic Force Microscopy (AFM)

Atomic force microcopy AFM is a useful tool for measuring the micro-structural parameters and atomic resolution characterization at Nano scale. AFM can be operated in three open loop modes, i.e. tapping mode, contact mode, and non-contact mode. It provides additional advantage over other microscopic methods by providing reliable measurements at nanometer scale. AFM consists of micro-machined cantilever probe, Photo detector and sharp tip mounted to a Piezoelectric (PZT) actuator as shown in Fig 4.14. The photo detector is used to provide cantilever deflection feedback. The working principle of AFM is to scan the sample using the tip over the surface which enables the PZT to maintain the tip at constant height and constant force over the surface. The tip is used to scan the surface moving up and down and providing the measurements of difference in light intensities between the lower and upper photo detectors. The photodiode difference signal is controlled by computer, in constant force mode real time height deviation is monitored while in constant height mode, deflection force is recorded [341-343].

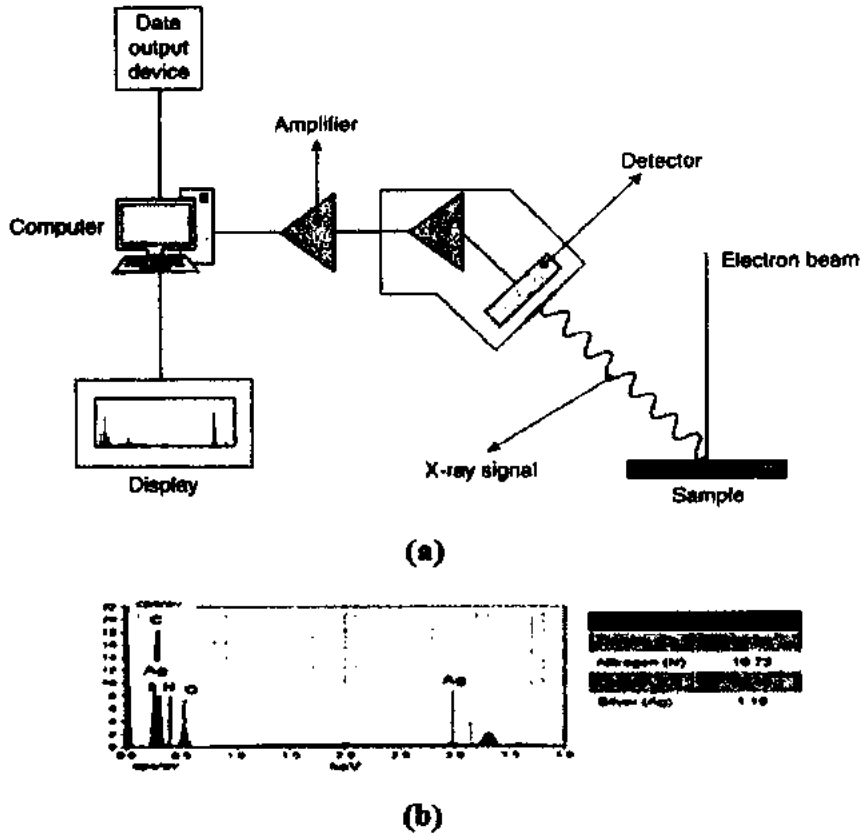

Fig 4.13: (a) Energy dispersive X-ray spectroscopy [339] (b) Elemental Composition mapping of sample analyzed via EDS [340]

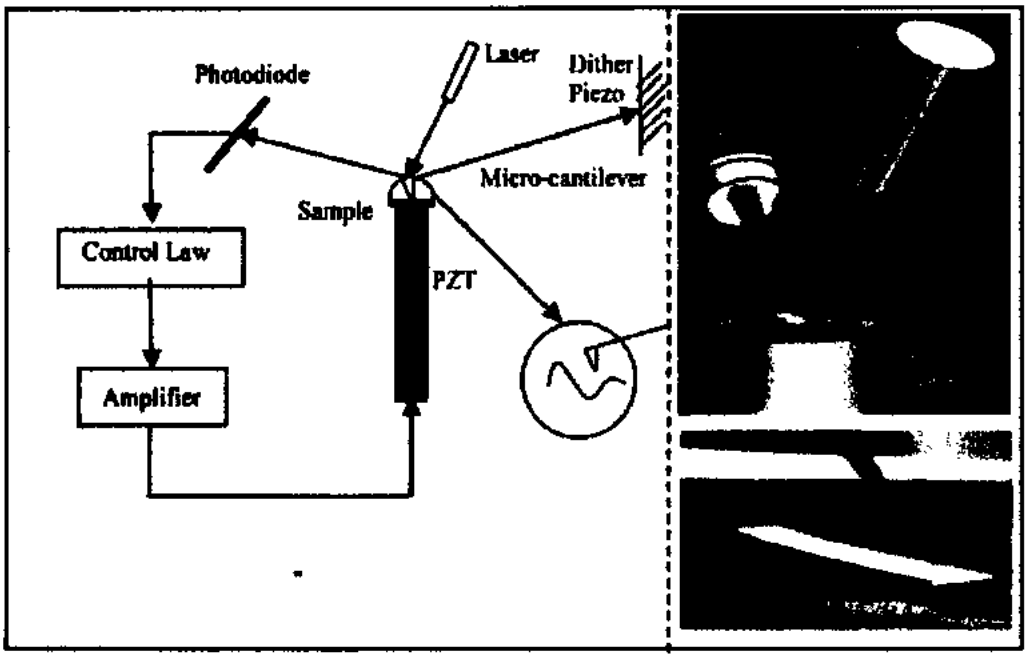

Fig 4.14: Schematic of basic AFM operation (left), real micro-cantilever and components (right) [340]

4.3 Precautions in Experimentation

The precaution regarding each respective experimental technique have been mentioned below.

Table 4.1 Precautions in Experimentation

Sr.No	Experimentation Technique	Precaution	Resolve
1.	Hall Effect System	Geometry of the sample	The geometry of the sample and the ohmic contact should be confined
2.	Automatic system for Material electro-physical characterization (ASMEC) System	Rare surface Physical contact	The rare surface of the sample should be physically adhere to enhance thermal conductivity and block electrical noises.
3.	Electro-chemical Impedance Spectroscopy (EIS)	Anode and Cathode contacts	The physical contacts of both anode and cathode should be properly contacted via standard clips.
4.	Photoluminance (PL) Spectroscopy	Light emission	In order to gauge the light emission after the absorption of laser radiation, the physical distance between the sample stage and the hieght of the assembly should be properly managed.
5.	Hot Plate and stirrer	High Temperature	The said machine contains high temperatures, to avoid any possible injury one should maintain a sutibale distance from the instrument.
6.	Scanning Electron Microscope (SEM)	High Voltage	The machine conatins high voltage assembly which can cause electric shock to its near permissive.
7.	Energy Dispersive Spectroscopy (EDS)	X-Ray Radiation	The equipment should be properly encapsulated in the led Cage.
8.	Atomic Force Microscopy (AFM)	Vibration	The instrument is highly sensitive to the vibrations, in order to gauge precise measurements the said instrument should be located onto the vibration free table.

4.4 Summary

Stretchable supercapacitors devices are fabricated by using spin coating and spray coating in our work. After device fabrication the testing and characterization can be done using different techniques like Nano chip reliability grade HALL effect system, ASMEC Electro-physical Characterization system, Electrochemical Impedance Spectroscopy (EIS) analysis, Photo-Luminance System, Hot Plate Magnetic Stirrer, Scanning Electron Microscopy (SEM), Energy Dispersive Spectroscopy (EDS) and Atomic Force Microscopy (AFM).

Chapter 5

Experiments, Results and Discussion

Four distinct approaches are used to conduct a systematic study on the fabrication and characterization of stretchable supercapacitors. One of the key findings have been published in Elsevier Journal of Energy Storage. However other work has been submitted in internationally renowned journal for the evaluation, also, the major findings have been submitted for National Patent Organization i.e. Intellectual Property Organization (IPO) of Pakistan. Experimental details, findings and discussion is presented in the following sections:

5.1 PEDOT:PSS based supercapacitor

Herein; a detailed account of an aged PEDOT:PSS based supercapacitor is presented in terms of Current-Voltage (I-V), Electrochemical Impedance Spectroscopy (EIS) and Charge Deep Level Transient Spectroscopy (Q-DLTS) measurements under 0.1-1V charging voltages at variable ambient temperatures. Evaluation of age-assisted defects and influence of temperature on the current kinetics of the supercapacitors is also presented with detailed reliability analysis for system level application of the fabricated device.

5.1.1 Experimental

Two Indium Tin Oxide (ITO) coated Glass strips were used as a starting material/substrate, as shown in Fig 5.1 (a). One side of ITO coated glass is conductive and optically transparent which could be tested using the short-circuit method through Digital Multi-Meter (DMM). ITO coated glass strips were cleaved into 1 inch x 1 inch structure and Copper tape is used to make ohmic contact on both strips at their edges to make anode and cathode. The PEDOT: PSS conducting polymer was spin-coated onto the both ITO coated cleaved glass strips. The

conducting side of the glass strips was caped using a specialized mask, so that the spin-coated material can be positioned at the desired space. Initially, the spin-coated material was in aqua phase, so to properly solidify this film, post-annealing was done using a hot plate at 85 °C for ~5 minutes to properly bind the material to the ITO surface as shown in Fig 5.1 (b). A liquid gel electrolyte of 1.2g of propylene carbonate, 1.2g of poly (ethylene glycol) diacrylate (Mn=700), 0.22g of trifluoto-methane-sulfonate, 3.5mg of 2,2-dimethoxy-2-phentlacetophenone (DMPAP) were mixed together and sonicated for ~1 hour; developed and published by our Chinese team [344]. After the process of PEDOT: PSS's annealing, this gel electrolyte was dropped at the center of one of the PEDOT:PSS's annealed films, and the ITO faced second strip was placed onto the gel to make a sandwich structure as shown in Fig 5.1 (c). After fabricating the supercapacitor, it was exposed by UV light for ~3 minutes to solidify the gel electrolyte from gel to solid as shown in Fig 5.1(d).

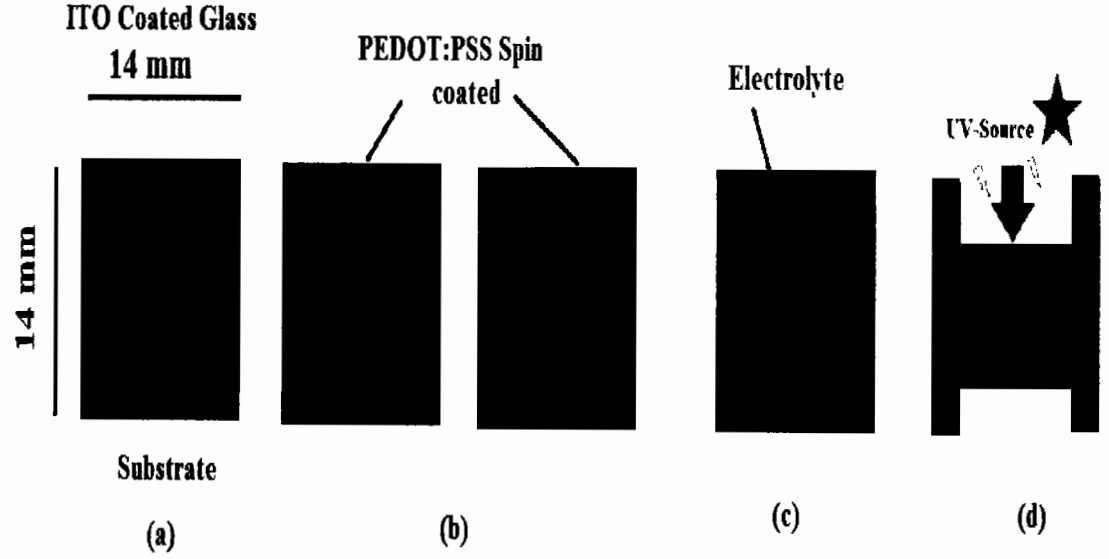

Fig 5.1: Fabrication of ITO Coated PEDOT: PSS based Supercapacitor:(a) ITO coated glass substrate, (b) Spin coated PEDOT:PSS onto the substrate , (c) drop casting of gel-electrolyte (d) U-V exposure to solidify the gel electrolyte

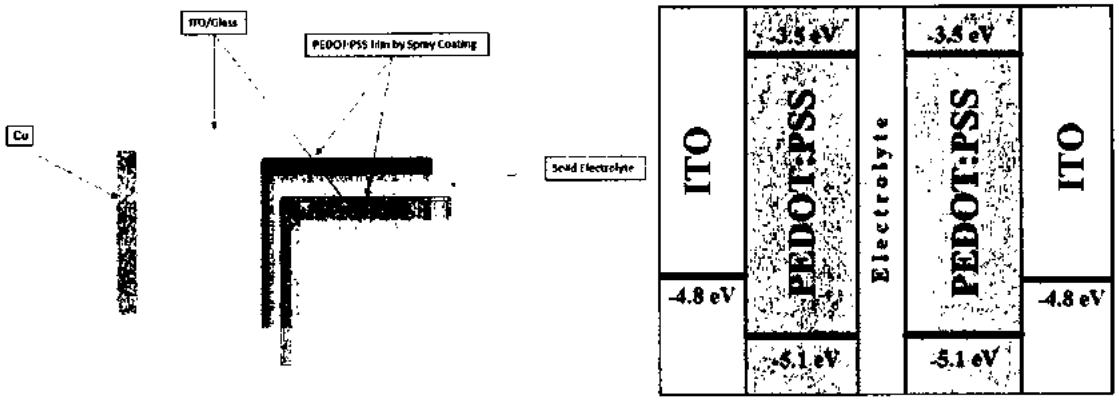

Fig 5.2: General schematic of PEDOT: PSS based Supercapacitor (a) layer-wise structure, (b) Energy band structure

As reference; the HOMO-LUMO of PEDOT: PSS was about -3.5 and -5.1 eV, respectively [345]. In order to understand the structure better for the follow-up characterization and analysis; the schematic and energy band diagram representation of ITO/PEDOT: PSS based supercapacitor is shown in Fig 5.2 (a) and (b).

5.1.2 Characterization

After physical growth of ITO/PEDOT:PSS/Electrolyte/PEDOT:PSS/ITO supercapacitor, the characterization of this device is done by Chinese team and published the initial results [344]. To specifically inspect the aging effect i.e. stability, quality and capacity of this supercapacitor, we have spanned this supercapacitor to age-out for ~120 days. After this time span; we inspected this supercapacitor with a variety of electrical and electro-chemical techniques including Charge-Deep Level Transient Spectroscopy (Q-DLTS) as rather newer method for the assessment of the supercapacitors. Q-DLTS is actually a charge relaxation technique already explained in previous chapter, which is used to study the physical defects of PEDOT: PSS's interface because PEDOT: PSS shows inhomogeneous electrical and morphological properties resulting in poor long-term stability and causes the limitation in its shelf-life [346]. Initially the PEDOT:PSS shows high conductivity but as the time elapses,

the conductivity magnitude decreases to its optimal limits. This is because of the "PSS" content i.e PEDOT part surrounded by a hydrophilic and insulating PSS rich shell in an aqua's dispersion [347]. Poor air ambient stability and the acidic nature of PEDT: PSS film, mainly due to water soluble ionic PSS, are significant hurdles which limit its performance on conductivity scales [348]. To enhance conductivity and stability of PEDOT:PSS films, various post treatment methods, such as annealing and solvent treatment with various chemicals have to be utilized to remove access PSS content which provides better performance of overall PEDOT:PSS films[349-350]. QDLTs technique has readily been adopted for diagnosing the organic material's defects [351]. Nguyen et al. has also reported that Q-DLTS is valid for evaluating the PEDOT: PSS based devices [352], to determine the trap defects. Thus, we have adopted this technique on the fabricated PEDOT: PSS based supercapacitor to evaluate the possible defects responsible for the device degradation. This is important as the charge storing capability may limit the PEDOT: PSS's shelf-life, owing the evolution of undesirable extent of trap centers within the interface [346]. The complexity of charging and discharging nature of any supercapacitor has still not properly been understood due to the complex nature of electrolytic behavior of monomers under charging and discharging mode of operation. In order to make an effort, we have utilized semiconductor's-based theory onto our subject supercapacitor. Literature [158], has suggested that for the charge flow in supercapacitors, a Randles cell of an equivalent circuit model is very popular for the ionic behavior at the electrolytic and PEDOT:PSS interface levels and is shown in Fig 2.11. Current-voltage (I-V) characteristics have been performed for gauging the charging current magnitudes with respect to the applied charging voltages. Kinetics of currents have also been gauged at different charging voltages in which detailed charging mechanism is envisaged using Equations 5.1 and 5.2. EIS study has been performed for same charging voltages to inspect the Bode and Nyquist nature of subject supercapacitors.

ASMEC system is used for mapping I-V, Q-DLTS and kinetics of current studies and BST8-STAT-EIS system is used for EIS measurements, are utilized in this work.

$$C = \frac{i}{\frac{dv}{dt}} \tag{5.1}$$

$$v_t = \frac{1}{C}\int_0^{10} i\,dt \tag{5.2}$$

Where, 'C' is capacitance, 'i' is electric current, 'v_t' is charging voltage.

5.1.2.1 Current Voltage (I-V) Analysis

After the physical growth of PEDOT: PSS based supercapacitor, Current-Voltage (I-V) analysis was performed on the devices using two probe method with copper contacted anode and cathode of the fabricated device. This analysis was done at multiple ambient conditions to inspect the thermal stability of the device and its sustainability. For this purpose, temperatures ranging from 26 °C to 86 °C were chosen with a step size of 10 °C. Electrical biasing for the evaluation of this technique was scanned from the ground (0V) to 5 volts. The voltage is applied and the current is recorded and plotted as a function of the dependent variable of voltages to inspect the bias dependent maximum charging current at which the supercapacitor shows saturation current. The extent of this saturation current is very important because of the charge storage capability (i.e. charging capability may limit at a particular level and the streaming charge from the charging source may get drained from the internal discharging resistor of the supercapacitor). This specific internal resistor is modeled as in a parallel combination with the charging capacitor. The graphical representation of I-V curves at multiple temperatures is shown in Fig 5.3. Most of the recent studies suggest that the internal temperature of the supercapacitor varies during the charging and discharging modes of operation [6]. In particular, for charging mode of operation, this temperature may rise rapidly [6]. In our study, we have increased the ambient temperature of the supercapacitor to inspect

the charging nature of the subject supercapacitor. The I-V characteristics provide an indirect measure of charge-storage capability of the device. The monomer-based electrolyte in our case provide substantially progressive trend for temperature ranging between 26°C to 36°C. If we further increase the temperature, the extent of charging current is seen to fall and get decreased to lower levels. This behavior is thought to be due to the internal chemistry of interfaces between the electrolyte and PEDOT: PSS layer. Fig 5.3 shows the electric current behavior as function of applied electric field and different ambient temperature. This spectra depicts that at rather higher temperatures i.e. >36°C, the charging current seems to decrease and reduces the charge collection mechanism of said supercapacitor.

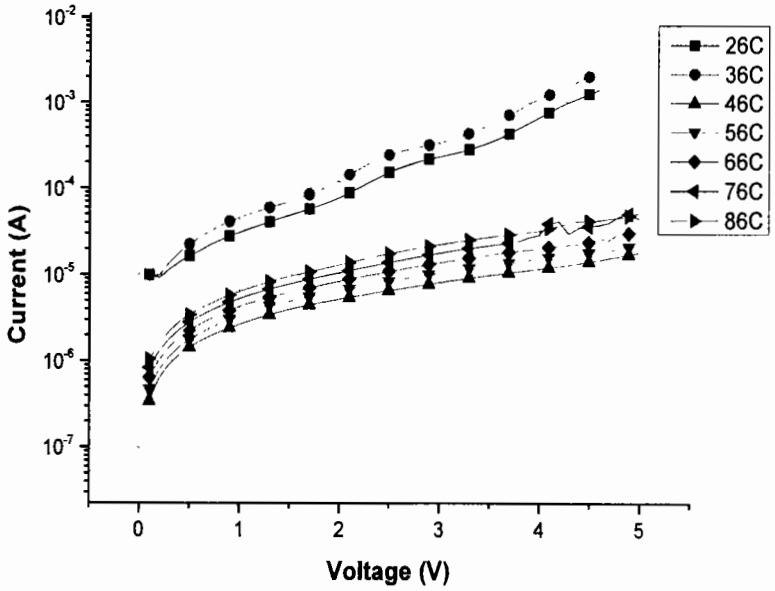

Fig 5.3: Current-Voltage characteristic of PEDOT:PSS based supercapacitor at variable temperatures.

5.1.2.2 Q-DLTS: Defect Analysis of PEDOT:PSS based Supercapacitor

Charge based Deep Level Transient Spectroscopy (Q-DLTS) technique [318] has been performed to better clarify the charging and discharging nature of the fabricated supercapacitors. The change in the charge magnitude (ΔQ) was recorded and plotted as a

function of charge/discharge events with special expression of rate window during these interruptions. To properly investigate the traps produced within the supercapacitor, one may apply the external charging bias, to charge the supercapacitor, at a specific level. When subject supercapacitor is fully charged at a certain bias level, followed by discharging events, these discharging levels decay exponentially at their respective ground levels (i.e. 0V) but during these events, the decay within the traps did not follow the normal exponential decay. These traps may discharge in another way as compared to the normal decay cycle and thus produce transients during the normal discharge (decay) cycle. During these discharge time intervals, which is expressed in the Equation 4.8 i.e. t_1 (initial discharge time) and t_2 (final discharge time), the change in charge magnitude is recorded and plotted as a function of rate window. In our study, the supercapacitor has been treated at 0V external bias and then 10mV charging bias has been applied for 10 milliseconds of charging time and then switched back to 0V. To practically charge these trap centers, these biases are applied within the band-gap of PEDOT:PSS. When the external bias is removed the charge magnitude decreases from +10mV to the ground state i.e. 0V. During these discharge events, the charge collected by the traps was released and recorded between respective time intervals as referred in equations 4.5 and 4.6.

$$\Rightarrow \quad Qt1 = Q_0 \exp(-e_n t_1) \qquad (4.5)$$

$$\Rightarrow \quad Qt2 = Q_0 \exp\left(-e_n t_2\right) \qquad (4.6)$$

Fig 5.4 Shows the Charge based transient analysis of PEDOT: PSS based supercapacitor at 26°C-66°C as a function of rate window 'τ'.

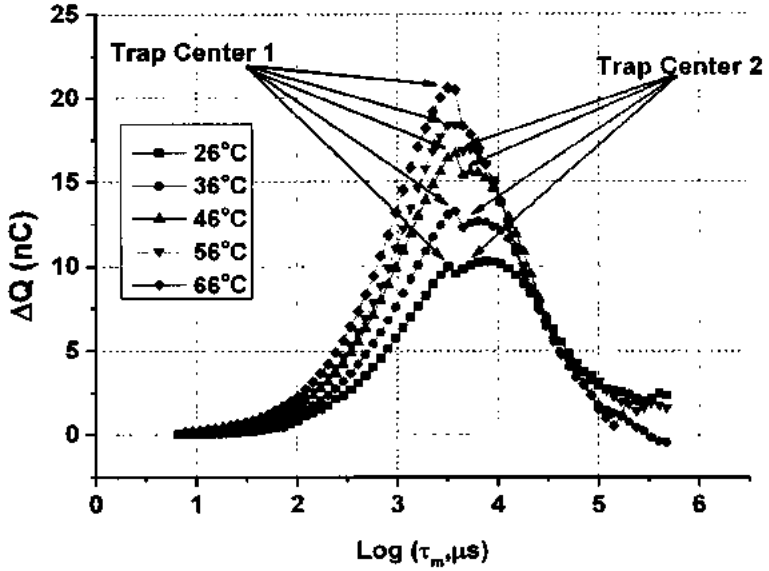

Fig 5.4: Charge based transient analysis of PEDOT:PSS based supercapacitor

As per equation 4.12, is used to calculate the trap density 'N_T':

$$\Rightarrow \qquad N_T = \frac{4\Delta Q_{max}}{qAd} \qquad (4.12)$$

Where 'A' is contact area (i.e. 14mm x 14mm = 196 mm^2) , 'N_T' is Trap concentration, 'q' is absolute charge constant (i.e. =1.6x10^{-19}C) , 'ΔQ' is change in charge magnitude, and the distance between two contacts is represented by 'd' i.e. separation between anode and cathode contacts of the device. Fig 5.4 shows the change in charge magnitudes as function of charge and discharge events. The peaks of these spectra provides the maximum native defects densities (and calculated from Equation 4.12) that may limit the Supercapacitor's operation. The peaks identified in these spectra may further contributes for the evaluation of Trap/Defect energies (i.e. the energy levels known as trap centers; within the band picture of PEDOT: PSS supercapacitors, and are responsible for the self-leakage of collected charge at the PEDOT: PSS's interface) and these trap energies are calculated from Equation 4.10. The trap levels may exist due to the formation of electronic defects which may cause recombination at the monomer-PEDOT: PSS interface and limits the overall functionality of

supercapacitor. Two peaks are observed in Fig 5.4, which indicates that two trap centers are imminent. The peak of the Q-DLTS signal may be defined as the maximum change in charge magnitude at a certain level for a particular rate window.

This may be noticed that, as the ambient temperature of the supercapacitor rises, the trap states also increase. This means that the available 'space discharge states i.e. N_T' during discharge time may rise in accordance with the Equation 4.12 i.e. $N_T \alpha \Delta Q_{max}$ and $\Delta Q_{max} \alpha Temperature$, and are reported in Table 5. 1. Thus, for increasing temperatures, the discharge states may rise which results in lesser time to store the effective charge within the PEDOT:PSS layer and thus decrease in current may be observed as shown in Fig 5.2.

Table 5.1: Surface Trap Densities of PEDOT: PSS based supercapacitor at multiple temperatures

Sr#	Temperature (°C)	N_T (cm^{-2}) Trap-1	N_T (cm^{-2}) Trap-2
01	26	1.25×10^{11}	1.30×10^{11}
02	36	1.65×10^{11}	1.61×10^{11}
03	46	2.08×10^{11}	1.99×10^{11}
04	56	2.31×10^{11}	2.17×10^{11}
05	66	2.60×10^{11}	----------

Fig 5.5 shows the Arrhenius analysis of Q-DLTS spectra using Equation 4.10 for the given temperature window.

$$\Rightarrow \; e_n = \sigma T_n T^2 exp\left(-\frac{E_T}{kT}\right)$$

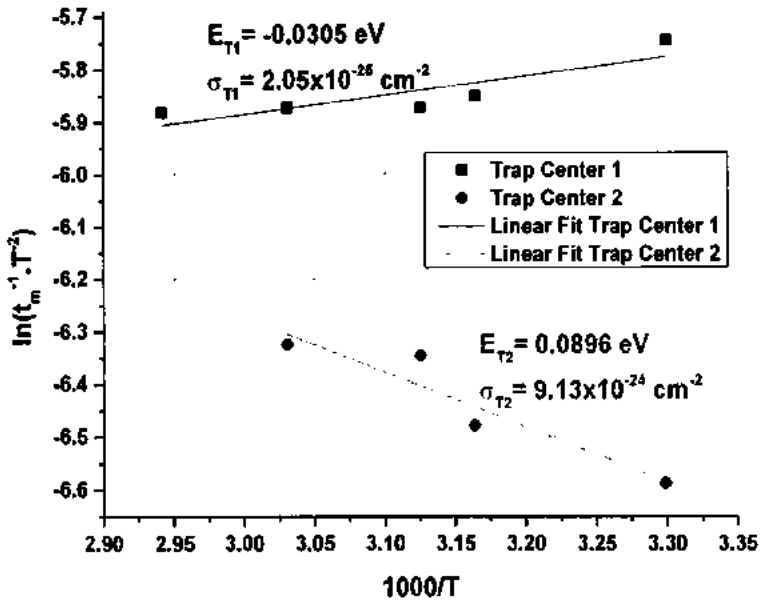

Fig 5.5: Arrhenius analysis of PEDOT:PSS based supercapacitor

We observe two trap centers from the Arrhenius analysis using Equation 4.12, as shown in Fig 5.5. Fig 5.5 represents the Arrhenius analysis of Fig 5.4. This is done from the linear approximation of Equation 4.10 i.e. straight line passing through each point. The line's slope is proportional to the subject supercapacitor's trap energy level and its y-intercept provides the capture cross-section magnitudes associated with subject trap level.

Arrhenius analysis shows that the two trap levels are populated within the energy band diagram and can be visualized in Fig 5.6:

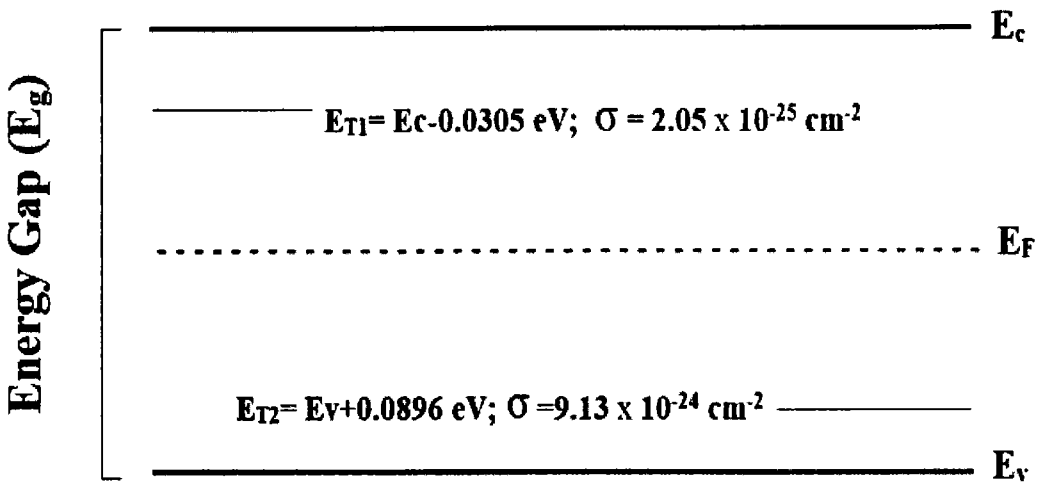

Fig 5.6: Visualized Trap levels within the energy band of PEDOT:PSS based supercapacitor

Fig 5.6 shows the trap levels within the energy band picture of PEDOT:PSS based supercapacitor. These levels may limits the supercapacitor's operation because the collected charge carriers may get trapped at these energy levels and recombine at their interface.

From Arrhenius analysis, there are two trap levels captured, thus, two associated capture cross-sections (σ) may be calculated from the linear approximation of Equation 4.10. Physically, the capture cross-section of a specific trap center is the ability of the trap center to capture the free charge carrier from its respective band edge. During charge time, the generation center (placed near the conduction band edge i.e. E_{T1}) may be activated, which may allow the larger ability to capture the free carrier from the charging source and during the discharge cycle, the recombination center (placed near the valence band edge i.e. E_{T2}) may contribute explicitly. The relatively larger capture cross-section near the valence band edge may cause larger leakage due to the recombination process irrespective of the parallel resistance model of a supercapacitor. The study presented in this work shows that during the discharge cycle, subject PEDOT: PSS based supercapacitor may cause larger recombination [353] and thus holds the captured charge from the charging source due to the self-recombination process and eventually may become connected with source for a small

duration to the active-load connected with the supercapacitor. One of the recent studies revealed that self- discharging resistor (parallel resistor of the equivalent model of the supercapacitor) may limit the load current duration during discharge cycle [354]. But in our study, this self-discharge mechanism may originate and caused from the recombination centers which may trap the charge carriers from their respective bands and recombine at their own interface rather than the load terminals.

5.1.2.3 EIS Analysis of PEDOT:PSS based Supercapacitor

For an ideal supercapacitor, series resistance (R_s) should approach to zero and Parallel resistance (R_p), to infinity. But for practical cases, these resistances may vary. Electrochemical Impedance Spectroscopy (EIS), has also been presented for the evaluation of supercapacitors. The EIS based Nyquist (Real Z vs Imaginary Z), and Bode (frequency-dependent impedance and phase) plot are considered to be important measure to describe the internal electrical metrology of the supercapacitors when treated under two probe analysis. Working/Sense Electrode and Counter/Reference electrode are connected in such a way that working and sense are connected together and treated as "Anode electrode", Whereas, Counter and Reference electrode as "Cathode electrode".

5.1.2.3.1 Nyquist Plot

The initial conditions for the said experiments were kept fixed i.e. pretreatment time= 5s, AC amplitude $0.1V_{ac}$, and the frequency window between 10 mHz – 10 kHz, followed by the different charging voltages ranging from $0.1\text{-}1V_{DC}$. For better clarity, we plotted two Nyquist plots with the same values but the only difference is the linear and log scaling which are shown in Figs 5.7 and 5.8, respectively.

The conductivity of commercially available PEDOT: PSS active layer was around 1 S/cm. From EIS analysis (shown in Fig. 5.7) the RESR is found to be around 400 ohms. This is

actually the resistance of PEDOT: PSS's active layer. Thus, the conductance magnitude may around 1/400=0.0025 S (mho). However, the conductance magnitude depreciated which results the degradation of charge storage capability of said supercapacitor.

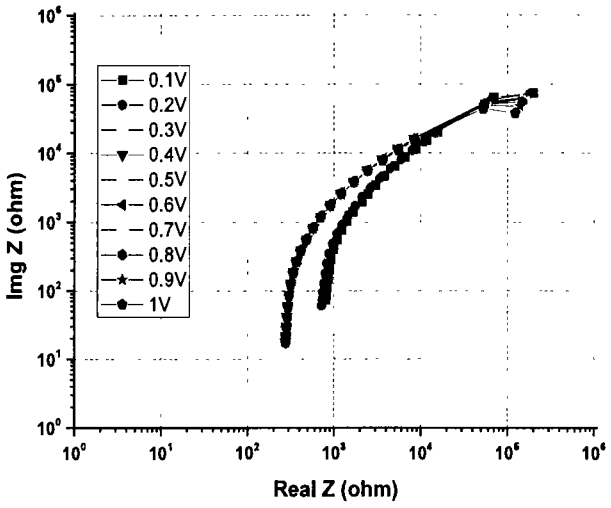

Fig 5.7: Logarithmic scaled Nyquist plot

Fig 5.7 shows the Nyquist plot, and from this Fig real-impedance (Re-Z) i.e. x-axis, provides the information about the integral part of passive components of Randles equivalent model (as shown in Fig 2.11) of said supercapacitor i.e. magnitudes of R_{ESR} and R_P may retrieved from said spectra.

The ESR values measured from Nyquist plot at 0.1V and 1V are 805.6 Ω and 274.1 Ω, respectively. The R_p values for all (ascending i.e. 0.1-1V) subject charging voltages are recorded as 2 $x10^5$, 1.82 $x10^5$, 1.57 $x10^5$,1.56 $x10^5$, 1.54 $x10^5$, 1.53 $x10^5$, 1.52 $x10^5$, 1.47 $x10^5$, 1.39 $x10^5$ and 1.23 $x10^5$ Ω, respectively. Fig 8 shows that by increasing the charging voltage, the parallel resistance of the supercapacitor may decrease. Meanwhile, ESR magnitudes may also get decreased.

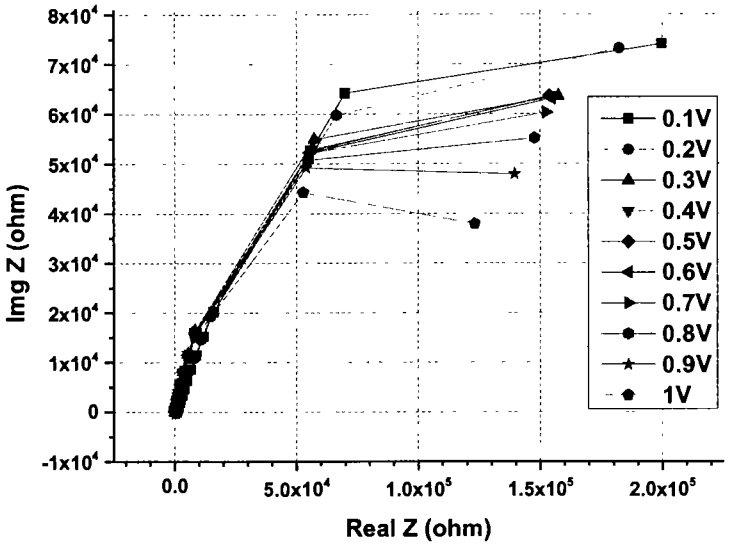

Fig 5.8: Normalize scaled Nyquist plot

These results reveal the pros and cons of subject resistances i.e. for better operable supercapacitor's, the R_p magnitude should be as high as possible and the value of ESR close to zero. However, by increasing the charging voltage, R_p tends to decrease gradually. This indicates that the self-discharging mechanism within the supercapacitor may dominate and this may be responsible for the shrinkage of the overall discharge time. For this study, one may tradeoff for selecting desirable charging bias for the viable operation of the supercapacitor. One can suggest that one may increase the charging voltage because this will lead to the lower ESR values, which is highly desirable for the quality operation of the device. We can ignore the effect of R_p for the selected charging biases. Because the extent of ESR for subject voltage's colonial order may decreases at larger extent as compared to R_p, thus, we can ignore the change of R_p magnitudes.

5.1.2.3.2 Bode Plot

The capacitive reactance of a capacitor is shown in equation 12 and can be measured from the Bode plot.

$$Xc = \frac{1}{2\pi fC} \qquad (5.3)$$

The Bode plot of the supercapacitor, under the same charging voltages, is shown in Fig 5.9. The impedance-based Bode plot is a signature for cross verifying the nature of Device Under Test (DUT). Fig 5.9 shows that by increasing the frequency, the impedance decreases and vice versa. For capacitors, the impedance shows the same trend i.e. the higher the frequency, the lower will be the impedance and vice versa. The R_p and R_s magnitudes can also be visualized from the lower and higher end of frequencies, respectively. This plot shows the same effect as Nyquist as depicted in Fig 5.7.

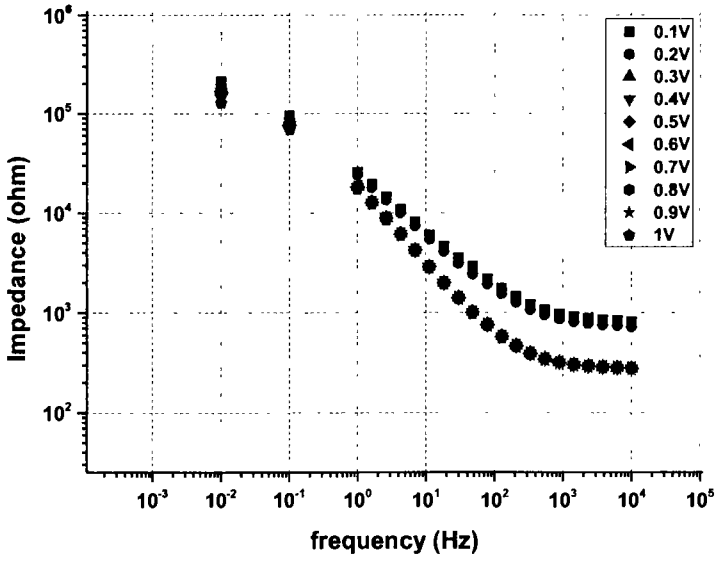

Fig 5.9: Impedance based Bode plot at multiple charging voltages

Fig 5.9 shows the impedance based Bode plot of said supercapacitor. This plot describes the overall impedance of subject supercapacitor with respect to applied frequencies and all spectra are collected at various charging bias conditions. From this analysis one can find real and imaginary impedance (resistance; *R*, reactance; *Xc*) response of the supercapacitor. This mimic behavior can be visualized from the applied frequencies because the passive

components may respond as open- or close; as function of applied frequencies e.g. at higher frequencies capacitors may like as short circuit and resistors may act as it is.

The phase difference based Bode plot of the supercapacitor, under the same charging voltages is shown in Fig 5.10. The graph is plotted to assess the charging phase operation. This phase magnitudes is the angle difference between the charging voltage and the current. For ideal supercapacitors, its magnitude must be at the phase difference of -90°. The negative sign indicates that the charging voltage is lagging behind the current by the 90° phase shift. The impedance-based spectra of bode plot decrease as a function of increasing frequency (as shown in Fig 5.9) while the phase based Bode spectra (as shown in Fig 5.10) decrease at some specific frequency and then increase in phase difference as observed. The specific frequency at which phase transition has occurred is known as critical frequency and this specific frequency is responsible where the maximum physical area of the supercapacitor may be accessed [355]. In our case, the critical frequency magnitude is about 4Hz with the phase difference of about -68°. Thus, at this frequency maximum area of the supercapacitor may remain unutilized effectively. It is known form the fundamental concepts of the conventional capacitor that at higher and lower frequencies the impedance of the capacitor approaches to zero and infinity, respectively. Thus, at the higher end of frequency i.e. 10 kHz, the impedance of the fabricated supercapacitor decreases and will act as a short circuit. So that charge will readily flow through ESR and the phase angle approaches to zero. It is because the phase difference between current and voltage in a pure resistor is zero. However, at lower frequency i.e. 10 mHz, the impedance of the capacitor may become high enough to behave like an open circuit. Thus, at this frequency, the major charge will flow through R_p rather than ESR. So, at this frequency, R_p will contribute mainly to the device operation, thus, the phase difference may again approach to zero. However, the extent of charge flow during

low frequencies may be limited through R_p due to the possible charge sharing to its parallel circuit element i.e. ESR and internal capacitance of supercapacitor.

Fig 5.10 shows the phase angle based Bode plot of said supercapacitor. This plot describes the phase difference between charging voltage and its obsessed electric current as function of applied frequency. From this analysis is one may evaluate the maximum physical area of supercapacitor and the response magnitude can be mapped from the applied frequency where the phase angle is maximum.

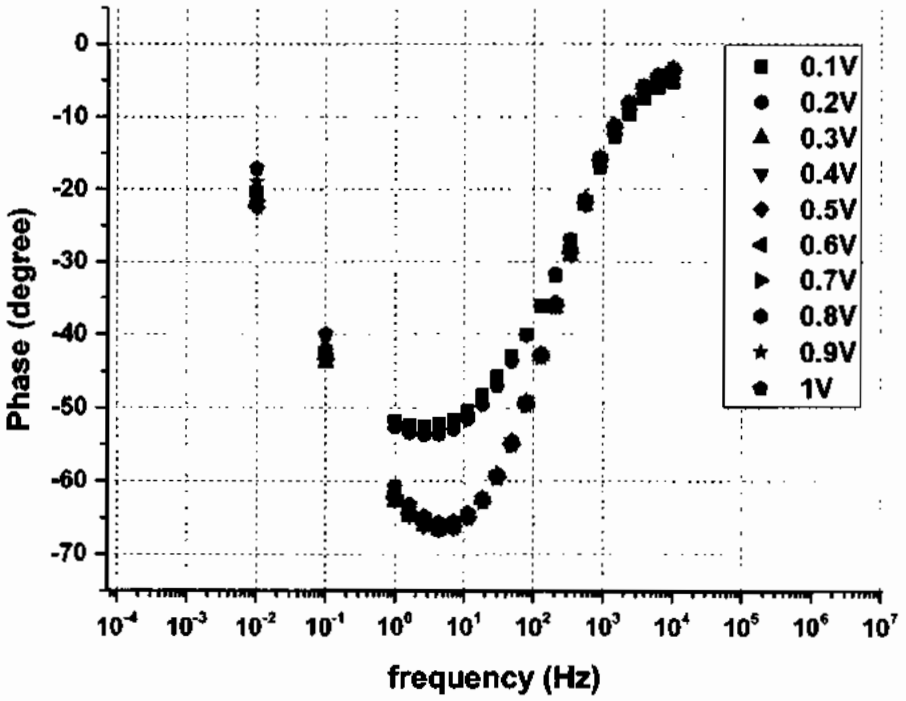

Fig 5.10: Phase based Bode plot at multiple charging voltages

5.1.2.4 Kinetics of electric current under charging voltage and temperature

Kinetics of electric current under charging voltages from 0.1 to 1V are also studied and shown in Fig 5.11. We inspected the charging mechanism of supercapacitor at variable ambient temperatures from 26 and 86°C. The graphical representation of charging current at 26 and 86°C is shown in Fig 5.11a and 5.11 b, respectively. We can analyze that by increasing the

charging voltage, charging current may also increase. Figs 5.11 (a) and 5.11(b) revealed that by increasing the ambient temperature the charging current decreases and limits the overall supercapacitor's operation/performance.

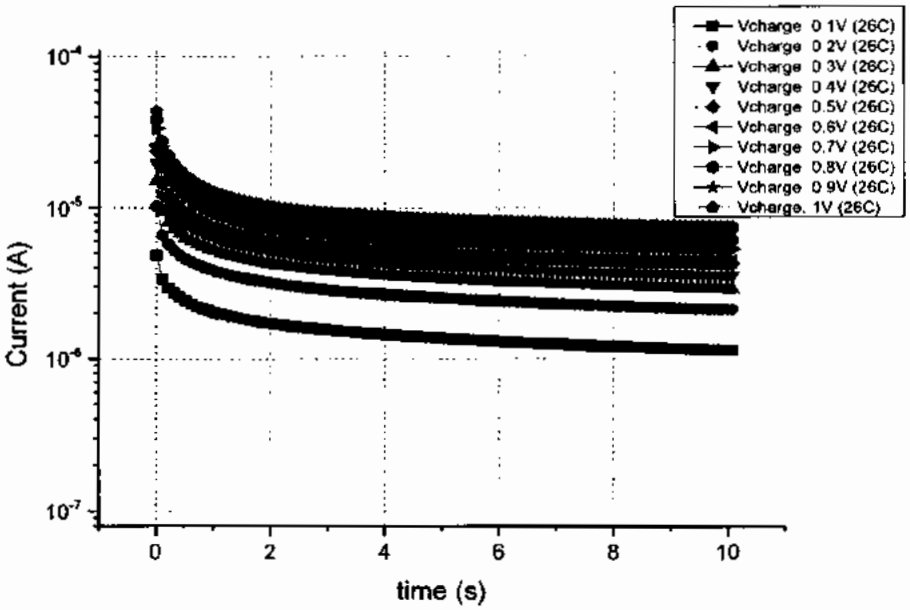

(a)

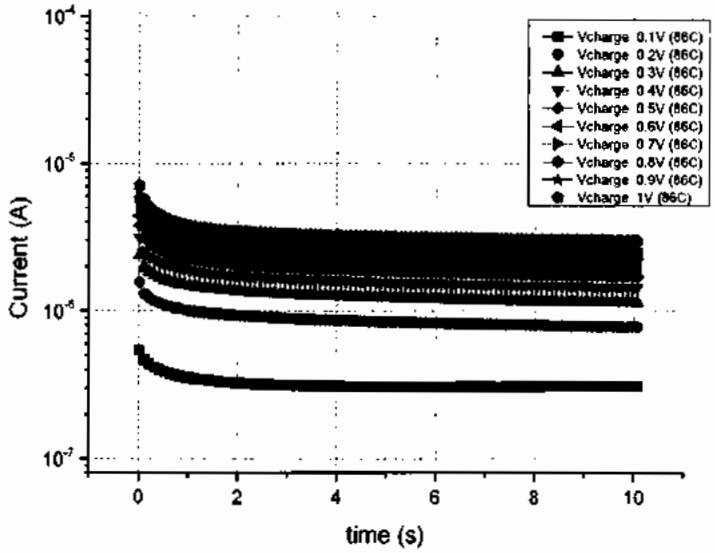

(b)

Fig 5.11: kinetics of electric current under subject charging voltages i.e. 0.1-1V (a) At 26 °C ambient temperature, (b) At 86 °C ambient temperature

Fig 5.11 shows the transient behavior of electric currents recorded at different charging voltages of said supercapacitor. In this analysis we have also worked out the same analysis at rather higher operating temperatures to sense the electric current nature of supercapacitor.

From the above, we can analyze the time-based charging mechanism i.e. capacitance, current, and charging voltage. Fig 5.12 is focused to provide an overall charging behavior of fabricated supercapacitor under charging voltage (1V) at 26/86°C ambient temperature. In both Figs 5.12(a-b), the blue line indicates how the charging voltage varies from ground (0V) to 1V and during this time span the charging current and its associated capacitance builds within the supercapacitor as a function of applied voltage (blue line). Thus, one may easily understand as to how these supercapacitors were charged. It is witnessed from both the Figs 5.12(a-b) that the charging current of higher ambient temperature is far less than that of its lower temperature case (26 °C). For instance; the charging current at 26°C is ~45μA and the charging current at 86°C is just about ~7 μA. This behaviour has also limited the magnitudes of capacitances and thus the overall performance of the supercapacitors.

From Fig 5.12, one can easily analyze the charging behavior i.e. how much time is needed for a particular super-capacitor to respond to its internal passive elements in order to fully charge during given applied charging bias at rather higher and lower ends of operating temperature. The voltage curve looks linear however at initial time intervals the spectra is exponential in nature which has already been mentioned in capacitor and current curves respectively.

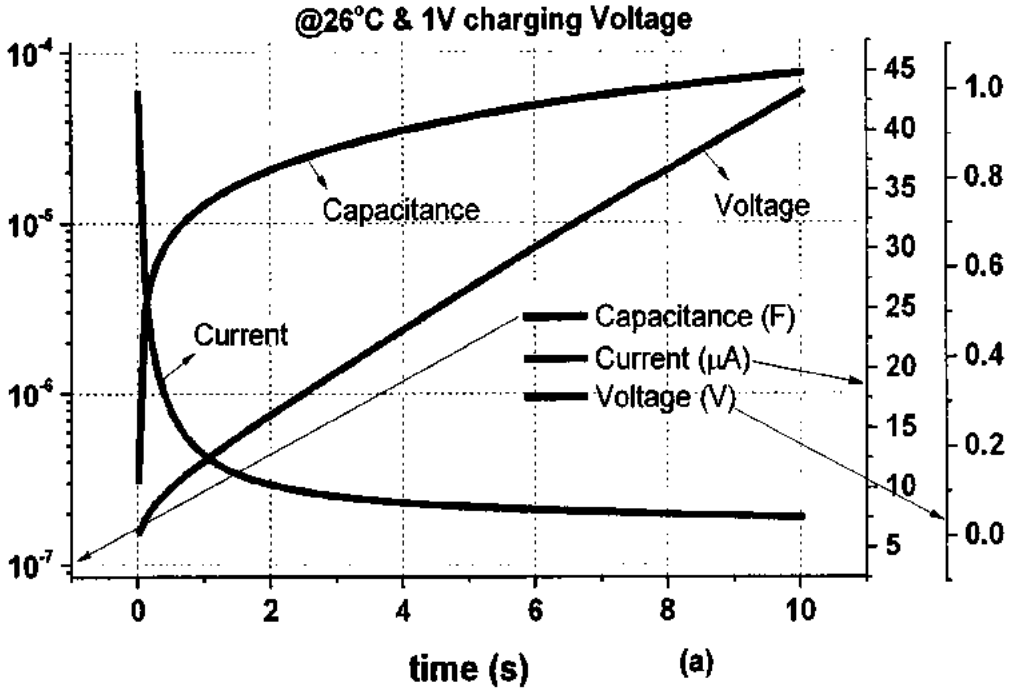

(a)

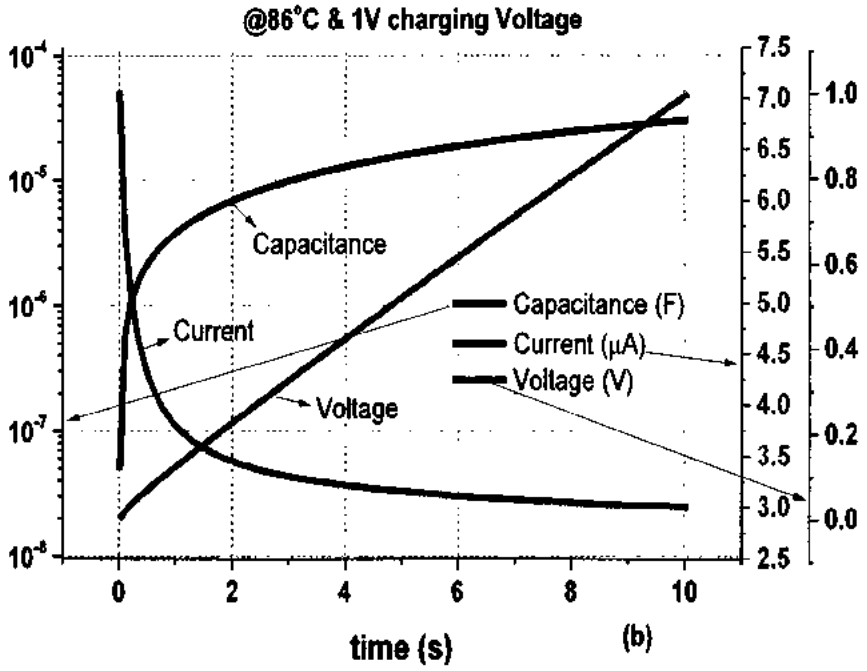

(b)

Fig 5.12: Overall charging behavior of subject supercapacitor under 1V charging voltage (a) At 26°C, (b) At 86°C ambient temperatures

Fig 5.13 shows the separate response of the capacitance of said supercapacitor as function of temperature variation. From this response one can examine that by increasing the ambient

temperature the capacitance of subject supercapacitor might fall and affect the overall device performance. PEDOT:PSS's inhomogeneous electrical and morphological properties result in poor long-term stability and cause the degradation; the supercapacitors were subjected to the detailed evaluation of interface defects and kinetics of current. Both aging-assisted defects and current kinetics due to variable operating temperatures may prove to be important parameters while designing the process strategies for flexible and stretchable PEDOT: PSS based supercapacitors for real-time system integration.

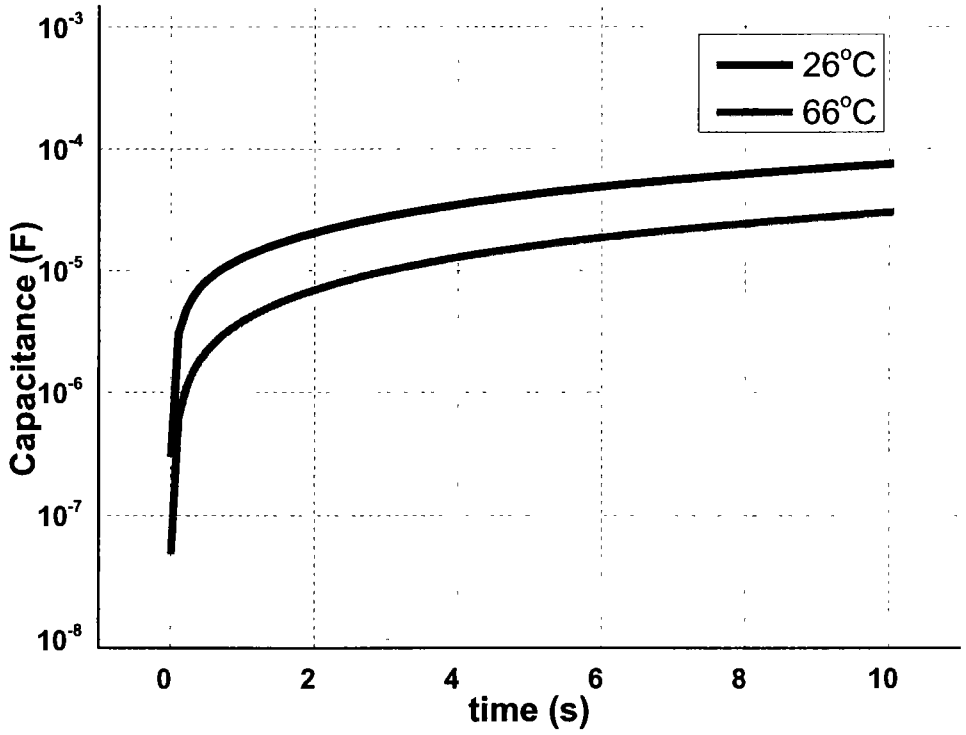

Fig 5.13: Capacitance of the PEDOT:PSS supercapacitor at varying temperature

5.2 Stretchable and Foldable Polyurethane Based Supercapacitors

Herein, a specialized Stretchable and Foldable Polyurethane Based Supercapacitors is fabricated in which the electrolyte is sandwiched between a dense metal net. A detail account of characterization is presented in terms of Current-Voltage (I-V) and Electrochemical Impedance Spectroscopy (EIS) at variable ambient temperatures. Charge based Transient Spectroscopy (Q-DLTS) measurements are performed on subject stretchable supercapacitor

in order to analyze the transient behavior of the device while under operation for its performance evaluation at charge level.

5.2.1 Experimental

The stretchable substrate of Polyurethane was used as a starting material in order to fabricate the partially stretchable and fully foldable supercapacitor. The length and width of the stretchable substrate was cleaved as length by width i.e. 45mm x 15mm, with an effective area of 675mm^2. Two stretchable and completely foldable substrates with effective geometrical dimensions were considered for subjecting each set onto the anode and cathode of the supercapacitor. A specifically prepared dense metal net with flexible and stretchable nature was selected as an anode and cathode metal contact with effective dimension each of 43mm (length) and 13mm (width), as shown in Fig.5.14. A specialized gel electrolyte was developed with some conical modifications, described in detail in publication [352]. All chemicals were purchased from Sigma-Aldrich and were used as received. The brief modified stoichiometry of subject electrolyte were, propylene carbonate (5-gram), polyethleneglycole diacrylate (Mn=700), trifluoromethene-sulfonate (1-gram) and DMPAP(2,2-dimethoxy-2-phenyle-acetophenone) of 17.5 mg , were added and mixed together and sonicated in an ultrasonic bath for about 17 minutes. The electrolyte was drop-casted onto the dense metal net and another set of dense metal net and stretchable substrate were placed in such a way that the electrolyte may be seen as sandwich layer. The UV light was exposed for ~5 minutes to solidify the gel-electrolyte. The detailed pictorial representation is shown in Fig 5.14.

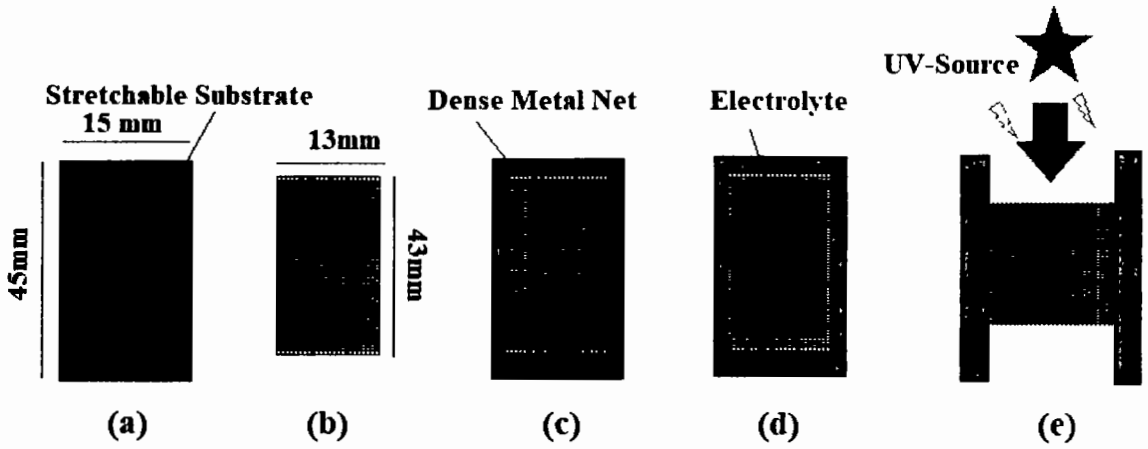

Fig 5.14: Fabrication of stretchable and foldable Supercapacitor:(a) stretchable and foldable Polyurethane substrate, (b) dense metal net, c) substrate/metal net stack, (d) drop casting of gel-electrolyte (e) U-V exposure and layer vise stack of stretchable supercapacitor.

5.2.2 Characterization

After physical growth of stretchable /flexible (Polyurethane substrate) supercapacitor's matrix i.e. Polyurethane /metal net/ Specialized Electrolyte/ dense metal/ Polyurethane. It was spanned for about ~15 days to properly mitigate the electrolyte with dense metal net and to investigate the essential device parameters i.e. R_{ESR}, R_p and effective capacitance etc. We inspected this stretchable and foldable supercapacitor with a variety of electrical and electro-chemical techniques including Current-Voltage (I-V) , Q-DLTS, kinetics of current I (t) techniques, potentiostatic based impedance techniques have been utilized charge based transient analysis is performed to investigate the interfaced defects that may contribute the leakage path for the collected charge. Current-voltage (I-V) characteristics have been performed for gauging the charging current magnitudes with respect to the applied charging voltages. ASMEC system is used for mapping I-V, Q-DLTS and kinetics of current studies and BST8-STAT-EIS system is used for EIS measurements, are utilized in this work.

5.2.2.1 Current Voltage (I-V) Analysis

Current-Voltage (I-V) analysis were performed after the fabrication of Stretchable and Foldable Polyurethane Based Supercapacitors. Two probe technique is used for I-V analysis, where the probes are connected to the copper contact of cathode and anode. The thermal stability and sustainability was inspected at different ambient temperatures. The temparture range selected with a step size of 10 °C for I-V analysis is from from 26 °C to 86 °C. Electrical biasing for the evaluation of this technique was scanned from the ground (0V) to 5 volts. The voltage is applied and the current is recorded and plotted as a function of the dependent variable of voltages to inspect the bias dependent maximum charging current at which the supercapacitor shows saturation current. The extent of this saturation current is very important because of the charge storage capability (i.e. charging capability may limit at a particular level and the streaming charge from the charging source may get drained from the internal discharging resistor of the supercapacitor). This specific internal resistor is modeled as in a parallel combination with the charging capacitor. The graphical representation of I-V curves at multiple temperatures is shown in Fig 5.15. Most of the recent studies suggest that the internal temperature of the supercapacitor varies during the charging and discharging modes of operation [6]. In particular, for charging mode of operation, this temperature may rise rapidly [6]. In our study, we have increased the ambient temperature of the supercapacitor to inspect the charging nature of the subject supercapacitor. I-V characteristics provide an indirect measure of charge-storage capability of the device.In start when we increase temperature from room temperature i.e. 26 °C to 36 °C and then 36 °C to 46 °C, the current is increased. But after 46 °C if we further increase the temperature, the extent of charging current is seen to fall and get decreased to lower levels. For higher temperature values, the spread of current becomes higher for just 300K, and after this temperature the current magnitude decreases limiting the overall charging capability at these specific temperatures. This

behavior is thought to be due to the internal chemistry of interfaces between the electrolyte and the substrate. Fig 5.15 shows the electric current behavior as function of applied electric field and different ambient temperature. This spectra depicts that at rather higher temperatures i.e. >46°C, the charging current seems to decrease and reduces the charge collection mechanism of said supercapacitor.

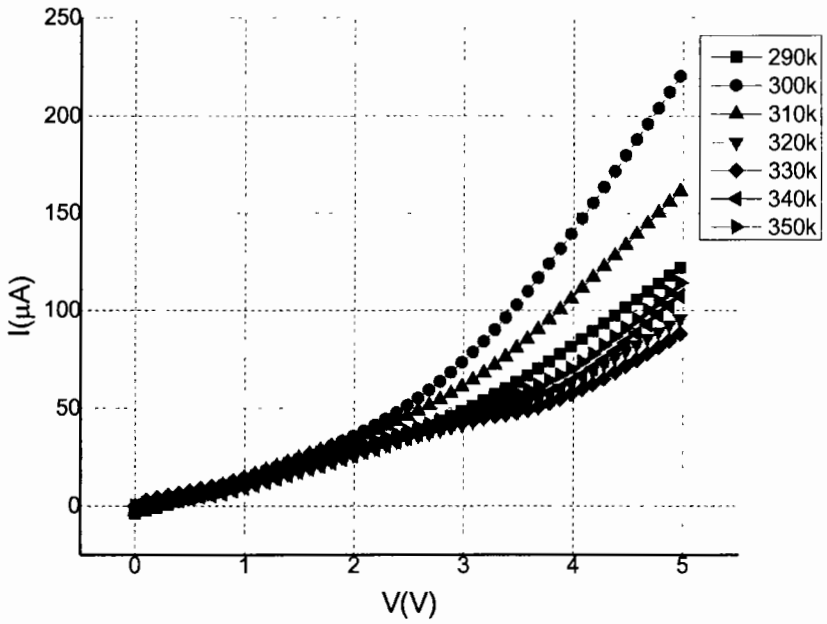

Fig 5.15: Current-Voltage characteristic stretchable and foldable polyurethane based based supercapacitor at variable temperatures

5.2.2.2 Q-DLTS: Defect Analysis of Strechable and foldable Supercapacitor

In order to study the lossy nature (because of internal discharge resistance, R_P) of intrinsic ability of supercapacitor, one has to envisage this at an atomistic scale and may evaluate the discharge nature. For that purpose, we have performed a very specialized charged based technique namely Charge Deep Level Transient Spectroscopy (Q-DLTS). It is explained at length the background theory along with the mathematical expression about Q-DLTS and its application in supercapacitors in previous topic and also published it [356]. In Q-DLTS spectra, we measure the change in charge magnitude during discharge cycle in order to map

the discharge states at dense metal net and UV- cured electrolyte interface. During this analysis the supercapacitor is pulsed for a duration by which said interface has been filled with the upcoming charges from the charging source as shown in Fig 5.16. From Fig 5.16, when switch is closed, the charge flows towards the internal capacitor and when the switch is turned open, the collected charge at the dense metal net and electrolyte layer discharges itself over the self-discharge resistance which is physically created by the interface as shown in Fig 5.16 (b).

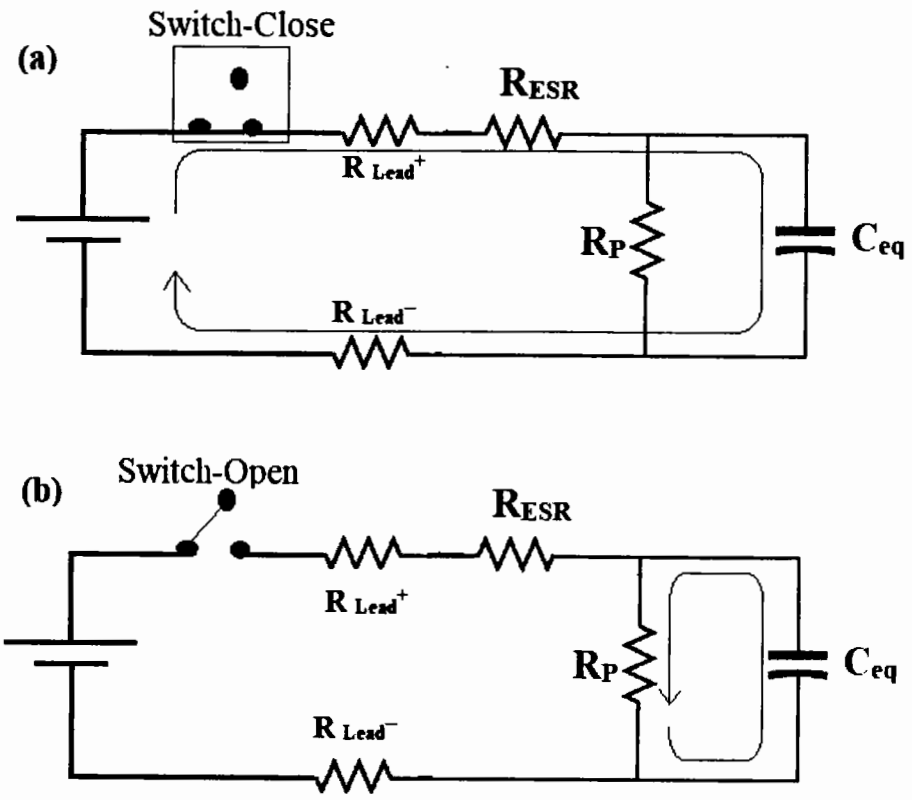

Fig 5.16: Charge-Discharge events of supercapacitor in Q-DLTS measurements (a) charging through R_{ESR} (b) discharging through R_P

In this study we apply the charging pulse of 20 mV for about 10ms duration because if we increase these limits (i.e. charging voltage and duration) the discharge time of transient may increase. Further; the temperature needs to be fixed, when these events are captured (especially in discharge cycle as highlighted in Fig 5.16(b)). When the interface is fully charged at 20 mV, the switch turned open and charge is measured when the internal capacitor

discharges itself via 'R_P' resistor. This is achieved when voltage of the capacitor decreases from maximum value (i.e. 20 mV) to ground level (i.e. zero volts).

Fig 5.17 shows the Q-DLTS spectra of the stretchable/foldable supercapacitor which is plotted against the change in charge magnitude as function of rate window (τ) [356]. The change in charge magnitude is recorded at multiple temperatures ranging from 300K-350K.The Trap densities of the device can be measured from the highest peak of ΔQ spectra and related by equation 4.12 => $N_T = \frac{4\Delta Q_{max}}{qA}$, Where '$N_T$' are the surface trap densities 'q' is the universal charge constant and 'A' is the area of dense metal net electrode which is interfaced with UV-cured electrolyte (which is equals to 546mm^2). The Trap densities are recorded at each ambient temperature and listed in Table 5.2, case wise.

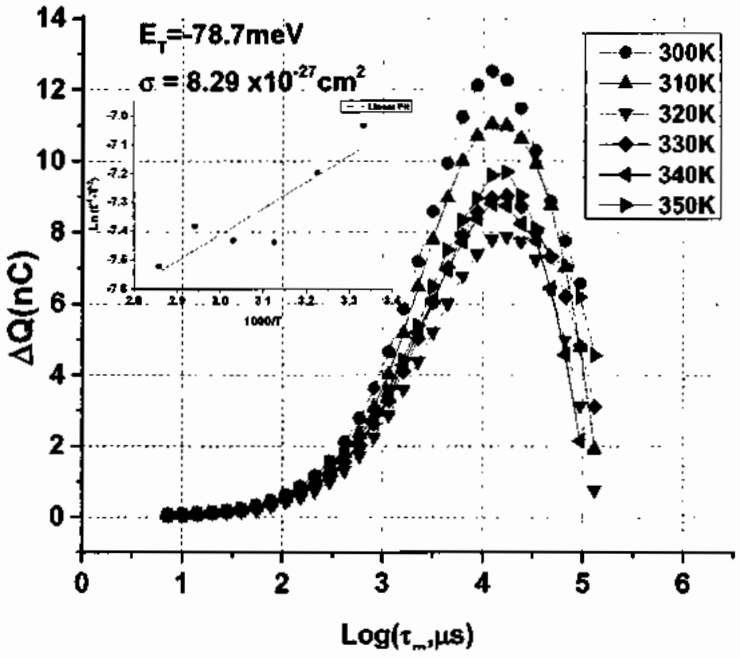

Fig 5.17: Q-DLTS spectra of stretchable/foldable supercapacitor

The trap energy (E_T) and capture cross section (σ) of the interface traps are calculated from the Arrhenius analysis of Equation (4.10). The inset of Fig 5.17 shows the Arrhenius plot

(i.e. the slope of the linearly fitted line proportional to the Trap energy and the y-intercept provides the capture cross section of the interface.

Trap energy (E_T) is the location near the conduction band edge of dense metal net electrolyte interface and its position predicted from measurements is 'E_C-78.7meV'. And the capture cross-section (σ) is actually the ability of 'E_C-78.7meV'energy level that it captures the collected carriers from the internal capacitor and discharges/conducts them at the dense metal net electrolyte interface i.e. 'R_P'. Thus, lower values of capture cross-sections are desirable [356], in order to have less ability to capture the collected charge at the internal capacitor of supercapacitor. Trap densities (N_T) are the physical states around 'E_C-78.7meV' (i.e. trap level) which are reported in Table 5.2.

Table 5.2: Trap parameters of stretchable/foldable supercapacitors

Sr.#	Temp [K]	Trap density(N_T) (cm^{-2})	E_T	σ (cm^2)
1	300	8.2×10^{10}	-78.7 meV	8.29×10^{-27}
2	310	5.07×10^{10}		
3	320	3.63×10^{10}		
4	330	4.15×10^{10}		
5	340	4.06×10^{10}		
6	350	4.49×10^{10}		

5.2.2.3 EIS Analysis of based Polyurethane Based Supercapacitors

Electrochemical Impedance Spectroscopy (EIS) analysis was carried out for the evaluation of Stretchable and Foldable Polyurethane Based Supercapacitors. The EIS based Nyquist (Real Z vs Imaginary Z), and Bode (frequency-dependent impedance and phase) plot is obtained by using two probe technique. Working/Sense Electrode and Counter/Reference

electrode are connected in such a way that working and sense are connected together and treated as "Anode electrode", whereas, Counter and Reference electrode as "Cathode electrode". EIS is considered to be important measure to describe the internal electrical metrology of the supercapacitors. The initial conditions for the said experiments were kept fixed i.e. pretreatment time= 5s, AC amplitude $0.1V_{ac}$, and the frequency window between 10 mHz – 10 kHz, followed by the different charging voltages ranging from $0.1\text{-}1V_{DC}$.

The value of R_p of 936 kΩ was calculated from the real impedance of the EIS spectra measured at 10mHz to 10KHz frequency range and the value of Capacitance was found to be around $7.34x10^{-5}$ F.

As mentioned earlier the lesser value of R_{ESR} is more favorable for any type of supercapacitor. In this type of supercapacitor one has scanned the applied biases ranged from 0.1-1V. Fig 5.18 shows the Nyquest plot of all said range of electrical potentials. From this analysis the value of R_{ESR} is low for just 1V of charging potential i.e. ~19.6KΩ. Contrary to that fact when the supercapacitor discharge itself the voltage drops may occurred and this may affects the R_{ESR} magnitude i.e. the increase in R_{ESR} ~35KΩ be observer. Due to significant increase in R_{ESR} magnitude, this fact decreases the efficiency of said supercapacitor.

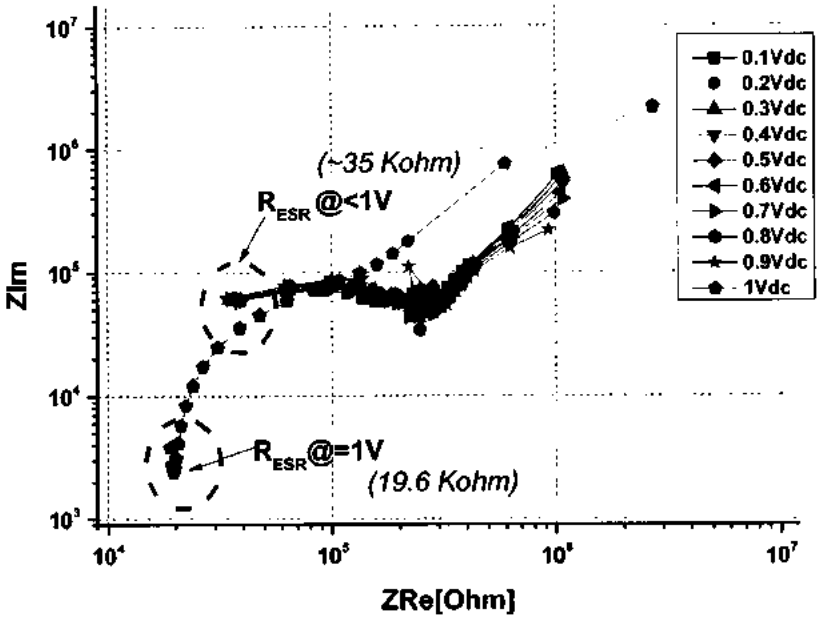

Fig 5.18: EIS based Nyquist plot

5.2.2.4 Kinetics of electric current under charging voltage and temperature

In recent literature, Martinovic et al. [357], have studied electrochemical behavior of supercapacitor's electrodes and used potentiostatic current-time analysis with the charging pulse of 100 mV for 50 seconds. They have calculated the values of 'R_{ESR}' and 'R_p' at $t=0^+$ and 50 seconds, respectively. Whereas, for our stretchable and completely foldable supercapacitor, we have applied a charging pulse of 100 mV-1000 mV (0.1V-1V) with the step size of 100 mV over 20 seconds, respectively, and recorded the values of current. In addition to the multi-charging voltage pulses, we have also applied multiple temperature cycles ranging from 300K – 350K, in order to inspect the thermal stability of the fabricated supercapacitor. Fig 5.19 (a-e) shows the potentiostatic measurements at multi-charging and multi temperature cycles.

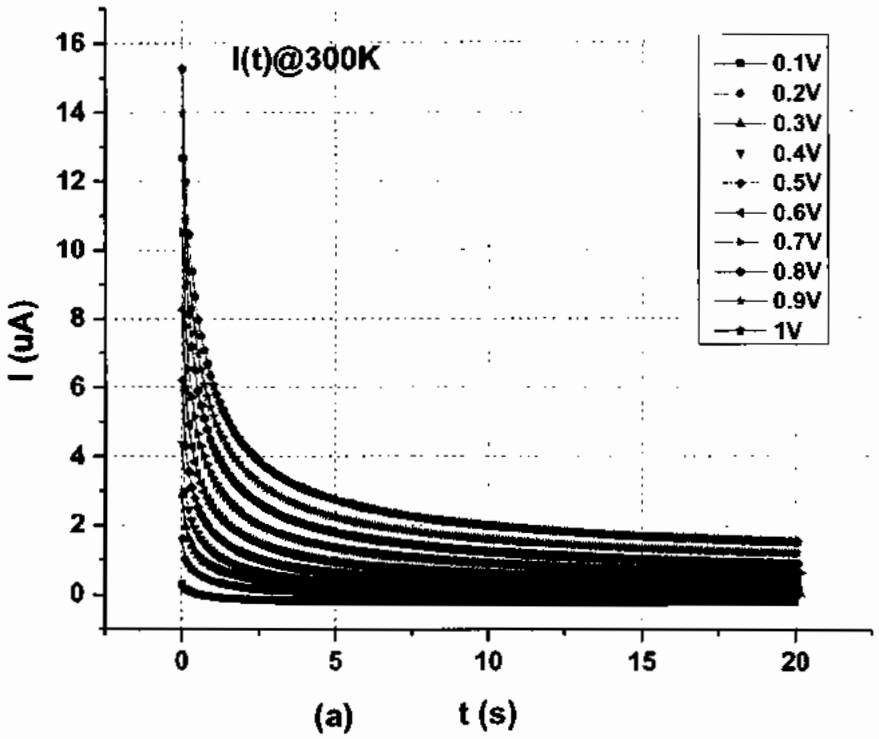
I(t)@300K
0.1V
0.2V
0.3V
0.4V
0.5V
0.6V
0.7V
0.8V
0.9V
1V
I (uA)
t (s)

(a)

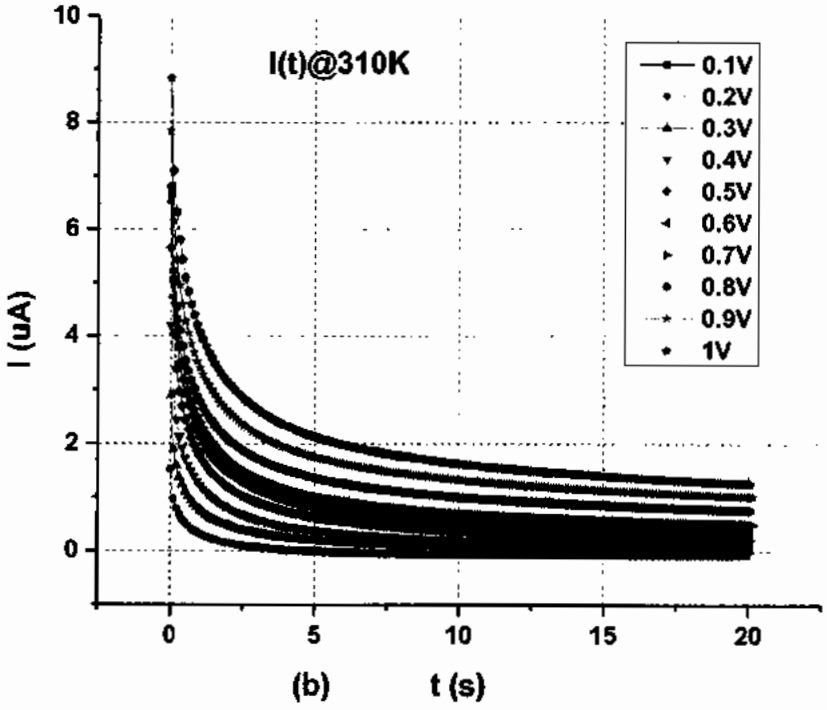
I(t)@310K
0.1V
0.2V
0.3V
0.4V
0.5V
0.6V
0.7V
0.8V
0.9V
1V
I (uA)
t (s)

(b)

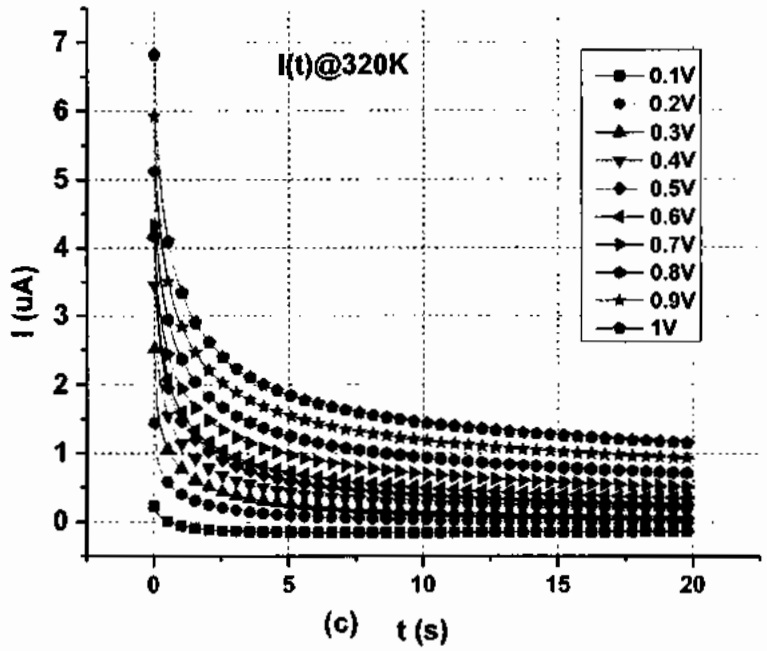
I(t)@320K
0.1V
0.2V
0.3V
0.4V
0.5V
0.6V
0.7V
0.8V
0.9V
1V
I (uA)
t (s)
(c)

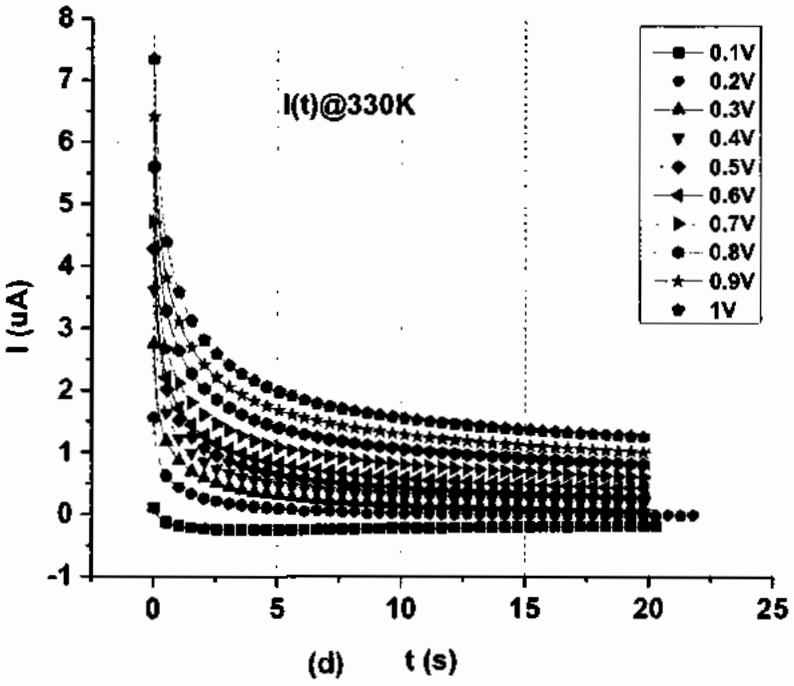
I(t)@330K
0.1V
0.2V
0.3V
0.4V
0.5V
0.6V
0.7V
0.8V
0.9V
1V
I (uA)
t (s)
(d)

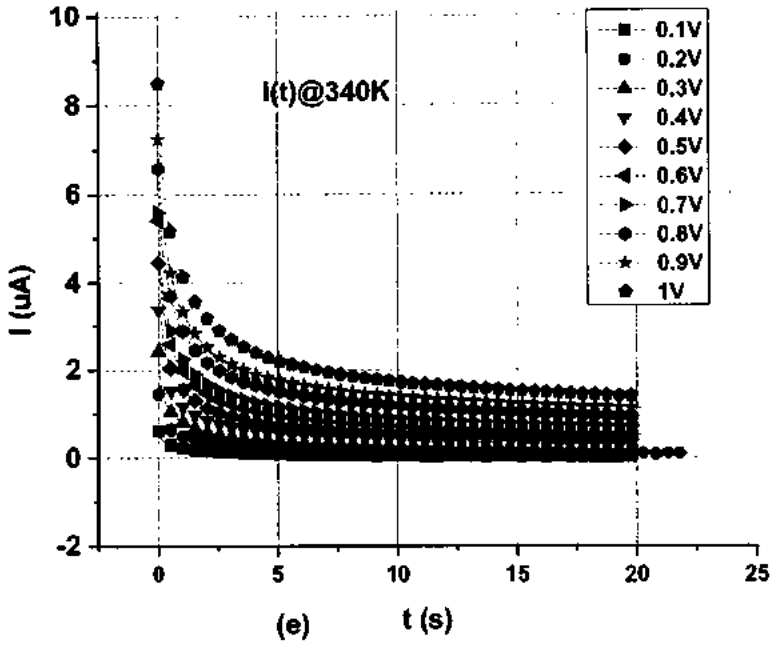

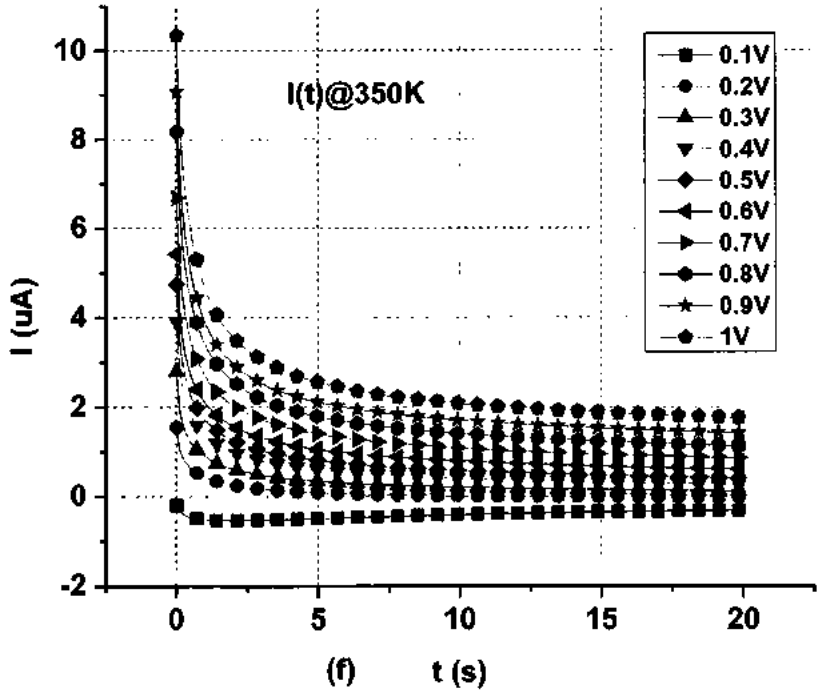

Fig 5.19: Current-time spectra's at multi-charging voltage pulses, (a) I(t) at 300K, (b) I(t) at 310K, (c) I(t) at 320K, (d) I(t) at 330K, (e) I(t) at 340K, (f) I(t) at 350K

We can analyze that by increasing the charging voltage, charging current may also increase. Figs 5.19 (a-e) revealed that by increasing the ambient temperature the charging current decreases and limits the overall supercapacitor's operation/performance. In our case we have applied the charging bias in descending orders i.e. 1V to 0.1V, to charge the said supercapacitor. In Fig 5.19 (f) the current is negative because the stray charge of more than 0.1V is already present at this particular (i.e. 0.1V) charging bias. Further, the internal resistance ($R_{Internal}$) of voltage source is very low. Thus, the current flows from higher potential side to the lower potential. Resultantly; the direction of current flow is from supercapacitor to the external 0.1V charging source. Thus, reverse polarity in current magnitude has been observed at this particular lower charging voltages. Fig 5.20 specifically clarifies this special behavior of the said supercapacitor device.

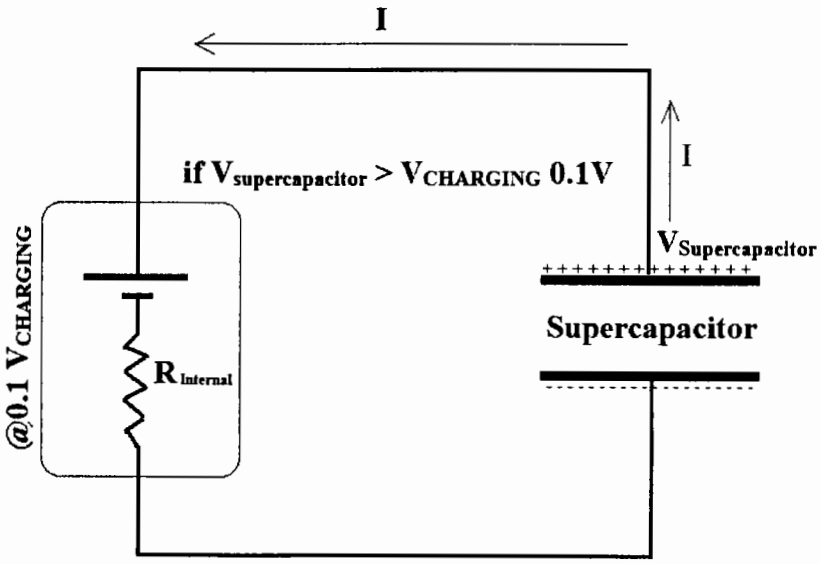

Fig 5.20: Reverse polarity in current magnitude

5.3 Alternating and Direct Current Analysis of said Supercapacitors

Herein, a detailed amount of mathematical analysis is done for Stretchable and Foldable Polyurethane Based Supercapacitors, in terms of alternating current (AC) and direct current (DC) techniques is carried out with multi-charge pulses ranging from 0.1V to 1V. For AC analysis, impedance spectroscopy has also been performed.

We can analyze that by increasing the charging voltage, charging current may also increase. Figs 5.19 (a-e) revealed that by increasing the ambient temperature the charging current decreases and limits the overall supercapacitor's operation/performance. In our case we have applied the charging bias in descending orders i.e. 1V to 0.1V, to charge the said supercapacitor. In Fig 5.19 (f) the current is negative because the stray charge of more than 0.1V is already present at this particular (i.e. 0.1V) charging bias. Further, the internal resistance ($R_{Internal}$) of voltage source is very low. Thus, the current flows from higher potential side to the lower potential. Resultantly; the direction of current flow is from supercapacitor to the external 0.1V charging source. Thus, reverse polarity in current magnitude has been observed at this particular lower charging voltages. Fig 5.20 specifically clarifies this special behavior of the said supercapacitor device.

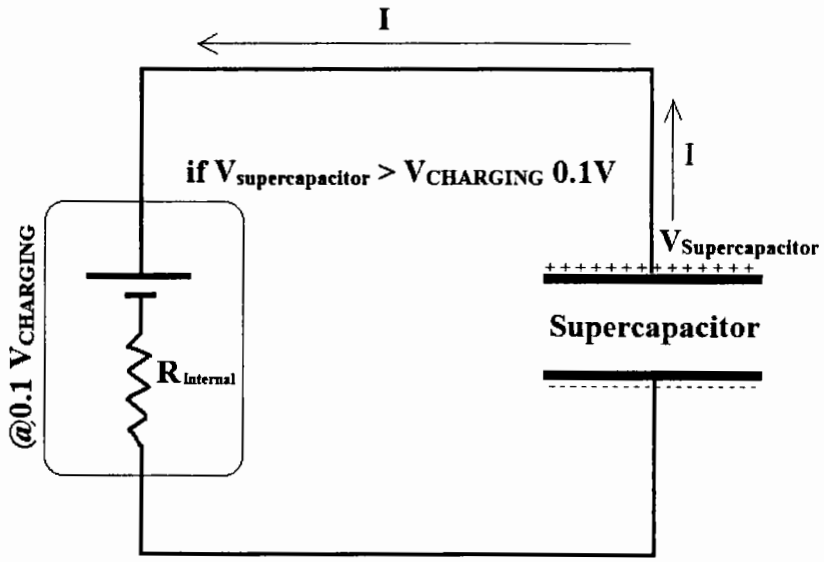

Fig 5.20: Reverse polarity in current magnitude

5.3 Alternating and Direct Current Analysis of said Supercapacitors

Herein, a detailed amount of mathematical analysis is done for Stretchable and Foldable Polyurethane Based Supercapacitors, in terms of alternating current (AC) and direct current (DC) techniques is carried out with multi-charge pulses ranging from 0.1V to 1V. For AC analysis, impedance spectroscopy has also been performed.

5.3.1 Characterization

It was spanned for about ~15 days to properly mitigate the electrolyte with dense metal net and to investigate the essential device parameters i.e. R_{ESR}, R_p and effective capacitance etc. Two different characterization approaches are adopted in order to evaluate self-discharge resistance (R_p) and effective capacitance (C_{eff}) of supercapacitor, by utilizing the DC and AC analysis at the circuit level.For DC analysis, we have used Current-Voltage (I-V) and kinetics of current I (t) techniques and for AC analysis, potentiostatic based impedance techniques have been utilized. The DC and charge measurements were done using ASMEC Electro-Physical Characterization system and the AC analysis was conducted using BST8-STAT-Electrochemical impedance Spectroscopy (EIS) system.

5.3.2 Alternating and Direct Current Analysis

There are three main equivalent parameters that have to be optimized in order to bridge technology ready solution of any supercapacitor. These parameters are named as R_{ESR}, R_p and equivalent capacitance and their circuit level representation is shown in Fig 2.11.

As in Fig 2.11, the 'R_{ESR}' indicates the ohmic resistance of electrodes, and 'R_p' indicates the self-discharge resistance (however from circuit's perspective; this resistance is always offered during charging and discharging mode of operation). When the supercapacitors get tied with the physical application in order to run/functionalize the loads, the degradation is observed, and viable solutions are needed to engineer the process. In order to solve the circuit (as shown in Fig 2.11), one has to evaluate Thevenin's equivalent resistance of said supercapacitor. As this study will focus on both AC and DC approaches, the term "resistance" may be swapped with impedance. Initially, the circuit was labeled as shown in Fig 5.21.

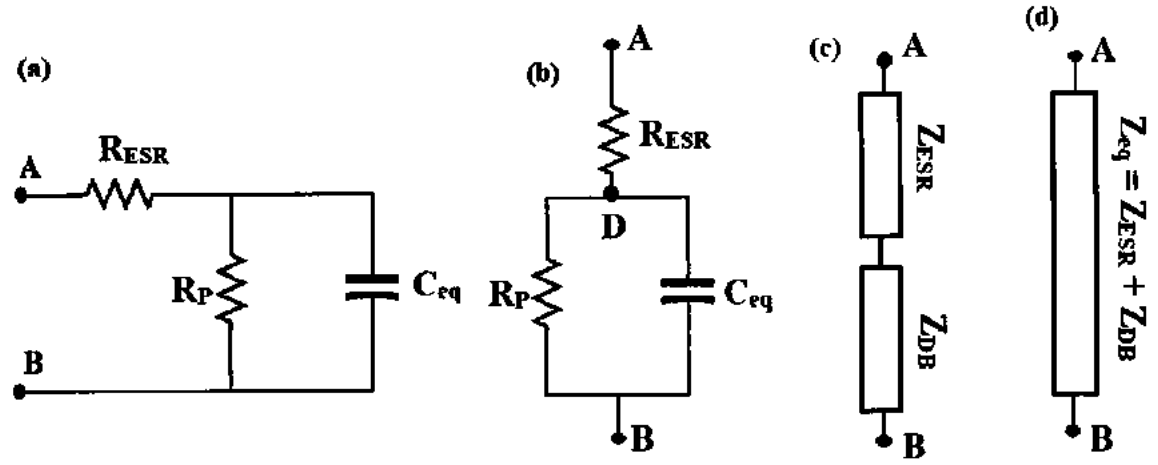

Fig 5.21. Thevenin's Equivalent circuit of stretchable Supercapacitor

In order to solve the circuit, each component would be represented by "Z" form as shown in Fig 5.21 (c-d). As R_p and C_{eq} are in parallel so, they would be solved by parallel impedance law i.e.

$$Z_{AB} = Z_{RESR} + Z_{DB} \tag{5.4}$$

$$Z_{DB} = Z_{RP} \parallel Z_{Ceq} \tag{5.5}$$

and,

$$Z_{Ceq} = X_{Ceq} = \frac{1}{2\pi f C_{eq}} \tag{5.6}$$

As Capacitance is complex term, thus '*j*' would be added before '*f*' term.

$$Z_{Ceq} = X_{Ceq} = \frac{1}{j2\pi f C_{eq}} \tag{5.7}$$

And equation (5.5) becomes as;

$$Z_{DB} = Z_{RP} \parallel \frac{1}{j2\pi f C_{eq}} \tag{5.8}$$

$$\frac{1}{Z_{DB}} = \frac{1}{Z_{RP}} + \frac{1}{\frac{1}{j2\pi f C_{eq}}} \tag{5.9}$$

$$Z_{DB} = \frac{1}{\frac{1}{Z_{RP}} + j2\pi f C_{eq}} \tag{5.10}$$

$$Z_{DB} = \frac{1}{\frac{1+j2\pi f C_{eq} Z_{RP}}{Z_{RP}}} \tag{5.11}$$

$$Z_{DB} = \frac{Z_{RP}}{1+j2\pi f C_{eq} Z_{RP}} \tag{5.12}$$

Putting the value of 'Z_{DB}' in equation (1)

$$Z_{AB} = Z_{RESR} + \frac{Z_{RP}}{1+j2\pi f C_{eq} Z_{RP}} \tag{5.13}$$

Also, we can write as;

$$\overrightarrow{Z_{AB}} = \overrightarrow{R_{ESR}} + \frac{\overrightarrow{R_P}}{1+j2\pi f C_{eq} Z_{RP}} \tag{5.14}$$

This is the vector form of Thevenin's equivalent impedance. The scalar magnitude of Thevenin's equivalent impedance of the supercapacitor would be calculated as:

$$|Z_{AB}| = \sqrt{(R_{ESR})^2 + \left(\frac{R_P}{1+j2\pi f C_{eq} Z_{RP}}\right)^2} \tag{5.15}$$

$$|Z_{AB}| = \sqrt{(R_{ESR})^2 + \frac{(R_P)^2}{(1+j2\pi f C_{eq} R_P)^2}} \tag{5.16}$$

$$|Z_{AB}| = \sqrt{(R_{ESR})^2 + \frac{(R_P)}{1+(j2\pi f C_{eq} R_P)^2+2(1)(j2\pi f C_{eq} R_P)}^2} \tag{5.17}$$

$$|Z_{AB}| = \sqrt{(R_{ESR})^2 + \frac{(R_P)}{1+j4\pi f C_{eq} Rp-4\pi^2 f^2 C_{eq}{}^2 Rp^2}^2} \tag{5.18}$$

As, $f=\frac{1}{T}$, Thus,

$$|Z_{AB}|=\sqrt{(R_{ESR})^2+\frac{(R_P)}{1+j4\pi\frac{1}{t}C_{eq}R_P-4\pi^2\left(\frac{1}{t}\right)^2C_{eq}{}^2Rp^2}^2} \quad (5.19)$$

Equation (5.18) and (5.19) represents the frequency and time domain Thevenin's equivalent impedance of the supercapacitor. Thus, the equivalent circuit of stretchable supercapacitor is shown in Fig 5.22.

Equation 5.19 provides an insight of overall Equivalent impedance and its respective entity-wise internal active and passive components. To properly envisage the values of internal ' R_{ESR}' and 'R_P', one has to apply mathematical limits on equation 5.19.

⇨ When $\lim_{t\to o}$ *i. e*

$$\lim_{t\to o}|Z_{AB}|=\lim_{t\to o}\left|\sqrt{(R_{ESR})^2+\frac{(R_P)}{1+j4\pi\frac{1}{t}Ceq\,R_P-4\pi^2\left(\frac{1}{t}\right)^2C_{eq}{}^2Rp^2)}^2}\right| \quad (5.20)$$

$$\lim_{t\to o}|Z_{AB}|=\sqrt{(R_{ESR})^2+\frac{(R_P)}{1+j4\pi\lim_{t\to 0}\frac{1}{t}Ceq\,R_P-4\pi^2\lim_{t\to 0}\left(\frac{1}{t}\right)^2C_{eq}{}^2Rp^2)}^2} \quad (5.21)$$

The term $\lim_{t\to o}\frac{1}{t}=\infty$. Thus, putting this value in equation 5.21.

$$\lim_{t\to o}|Z_{AB}|=\sqrt{(R_{ESR})^2+\frac{(R_P)}{1+\infty-(\infty)^2}^2} \quad (5.22)$$

$$\lim_{t\to o}|Z_{AB}|=\sqrt{(R_{ESR})^2+\frac{(R_P)^2}{\infty}} \quad (5.23)$$

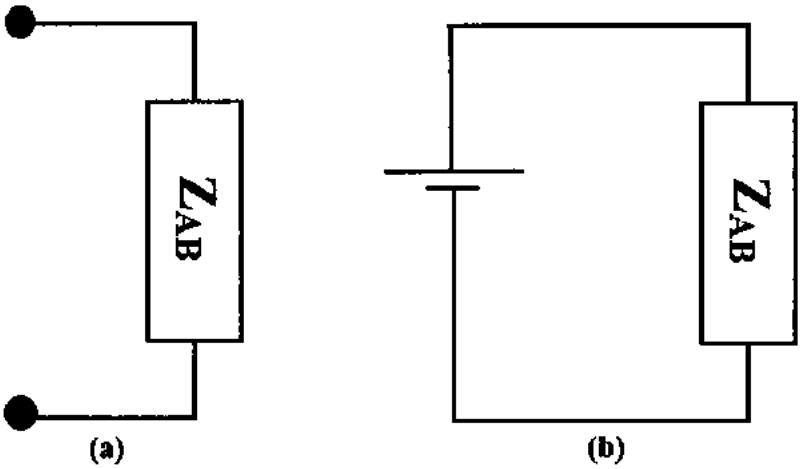

Fig 5.22: Thevenin's Equivalent impedance model (a), Thevenin's Equivalent impedance (b) Thevenin's Equivalent impedance with DC source

The term $\frac{(Rp)^2}{\infty} = 0$, thus

$$\lim_{t\to o}|Z_{AB}| = \sqrt{(R_{ESR})^2 + 0} \tag{5.24}$$

$$\lim_{t\to o}|Z_{AB}| = R_{ESR} \tag{5.25}$$

And when $\lim_{t\to\infty}$, the term $\lim_{t\to\infty}\frac{1}{t} = 0$. Thus, Equation 5.21 becomes as;

$$\lim_{t\to\infty}|Z_{AB}| = \sqrt{(R_{ESR})^2 + \frac{(R_P)^2}{1+0-(0)^2}} \tag{5.26}$$

$$\lim_{t\to\infty}|Z_{AB}| = \sqrt{(R_{ESR})^2 + R_P{}^2} \tag{5.27}$$

In practical cases the value of $R_P >> R_{ESR}$, thus term R_{ESR} can be neglected; and Equation (5.27) becomes as:

$$\lim_{t\to\infty}|Z_{AB}| = \sqrt{(R_P)^2} \tag{5.28}$$

$$\lim_{t\to\infty}|Z_{AB}| \cong R_P \tag{5.29}$$

From Equation (5.25) and (5.29), one can easily understand that when time approaches to zero i.e. at pico and femto seconds, the value of 'R_{ESR}' can be calculated and when time approaches to infinity i.e. when supercapacitor almost charged in a few seconds. After that, the value of 'R_p' can be estimated.

In DC analysis also known as potentiostatic measurement as reported in [353], the value of 'R_{ESR}' and 'R_p' are calculated from current-time graph at a certain/particular charging voltage.

From application point of view, following circuit diagram is sketched for practical scenarios as shown in Fig 5.23 (a-d).

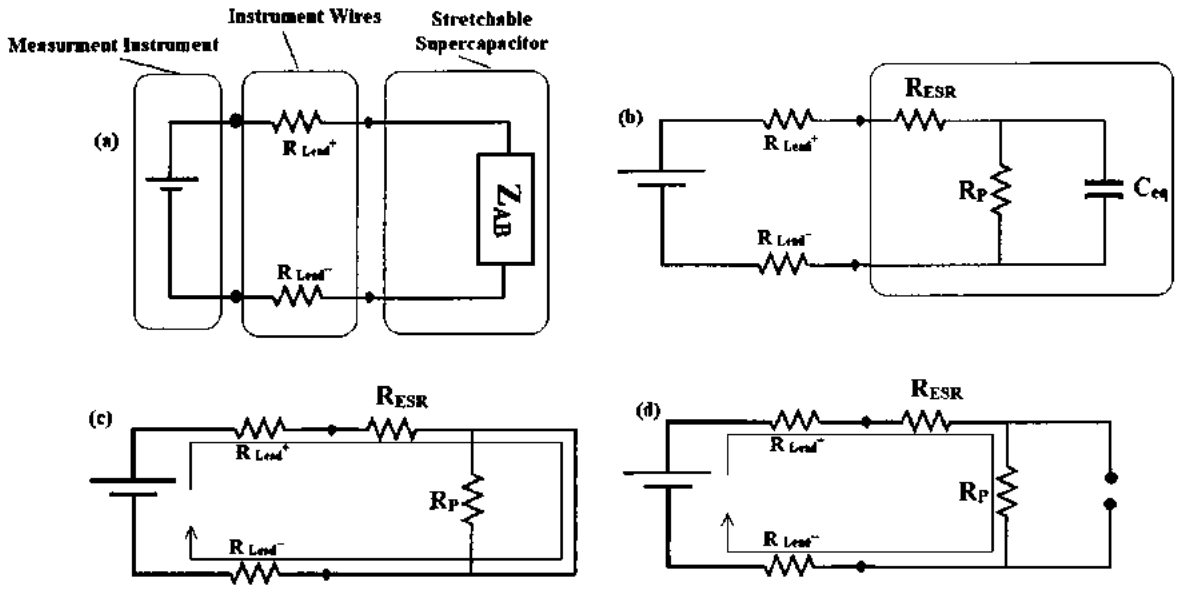

Fig 5.23: Charging Circuit of stretchable supercapacitor, (a) supercapacitor charging along with positive and negative series wires. (b) Charging circuit diagram (practical), (c) equivalent circuit diagram during charging phase, (d) Equivalent circuit diagram during charged phase

From both Equation (5.25) and Fig 5.23(c), it is analyzed that when time approaches to zero, the practical circuit's resistance would be equalized as; $\lim_{t\to 0} R_{Eq} = R_{Lead}^{+} + R_{ESR} + R_{Lead}^{-}$.

Thus, the charging current is limited by R_{eq} ($=R_{Lead}^{+} + R_{ESR} + R_{Lead}^{-}$) and not only by '$R_{ESR}$'.

As the 'R_{ESR}' is the joint ohmic resistance of both (positive and negative) electrodes of supercapacitor, thus, to properly envisage the value of 'R_{ESR}', one can only measure it before the fabrication of any supercapacitor.

Following circuit diagram (Fig (5.24)), is suggested for the determination of precise value of 'R_{ESR}'.

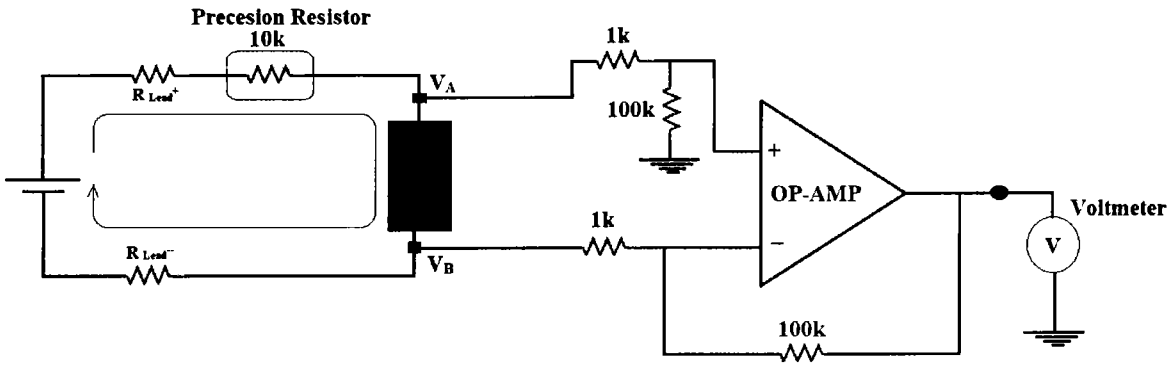

Fig 5.24-I-: Circuit Diagram of Precise R_{ESR} determination

Fig 5.24-I provides the precise evaluation of R_{ESR} as:

$$R_{ESR} = R_{Dense\ MetalNet\text{-}\ Electrode\ 1} + R_{Dense\ MetalNet\text{-}\ Electrode\ 2} \qquad (5.30)$$

In our case, we have chosen identically dimensioned dense metal nets. Thus, equation 5.30 can be seen as;

$$R_{ESR} = 2\ R_{Dense\ MetalNet} \qquad (5.31)$$

Referring to Fig5.32 as; and by applying Kirchhoff's voltage law, V_{source} can be written as:

$$V_{source} = V_{Rlead^+} + V_{10K\Omega} + V_{AB} + V_{Rlead^-} \qquad (5.32)$$

The value of current 'I' can be measured from the 'ampere meter' connected in series as shown in Fig (5.24-I). The potential difference of dense metal net can be calculated from 'V_{AB}'. This is because we have to get rid from the parasitic voltages developed across *lead*$^+$ and *lead*$^-$. The value 'V_{AB}' can be in the range of few 'μV' and to measure these ultra-low

level of voltages, one can adopt differential amplifier analogy [358]. For that purpose, one can use very precise family of operational amplifier i.e. Instrumentation Amplifier. From circuit designing perspective we have adjusted the gain of Instrumentation Amplifier of about 100 i.e. the voltage measured from the output terminal of operational amplifier (op-amp) be multiplied by the factor 100. It is done because the output stage of op-amp is fed to normal digital multimeter, and thus easily be measured. 'V_{AB}' can be measured from the output stage of op-amp and connected via digital multimeter by following equation.

$$V_{AB} = \frac{Vo}{Gain} \quad \text{(where Gain= 100)} \tag{5.33}$$

The $R_{\text{Dense MetalNet}}$ can be calculated from Equation (5.33) and the measured current through ampere meter as ;

$$R_{\text{Dense MetalNet}} = \frac{V_{AB}}{I} = \frac{Vo}{100I} \quad \text{(where 'I' is the current)} \tag{5.34}$$

And the value of R_{ESR} can be determined from Equation (5.31) as;

$$R_{ESR} = 2\left(\frac{Vo}{100I}\right) \tag{5.35}$$

From Equation (5.35) one can precisely calculate the value of R_{ESR}.

The value of 'R_P' can be calculated from Equation (5.29) when $\lim_{t\to\infty}$ and can be visualized from circuit level analysis, as highlighted in Fig 5.23(d). Literature [330], also reported that at final time (like in our case when $\lim_{t\to\infty}$) the value of current (I) provides the value of R_P. It is because when $t\to\infty$, the capacitor is almost charged, and no current should be migrated from the capacitor. But at final time the very limited current be observed that has to be found from 'R_P', as can be seen in Fig 5.23(c). Thus, at this time the value of current is mainly due to the R'_{eq} and related as;

$$R'_{eq} = R_{Lead}^{+} + R_{ESR} + R_P + R_{Lead}^{-} \tag{5.36}$$

From practical point of view, the value of R_{Lead}^{+} and R_{Lead}^{-} is of few ohms and 'R_{ESR}' is also from few ohms to mili-ohm range. Thus, $R_P >> R_{Lead}^{+}, R_{ESR}, R_{Lead}^{-}$. So one can relate R_P as;

$$R'_{eq} \cong R_P \tag{5.37}$$

Thus, to evaluate 'R_P', potentiostatic measurements may be carried out at relatively higher intervals.

The value of capacitance can be calculated when the capacitor is fully charged i.e. $\lim_{t\to\infty}$. The instantaneous value of capacitance can be measured from the relation given in equation 5.38.

$$C_{inst} = \frac{I_{inst}}{\frac{dV}{dt}} \tag{5.38}$$

Where 'C_{inst}' is the instantaneous capacitance, 'I_{inst}' is the instantaneous current, 'V' is the applied voltage and 't' is the instantaneous time.

R_{ESR}' as known from the literature, can be determined from I(t) graph at maximum peak current [353]. In our case as shown in Fig 5.19, for 300K and 1V charging voltage pulse, the value of maximum current (near zero seconds) is about 15.2 μA. Thus, the value of 'R_{ESR}' would be 1V/(15.2μA)=65.7kΩ. As the 'R_{ESR}' is the ohmic resistance [359-360], this resistance would never reach practically closed to the value obtained. Thus, to properly envisage this specific 'R_{ESR}' the current would be measured when limit of $t\to0$ is applied. For practical applications; this time may be around pico and femto second's interval. To capture the current at such small intervals, very fast Analog to Digital Converters (ADC) are required. On contrary, even if the powerful instrument measure that interval, still the value of 'R_{ESR}' would never be estimated, as per Fig 5.22(c). The current during this particular interval would be due to the R_{lead}^{+}, R_{ESR} and R_{lead}^{-}. Thus, the method suggested for lead free resistance as shown in Fig 5.23 may prove to be way forward. However, the value of 'R_p' can be preferably predicated from final current when $\lim_{t\to\infty}$ and can be evaluated from

Equation. (5.37). For 300K and 1V charging pulse the value of 'R_p' is calculated as ~656kΩ. The case wise magnitudes of 'R_p' at multi-charging voltage pulses and multi-temperatures are calculated and are reported in Table 5.3.

Table 5.3: Parallel Resistance magnitudes measured from potentiostatic DC Analysis

Sr#	Voltage	@290K	@300K	@310K	@320K	@330K	@340K	@350K
01	0.1V	6.33E5	5.21E5	2.84E5	7.10E5	5.45E5	7.52E6	3.28E5
02	0.2V	6.80E8	5.80E6	2.40E6	3.57E7	1.28E7	2.16E6	1.28E7
03	0.3V	2.28E6	8.20E6	1.80E7	3.98E6	3.36E6	1.70E6	2.53E6
04	0.4V	2.28E6	3.50E6	3.60E6	2.52E6	2.15E6	1.42E6	1.48E6
05	0.5V	1.98E6	2.20E6	2.20E6	2.00E6	1.77E6	1.20E6	1.22E6
06	0.6V	1.57E6	1.50E6	1.79 E6	1.74E6	1.41E6	1.14 E6	9.9.E5
07	0.7V	1.20E6	1.09E6	1.40E6	1.37E6	1.16E5	9.80E5	8.20E5
08	0.8V	9.40E5	8.83E5	1.05E6	1.13E6	9.92E5	8.59E5	7.10E5
09	0.9V	7.90E5	7.46E5	8.86E5	9.76E5	8.93E5	7.96E5	6.35E5
10	1.0V	7.20E5	6.50E5	7.96E5	8.72E5	8.01E5	7.14E5	5.70E5

In order to inspect the thermal stability of capacitance and parallel resistance magnitudes, we have to visualize respective parameters at multi-ambient temperatures. Fig 5.24-II (a) (b) shows the effective capacitance and parallel resistance (R_p) magnitude which are calculated while applying the limit $t \rightarrow \infty$.

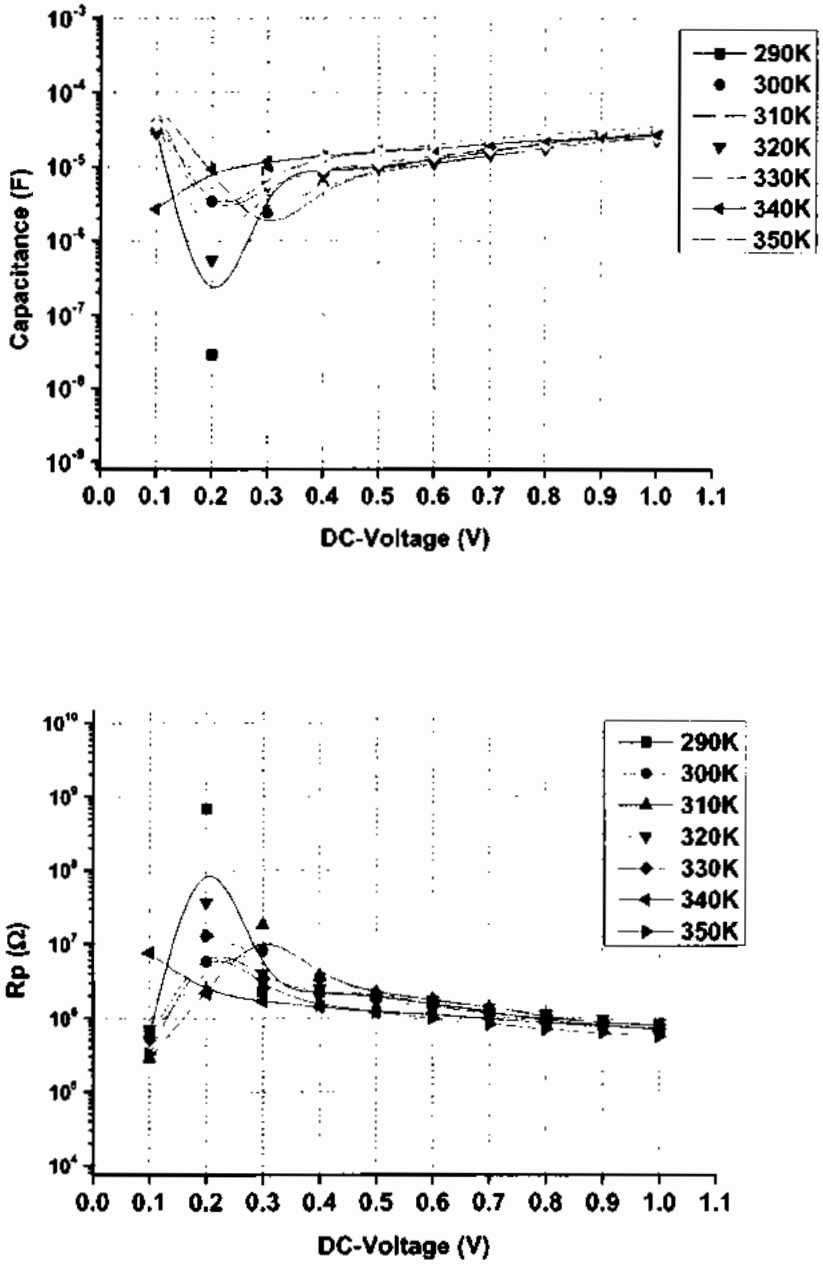

Fig 5.24-II: Effect of the ambient temperature on stretchable supercapacitor performance parameters. (a) Effect of the DC voltage on effective capacitance at multi temperature. (b) Effect of the DC voltage on Parallel resistance at multiple temperatures

From Fig 5.24-II, one can observe that the value of effective capacitance and the parallel resistance magnitude are stable at 0.5V - 1V of charging pulses. It is evident that during discharge event the capacitance is responsible to decreases the voltage from 1V- 0.5V (discharge event). The connected load tends to stabilize itself by supercapacitor but after 0.5V i.e. 0.5V – 0.1V of discharge event the stability over temperature loses.

Another approach for mapping 'R_p' and equivalent capacitance 'C_{eq}' is the AC analysis of stretchable/foldable supercapacitor. It is established that the supercapacitor is charged under DC biased only but the load connected with it may be active (resistive) or passive (capacitive or inductive) in nature. Thus, in order to see the small AC-signals, one needs to properly polarize the supercapacitor under AC drift mechanism. The AC-test signal, alone, would have no importance because the main objective is to gauge both the capacitance and the self-discharge parasitic resistance. Thus, we have to superimpose AC-signal of specific amplitude and vary the frequency of that signal. From data logging perspective, we will record the real and imaginary part of Impedances to practically gauge the physical extent of 'R_P' and effective capacitance magnitude under such AC-conditions. The electrical charge will be pumped into the said stretchable/foldable supercapacitor by adding an AC-source off-setted with respective direct current voltage source. The electronic circuit diagram for the proposed assembly is sketched and shown in Fig 5.25.

There are three main sections of AC-Equivalent power source for the stretchable supercapacitor i.e. power section, wiring section and the supercapacitor itself. The spectral response of each drift source for charge pumping into the stretchable supercapacitor is shown in Fig 5.26. In Fig 5.26(c), this can be analyzed that the instantaneous voltage fluctuates its level at a particular DC-offset. In order to find equivalent voltage of fixed level V_{eq}, one should determine that specific voltage.

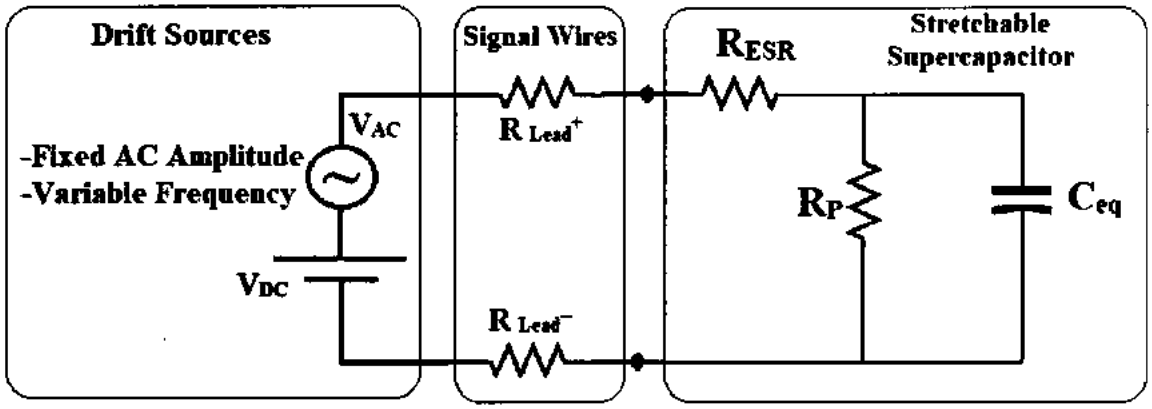

Fig 5.25: AC-induced power source for measuring stretchable super-capacitor: Proposed Assembly

Following expressions are used to find out the particular solutions for the determination of V_{eq}.

$$\text{DC voltage level} = V_{DC} \tag{5.39}$$

$$\text{AC maximum voltage Level} = V_{AC} \tag{5.40}$$

The instantaneous level of DC voltage will remain fixed, however the instantaneous value of AC voltage will be varied as;

$$V_{i(AC)} = V_{AC} \sin\omega t \tag{5.41}$$

Where 'ω' is the angular frequency (i.e. $\omega = 2\pi f$), similarly $V_{i(DC)} = V_{DC}$.

The effective value of both sources will be the instantaneous addition of both voltage sources as shown in Fig 5.26 (c).

$$V_{effective} = V_{i(DC)} + V_{i(AC)} \tag{5.42}$$

From Equation (5.41) and Equation (5.42),

$$V_{effective} = V_{DC} + V_{AC} \sin\omega t \tag{5.43}$$

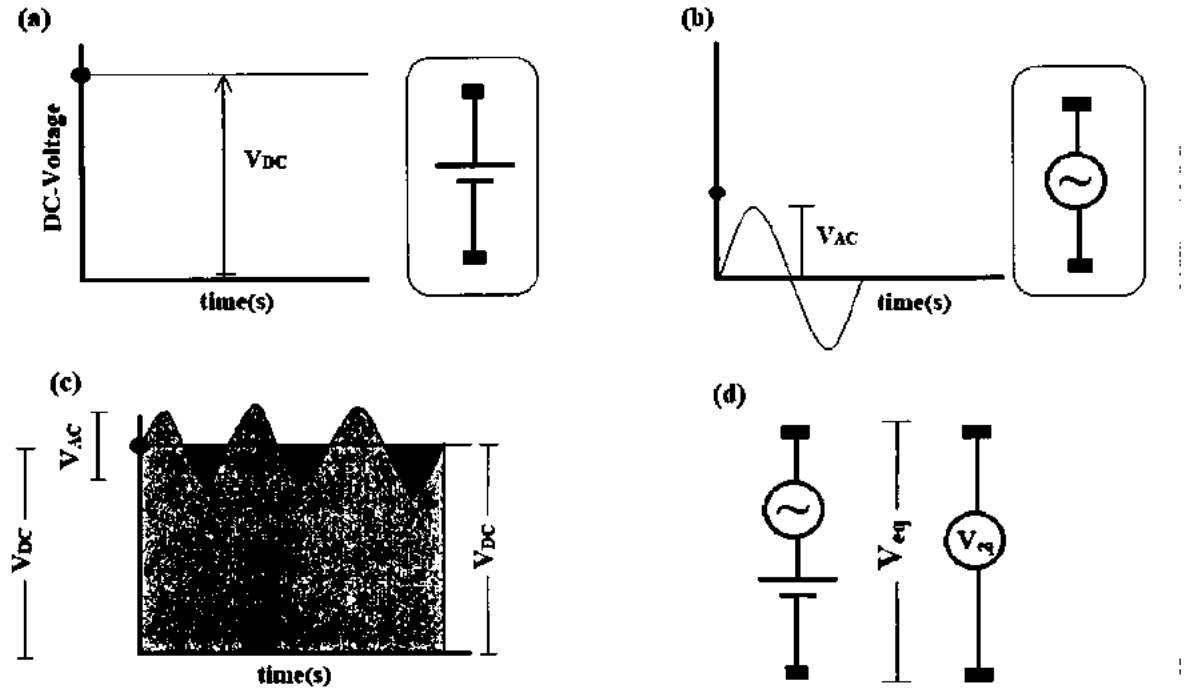

Fig 5.26: Spectral response of individual and combine voltages for charging of super-capacitor, (a) DC-voltage spectral response. (b) AC- Voltage spectral response. (c) Spectral response of off-setted AC combined voltage and red colored part shows the DC-level clipping due to negative half of AC. (d) Equivalent voltage source for charging super-capacitors

Equation (5.43) is equalized form of Fig 5.26(c), but we have to find a fixed equivalent voltage level as shown in Fig 5.26(d). The equivalent voltage (V_{eq}) is actually the overall Root Mean Square (RMS) magnitude of both sources and can be related with effective voltage 'V_{eq}' as [361];

$$(V_{Eq})^2 = \frac{1}{T}\int_0^T \left(V_{effective}{}^2\right)dt \qquad (5.44)$$

Where 'T' is the time period of AC-signal, and after putting the value of $V_{effective}$, we get

$$(V_{Eq})^2 = \frac{1}{T}\int_0^T (V_{DC} + V_{AC}\sin\omega t)^2 dt \qquad (5.45)$$

As $(a+b)^2 = a^2+b^2+2ab$, so,

$$(V_{Eq})^2 = \frac{1}{T}\left[\int_0^T (V_{DC}{}^2 + V_{AC}{}^2 \sin^2\omega t + 2V_{DC}\, V_{AC} \sin\omega t)dt\right] \quad (5.46)$$

$$(V_{Eq})^2 = \frac{1}{T}\left[\int_0^T V_{DC}{}^2 dt + \int_0^T V_{AC}{}^2 \sin^2\omega t dt + \int_0^T 2V_{DC}\, V_{AC} \sin\omega t)dt\right] \quad (5.47)$$

As 'V_{DC}' and 'V_{AC}' are fixed or constant, thus they can be separated from the integral part as;

$$(V_{Eq})^2 = \frac{1}{T}\left[V_{DC}{}^2 \int_0^T dt + V_{AC}{}^2 \int_0^T \sin^2\omega t dt + 2V_{DC}\, V_{AC} \int_0^T \sin\omega t)dt\right] \quad (5.48)$$

As, $\sin^2\omega t = \frac{1-Cos2\omega t}{2}$ and $\int \sin\omega t dt = -\frac{cos\omega t}{\omega}$

$$(V_{Eq})^2 = \frac{1}{T}\left[V_{DC}{}^2 [t]_0^T + V_{AC}{}^2 \int_0^T \frac{1-Cos2\omega t}{2} dt + 2V_{DC}\, V_{AC} \left(-\frac{cos\omega t}{\omega}\right)_0^T\right] \quad (5.49)$$

$$(V_{Eq})^2 = \frac{1}{T}\left[V_{DC}{}^2 T + V_{AC}{}^2 \left[\int_0^T \frac{1}{2} dt - \int_0^T \frac{Cos2\omega t}{2} dt\right] + 2V_{DC}\, V_{AC} \left(-\frac{cos\omega t}{\omega}\right)_0^T\right] \quad (5.50)$$

The term $\left(-\frac{cos\omega t}{\omega}\right)_0^T = 0$, and $\int_0^T \frac{Cos2\omega t}{2} dt = 0$, putting the values, we get:

$$(V_{Eq})^2 = \frac{1}{T}\left[V_{DC}{}^2 T + V_{AC}{}^2 \left[\int_0^T \frac{1}{2} dt - 0\right] + 2V_{DC}\, V_{AC}(0)\right] \quad (5.51)$$

$$(V_{Eq})^2 = \frac{1}{T}\left[V_{DC}{}^2 T + V_{AC}{}^2 (\frac{1}{2} T)\right] \quad (5.52)$$

$$(V_{Eq})^2 = \frac{1}{T} T \left[V_{DC}{}^2 + \frac{V_{AC}{}^2}{2}\right] \quad (5.53)$$

$$(V_{Eq})^2 = \left[V_{DC}{}^2 + \frac{V_{AC}{}^2}{2}\right] \quad (5.54)$$

$$V_{Eq} = \sqrt{(V_{DC}{}^2 + \frac{V_{AC}{}^2}{2})} \quad (5.55)$$

Thus Equation (5.55), provides the "particular solution" for equivalent voltage source magnitude (i.e. $\sqrt{{V_{DC}}^2 + \frac{{V_{AC}}^2}{2}}$) for evaluating the internal element of supercapacitors (i.e. active and passive elements).

From Equation (5.18) and Fig 5.25; we conclude that the value of total impedance "Z_{AB}" of the supercapacitor depends upon the applied frequency of the AC-source as shown in Fig 5.25.

The circuit diagram for evaluating the impedance of supercapacitor through combined effect of voltage sources as evaluated from Equation 5.55 as shown in Fig 5.27.

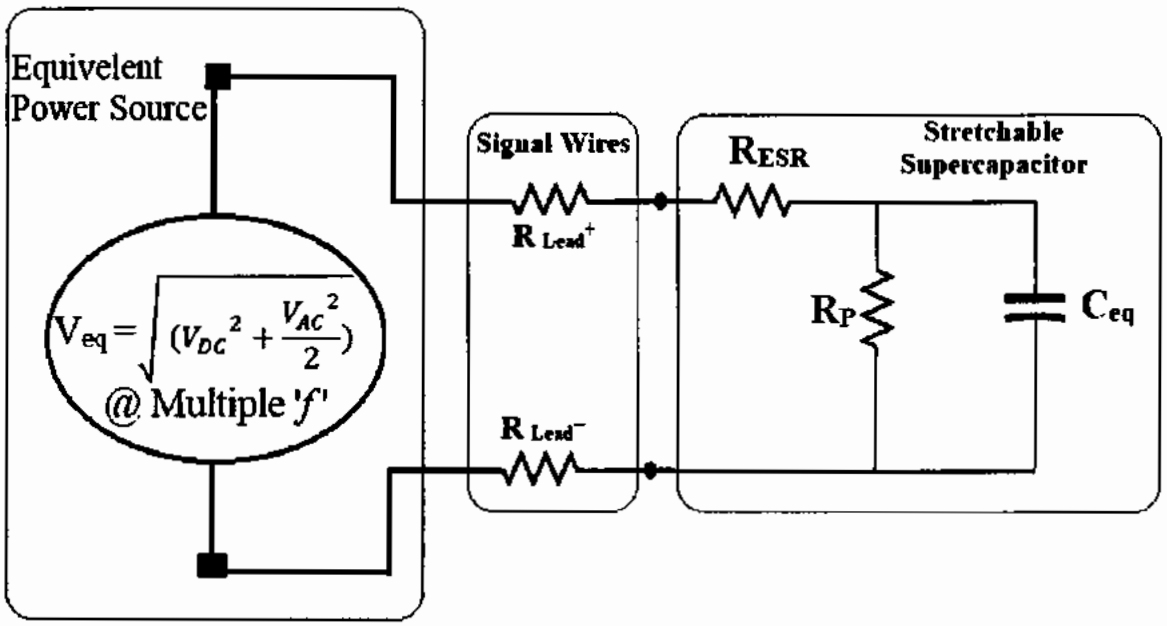

Fig 5.27: Supercapacitor's Equivalent Circuit coupled with Equivalent Voltage Source.

For this Analysis we have characterized said supercapacitor using potentiostatic based Electrochemical Impedance Spectroscopy (EIS). For this, we have fixed the AC amplitude of V_{AC}= 100mV and vary the frequency range from 10 mHz to 10 kHz at same multi-charge DC pulses of $0.1V_{DC}$ to $1V_{DC}$. Thus, from Equation 5.18:

$$=> |Z_{AB}| = \sqrt{(R_{ESR})^2 + \frac{(R_P)}{1+j4\pi f C_{eq}\, Rp - 4\pi^2 f^2 C_{eq}{}^2 Rp^2}^2} \quad (5.18)$$

As impedance Z_{AB} of overall supercapacitors equivalent circuit depends upon the value of frequency 'f' and the equivalent voltage source (from Equation 5.55) as; for V_{AC}=100mV and V_{DC} varies at multi-spectrum. For these boundary conditions of charging source, we have evaluated the real and imaginary impedances from EIS characterization, as a function of frequency spectrum range and are shown in Fig 5.18.

As in DC analysis, we applied the limits of zero and Infinity on I(t) measurements. Likewise, in AC- analysis we have to apply mathematical limits on Frequency domain, and Thevenin's equivalent of 'Z_{AB}' of equation 5.18.

When $\lim_{f\to 0}$ then equation 5.18 becomes as:

$$\lim_{f\to 0}|Z_{AB}| = \lim_{f\to 0}\sqrt{(R_{ESR})^2 + \frac{(R_P)}{1+j4\pi f C_{eq}\, R_P - 4\pi^2 f^2 C_{eq}{}^2 R_P{}^2}^2} \quad (5.56)$$

$$\lim_{f\to 0}|Z_{AB}| = \sqrt{(R_{ESR})^2 + \frac{(R_P)}{1+j4\pi \lim_{f\to 0} f C_{eq}\, R_P - 4\pi^2 \lim_{f\to 0} f^2 C_{eq}{}^2 R_P{}^2}^2} \quad (5.57)$$

The term $\lim_{f\to 0}$(f)=0, then

$$\lim_{f\to 0}|Z_{AB}| = \sqrt{(R_{ESR})^2 + \frac{(R_P)}{1+0-0}^2} \quad (5.58)$$

$$\lim_{f\to 0}|Z_{AB}| = \sqrt{(R_{ESR})^2 + (R_P)^2} \quad (5.59)$$

As, $R_{ESR} << R_P$, Thus the term 'R_{ESR}' can be neglected

$$\lim_{f\to 0}|Z_{AB}| = \sqrt{((R_P))^2} = R_P \quad (5.60)$$

Whereas; when $\lim_{f\to\infty}$, the term $\lim_{f\to\infty} f = \infty$, and

$$\lim_{f\to\infty}|Z_{AB}| = \sqrt{(R_{ESR})^2 + \frac{(R_P)^2}{\infty}} \tag{5.61}$$

$$\lim_{f\to\infty}|Z_{AB}| = \sqrt{(R_{ESR})^2 + 0} \tag{5.62}$$

$$\lim_{f\to\infty}|Z_{AB}| = R_{ESR} \tag{5.63}$$

Thus, when one may increase the frequency of the AC source, the capacitor's reactance (impedance) becomes low enough and the serially connected R_{ESR} can be determined. But in any case, we can't measure exact value of R_{ESR} because of the wiring resistance as already explained at length (as referred in Equation. 5.25).

When we apply these limits (as derived from Equation 5.60 and 5.63), on experimental data measured using EIS analysis (as shown in Fig 5.18(a)); the value of 'R_P' can be estimated from the real Z vs frequency spectra intercepts at lower limit of frequency i.e. at 10 mHz (as $\lim_{f\to 0}$). Also, the capacitance magnitudes can be determined from the imaginary part of Impedance versus frequency graph (as shown in Fig 5.18-b). As the values of R_{ESR} are very small, the capacitance of the capacitor can directly be equalized as;

$$j\,Z_{imaginary} = X_c = \frac{1}{j2\pi fC} \tag{5.64}$$

where the capacitive reactance 'j' is the complex term

$$j^2\,Z_{imaginary} = \frac{1}{2\pi fC} \tag{5.65}$$

as mathematically $j^2 = -1$, so

$$-Z_{imaginary} = X_c = \frac{1}{2\pi fC} \tag{5.66}$$

From EIS analysis we have evaluated the spectra of $-Z_{Imaginary}$ vs frequency (as shown in Fig 5.18-b). Thus, the value of capacitance can be determined as:

$$C = \frac{1}{2\pi f|-Z_{imaginary}|} \tag{5.67}$$

From Equation. (5.67), the maximum value of capacitance can be determined from the minimum value of frequency $-Z_{Imaginary}$ graph.

Thus, to see the extent of AC and DC analysis as also reported by Negroius et al. [362], on the same EIS technique but on multiple set of supercapacitors, we have provided the comparative nurture of both the techniques as shown in Fig 5.28.

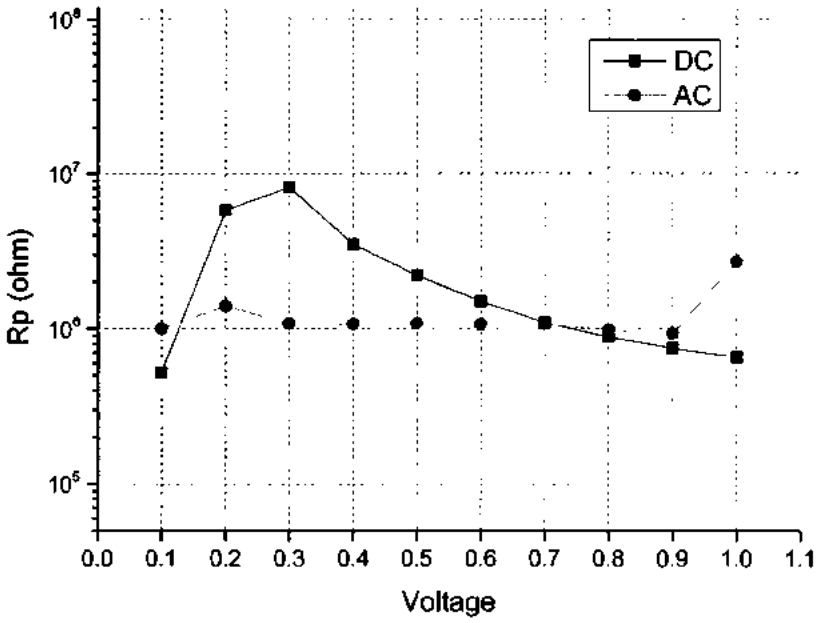

(a)

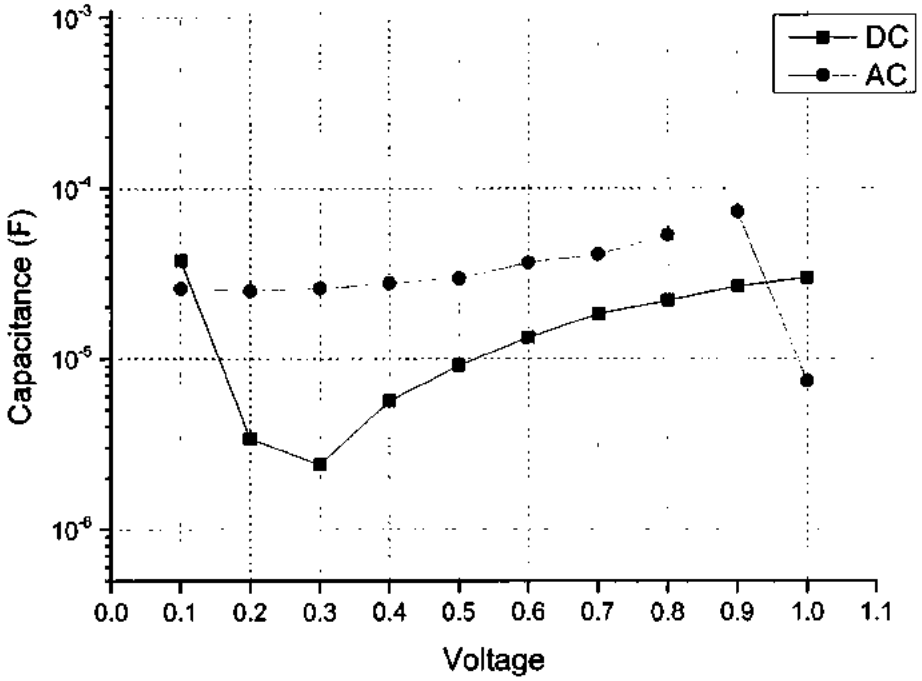

(b)

Fig 5.28: Comparative analysis of AC and DC technique for supercapacitors evaluation characteristic parameters, (a) comparative analysis of 'R_P' (b) Comparative analysis of 'C'

This can be visualized from Fig (5.28), that AC-method shows approximately same extent of magnitudes of both 'R_P' and 'C'. It is because that, the said supercapacitor is powered by both fluctuating AC and DC-offset voltages. From capacitance point of view, the value of DC technique shows the rapid fall when voltage decreases (in discharge mode) when compared with AC-mode. This is because the AC-source is continuously influenced by the applied frequency on the capacitance element, more actively as compared to 'R_P'.In addition, alternating source's frequency does not alter the resistive elements.

5.4 PVA-KOH Gel Electrolyte Based Supercapacitor

Herein, a specialized PVA-KOH electrolyte has been synthesized to fabricate the super-capacitor with activated Carbon and graphene ink as an electrode. After successful fabrication

of said super-capacitor, the initial charge cycle of 1Volt have been spanned to record the discharge spectra on current and voltage scales separately. For electrical characterization, we have used multiple techniques in order to assess the said PVA electrolyte including Electrochemical Impedance Spectroscopy (EIS), Nyquist Plots, Current-Voltage and Charge Deep Level Transient Spectroscopy (Q-DLTS). Scanning Electron Microscope (SEM), Electron Dispersive Spectroscopy (EDS), Photo-Luminescence (PL) and Atomic Force Microscopy (AFM) are also utilized to provide supplementary information to understand the device functionality in a better way.

5.4.1 Experimental

For the synthesis and fabrication of said super-capacitor, polymer sheet and dense metal net are cleaved into 5 cm x 3cm structure and are stuck to each other making current collector of super-capacitor. The ohmic contacts were made using copper tape at the edges to make cathode and anode. The active material for electrodes are developed by the mixture of ink-based graphene flakes and the activated carbon. The one side (anode) of the activated carbon was chosen about 0.417g and is then encapsulated into the fabric (fabric mass = 0.191g) which have relatively larger pore size. This encapsulation may provide the mechanical stability over larger time spans. The PVA/KOH gel electrolyte was prepared by taking 5 grams (56.1056 g/mol) of KOH, 10 grams (44.05 g/mol) of PVA and are dissolved homogeneously in 150 ml of distilled water at 120 °C with continuous magnetic stirrer for ~ 10hrs. After successfully formation of homogenized solution, it was poured into Petri plates for drying. This process was cured again for ~10hrs. All chemicals was purchased from Sigma Aldrich. The fabrication steps are highlighted in Fig 5.29 below:

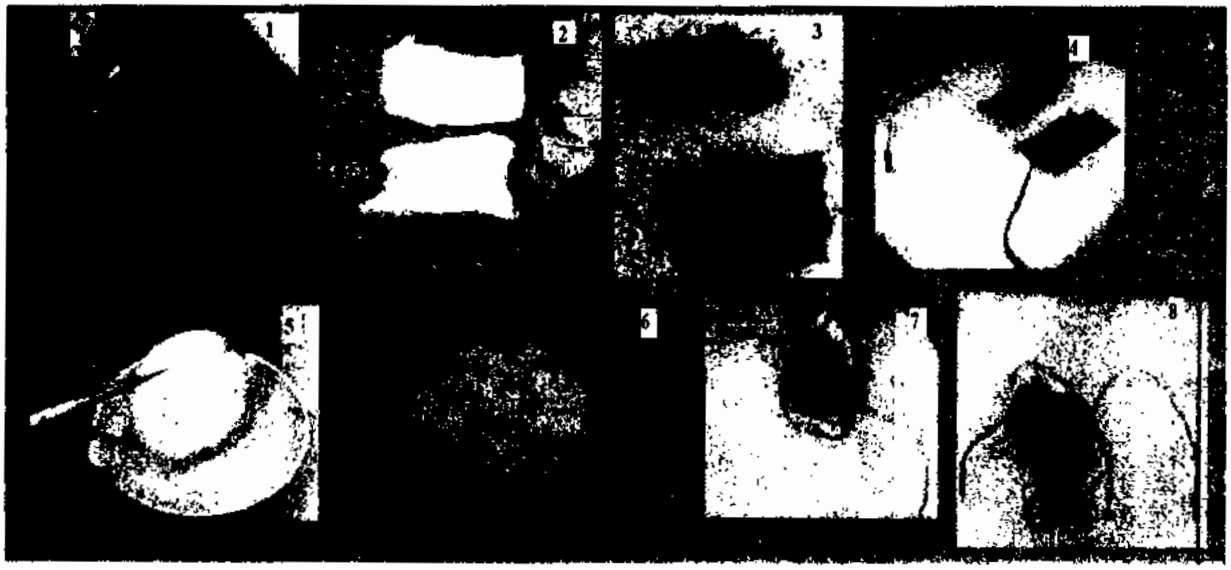

Fig 5.29: Fabrication steps of PVA based Super-capacitor, (1) Polymer sheets for encapsulation, (2) larger pore fabric for active material encapsulation, (3) Activated Carbon dropped with Graphene Ink, (4) Interconnection of Anode and Cathode with Copper wire, (5-6) PVA based Electrolyte, (7-8) Super-capacitor ready for charge/discharge activity

5.4.2 Characterization

Post –fabrication analysis of the device using the standard imaging/microscopy techniques was carried out as initial diagnostic test for detailed electrical and charge-based evaluation. The scanning electron microscope (SEM) imaging of each active region of PVA based super-capacitor are shown in Fig 5.30. It is analyzed from Fig 5.30 that there is a huge difference of contrast between standalone activated carbon and graphene induced one i.e. high level of contrast is a signature of high conductivity when compared with other elements. For elemental analysis, Electron Dispersive Spectroscopy (EDS) analysis has been performed and shown in Fig 5.31 It is noticed that dense metal net is the alloy of different active metals i.e. Fe, Cr, and Co. The EDS analysis of PVA electrolyte shows the presence of potassium (K) and oxygen (O) elements along with Carbon.

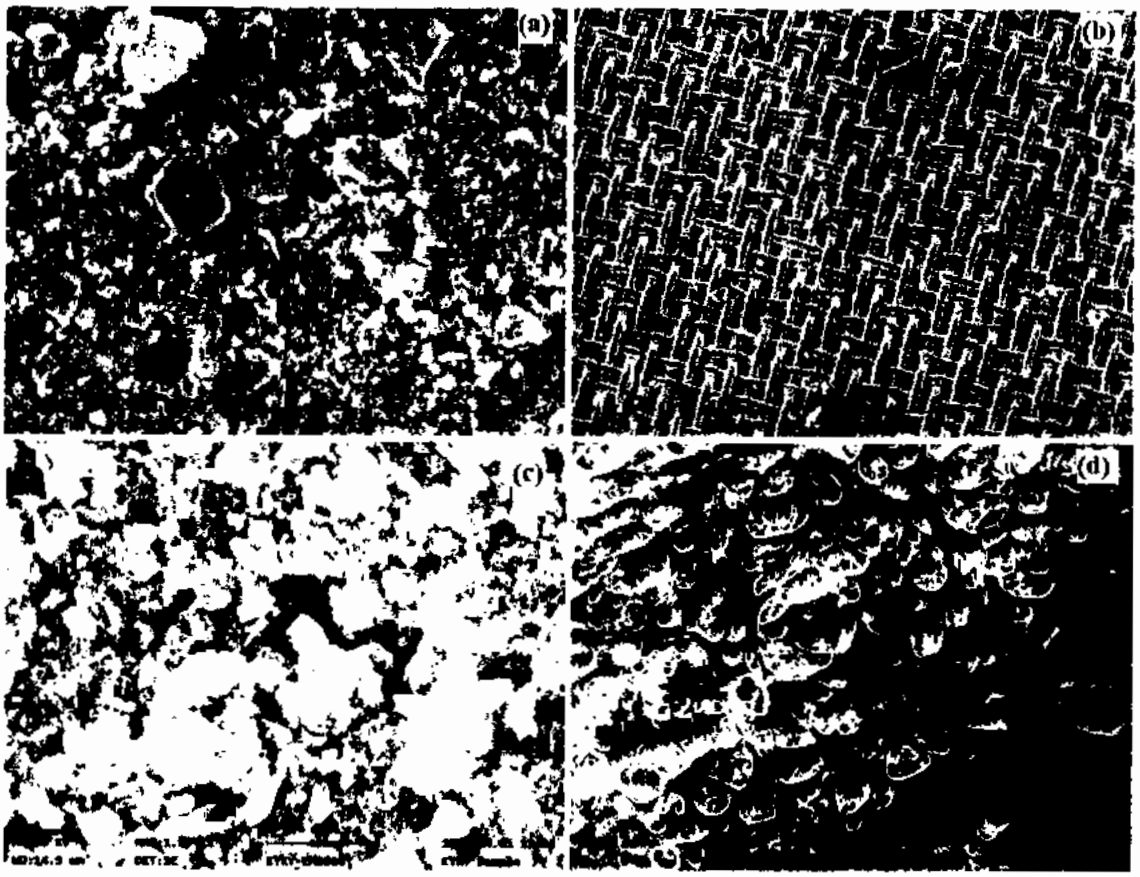

Fig 5.30: SEM imaging of PVA based super-capacitor's elements, (a) Activated carbon mixed with graphene ink, (b) dense metal net, (c) standalone activated carbon and (d) PVA electrolyte

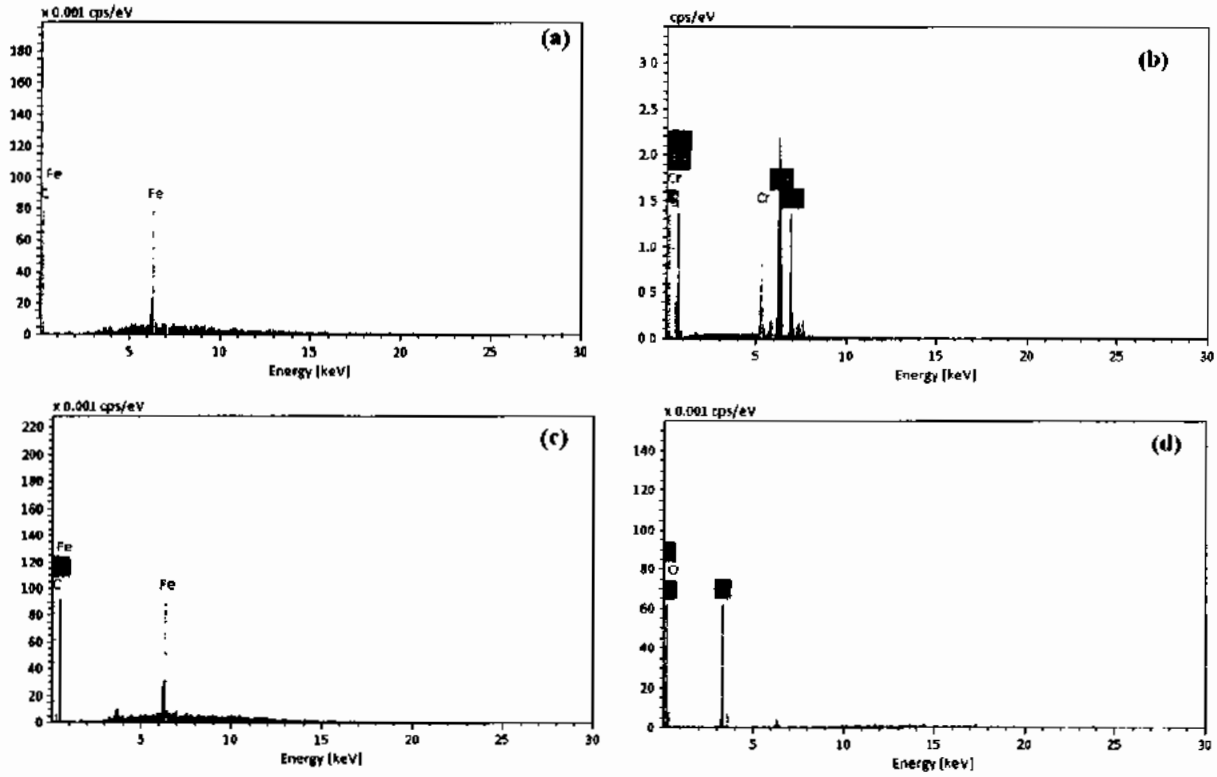

Fig 5.31: EDS analysis of PVA based super-capacitor's elements, (a) Activated carbon mixed with graphene ink, (b) dense metal net, (c) standalone activated carbon and (d) PVA electrolyte

In order to map the surface roughness of electrolyte, Atomic Force Microscopy (AFM) was performed on said PVA layer and is shown in Fig 5.32. AFM image indicates that number of small sized pores are available within the device region that may act as the conduction as well as diffusion centers against charge carriers and ions, respectively.

Fig 5.32: AFM image of PVA electrolyte

After successful fabrication and encapsulation of PVA based super-capacitor, it is tested on different physical loads. There are two physical loads considered for this purpose i.e. Full Load and No Load. In "Full Load", the impedance of the derived circuit is subjected to absolute value which may be about less than 1 ohm i.e. maximum current can flow through the external circuitry for which subject super-capacitor behaves as charge source. In "No Load", the impedance of the external circuit is kept to ~100 MΩ (very high) i.e. no current can flow to the external circuit. In both cases (Full Load and No Load) the current and voltage magnitudes have been observed. In order to gauge these practical limits, one has coupled '*Ammeter*' is coupled for gauging full load electric currents. This is because of fact that the internal resistance of '*Ammeter*' is extremely low. For gauging the voltage of the super-capacitor, the input of Analog-to-Digital Converter (ADC) is measured because the input resistance of ATMega328 ADC is ~100MΩ [363]. Fig 5.33 shows the schematic diagram and it's *Full* and *No load* circuits operated by the fabricated PVA based Super-capacitor.

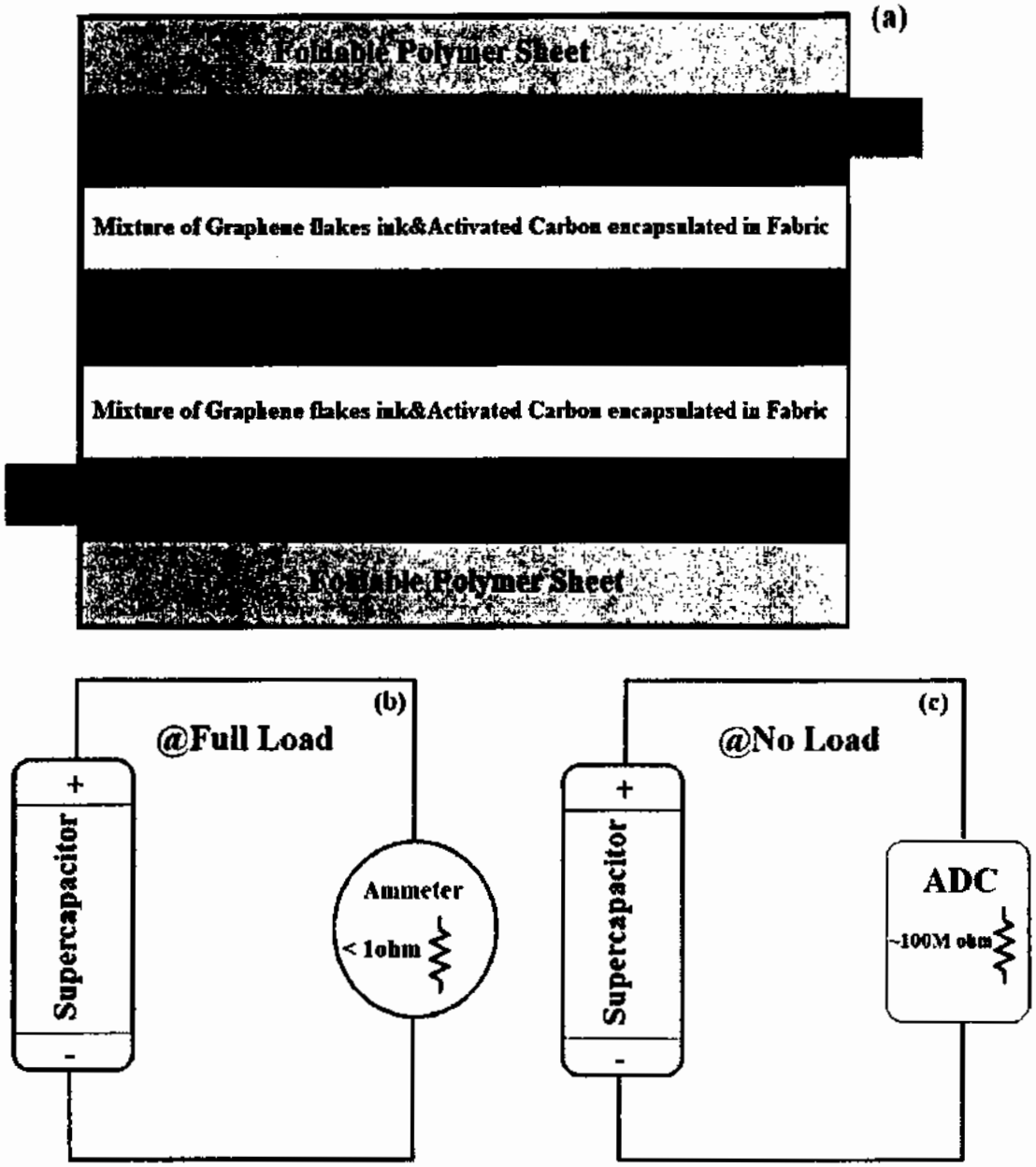

Fig 5.33: Schematic diagram of PVA + KOH based SC, (a) Layer wise structure of SC, (b) Full load equivalent circuit of SC, (c) No Load equivalent circuit

For practical perspectives, the super-capacitor is physically charged at 1 volt using Switch Mode Power Supply (SMPS) for a 1 minute duration. After charging, the discharge nature is inspected and the full load current and no load voltages are scanned, respectively. Fig 5.34 shows the discharge current and voltage characteristics as function of time. During discharge analysis, each parameter has been recorded at ~30 minutes span. For current and voltage measurements, a FLUKE 15B and ATMega328P Integrated Chip (IC) has been used, respectively.

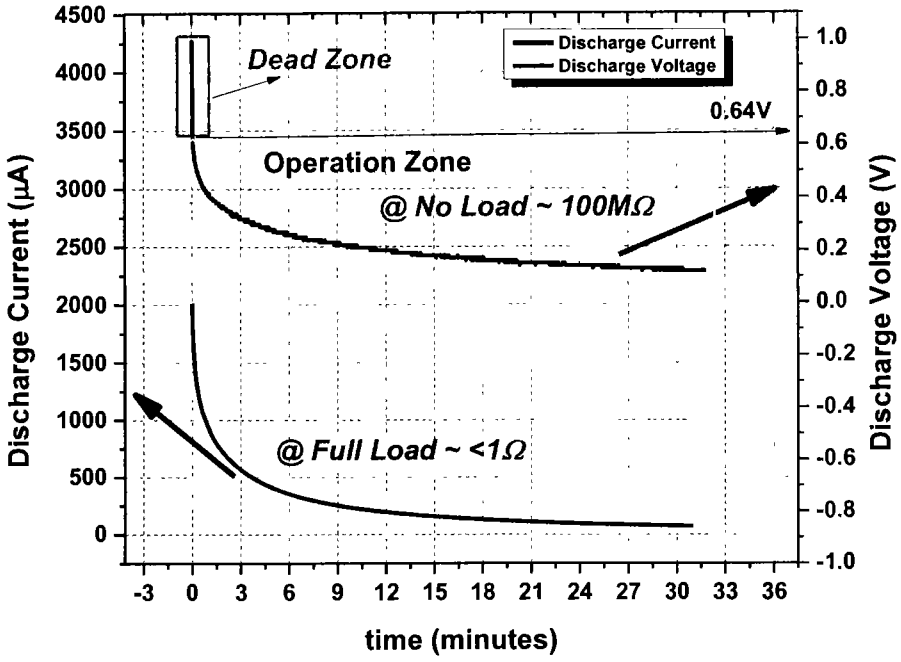

Fig 5.34: Discharge characteristics at Full and No Load conditions

In order to gauge the extent of voltage sustainability, the discharge voltage curve at no load is shown in Fig 5.34. This has been noticed from discharge voltage spectra that as soon as the charging source was removed, the initial discharge voltage level suddenly decreased from 1 volts to ~0.64V. This rapid initial discharge is due to the possible trap centers placed within the band gap of PVA based electrolyte. This possibly due to the fact that whenever the charging voltage drops the columbic charges recombine themselves at a relatively low energy level rather than the entire band gap energy (which will be explained at length in next section). Thus, an eventual rapid drop of voltage is observed. During this time span, whenever the voltage drops, we call it as 'Dead Zone' because in this time interval no voltage can be sensed at the load terminals. After the 'Dead Zone' interval, the extent of charge is going to decrease at the internal self-discharge resistance [356], thus, the voltage magnitude at the anode/cathode terminals falls. The stored charge in form of voltage sustains 0.64V to 0.2V at ~10 minutes duration which is called 'Operation Zone' of the super-capacitor. This magnitude may increase by increasing the cascade architecture of super-capacitor's network. For discharge current magnitude, literature [6] has suggested that super-capacitor may be inspected at variable physical resistive loads i.e. higher the load resistance larger will be the charge storage capability [6]. However, in this study, we plan to apply maximum load (i.e. extremely low resistance) in order to asses as to how much time is needed to fully discharge the said PVA based super-capacitor at full physical loads. Fig 5.34 shows that discharge current

magnitude falls exponentially from 2000μA - 10μA within ~30 minutes span. For low current applications, this may provide significant time power backup at just 1 minute of charging. If one's application needs relatively higher currents i.e. ~ 2mA-0.5mA; this super-capacitor may provide it for 3 minutes. If physical load needs the power for a larger time duration, one needs to add more super-capacitor in a parallel fashion. The electrical circuitry of the subject electrical loads is depicted in Fig 5.35. This can be visualized that super-capacitor is connected with 1Volt charging source for ~1minute and after this interval the selector knob revives to the physical load and super-capacitor discharges itself on that specific load.

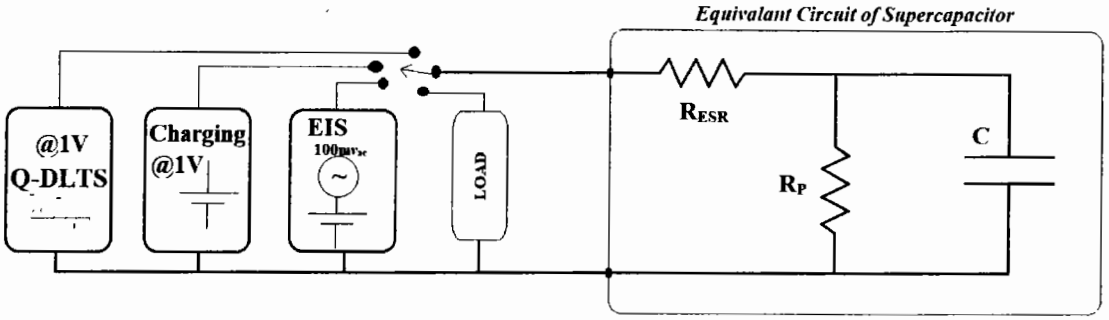

Fig 5.35: Electrical schematic overview of the super-capacitor's equivalent circuit and the test bench

In order to see the impact of PVA based said electrolyte on the charge transfer mechanism and impact of graphene based activated carbon electrode; Electro-Chemical Impedance (EIS) is used as diagnostic technique. In this technique, oscillating electric potential superimposed onto the desired DC potential and the Impedance of the system can be calculated. It can be seen from Fig 5.34 that the discharge voltage continuously decreases exponentially from 1V to the level zero. During this time span, each voltage level impacts on the overall functionality of the super-capacitor. Fig 5.36 shows the pictorial diagram of the said super-capacitor at desired charged potential. Poly-Vinyl Alcohol (PVA) would act like a separator and the KOH splits into K^+ and OH^- ions during the charged state. Both ions may play a significant role during charge collection and storage mechanism. These ions form electronic double layers at the electrodes and the interface of electrolyte. The main advantage of this scheme is to provide high columbic interaction which separates opposite charges to reduce recombination at their interface and consequently causes larger time to store charge. Contrary to that fact, if the separator layer provides conduction to the collected charges as a result of diffusion of ions into the electrolyte; the

super-capacitor may self-discharge. Thus, higher the ionic conduction extent lower will be the charge storage time.

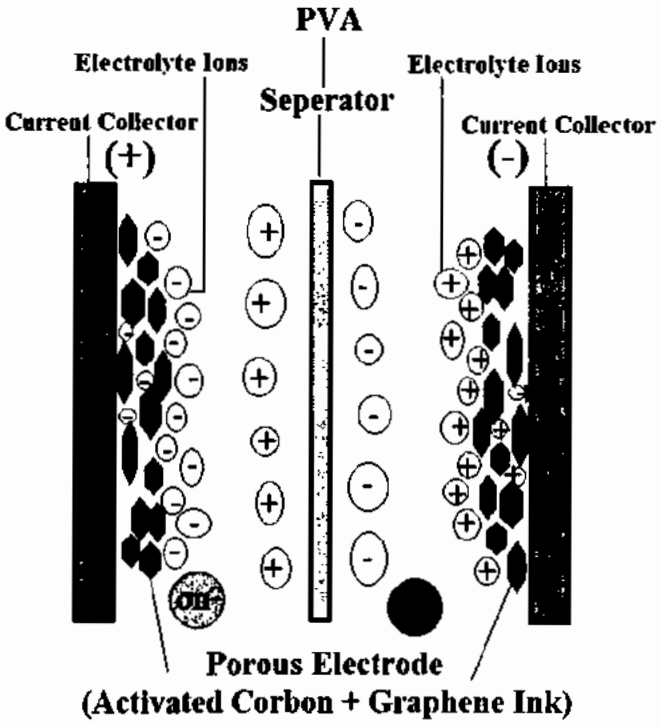

Fig 5.36: Ionic charge state for PVA and KOH based Electrolyte

In order to further understand this phenomena the Nyquist Plot obtained using EIS is presented in Fig 5.37. The plot shows the behavior of the fabricated super-capacitor at different DC charging potentials in order to evaluate the overall discharge mechanism that was reported in Fig 5.34. The Nyquist analysis has been performed at each particular bias and shown in Fig 5.37. Referring to Fig 5.35, when the super-capacitor knobbed at EIS terminals, this has indicated that the alternating signal was superimposed onto the DC level. In our work, we have fixed the amplitude of the AC source and varied the frequency ranging from 100mHz to 10kHz. At higher frequency, the capacitive element in Fig 5.35 shows almost short circuit to the relevant fluctuating signal and the electric current density is only limited by the value of R_{ESR}. However, at extremely lower frequency i.e. ~100mHz, the capacitive element provides maximum opposition to charge flow, thus, the current density is limited by both R_{ESR} and R_P.

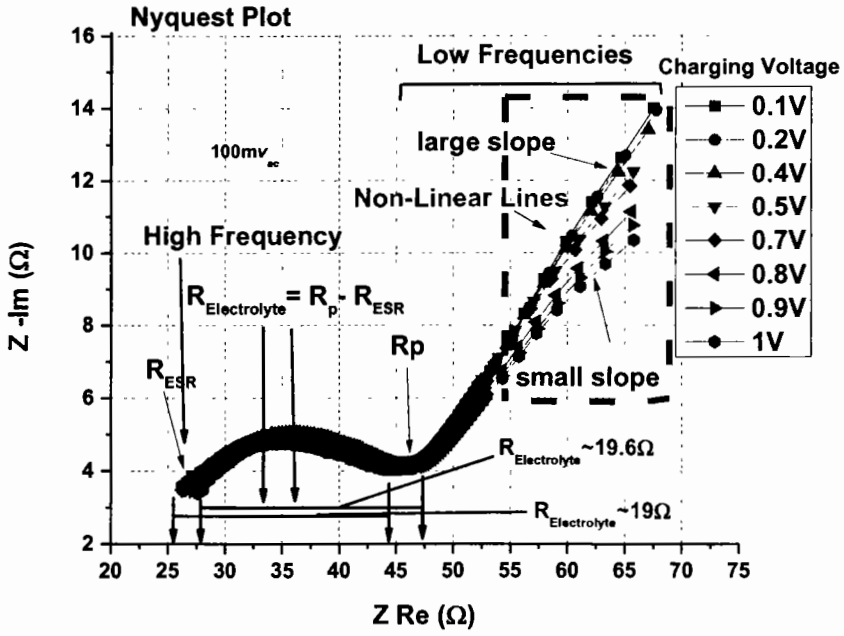

Fig 5.37: Nyquist Plot against each discharge DC potentials

Fig 5.37 shows the Rp and R_{ESR} magnitude on Real-Z scale. From this approach, one can calculate the electrolyte resistance which is ~19Ω for all said charging conditions. Physically, R_{ESR} value corresponds to the electrode resistance and Rp is the self-discharge resistance. The value of R_{ESR} should be as low as possible and Rp as high as possible for practical purposes (desirable functionality of super-capacitor). The value to R_{ESR} and Rp corresponds to 26-28Ω and 44-47.6Ω, respectively. For any super-capacitor 'Rp' is the danger mode of resistance because if its value is too small the super-capacitor may charge itself quickly but as soon as the charging source is removed it discharges itself very quickly because of lower Rp magnitude. For such case, we measured this value as 44.5-47.5Ω (Rp) for the fabricated super-capacitor. Another approach that can be predicted from Nyquist Plot of said super-capacitor is the non-linear region near the low-frequency scans i.e. how the charge is localized during the charging process. Fig 9 also points towards this specific nurture. Also, this phenomena is inspected from the slope of non-linear region i.e. if the slope is higher the charging process could be controlled by the Electronic Double Layer (EDL) formation and

if the slope is lower, the charging process could be limited by the ionic diffusion into the electrolyte itself [364]. For the PVA based super-capacitor in our case; the 0.7-1V charging voltages shows ionic diffusion which may limit the entire process. For relatively lower charging biases less than 0.7V the EDL mechanism may get strengthened and charge may be governed by this phenomena. While comparing this specific behavior with the discharge characteristics (Fig 5.34), the super-capacitor's voltage from 1V to 0.64V drops very quickly without any further electronic load and hence lie in the 'Dead Zone' i.e. no voltage signal can stay between this operational range (1-0.64V).

There are two possible directions of current flow which are highlighted in Fig 5.38. One is from x-axis to z-axis (*xz*) direction during charging mode of course as highlighted in Fig 5.34. Another critical dimension is *xy*-plane because there is electrical resistance in this plane of PVA electrolyte.

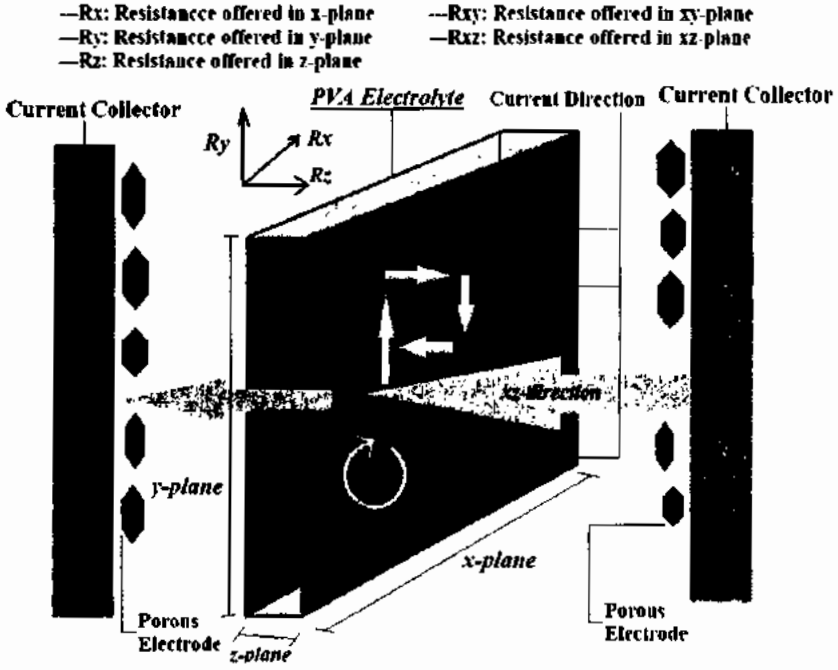

Fig 5.38: Direction of Current Flow with respect to geographical planes

In order to gauge this behaviour two points are probed at *xy*-plane and current-voltage (I-V) analysis is performed. The 1/slope of I-V curve provides the resistance between two points placed onto the plane i.e. ~100 kΩ at a temperature of 300K. For an optimum super-capacitor, the resistance of the electrolyte at *xy*-plane should be as high as possible because no charge

carrier may flow towards this plane. The current however flows (as shown in Fig 5.37) and may cause to reduce the energy of the charge carriers collected by the charging mechanism From band gap analysis perspective, the energy needed to conduct the collected charge carriers on *xy*-plane can be calculated by Arrhenius Equation 5.68 [319].

$$\sigma s = \sigma o e^{Ea/KT} \quad \text{(5.68)}$$

Where 'σ_s' is the conductance of the two points placed on the *xy*-plane at temperature '*T*' and 'σ_o' is the conductivity at absolute temperature, '*K*' is the Boltzmann constant and '*Ea*' is the activation energy needed to conduct the charge carrier (which should be as high as can be achieved). In order to calculate the activation energy of the fabricated device, it was probed at given *xy*-plane with current-voltage spectra recorded at 300-325K temperature range. The activation energy was calculated by the linear approximation of Equation 1 i.e. ~0.724eV. Fig 5.39 shows the current voltage analysis of subject PVA based super-capacitor at given temperatures.

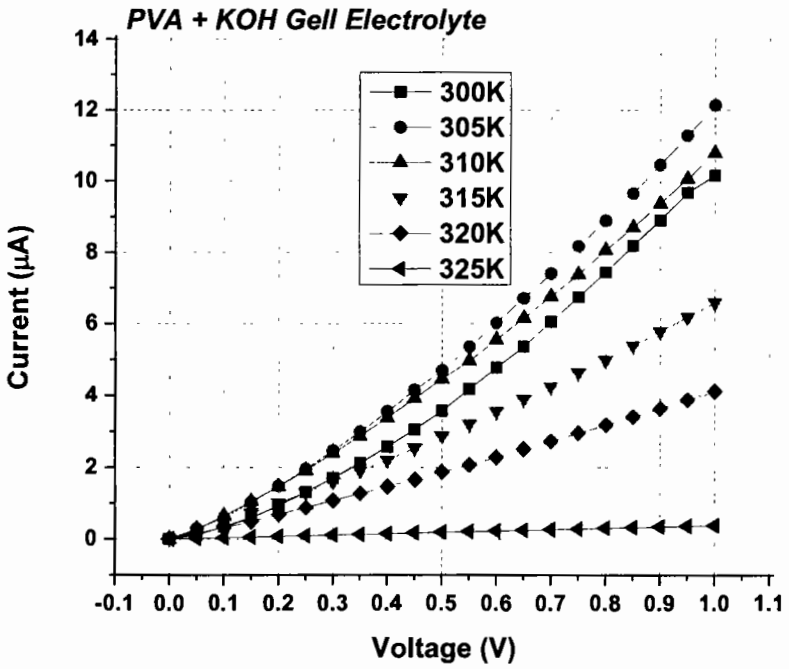

Fig 5.39: Current-Voltage analysis of PVA based Electrolyte at variable temperatures

The 'Dead Zone' (refer to Fig 5.34) is the region where charge does not become static at a given charging voltage which may due to the available trap centers that provide instant leakage path to the collected charge carriers. In order to locate the possible trap centers available within the PVA electrolyte, we have performed two different techniques i.e. Charge Deep Level Transient Spectroscopy (Q-DLTS) and Photo-Luminescence (PL) spectroscopy to help us understand it better.

Q-DLTS is the charge relaxation technique based on the measurement of transients produced during discharge time interval followed by required charging potential [365-367]. In our case, we have intentionally subjected the PVA electrolyte at ground zero potential and applied 1 V charging bias to the *xy*-plane for a limited duration of ~10ms. After this duration, the applied bias was removed and the device reduced its potential from 1V to the ground zero in a time duration known as 'Discharge time'. During this specific time interval the device reduced its voltage level followed by the charge transients. The overall Voltage-Charge (V-Q) curve concept of given technique has shown in Fig 5.40 below:

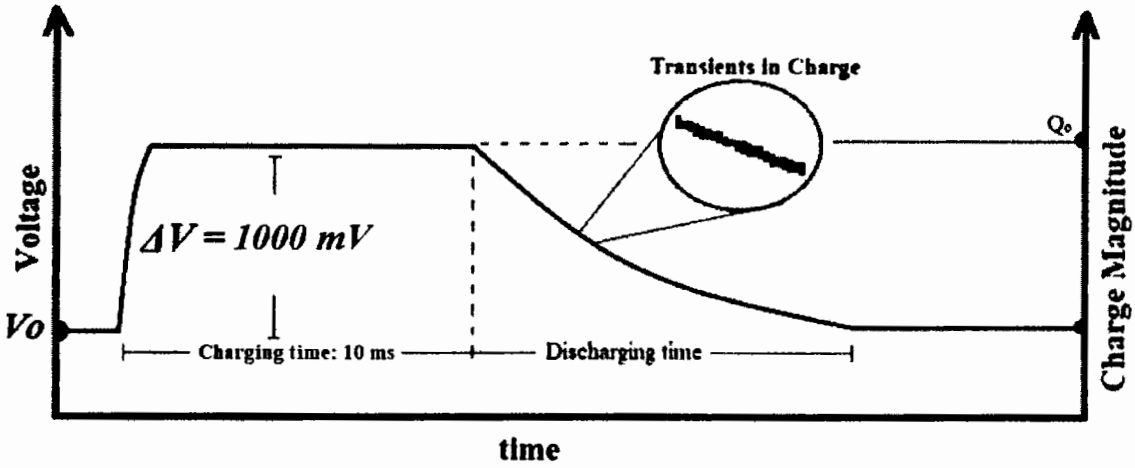

Fig 5.40: Voltage-Charge (V-Q) analysis of PVA based Electrolyte

From discharge events the change in the charge magnitude (ΔQ) was recorded and plotted as a function of special expression i.e. rate window (τ). This rate window is a function of time for which change in charge magnitude has been recorded i.e. the initial discharge time (t_1) and the final discharge time (t_2). In order to minimize phase-assisted errors, times t_2 and t_1 should be perfectly matched i.e. t_2/t_1 = constant.

Where 'e_n' is the emission rate of the charge carrier and can be related as:

$$e_n = \sigma\, 2\sqrt{3}\, \sqrt[3]{\frac{2\pi}{h^2}} k m_n T^2 \exp\left(-\frac{E_T}{kT}\right) \quad \text{(5.69)}$$

Where, 'σ' is the capture cross section, 'k' is the Boltzmann constant, 'm_n' is the effective mass of electron, 'T' is the temperature, 'h' is the plank's constant and 'E_T' is the trap level energy localized within the band gap of PVA.

For the trap level localization of such PVA electrolyte specifically associated to given 1V charging potential, one needs to scan Q-DLTS spectra against multiple temperature scans. The temperature window was chosen same as for current-voltage scenario. The Q-DLTS

scans of given PVA based electrolyte are shown in Fig 5.41. The maximum magnitude of the change in charge level against respective rate window (τ) points the trap center and its value can be emulated by linear approximation of Equation 5.69. From such analysis, one can find the trap level location and its respective capture cross section. The graphical representation of current-voltage and Q-DLTS based Arrhenius plots are shown in Fig 5.42.

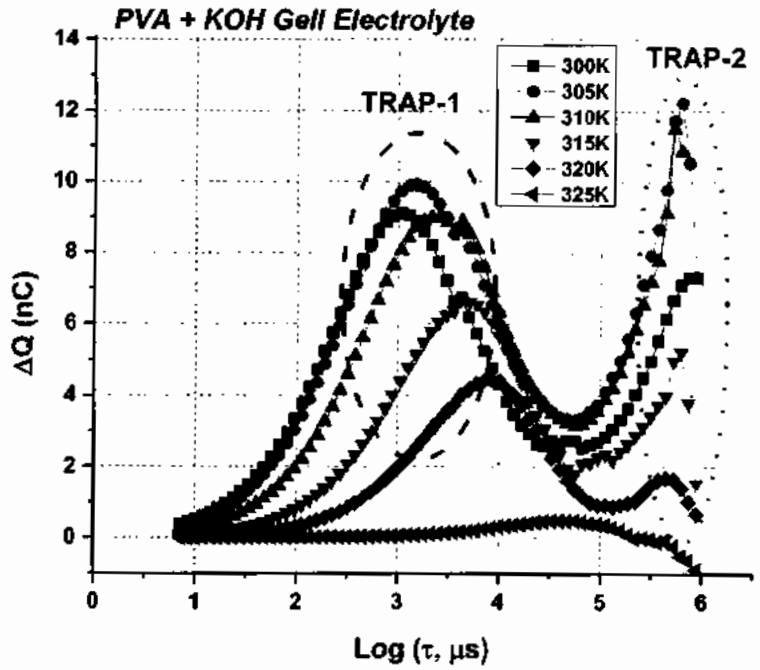

Fig 5.41: Q-DLTS scans of PVA based Electrolyte

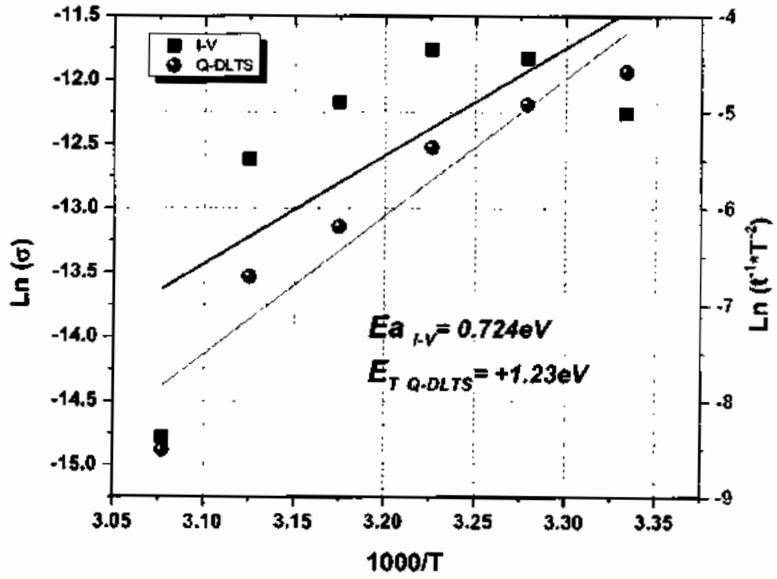

Fig 5.42: Arrhenius analysis of Current-voltage and Q-DLTS scans

The trap level sign is positive i.e. +1.23eV, which directs that this level is above the valance band edge (Ev+1.23eV). The capture cross section (with the units of 'area') actually corresponds to the power of said trap level. It is the ability of the trap to capture the free

charge carriers from its respective band edge, thus, higher the capture cross section higher will be the carrier loss at each respective trap position. In our case, the charge at 1V quickly diminish due to this specific trap energy level located into the PVA polymer.

High energy laser light of 325nm wavelength was shone onto the device through optical circuits and spectral response was mapped in Photo-Luminescence (PL) spectroscopy setup and shown in Fig 5.43. As the PVA absorbed the high energy light, the carriers in PVA electrolyte gains this specific energy and crossed its band gap. From this approach, one can find the band gap energy of PVA electrolyte as well as the trap centers can also be estimated from these spectra.

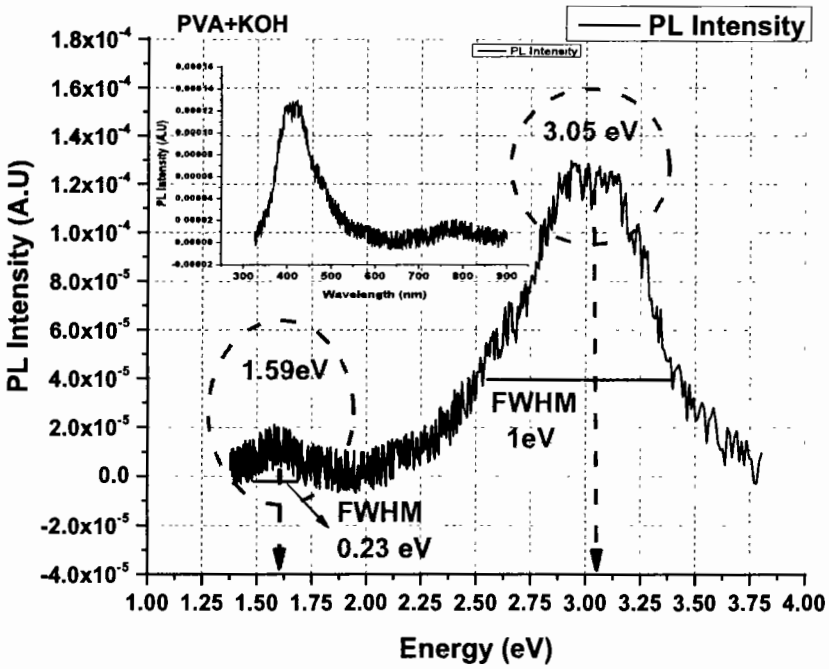

Fig 5.43: Photo-Luminescence (PL) scans of PVA based Super-Capacitor Electrolyte

From this analysis it is found that the band gap of PVA is ~ 3.05eV which is in close agreement to the reported literature [368]. It is also noticed that a trap center at 1.59eV exists within the band gap of PVA electrolyte. The Full Width and Half Maxima (FWHM) identified against each mapped energy actually points towards the defect states at a given energy level. The energy band picture of PVA based electrolyte along with the trap centers measured by Q-DLTS and PL spectra is shown in Fig 5.44. This can be observed from Fig 5.44 that the trap level measured by Q-DLTS technique is recombination in nature i.e. around this energy level maximum carriers may be captured as soon as one may charge the super-capacitor against 1V potential. As the carrier gets captured by this trap center, less carriers are available to the device and as a result lesser magnitude of voltage may be observed even

at no-load condition. As for the PL assisted trap center is concerned; this may be either the recombination or generation one. To our assessment; this center may likely be recombination one because carriers continuously diminish at the internal self-discharge resistance which is mainly due to electron-hole pair recombination phenomena.

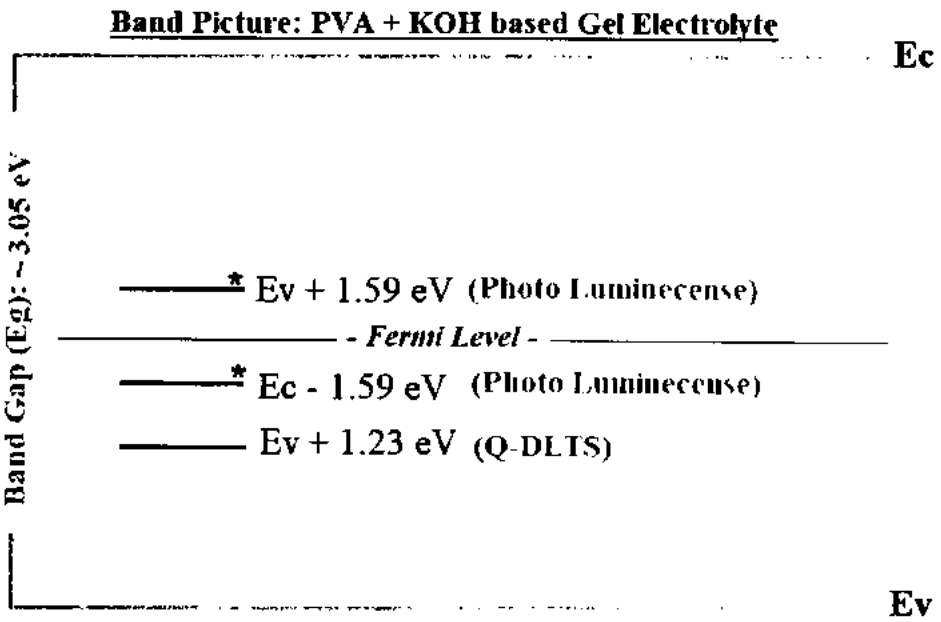

Fig 5.44: Energy band picture of PVA based Electrolyte

5.5 Comparison with the reported Devices

Based on our methodology, fabrication and characterization of stretchable supercapacitor is echived with the following three strategies:

- PEDOT:PSS based Supercapacitor
- AC-DC Analysis of Supercapacitor
- PVA-KOH based Supercapacitor

The details pertaining to the key works published in literature compared with the findings presented in sections 5.1-5.4 are given in the following section.

PEDOT: PSS: Conductive Polymers (CPs) show unique properties like toughness, low-temperature synthetic routes, high elasticity, and solution processability. Several properties of conductive polymers are shown in Table 5.4.

Table 5.4: Conductivity and Properties of common conductive polymers.

Polymer	Conductivity S/cm	Properties	Limitations	Ref.
PPy	2000	High electrical Conductivity, easy preparation, ease of surface modification	Stiff, inelastic and insoluble	[369]
PANI	112	Various structural forms, low cost	Hard to process, limited solubility	[370]
PTh	560	High electrical Conductivity, ease of preparation, good optical properties	Hard to process	[371]
PEDOT:PSS	4700	High electrical Conductivity, use as transparent electrode	More process steps	[372]

PEDOT: PSS is used as the most researched and successful conducting polymer due to its high chemical stability and electrical conductivity.

Khasim et al. reported high performing PEDOT: PSS based flexible supercapacitor. By secondary doping, reduced graphene oxide (rGO) is incorporated with PEDOT:PSS [373]. Room temperature conductivity of PEDOT:PSS film is enhanced from 3 $S.cm^{-1}$ to nearly 1225 S cm^{-1} for a 10 wt% composite, by secondary doping of Ehtylne glycol(EG) with rGO. Energy density of 810 (W h kg^{-1}) and specific capacitance of 174 ($F.g^{-1}$) is achieved by secondary doped PEDOT–PSS:EG/rGO composite film. Long term stability is shown with 5000 cycles of charging discharging are achieved with capacitance retention of over 90%. Fig 5.45 shows the schematic diagram of fabrication process of flexible electrode. EIS is used to study the capacitive behavior of PEDOT–PSS:EG/rGO nanocomposites and pristine PEDOT–PSS by measuring equivalent-series resistance 'Req', and charge-transfer resistance 'Rct'. Fig 5.46 shows Nyquist plots of differnet composites of PEDOT–PSS:EG/rGO. It shows vertical plot at low frequencies region where the electrodes are

dominated by purely capacitive behavior. A rolled up device is also constructed to show the practical applications which shows that when the capacitor is fully charged it can switch red LED for 40 seconds [373].

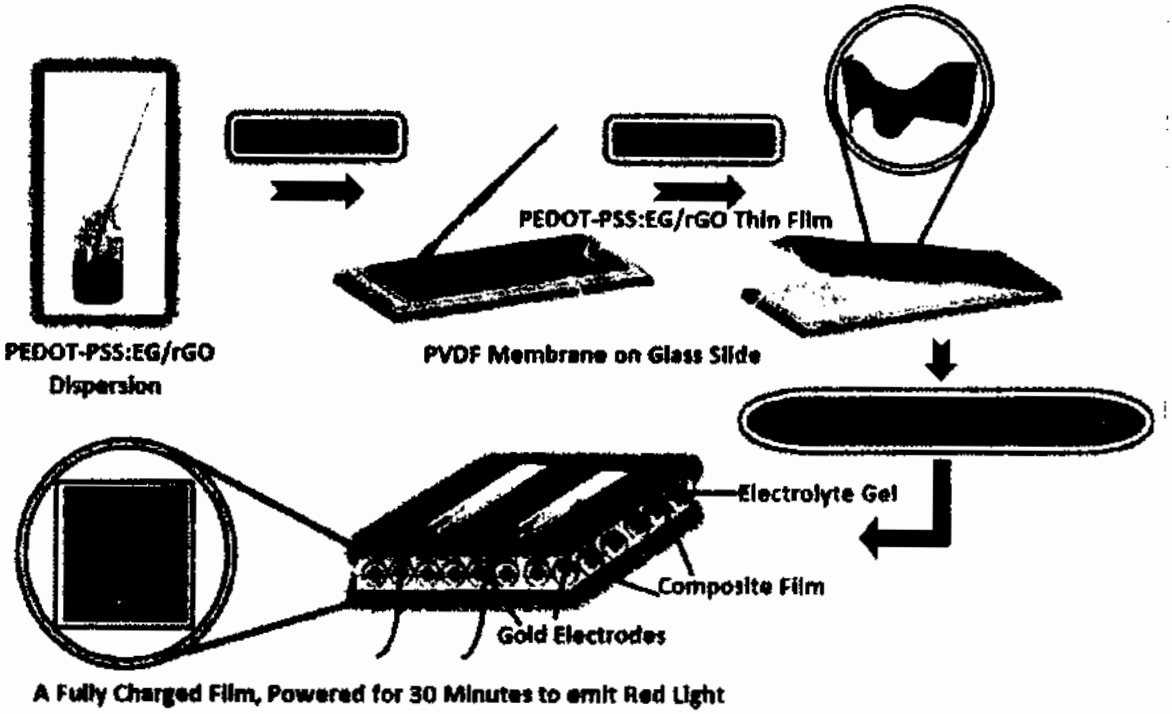

Fig 5.45: Schematic representation of flexible electrode fabrication [369]

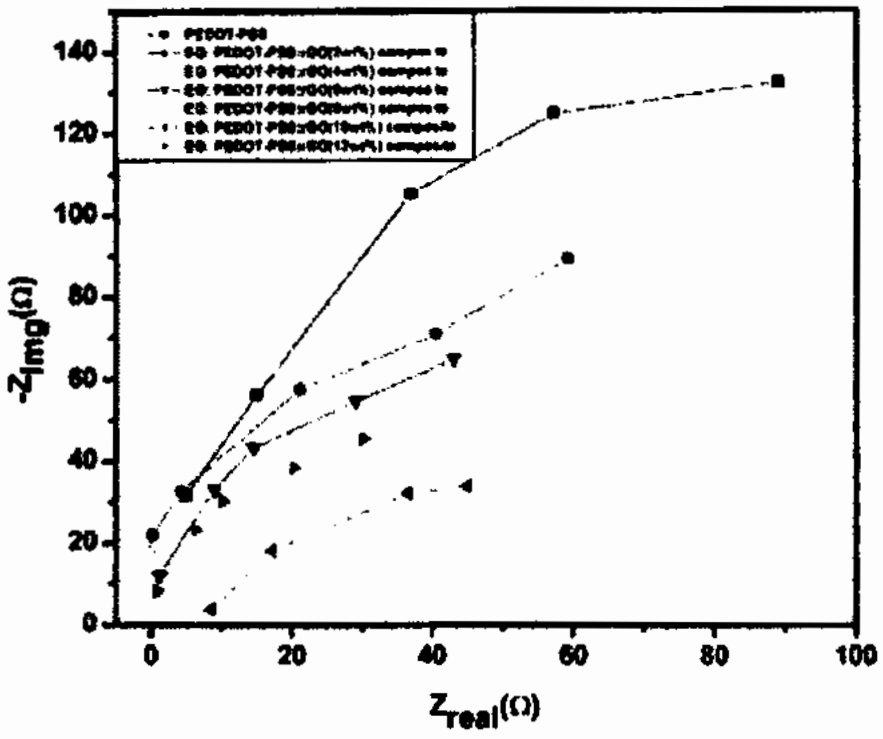

Fig 5.46: Nyquist plots for pure PEDOT–PSS and EG doped PEDOT–PSS:rGO composites [369]

Manjakkal et al reported sweat-based flexible supercapacitor for self-powered smart textiles and wearable systems. PEDOT: PSS is selected as active electrode while sweat is selected as electrolyte, for fabrication of SC. [374]. Fig 5.47 shows the fabrication process the textile SC and electrodes.

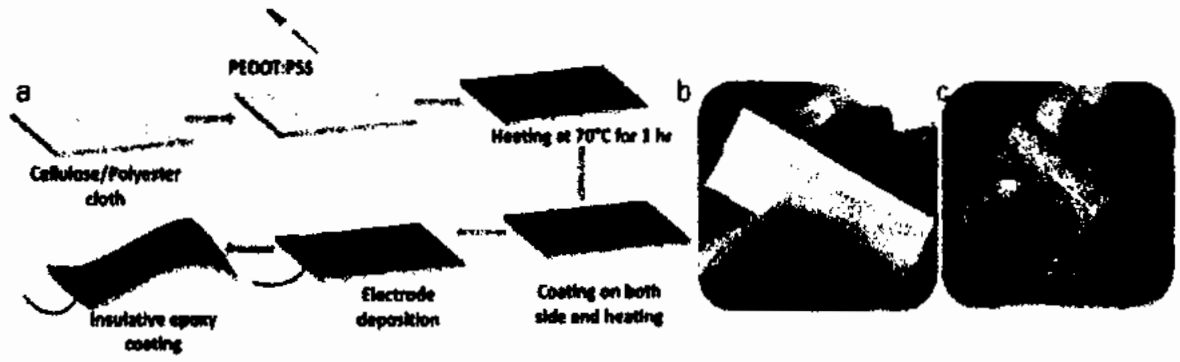

Fig 5.47: a) Fabrication Process of PEDOT:PSS-based electrodes on cloth. b) Cloth before coating (c) cloth after PEDOT: PSS coating [374]

SC shows specific capacitance of 8.94 F g^{-1} (10 mF cm^{-2}) at 1 mV s^{-1}, when PEDOT:PSS coated onto cellulose/polyester cloth. With artificial sweat , the specific capacitance of SC is 5.65 F g^{-1} , power and energy densities are 329.70 W kg^{-1} and 1.36 Wh kg^{-1} respectively for 1.31 V. While using real human sweat the values of power and energy densities are 30.62 W kg^{-1}, and 0.25 Wh kg^{-1}, respectively. The performance of SC is evaluated with different volumes of sweat (20, 50, and 100 μL), charging/discharging stability (4000 cycles), washability, and bending radii (10, 15, 20 mm). Fig 5.48 shows the performance of sweat-based SC in real life.

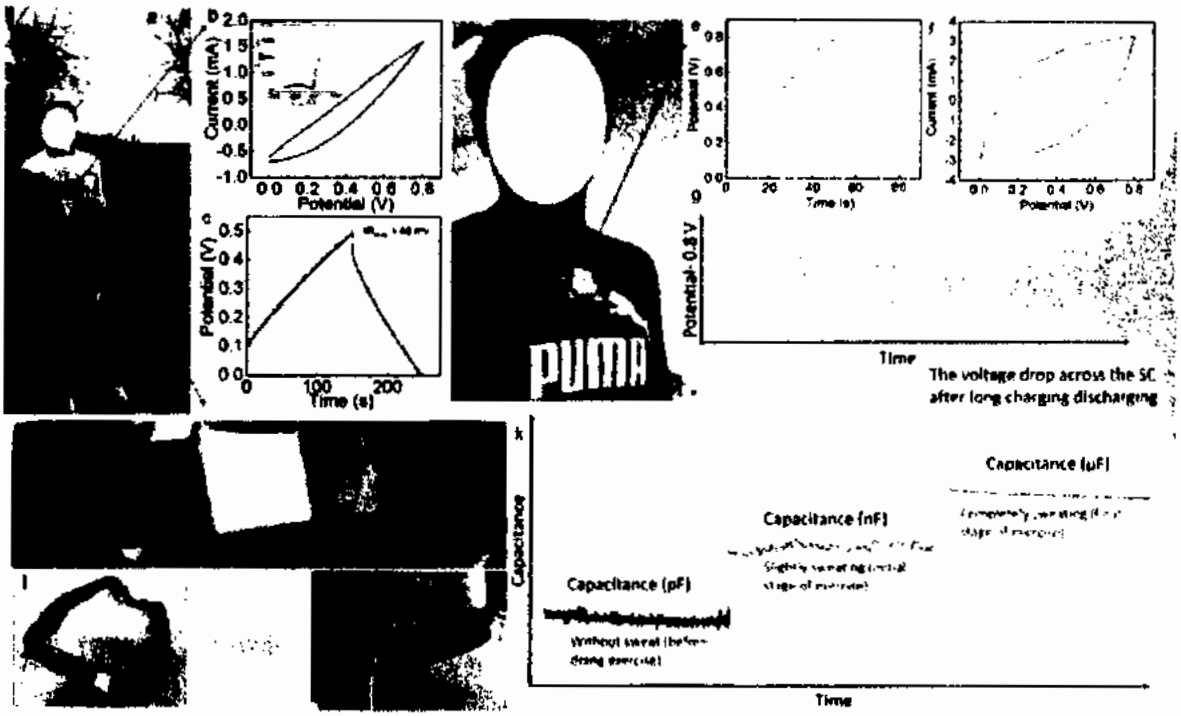

Fig5.48: Performance of the sweat-based SC in real application. a) SC attached to clothes of a person who is partly wet due to sweat. b) The CV (inset EIS) and c) GCD analysis d) SC attached to clothes of a person who is fully wet due to sweat e,f) GCD and CV analysis of the fully wet SC. h–j) The textile SC on a polar pro strap for conformal contact and k) SC performance with sweat during workout

Song et al reported a PEDOT: PSS based flexible high conductivity transparent electrode - (denoted as S-PH1000) for semitransparent supercapacitor [375]. Flexible plastic substrate and transparent electrode via H_2SO_4 treatment was used to achieve high conductivity of 2673

S/cm. This is the top electrical conductivity of flexible substrates with PEDOT: PSS films. High rate property of this electrode is achieved by finding the electrochemical properties. It shows specific capacitance of 121 F/g and 161 F/g and was obtained from electrode at current density of 100 A/g and 1 A/g. It also shows high transparency over 60% at 550 nm. Due to high electrical conductivity, excellent flexibility, and transparency, these flexible transparent electrodes are expected to be applied to electronic devices.

Critical Analysis:

From above mentioned works [369-375], it was found that PEDOT:PSS is among most researched and successful conducting polymers due to its high chemical stability and electrical conductivity. However, PEDOT: PSS shows inhomogeneous electrical and morphological properties resulting in poor long-term stability and causes the limitation in its shelf-life [346]. Thus, a detailed amount of investigations are needed in order to practically gauge the actual cause that may limit its long term performance.

Our Contribution:

In order to do so, a detailed account of an aged PEDOT:PSS based supercapacitor was performed in terms of Current-Voltage (I-V), Electrochemical Impedance Spectroscopy (EIS) and Charge Deep Level Transient Spectroscopy (Q-DLTS) measurements under 0.1-1V charging voltages at variable ambient temperatures. Evaluation of age-assisted defects and influence of temperature on the current kinetics of the supercapacitors were also presented with detailed reliability analysis for system level application of the fabricated device. PEDOT: PSS based supercapacitor was fabricated and spanned over more than ~120 days to be subsequently characterized with a special focus to evaluate the charging and discharging nature of aged supercapacitor. From Q-DLTS study, the two defect centers are measured and calculated i.e. E_{T1} = Ec-0.0305 eV with capture cross section of 2.05×10^{-25} cm^{-}

^{2} and E_{T2} = Ev+0.0896 eV with capture cross section of $9.13x10^{-24}$ cm^{-2}. While increasing the ambient temperature of the supercapacitor and to inspect the charging nature; the said supercapacitor provided better charge storage capability at near ambient temperatures i.e. 26-36 °C when compared with higher operating temperatures i.e. >36°C; at these temperatures; the charging current was observed to fall dramatically. The ambient temperature of the device is also found to be responsible to raise the extent of trap states which might also increase the available 'space discharge states' and thus decreases the charging current. Also, from this study the Self-discharge (especially during standby time) is readily evaluated effectively due to the recombination mechanism. These recombination centers are thought to trap the charge carriers from their respective bands and recombine at their own interface rather at the load terminals and degrades the overall supercapacitor's performance. From EIS study, it is analyzed that by increasing the charging voltage, the parallel resistance (Rp) of the supercapacitor might decrease which consequently increase the self-discharge capability and limits the supercapacitor's performance. The kinetics of current (I-t) analysis of the said supercapacitors revealed that higher temperatures might limit the device performance for system level applications. In this wake, it is found that at 1V charging bias, the charging current is recorded as 45 μA and 7 μA at 26°C and 86°C, respectively. Both aging-assisted defects and current kinetics due to variable operating temperatures may prove to be important parameters while designing the process strategies for flexible and stretchable PEDOT:PSS based supercapacitors for real-time system integration. This approach is an altogether novel one while comparing with the published works on PEDOT: PSS based supercapacitors.

AC/DC Analysis of Supercapacitors:

Pico et al reported the fabrication of single walled carbon nanotubes (SWCNT) and commercial activated carbon based supercapacitors [376]. The relative content of the two carbons has been varied in the range 0–100 wt %. Fabricated supercapacitor is being studied

at room temperature by AC and DC measurements. AC response is analyzed on the basis of equivalent circuit of supercapacitor for two relaxation times τ_1 and τ_2, i.e. initial time 1–10 s and the latter time of the order of 10^{-6}–10^{-5} s. Impedance plots of real impedance vs imaginary impedance is plotted at different frequencies for different compositions as active electrodes composites 90 wt % activated carbon and 10 wt % SWCNT, and 30 wt % activated carbon 70 wt % SWCNT as shown in Fig 5.49.

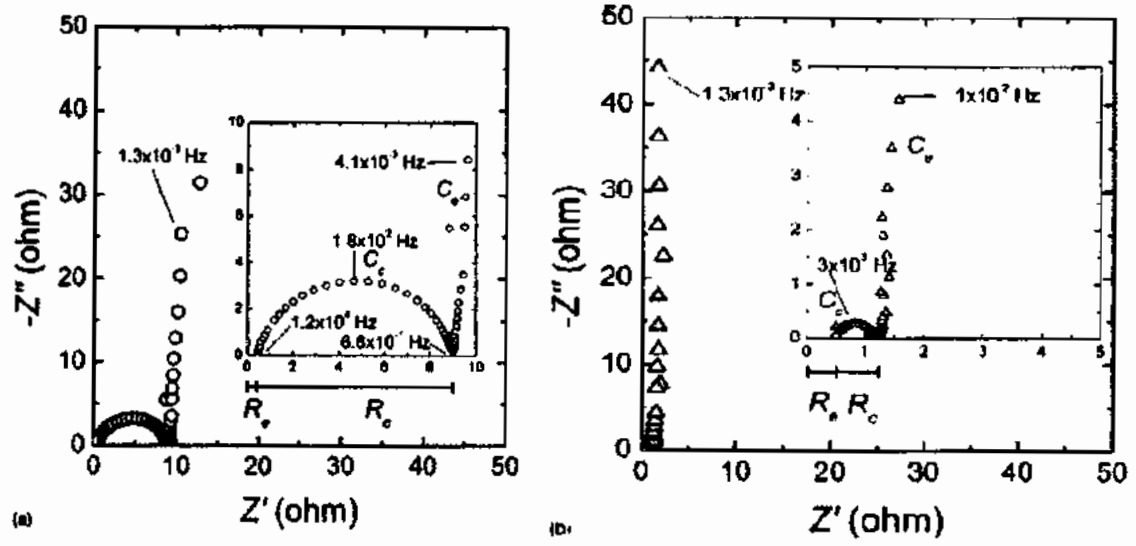

Fig 5.49: Imaginary impedance vs real impedance recorded on the supercapacitor cells having as active electrodes composites (a) 90 wt % activated carbon and 10 wt % SWCNT (b) 30 wt % activated carbon 70 wt % SWCNT [376]

From the two graphs we can see (i) electrolyte Resistance Re 0.5, (ii) Resistance Rc associated to Capacitance of the order of 10^{-5} F and gives to an arc (iii) a spike (vertical line), which is characteristic of the double layer capacitive behavior Ce of the cell; the capacitance Ce is of the order of 1 F and it can be estimated from the ideal equation $Z = -1/Ce\,\omega$ at the spike. DC measurements were performed by taking charge/discharge curve of supercapacitor at 20 mA with 55 wt % of active carbon and 45 wt% SWCNT as shown in Fig 5.50.

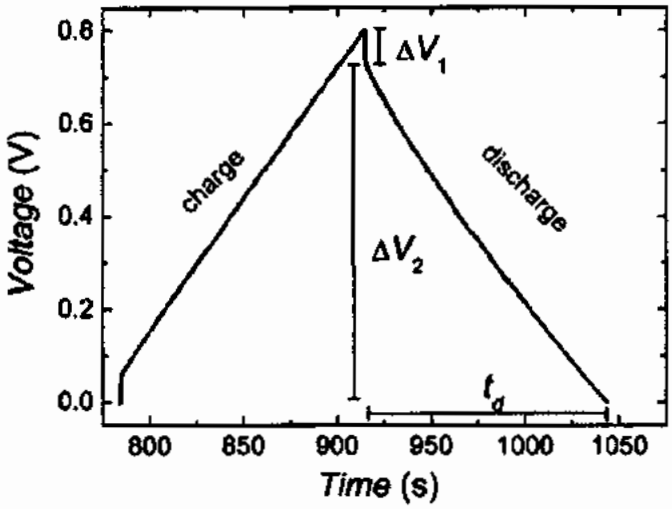

Fig 5.50: Charge/discharge curve of supercapacitor at 20 mA with 55 wt % of active carbon and 45 wt% SWCNT

From the discharge plots the Equivalent series resistance of the supercapacitor cell can be estimated by ESR = $\Delta V_1/2I$ and capacitance can also be determined by C= $It_d/\Delta V_2$. It is found that ESR is approximately equal to Rc + Re found from AC measurements. ESR different values are obtained by varying Rc , as Re is almost constant from cell to cell.

Zhao et al reported a method to determine the DC internal resistance of supercapacitor. Supercapacitor with 350 F capacitance is tested to validate the results. Voltage data were taken at 30s, 2 s and 10 ms after current pulse.. The internal resistance was measured by equation 5.70.

$$R_s = (V_2 - V_1)/(I_2 - I_1) \qquad (5.70)$$

where I_1 and I_2 are the current values before and after the current change, either interruption or pulse and V_1 is the voltage before the current change, V_2 is the voltage taken at 30 s, 2 s or 10 ms or after the current change. AC resistance of 1 KHz of the supercapacitor were measured and compared with DC values and found that it is good parallel reference for dc resistance measurement at 1 ms time frame [377].

Critical Analysis:

From above mentioned works [376-377], only the characterizations based on AC and DC analysis have been performed however the background theoretical framework specific to the tailored stretchable supercapacitors is missing. In our study, both AC and DC approaches and have been rigorously worked out with the relevant mathematical frame work from ab initio.

Our Contribution:

Internal passive components of the supercapacitor are rigorously studied in the wake and the conventional circuit theory. From this approach, we have numerically solved the supercapacitor's internal parameters in view of frequency and time domain. In order to do so, a stretchable supercapacitor is fabricated using a specialized gel electrolyte and a dense metal net. A detailed mathematical analysis in special preview of alternating current (AC) and direct current (DC) techniques has been carried out with multi-charge pulses ranging from 1V to 0.1V. For AC and DC Analysis, impedance spectroscopy and kinetics of currents has been performed. Additionally, the Charge based Transient Spectroscopy (Q-DLTS) measurements are performed in order to analyze the transient behavior. AC and DC analysis are perfomed to estimate R_{ESR}, R_P, and effective Capacitance of the supercapacitor. Thevenin equivalent model along with complete mathematical expressions is solved rigorously. Additionally, Frequency and time domain analysis of supercapacitor have been also carried out with mathematical limits applied for each boundary conditions. For DC analysis, we have biased the supercapacitor under 0.1-1V range at multiple temperatures and calculated the performance parameters. When $\lim_{t\to 0}$ is applied, the value of R_{ESR} was found to be limited by the wiring of the measurand instrument. We have concluded that the value of R_{ESR} would not be retrieved from its original nature alone, because of the serially connected wires of the measuring instrument. To solve this ambiguity, we proposed a differential amplifier based

model. Additionally, the internal discharge resistance (Rp) and the capacitance magnitudes are measured by DC and are compared with AC technique. The value of R_P was calculated around ~656kΩ and 936kΩ for DC and AC analysis, respectively. The Capacitance magnitudes were calculated around 3E-5 F and 7.34E-5 F for DC and AC analysis, respectively. In order to study the lossy nature of said supercapacitor (caused by R_p.), we have envisaged this phenomenon by using Q-DLTS and evaluated the possible reason behind this self-discharge nature. From these measurements we have obtained the trap energy level (~Ec-78.7meV) that is responsible for the charge leakage at the internal self-discharge resistance of the supercapacitor.

PVA/KOH based Supercapacitor:

Yuan et al reported fabrication of hybrid supercapaitor with activate carbon as electrodes and PVA-KOH- H_2O containing 5 M KOH as alkaline polymer gel electrolyte as shown in Fig 5.51. EIS, Cyclic Voltammetry and galvanostatic charge discharge measurements were applied to find the characteristics of hybrid supercapacitor at different tempeartures i.e -20 to 40 °C. it revealed interesting results like by increasing the temperature the conductivity of alkaline polymer gel electrolyte increases, and decreasing the charge transfer resistance. Energy density of 26.1 Wh/kg and specific capacitance of 73.4 F/g was achived at current density of 0.1 A/g at 40°C is achieved [378].

Vandana et al. reported fabrication of solid state supercapcaitor based on conjugated polymer-quantum dots. Polypyrrole-graphene quantum dots composites (PGC) are used as electrode while PVA/ H_3PO_4 , PVA/ KOH, PVA/KCL and PVA/ H_2SO_4 gel as electrolytes. Nyquists plots were ploted for all these combination of gel electrolytes. The Specific capacitance is calculated and comparison is plotted in Fig 5.52 [379].

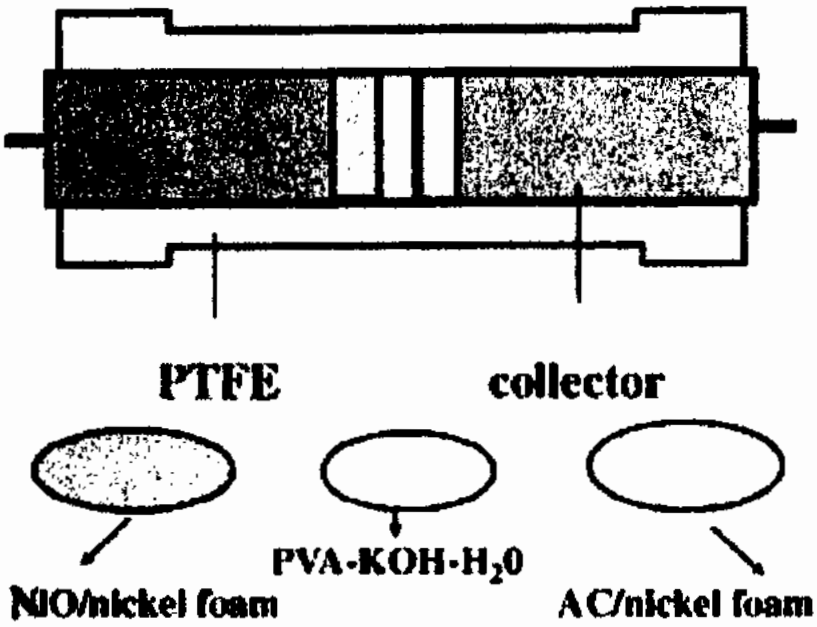

Fig 5.51: Schematic design of the hybrid supercapacitor [378]

QianZhang et al reported fabrication of high performance MnO_2//PVA-KOH//carbon nanotubes based wire-shaped supercapacitor. MnO_2 is poor electrical conductor, so to improve its conductivity copper wire is used as current collector in inner electrode. Hydrothermal method is used to insert PVA-KOH gel electrolyte and removal of SiO_2, simultaneously. High energy density (0.16 mWh cm^{-3}), good capacitive performance (1.98 F cm^{-2}) and long term cycling stability (90.38% of capacitance retention at 0.15 A cm^{-3}after 4000 cycles) with flexibility is achieved by wire shaped supercapacitor [380].

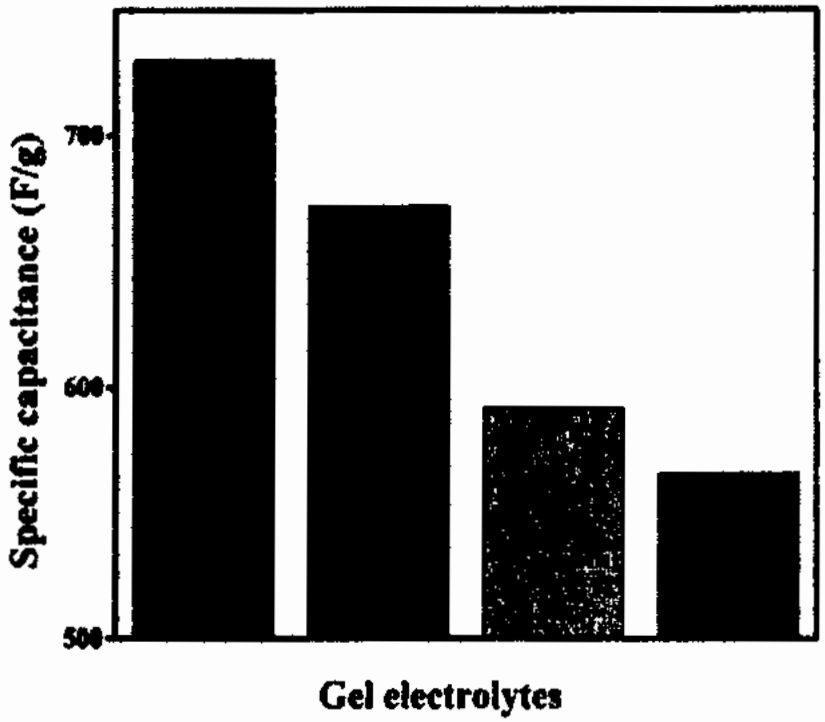

Fig 5.52: Specific capacitance comparison of different Gel eletrolytes [379]

Critical Analysis:

From above mentioned works [378-380], it was found that PVA/KOH has been widely studied and used as PVA based gel electrolyte for supercapacitors. PVA/KOH based supercapacitor is characterized on a well-known charge and discharge based technique that is cyclic voltammetry in which forward and reverse cycles are applied in order to obtain the charge and discharge hysteresis of subject supercapacitor. However the real time charging and discharging nature at specific loads were not gauged in any PVA/KOH based supercapacitor.

Our Contribution:

In our study, a specialized PVA-KOH electrolyte has been synthesized to fabricate the super-capacitor with activated Carbon and graphene ink as an electrode. After successful fabrication of said super-capacitor, the initial charge cycle of 1Volt have been spanned to

record the discharge spectra on current and voltage scales separately. For electrical characterization, we have used multiple techniques in order to assess the said PVA electrolyte including Electrochemical Impedance Spectroscopy (EIS), Nyquist Plots, Current-Voltage and Charge Deep Level Transient Spectroscopy (Q-DLTS). Scanning Electron Microscope (SEM), Electron Dispersive Spectroscopy (EDS), Photo-Luminescence (PL) and Atomic Force Microscopy (AFM) are also utilized to provide supplementary information to understand the device functionality in a better way. After successful synthesis of PVA based electrolyte, active layers of said super-capacitor was stacked. The active electrode was developed by intermixing of graphene flakes and activated carbon and subsequently sandwiched into the larger pore sized fabric layers. After successful development of super-capacitor it was charged at 1V for just one minute duration and the discharge characteristics were mapped. The fabricated super-capacitor discharged itself completely at ~30minutes both at no and full load operation. There was a dead zone observed with effective window of 1-0.64V where no physical charge would be measured. Thus, for such type of super-capacitor, 0.64V was the charging potential in order to physically monitor the charge without lacking the charging voltage. For discharge cycle, the full load current was scanned from 2000-10μA for the same duration of 30 minutes at just 1V and 1minutes charging span. In order to gauge the physical extent of Randles cell of super-capacitor, the EIS spectroscopy was performed and the Nyquist plot was analyzed. It was found that 1-0.6V potential provided ionic diffusion into the PVA electrolyte that maight degrade the super-capacitor's efficiency, which provided cross-verification of discharge characteristics observed from the discharge cycle. The self-discharge resistance (Rp), equivalent series resistance, electrolyte resistance was calculated to be ~ 47Ω, 28Ω and 19Ω, respectively. The fabricated device was also studied with special reference to the direction of current flow within electrolyte as a function of different geometrical planes (possible current associated with each respective

plane). The charge based transient analysis of PVA electrolyte was performed in order to investigate the dead zone. It was found that recombination center at Ev+1.23eV available within the band-gap of PVA electrolyte might provide the conducting path to the free carriers and eventually degraded the super-capacitor's performance. Photo-Luminescence (PL) study also revealed that the band gap of PVA is ~3.05eV and the trap center was localized at 1.59 eV. The SEM and EDS analysis was also performed for morphological and elemental studies for each device element of the super-capacitor. The AFM analysis was also performed to investigate the surface roughness which may provide an insight of the surface area connected with the active electrodes. This study provided an insight to the charge dynamics with in the active device regions and their roles in operational efficiency of the PVA-based electrolyte for the stretchable super-capacitors manufacturing.

A detailed conclusive summary of this specified chapter has been asserted in Chapter 6.

Chapter 6

Conclusion & Future Work

We have extensively envisaged the PEDOT:PSS, AC/DC analysis of Polyurethane based Supercapacitor and PVA based Supercapacitor. The case wise conclusion and corresponding future work has been elaborated below:

6.1 Conclusion

The section wise conclusion has been postulated and discussed in detail as:

6.1.1 PEDOT:PSS Based Super-capacitor:

PEDOT: PSS based supercapacitor was fabricated and spanned over more than ~120 days to be subsequently characterized with a special focus to evaluate the charging and discharging nature of aged supercapacitor's for the very first time, to the best of our knowledge. In this work, we have utilized Q-DLTS to study the native defects placed at the PEDOT: PSS/electrolyte interface which are responsible for the inhomogeneous nature of subject device. Summary of the major findings are as follows:

- From Q-DLTS study, the two defect centers are measured and calculated i.e. E_{T1} = Ec-0.0305 eV with capture cross section of 2.05×10^{-25} cm^{-2} and E_{T2} = Ev+0.0896 eV with capture cross section of 9.13×10^{-24} cm^{-2}.
- The ambient temperature of the device is also found to be responsible to raise the extent of trap states which might also increase the available 'space discharge states' and thus decreases the charging current.
- The Self-discharge (especially during standby time) is readily evaluated effectively due to the recombination mechanism. These recombination centers are thought to trap

the charge carriers from their respective bands and recombine at their own interface rather at the external load terminals and degrades the overall performance of the supercapacitor.

- From EIS study, it is analyzed that by increasing the charging voltage, the parallel resistance (Rp) of the supercapacitor may decrease which consequently increases the self-discharge capability and limits the supercapacitor's performance.
- The kinetics of current (I-t) analysis of PEDOT:PSS supercapacitors revealed that higher temperatures might limit the device performance for system level applications. In this wake, it is found that at 1V charging bias, the charging current is recorded as 45 μA and 7 μA at 26°C and 86°C, respectively.
- The aging-assisted defects and their respective current kinetics at variable operating temperatures may prove to be important parameters while designing the process strategies for flexible and stretchable PEDOT:PSS based supercapacitors for real-time system integration.

6.1.2 Alternating and Direct Current (AC/DC) analysis of Polyurethane Based Super-capacitor:

A stretchable and foldable Polyurethane substrate along with dense metal net was fabricated and spanned for ~15 days, in order to properly mitigate the electrolyte with anode and cathode within the device matrix. In this study, we performed AC and DC analysis to estimate R_{ESR}, R_P, and effective Capacitance of the supercapacitor. Thevenin equivalent model along with complete mathematical expressions was also solved at length. Additionally, Frequency and time domain analysis of supercapacitor was carried out with real time physical mathematical limits applied for each boundary conditions. During the experiments for DC analysis, the supercapacitor was biased under 0.1-1V range at multiple temperatures and performance parameters were conducted. Summary of major findings are:

- For such type of supercapacitor; when $\lim_{t \to 0}$ was applied, the value of R_{ESR} was found to be limited by the wiring of the measurand instrument.
- During these characterizations we concluded that the value of R_{ESR} would not be retrieved from its original nature alone, because of the serially connected wires of the measuring instrument. A differential amplifier based model may overcome this ambiguity, when used to model the device operational behavior.
- The internal discharge resistance (Rp) magnitudes was measured and compared by both the techniques. The value of R_P was calculated around ~656kΩ and 936kΩ for DC and AC analysis, respectively.
- The Capacitance (C) magnitudes was measured and compared as $3x10^{-5}$ F and $7.34x10^{-5}$ F for DC and AC analysis, respectively.
- In order to study the lossy nature of said supercapacitor (caused by $R_{p.}$), we envisaged this phenomenon by using Q-DLTS and evaluated the possible reason behind this self-discharge nature. From Q-DLTS measurements, it was found that the trap energy level (~Ec-78.7meV) was responsible for the charge leakage at the internal self-discharge resistance of the supercapacitor.

6.1.3 PVA-KOH Based Super-capacitor:

A detailed study was carried out for the evaluation of duly synthesized KOH based PVA electrolyte for stretchable super-capacitors.The active electrode was developed by intermixing of graphene flakes and activated carbon and subsequently sandwiched into the larger pore sized fabric layers. After successful development of super-capacitor it was charged at 1V for just one minute duration and the discharge characteristics were mapped. Major findings of this work is as follows:

- The fabricated super-capacitor completely discharged itself in ~30minutes both at no and full load operation.
- There was a dead zone observed with effective window of 1-0.64V where no physical charge would be measured. Thus, for such type of super-capacitor, 0.64V was the charging potential in order to physically monitor the charge without lacking the charging voltage.
- For discharge cycle, the full load current was scanned from 2000-10μA for the same duration of 30 minutes at just 1V and 1minutes charging span.
- In order to gauge the physical extent of Randles cell of super-capacitor, the EIS spectroscopy was performed and the Nyquist plot was also analyzed. It was found that 1-0.6V potential provided the ionic diffusion into the PVA electrolyte that might degrade the supercapacitor's efficiency, which provided cross-verification of discharge characteristics.
- The self-discharge resistance (Rp), equivalent series resistance, and electrolyte resistance were calculated to be ~ 47Ω, 28Ωand 19Ω, respectively.
- The direction of current flow within electrolyte as a function of different geometrical planes (possible current associated with each respective plane) was also envisaged in these experiments.
- In order to investigate the dead zone, the charge based transient analysis of PVA electrolyte was performed. It was found that recombination center at Ev+1.23eV available within the band-gap of PVA electrolyte might provide the conducting path (leakage) to the free carriers and eventually degrade the super-capacitor's performance.
- Photo-Luminescence (PL) study also revealed that the band gap of PVA is ~3.05eV and the trap center was localized at 1.59 eV within the device active region.

- The SEM and EDS analysis was carried out for morphological and elemental studies for each device element of the supercapacitor. Similarly; the AFM measurements were done to investigate the surface roughness which provided an insight of the surface area connected with the active electrodes.
- This study provided an insight to the charge dynamics with in the active device regions and their roles in operational efficiency of the PVA-based electrolyte for the stretchable supercapacitor's manufacturing.

6.2 Future Work

In future, a range of organic materials may be examined for the optimum utility and efficiency of stretchable supercapacitors. Some of the key domains that need to be addressed in detail for next generation supercapacitor technologies are as follows:

- Different conducting polymers including metal oxides such as MnO_2, RuO_2, V_2O_5, and MoO_3 could be utilized in electrodes which have higher energy storage capacity than the EDLC base electrodes.
- The main hindrance to compete the energy storage market is to properly address and control the internal discharge resistance of any type of supercapacitor, thus, major work needs to be carried out in order to address this device electronics issue.
- Another challenge for maximum utilization of flexible supercapacitor is of its electrode material i.e. by molding, folding and stretching the electrode material may become open circuited at harsh conditions. Polyurethane substrate may compensate this issue but this material only supports the mechanical stability of the outer-cover of the stretchable supercapacitor. This material has self-healable properties and provides the protection of overall structure. For future perspectives, this requires to

be studied in detail with the possibility to exploit the technology on mass manufacturing level.

- Materials with a high surface area such as foam-structured materials or nanocarbon-based materials could be utilized to reduce the weight and size of the supercapacitor which would eventually increase the amount of energy stored on the electrode's surface.
- In order to overcome the disadvantages of supercapacitors, such as lower operating voltage compared to metal (Li)-ion batteries (and other such alternatives) and lower energy density requires considerable effort to improve their electrochemical performance, including operating voltage window, enhancing their capacitance and energy density.
- Another area that needs to be addressed is to reduce the e-waste produced by supercapacitors, thus, auto degradable materials needs to be developed which may degrade themselves whenever needed. The electronics of such base materials will also be another interesting problem to solve.
- A new concept of an integrated selfpowered system by combining an energy harvesting device with an energy storage device can be established to harvest renewable energy and simultaneously store it for sustainable operation of electronic devices.
- With the continued increase in renewable distributed generation, PV energy supply can be more of a stumbling block than generating it. Utilities desire a firm, consistent supply of energy, from all of its sources, in order to meet the demand instantaneously. If supply is not consistent, whether from overcast days or shifting cloud cover, then it can be taken offline as it cannot reliably support grid needs. This can drastically reduce the utilization of the renewable source and effect the revenue return on the

physical assets. To assist with this firming of renewable generation, energy storage is often integrated to balance supply and demand. Supercapacitor can be used as the sole energy storage solution or used in combination with batteries to increase the life of an energy storage system and eliminate the need for replacement parts and batteries. Having the right power system helps improve return on investment in alternative energy applications.

- Both flexible energy harvesting and storage devices have been widely reported separately to satisfy part of the needs in the emerging areas, including wearable electronics, and low-density applications such as rooftop solar collectors. However, a flexible energy system with mechanical robustness and light-weight is the integrated device that will serve the real demand.
- Fabric supercapacitor is a flexible electrochemical device for energy storage application. It is designed to power up flexible electronic systems used for the Information sensing, Data computation and Communication. The development of a flexible supercapacitor is important for e-textiles since supercapacitor can achieve higher energy density than a standard parallel plate capacitor and a larger power density compared with a battery. A lot of research needs to be done on design, fabrication and characterization on prototype fabric supercapacitors with cost efficient electrode material, fast and reliable fabrication method and improve device structure. Various prototype flexible supercapacitors with fabric electrode can be achieved with the multilayer layer supercapacitor with dip coated fabric electrode and aqueous electrolyte. supercapacitors can achieve an excellent cycling stability over 15000 cycles.
- Increasing power and energy demands for next-generation portable and flexible electronics such as roll-up displays, photovoltaic cells, and wearable devices have

stimulated intensive efforts to explore flexible, lightweight, and environmentally friendly energy storage devices. Flexible solid-state supercapacitors (SCs) have attracted increasing interest because they can provide substantially higher specific/volumetric energy density compared to conventional capacitors. Additionally, flexible solid-state SCs are typically small, highly reliable, lightweight, easy to handle, and have a wide range of operation temperatures. In this regard, solid-state SCs hold great promise as new energy storage devices for flexible and wearable electronics

- Nanocarbon materials such as single-wall carbon nanotubes (SWCNTs) and reduced graphene oxide (rGO) and their composites are used for stretchable and flexible energy storage applications. To fabricate the stretchable and flexible supercapacitor, one can introduce an appropriate polymer with high stretchability and flexibility so that latex (natural rubber), biomedical grade polyurethane (PU) and polycaprolactone (PCL) can conducted for fabricating of stretchable and flexible supercapacitor by their high stretchability and flexibility. All these materials can be suitable for fabrication of stretchable and flexible substrate.

References

[1] Da Silva Lima, L., Quartier, M., Buchmayr, A., Sanjuan-Delmás, D., Laget, H., Corbisier, D., Mertens, J. and Dewulf, J. (2021). Life cycle assessment of lithium-ion batteries and vanadium redox flow batteries-based renewable energy storage systems. Sustainable Energy Technologies and Assessments, 46, 101286.

[2] Haque, S. A., & Islam, M. A. (2021). Artificial Neural Network-Based Short-Term Load Forecasting for Mymensingh Area of Bangladesh. International Journal of Electrical and Computer Engineering, 15(3), 99-103.

[3] Machado, P. G., Mouette, D., Rathmann, R., dos Santos, E., and Peyerl, D. (2020). Is Energy Planning Moving Towards Sustainable Development? A Review of Energy Systems Modeling and Their Focus on Sustainability. In International Business, Trade and Institutional Sustainability (pp. 629-644). Springer, Cham.

[4] Samsudin, N. A., Zainal, Z., Lim, H. N., Sulaiman, Y., Chang, S. K., Lim, Y. C., and Mohd Amin, W. N. (2018). Enhancement of capacitive performance in titania nanotubes modified by an electrochemical reduction method. Journal of Nanomaterials, 2018.

[5] Gonzalez-Salazar, M. A., Kirsten, T., and Prchlik, L. (2018). Review of the operational flexibility and emissions of gas-and coal-fired power plants in a future with growing renewables. Renewable and Sustainable Energy Reviews, 82, 1497-1513

[6] Cultura, A. B., and Salameh, Z. M. (2015, June). Modeling, evaluation and simulation of a supercapacitor module for energy storage application. In International conference on computer information systems and industrial applications. Atlantis Press.

[7] Wei, L., Wu, M., Yan, M., Liu, S., Cao, Q., and Wang, H. (2019). A Review on Electrothermal Modeling of Supercapacitors for Energy Storage Applications. IEEE Journal of Emerging and Selected Topics in Power Electronics, 7(3), 1677-1690.

[8] Malinowski, A., Chen, J., Mishra, S. K., Samavedam, S., and Sohn, D. K. (2019, June). What is Killing Moore's Law? Challenges in Advanced FinFET Technology Integration. In 2019 MIXDES-26th International Conference" Mixed Design of Integrated Circuits and Systems" (pp. 46-51). IEEE.

[9] Mayberry, M. (2013, March). Pushing past the frontiers of technology. In 2013-03)[2015-11-17]. http://www. nist. gov/pml/div683/conference/upload/Mayberry_final. pdf.

[10] Koydemir, H. C., and Ozcan, A. (2018). Wearable and implantable sensors for biomedical applications. Annual Review of Analytical Chemistry, 11, 127-146. https://doi.org/10.1146/annurev-anchem-061417-125956

[11] Lee, T. (2014). The Hardware Enablers for the Internet of Things–Part II (More than Moore). Newsletter, 2014.

[12] Whitmore, A., Agarwal, A., and Da Xu, L. (2015). The Internet of Things—A survey of topic and trends. Information Systems Frontiers, 17(2), 261-274. DOI 10.1007/s10796-014-9489-2.

[13] Liu, J. G., Ni, H. J., Wang, Z. H., Yang, S. Y., and Zhou, W. F. (2015). Colorless and transparent high-temperature-resistant polymer optical films–current status and potential applications in optoelectronic fabrications. Optoelectronics—Materials and Devices, 57-81.

[14] Chen, A., Tan, J., Henry, P., and Tao, X. (2020). The design and development of an illuminated polymeric optical fibre (POF) knitted garment. The Journal of The Textile Institute, 111(5), 745-755.

[15] Zeng, W., Tao, X. M., Lin, S., Lee, C., Shi, D., Lam, K. H.,and Zhao, Y. (2018). Defect-engineered reduced graphene oxide sheets with high electric conductivity and controlled thermal conductivity for soft and flexible wearable thermoelectric generators. Nano Energy, 54, 163-174.

[16] Zhu, H., Fang, Z., Preston, C., Li, Y., and Hu, L. (2014). Transparent paper: fabrications, properties, and device applications. Energy and Environmental Science, 7(1), 269-287.

[17] Gaspar, D., Fernandes, S. N., De Oliveira, A. G., Fernandes, J. G., Grey, P., Pontes, R. V.,and Fortunato, E. (2014). Nanocrystalline cellulose applied simultaneously as the gate dielectric and the substrate in flexible field effect transistors. Nanotechnology, 25(9), 094008.

[18] Fujisaki, Y., Koga, H., Nakajima, Y., Nakata, M., Tsuji, H., Yamamoto, T., and Shimidzu, N. (2014). Transparent nanopaper-based flexible organic thin-film transistor array. Advanced Functional Materials, 24(12), 1657-1663.

[19] Martins, R. F., Ahnood, A., Correia, N., Pereira, L. M., Barros, R., Barquinha, P. M., and Fortunato, E. E. (2013). Recyclable, flexible, low-power oxide electronics. Advanced Functional Materials, 23(17), 2153-2161.

[20] Martins, R., Nathan, A., Barros, R., Pereira, L., Barquinha, P., Correia, N., and Fortunato, E. (2011). Complementary metal oxide semiconductor technology with and on paper. Advanced Materials, 23(39), 4491-4496.

[21] Martins, R., Barquinha, P., Pereira, L., Correia, N., Gonçalves, G., Ferreira, I., and Fortunato, E. (2008). Write-erase and read paper memory transistor. Applied physics letters, 93(20), 203501.

[22] K. Nagashima, H. Koga, U. Celano, F. Zhuge, M. Kanai, S. Rahong, G. Meng, Y. He, J. D. Boeck, M. Jurczak, W. Vandervorst, T. Kitaoka, M. Nogi and T. Yanagida, Sci. Rep., 2014, 4, 5532.

[23] Nogi, M., Komoda, N., Otsuka, K., and Suganuma, K. (2013). Foldable nanopaper antennas for origami electronics. Nanoscale, 5(10), 4395-4399.

[24] Inui, T., Koga, H., Nogi, M., Komoda, N., and Suganuma, K. (2015). A miniaturized flexible antenna printed on a high dielectric constant nanopaper composite. Advanced Materials, 27(6), 1112-1116.

[25] Yang, P. K., Lin, Z. H., Pradel, K. C., Lin, L., Li, X., Wen, X., He, J.H and Wang, Z. L. (2015). based origami triboelectric nanogenerators and self-powered pressure sensors. ACS nano, 9(1), 901-907.

[26] He, Y., Chen, W., Gao, C., Zhou, J., Li, X., and Xie, E. (2013). An overview of carbon materials for flexible electrochemical capacitors. Nanoscale, 5(19), 8799-8820.

[27] Nguyen, T. H., Fraiwan, A., and Choi, S. (2014). based batteries: A review. Biosensors and Bioelectronics, 54, 640-649.

[28] Wang, X., Liu, B., Wang, Q., Song, W., Hou, X., Chen, D., Cheng, Y.B.and Shen, G. (2013). Three-Dimensional Hierarchical GeSe2 Nanostructures for High Performance Flexible All-Solid-State Supercapacitors. Advanced Materials, 25(10), 1479-1486.

[29] Wicaksono, I., Tucker, C. I., Sun, T., Guerrero, C. A., Liu, C., Woo, W. M., Pence, E.J. and Dagdeviren, C. (2020). A tailored, electronic textile conformable suit for large-scale spatiotemporal physiological sensing in vivo. npj Flexible Electronics, 4(1), 1-13.

[30] Prasad, G. G., Shetty, N., Thakur, S., and Bommegowda, K. B. (2019, October). Supercapacitor technology and its applications: a review. In IOP Conference Series: Materials Science and Engineering (Vol. 561, No. 1, p. 012105). IOP Publishing.

[31] Meng, C., Gall, O. Z., and Irazoqui, P. P. (2013). A flexible super-capacitive solid-state power supply for miniature implantable medical devices. Biomedical microdevices, 15(6), 973-983.

[32] Park, S., Wang, G., Cho, B., Kim, Y., Song, S., Ji, Y., Yoon, M.H. and Lee, T. (2012). Flexible molecular-scale electronic devices. *Nature nanotechnology*, 7(7), 438

[33] Wang, Y., Song, Y., and Xia, Y. (2016). Electrochemical capacitors: mechanism, materials, systems, characterization and applications. Chemical Society Reviews, 45(21), 5925-5950

[34] Raza, W., Ali, F., Raza, N., Luo, Y., Kim, K. H., Yang, J., Kumar, S., Mehmood, A. and Kwon, E. E. (2018). Recent advancements in supercapacitor technology. Nano Energy, 52, 441-473.

[35] Genc, R., Alas, M. O., Harputlu, E., Repp, S., Kremer, N., Castellano, M., Colak, S.G., Ocakoglu, K. and Erdem, E. (2017). High-capacitance hybrid supercapacitor based on multi-colored fluorescent carbon-dots. Scientific reports, 7(1), 1-13.

[36] Repp, S., Harputlu, E., Gurgen, S., Castellano, M., Kremer, N., Pompe, N., Wörner, J., Hoffmann, A., Thomann, R., Emen, F.M. and Weber, S. (2018). Synergetic effects of Fe 3+ doped spinel Li 4 Ti 5 O 12 nanoparticles on reduced graphene oxide for high surface electrode hybrid supercapacitors. Nanoscale, 10(4), 1877-1884.

[37] Sarac Oztuna, F. E., Unal, O., Erdem, E., Yagci Acar, H., and Unal, U. (2019). Layer-by-layer grown electrodes composed of cationic Fe3O4 nanoparticles and graphene oxide nanosheets for electrochemical energy storage devices. The Journal of Physical Chemistry C, 123(6), 3393-3401.

[38] Sadak, O., Wang, W., Guan, J., Sundramoorthy, A. K., and Gunasekaran, S. (2019). MnO2 Nanoflowers Deposited on Graphene Paper as Electrode Materials for Supercapacitors. ACS Applied Nano Materials, 2(7), 4386-4394

[39] Shown, I., Ganguly, A., Chen, L. C., and Chen, K. H. (2015). Conducting polymer-based flexible supercapacitor. *Energy Science and Engineering*, *3*(1), 2-26.

[40] Kularatna, N. (2014). Energy Storage Devices for Electronic Systems: Rechargeable Batteries and Supercapacitors. Academic Press

[41] Williard, N., Baek, D., Park, J. W., Choi, B. O., Osterman, M., and Pecht, M. (2015). A life model for supercapacitors. IEEE Transactions on Device and Materials Reliability, 15(4), 519-528.

[42] Gualous, H., Chaoui, H., and Gallay, R. (2016, October). Supercapacitor calendar aging for telecommunication applications. In Telecommunications Energy Conference (INTELEC), 2016 IEEE International (pp. 1-5). IEEE.

[43] Yuan, C., Zhang, X., Wu, Q., and Gao, B. (2006). Effect of temperature on the hybrid supercapacitor based on NiO and activated carbon with alkaline polymer gel electrolyte. Solid State Ionics, 177(13-14), 1237-1242.

[44] Shen, C., Xu, S., Xie, Y., Sanghadasa, M., Wang, X., and Lin, L. (2017). A Review of On-Chip Micro Supercapacitors for Integrated Self-Powering Systems. Journal of Microelectromechanical Systems, 26(5), 949-965.

[45] Masarapu, C., Zeng, H. F., Hung, K. H., and Wei, B. (2009). Effect of temperature on the capacitance of carbon nanotube supercapacitors. ACS nano, 3(8), 2199-2206

[46] Li, Z., Ma, K., Mi, H., Ji, C., Li, Z., Guo, F., ... & Pang, H. (2020). Solid-State Hybrid Supercapacitor Assembled from a Heterostructured Co− Ni Battery-like Cathode and Supercapacitor-Type Highly Disordered Carbon Nanosheets. *ChemElectroChem*, *7*(2), 517-525.

[47] Ajuria, J., and Aguesse, F. (2020). An ultrafast battery performing as a supercapacitor: Electrode tuning for high power performance. Electrochimica Acta, 334, 135587.

[48] Joshi, P. S., and Sutrave, D. S. (2017). Mn doped Ruthenium Oxide Permeable Structures and Their Electrochemical properties.

[49] Shao, Y., El-Kady, M. F., Sun, J., Li, Y., Zhang, Q., Zhu, M., Wang, H., Dunn, B.and Kaner, R. B. (2018). Design and mechanisms of asymmetric supercapacitors. Chemical reviews, 118(18), 9233-9280.

[50] Liang, Z., Qu, C., Guo, W., Zou, R., and Xu, Q. (2018). Pristine metal–organic frameworks and their composites for energy storage and conversion. Advanced Materials, 30(37), 1702891.

[51] Méndez-Morales, T., Ganfoud, N., Li, Z., Haefele, M., Rotenberg, B., and Salanne, M. (2019). Performance of microporous carbon electrodes for supercapacitors: Comparing graphene with disordered materials. Energy Storage Materials, 17, 88-92

[52] Mishra, P., and Bhat, B. R. (2020). Correlation between Synthesis and Properties of Graphene. Materials Research Foundations, 64, 25-62.

[53] Yaglikci, S., Gokce, Y., Yagmur, E., and Aktas, Z. (2020). The performance of sulphur doped activated carbon supercapacitors prepared from waste tea. Environmental technology, 41(1), 36-48.

[54] Simon, P., and Gogotsi, Y. (2013). Capacitive energy storage in nanostructured carbon–electrolyte systems. Accounts of chemical research, 46(5), 1094-1103.

[55] Augustyn, V., Simon, P., and Dunn, B. (2014). Pseudocapacitive oxide materials for high-rate electrochemical energy storage. Energy and Environmental Science, 7(5), 1597-1614.

[56] Wang, H., Forse, A. C., Griffin, J. M., Trease, N. M., Trognko, L., Taberna, P. L., Simon, P. and Grey, C. P. (2013). In situ NMR spectroscopy of supercapacitors: insight into the charge storage mechanism. Journal of the American Chemical Society, 135(50), 18968-18980.

[57] Jiang, H., Lee, P. S., and Li, C. (2013). 3D carbon based nanostructures for advanced supercapacitors. Energy and Environmental Science, 6(1), 41-53.

[58] He, Y., Chen, W., Gao, C., Zhou, J., Li, X., and Xie, E. (2013). An overview of carbon materials for flexible electrochemical capacitors. Nanoscale, 5(19), 8799-8820.

[59] Hu, S., Rajamani, R., and Yu, X. (2012). Flexible solid-state paper based carbon nanotube supercapacitor. Applied Physics Letters, 100(10), 104103.

[60] Niu, Z., Zhou, W., Chen, J., Feng, G., Li, H., Ma, W., Li, J., Dong, H., Ren, Y., Zhao, D.and Xie, S. (2011). Compact-designed supercapacitors using free-standing single-walled carbon nanotube films. Energy and Environmental Science, 4(4), 1440-1446.

[61] Frackowiak, E.; Beguin, F. Electrochemical Storage of Energy in Carbon Nanotubes and Nanostructured Carbons. Carbon 2002, 40, 1775–1787.

[62] Urade, A. R., Kaur, G., and Lahiri, I. (2020). Graphene-Based Materials for Micro-Supercapacitors. Materials Research Foundations, 64, 129-166.

[63] Ma, W. L., Cai, Z. H., Zhang, Y., Wang, Z. Y., Xia, L., Ma, S. P., Li, G.H and Huang, Y. (2020). An Overview of Stretchable Supercapacitors Based on Carbon Nanotube and Graphene. Chinese Journal of Polymer Science, 1-15.

[64] Qin, C., Gao, Y., Zhang, L., Liang, X., He, W., Zhang, G., Chen, R., Hu, J., Xiao, L. and Jia, S. (2020). Flexible engineering of light emission in monolayer MoS2 via direct laser writing for multimode optical recording. AIP Advances, 10(4), 045230.

[65] Xu, Z., Zhang, Z., Yin, H., Hou, S., Lin, H., Zhou, J., and Zhuo, S. (2020). Investigation on the role of different conductive polymers in supercapacitors based on a zinc sulfide/reduced graphene oxide/conductive polymer ternary composite electrode. RSC Advances, 10(6), 3122-3129.

[66] Long, S., Wang, H., He, K., Zhou, C., Zeng, G., Lu, Y., Cheng, M., Song, B., Yang, Y., Wang, Z.and Luo, X. (2020). 3D graphene aerogel based photocatalysts: synthesized, properties, and applications. Colloids and Surfaces A: Physicochemical and Engineering Aspects, 124666.

[67] Tingfeng, L., Zhong, J., Dong-Xin, L., Chunmiao, D., Wang, L., Lin, H., and Li, Y. (2020). A density functional theory study of high-performance pre-lithiated MS 2 (M= Mo, W, V) Monolayers as the Anode Material of Lithium Ion Batteries. Scientific Reports (Nature Publisher Group), 10(1).

[68] Zhang, L. L., and Zhao, X. S. (2009). Carbon-based materials as supercapacitor electrodes. Chemical Society Reviews, 38(9), 2520-2531.

[69] Ingole, S. M., Navale, Y. H., Jadhav, Y. M., Salunkhe, A. S., and Patil, V. B. (2020). High-Performance Potentiostatic Electro-Polymerized Polypyrrole (PPy) Electrode for Electrochemical Performance. In Techno-Societal 2018 (pp. 323-328). Springer, Cham.

[70] Jewell, D., Duong, H. M., and Cheng, H. (2017). Advanced Supercapacitors Using Carbon Nanotubes. Materials Research Foundations, 12.

[71] Chu, Z., Wang, Y., Jiao, L., and Zhang, X. (2019). Laser-scribed reduced graphene oxide as counter electrode for dye-sensitized solar cell. Fullerenes, Nanotubes and Carbon Nanostructures, 27(12), 914-919.

[72] Wang, S., Wang, G., Che, X., Wang, S., Li, C., Li, D., Zhang, Y., Dong, Q. and Qiu, J. (2019). Enhancing the capacitive deionization performance of NaMnO 2 by interface engineering and redox-reaction. Environmental Science: Nano, 6(8), 2379-2388.

[73] Ozkan, S. Z., Karpacheva, G. P., and Kolyagin, Y. G. (2019). Hybrid nanocomposite based on poly-3-amine-7-methylamine-2-methylphenazine and single-walled carbon nanotubes. Polymer Bulletin, 76(10), 5285-5300.

[74] Du Pasquier, A., Laforgue, A., Simon, P., Amatucci, G. G., and Fauvarque, J. F. (2002). A Nonaqueous Asymmetric Hybrid Li4Ti5 O 12/Poly (fluorophenylthiophene) Energy Storage Device. Journal of the Electrochemical Society, 149(3), A302-A306.

[75] Muzaffar, A., Ahamed, M. B., Deshmukh, K., and Thirumalai, J. (2019). A review on recent advances in hybrid supercapacitors: Design, fabrication and applications. Renewable and sustainable energy reviews, 101, 123-145.

[76] Zhang, M., He, L., Shi, T., and Zha, R. (2018). Nanocasting and direct synthesis strategies for mesoporous carbons as supercapacitor electrodes. Chemistry of Materials, 30(21), 7391-7412.

[77] Long, J. W., Bélanger, D., Brousse, T., Sugimoto, W., Sassin, M. B., and Crosnier, O. (2011). Asymmetric electrochemical capacitors-stretching the limits of aqueous electrolytes. NAVAL RESEARCH LAB WASHINGTON DC.

[78] Buiel, E. (2006). Development of lead-carbon hybrid battery/super capacitors. Proc. Advanced Capacitor World Summit 2006, 17-19.

[79] Panda, P. K., Grigoriev, A., Mishra, Y. K., and Ahuja, R. (2020). Progress in supercapacitors: roles of two dimensional nanotubular materials. Nanoscale Advances, 2(1), 70-108.

[80] Bashid, H. A. A., Lim, H. N., Kamaruzaman, S., Rashid, S. A., Yunus, R., Huang, N. M., ... and Alagarsamy, P. (2017). Electrodeposition of polypyrrole and reduced graphene oxide onto carbon bundle fibre as electrode for supercapacitor. Nanoscale research letters, 12(1), 246.

[81] Chen, X., Paul, R., and Dai, L. (2017). Carbon-based supercapacitors for efficient energy storage. National Science Review, 4(3), 453-489.

[82] Rogers, J. A., Someya, T., and Huang, Y. (2010). Materials and mechanics for stretchable electronics. science, 327(5973), 1603-1607.

[83] Sekitani, T., and Someya, T. (2010). Stretchable, large-area organic electronics. Advanced Materials, 22(20), 2228-2246.

[84] An, B. W., Shin, J. H., Kim, S. Y., Kim, J., Ji, S., Park, J., ... and Jo, S. (2017). Smart sensor systems for wearable electronic devices. Polymers, 9(8), 303.

[85] Gu, Y., Wang, X., Gu, W., Wu, Y., Li, T., and Zhang, T. (2017). Flexible electronic eardrum. Nano Research, 10(8), 2683-2691.

[86] Zhou, W., Yao, S., Wang, H., Du, Q., Ma, Y., and Zhu, Y. (2020). Gas-Permeable, Ultrathin, Stretchable Epidermal Electronics with Porous Electrodes. ACS nano, 14(5), 5798-5805.

[87] Benight, S. J., Wang, C., Tok, J. B., and Bao, Z. (2013). Stretchable and self-healing polymers and devices for electronic skin. Progress in Polymer Science, 38(12), 1961-1977.

[88] Shi, Y., Wang, X., Luo, J., and Xie, Q. (2019). Fabrication and characterization of polyoxometalate/2D graphene-based flexible supercapacitors for wearable electronic pulse-beat application. Journal of Materials Science: Materials in Electronics, 30(4), 3692-3700.

[89] Zhu, H. W., Ge, J., Peng, Y. C., Zhao, H. Y., Shi, L. A., and Yu, S. H. (2018). Dip-coating processed sponge-based electrodes for stretchable Zn-MnO 2 batteries. Nano Research, 11(3), 1554-1562.

[90] Yan, C., Wang, X., Cui, M., Wang, J., Kang, W., Foo, C. Y., and Lee, P. S. (2014). Batteries: Stretchable Silver-Zinc Batteries Based on Embedded Nanowire Elastic Conductors (Adv. Energy Mater. 5/2014). Advanced Energy Materials, 4(5).

[91] Wang, H., Wang, C., Jian, M., Wang, Q., Xia, K., Yin, Z., Zhang, M., Liang, X.and Zhang, Y. (2018). Superelastic wire-shaped supercapacitor sustaining 850% tensile strain based on carbon nanotube@ graphene fiber. Nano Research, 11(5), 2347-2356.

[92] Kim, H., Yoon, J., Lee, G., Paik, S. H., Choi, G., Kim, D., B.M., Zi, G. and Ha, J. S. (2016). Encapsulated, high-performance, stretchable array of stacked planar micro-supercapacitors as waterproof wearable energy storage devices. ACS applied materials and interfaces, 8(25), 16016-16025.

[93] Kim, W., and Kim, W. (2016). 3 V omni-directionally stretchable one-body supercapacitors based on a single ion–gel matrix and carbon nanotubes. Nanotechnology, 27(22), 225402.

[94] Jung, S., Hong, S., Kim, J., Lee, S., Hyeon, T., Lee, M., and Kim, D. H. (2015). Wearable fall detector using integrated sensors and energy devices. Scientific reports, 5, 17081.

[95] Li, X., Gu, T., and Wei, B. (2012). Dynamic and galvanic stability of stretchable supercapacitors. Nano letters, 12(12), 6366-6371.

[96] He, X., Song, P., Shen, X., Sun, Y., Ji, Z., Zhou, H., and Li, B. (2019). Chitosan-assisted synthesis of wearable textile electrodes for high-performance electrochemical energy storage. Cellulose, 26(17), 9349-9359.

[97] Kim, D., Shin, G., Kang, Y. J., Kim, W., and Ha, J. S. (2013). Fabrication of a stretchable solid-state micro-supercapacitor array. Acs Nano, 7(9), 7975-7982.

[98] Zhu, H. W., Ge, J., Peng, Y. C., Zhao, H. Y., Shi, L. A., and Yu, S. H. (2018). Dip-coating processed sponge-based electrodes for stretchable Zn-MnO 2 batteries. Nano Research, 11(3), 1554-1562.

[99] Lv, Z., Li, W., Yang, L., Loh, X. J., and Chen, X. (2019). Custom-made electrochemical energy storage devices. Acs Energy Letters, 4(2), 606-614.

[100] Song, J., Feng, X., and Huang, Y. (2016). Mechanics and thermal management of stretchable inorganic electronics. National science review, 3(1), 128-143.

[101] Raza, W., Ali, F., Raza, N., Luo, Y., Kim, K. H., Yang, J., Kumar, S., Mehmood, A.and Kwon, E. E. (2018). Recent advancements in supercapacitor technology. Nano Energy, 52, 441-473.

[102] Zhang, K., Liu, M., Si, M., Wang, Z., Zhuo, S., Chai, L., and Shi, Y. (2019). Polyhydroxyalkanoate-Modified Bacterium Regulates Biomass Structure and Promotes Synthesis of Carbon Materials for High-Performance Supercapacitors. ChemSusChem, 12(8), 1732-1742.

[103] Guan, L., Yu, L., and Chen, G. Z. (2016). Capacitive and non-capacitive faradaic charge storage. Electrochimica Acta, 206, 464-478.

[104] Ogoshi, T., Yoshikoshi, K., Sueto, R., Nishihara, H., and Yamagishi, T. A. (2015). Porous Carbon Fibers Containing Pores with Sizes Controlled at the Ångstrom Level by the Cavity Size of Pillar [6] arene. Angewandte Chemie International Edition, 54(22), 6466-6469.

[105] Yu, S., Yang, N., Zhuang, H., Mandal, S., Williams, O. A., Yang, B., Huang, N and Jiang, X. (2017). Battery-like supercapacitors from diamond networks and water-soluble redox electrolytes. Journal of Materials Chemistry A, 5(4), 1778-1785.

[106] Shayeh, J. S., Sadeghinia, M., Siadat, S. O. R., Ehsani, A., Rezaei, M., and Omidi, M. (2017). A novel route for electrosynthesis of CuCr2O4 nanocomposite with p-type conductive polymer as a high performance material for electrochemical supercapacitors. Journal of colloid and interface science, 496, 401-406.

[107] Picó, F., Rojo, J. M., Sanjuan, M. L., Anson, A., Benito, A. M., Callejas, M. A., Maser, W.K and Martinez, M. T. (2004). Single-walled carbon nanotubes as electrodes in supercapacitors. Journal of the Electrochemical Society, 151(6), A831.

[108] Frackowiak, E., Gautier, S., Gaucher, H., Bonnamy, S., and Beguin, F. (1999). Electrochemical storage of lithium in multiwalled carbon nanotubes. Carbon, 37(1), 61-69.

[109] Chen, X., Paul, R., and Dai, L. (2017). Carbon-based supercapacitors for efficient energy storage. National Science Review, 4(3), 453-489.

[110] Chavhan, M. P., and Ganguly, S. (2017). Charge transport in activated carbon electrodes: the behaviour of three electrolytes vis-à-vis their specific conductance. Ionics, 23(8), 2037-2044.

[111] Seyedsalehi, M., Goodarzi, M., and Barzanouni, H. (2014). Use of carbon in increasing the quality of drinking water-Case study: the wells of Savejbolagh villages. J Biodivers Environ Sci, 4(5), 102-111.

[112] Dang, Y. L., Cao, J. P., Hao, Z. Q., Wu, Y., Zhao, X. Y., Zhuang, Q. Q., Zhou, Z. and Wei, X. Y. (2019). Preparation of Porous Carbon Spheres Under Different Activation Conditions from 2-Keto-l-gulonic Acid Mother Liquor for Electric Double-Layer Capacitor. Waste and Biomass Valorization, 1-12.

[113] Sołoducho, J., Cabaj, J., and Zając, D. (2016). Advances in electrode materials. Advanced Electrode Materials, 1.

[114] Kado, Y., Soneda, Y., Horii, D., Okura, K., and Suematsu, S. (2020). Mechanochemical Processing of Natural Graphite under Different Atmospheres for Fabricating Electrodes Used in Electric Double-layer Capacitors. Electrochemistry, 88(3), 94-98.

[115] Choi, H., and Yoon, H. (2015). Nanostructured electrode materials for electrochemical capacitor applications. Nanomaterials, 5(2), 906-936.

[116] Wang, K., Cao, Y., Wang, X., Castro, M. A., Luo, B., Gu, Z., Liu, J., Hoefelmeyer, J.D.and Fan, Q. (2016). Rod-shape porous carbon derived from aniline modified lignin for symmetric supercapacitors. Journal of Power Sources, 307, 462-467.

[117] Inoue, A., and Matsumoto, A. (2017, July). Rapid adsorption removal of hydrogen sulfide by surface-modified activated carbon. In AIP Conference Proceedings (Vol. 1865, No. 1, p. 020003). AIP Publishing LLC.

[118] Grigorova, E., Khristov, M., Stoycheva, I., Tsyntsarski, B., Nihtianova, D., and Markov, P. (2017). Effect of activated carbons derived from apricot stones or polyolefin wax on hydrogen sorption properties of MgH2. Bulg. Chem. Commun, 49, 109-114.

[119] Saito, Y., Meguro, M., Ashizawa, M., Waki, K., Yuksel, R., Unalan, H. E., and Matsumoto, H. (2017). Manganese dioxide nanowires on carbon nanofiber frameworks for efficient electrochemical device electrodes. RSC advances, 7(20), 12351-12358.

[120] Qin, T., Xu, Z., Wang, Z., Peng, S., and He, D. (2019). 2.5 V salt-in-water supercapacitors based on alkali type double salt/carbon composite anode. Journal of Materials Chemistry A, 7(45), 26011-26019.

[121] Haider, W. A., He, L., Mirza, H. A., Tahir, M., Khan, A. M., Owusu, K. A., and Mai, L. (2020). Bilayered microelectrodes based on electrochemically deposited MnO 2/polypyrrole towards fast charge transport kinetics for micro-supercapacitors. RSC Advances, 10(31), 18245-18251.

[122] Verma, K. D., Sinha, P., Banerjee, S., and Kar, K. K. (2020). Characteristics of Electrode Materials for Supercapacitors. In Handbook of Nanocomposite Supercapacitor Materials I (pp. 269-285). Springer, Cham.

[123] Liu, T., Jiang, C., You, W., and Yu, J. (2017). Hierarchical porous C/MnO 2 composite hollow microspheres with enhanced supercapacitor performance. Journal of Materials Chemistry A, 5(18), 8635-8643.

[124] Zang, L., Liu, Q., Qiu, J., Yang, C., Wei, C., Liu, C., and Lao, L. (2017). Design and fabrication of an all-solid-state polymer supercapacitor with highly mechanical flexibility based on polypyrrole hydrogel. ACS applied materials and interfaces, 9(39), 33941-33947.

[125] Mike, J. F., and J. L. Lutkenhaus. 2013. Recent advances in conjugated polymer energy storage. J. Polym. Sci. Part B: Polym. Phys. 51:468–480. 24. Ramya, R., R. Sivasubramanian, and M. V. Sangaranarayanan. 2013.

[126] Ramya, R., Sivasubramanian, R., and Sangaranarayanan, M. V. (2013). Conducting polymers-based electrochemical supercapacitors—progress and prospects. Electrochimica Acta, 101, 109-129.

[127] Burke, A. (2007). RandD considerations for the performance and application of electrochemical capacitors. Electrochimica Acta, 53(3), 1083-1091.

[128] Rantho, M. N., Madito, M. J., Oyedotun, K. O., Tarimo, D. J., and Manyala, N. (2020). Hybrid electrochemical supercapacitor based on birnessite-type MnO2/carbon composite as the positive electrode and carbonized iron-polyaniline/nickel graphene foam as a negative electrode. AIP Advances, 10(6), 065113.

[129] Berrueta, A., Ursúa, A., San Martín, I., Eftekhari, A., and Sanchis, P. (2019). Supercapacitors: Electrical Characteristics, Modeling, Applications, and Future Trends. IEEE Access, 7, 50869-50896. Doi: 10.1109/ACCESS.2019.2908558

[130] Zhang, J., Chen, Z., Wang, Y., Yan, X., Zhou, Z., and Lv, H. (2019). All-Solid-State Flexible Asymmetric Supercapacitor with Good Cycling Performance and Ultra-Power Density by Electrode Materials of Core-Shell CoNiO 2@ NiAl-Layered Double Hydroxide and Hollow Spherical α-Fe 2 O 3. Nanoscale research letters, 14(1), 87. DOI: https://doi.org/10.1186/s11671-019-2910-5

[131] Lu, B., Yuk, H., Lin, S., Jian, N., Qu, K., Xu, J., and Zhao, X. (2019). Pure PEDOT: PSS hydrogels. Nature communications, 10(1), 1043. doi:10.1038/s41467-019-09003-5

[132] Chen, Q., Wang, X., Chen, F., Zhang, N., and Ma, M. (2019). Extremely strong and tough polythiophene composite for flexible electronics. Chemical Engineering Journal, 368, 933-940. https://doi.org/10.1016/j.cej.2019.02.203

[133] Liu, Q., Bai, Z., Fan, J., Sun, Z., Mi, H., Zhang, Q., and Qiu, J. (2018). A hydrogel-mediated scalable strategy toward core-shell polyaniline/poly (acrylic acid)-modified carbon nanotube hybrids as efficient electrodes for supercapacitor applications. Applied Surface Science, 436, 189-197. https://doi.org/10.1016/j.apsusc.2017.11.209

[134] Zhang, W., Xin, W., Hu, T., Gong, Q., Gao, T., and Zhou, G. (2019). One-step synthesis of NiCo2O4 nanorods and firework-shaped microspheres formed with necklace-like structure for supercapacitor materials. Ceramics International,45(7),8406-8413. https://doi.org/10.1016/j.ceramint.2019.01.149

[135] Lee, S., Cho, M. S., Lee, H., Nam, J. D., and Lee, Y. (2012). A facile synthetic route for well defined multilayer films of graphene and PEDOT via an electrochemical method. Journal of Materials Chemistry, 22(5), 1899-1903. DOI:10.1039/C1JM13739E

[136] Chu, C. Y., Tsai, J. T., and Sun, C. L. (2012). Synthesis of PEDOT-modified graphene composite materials as flexible electrodes for energy storage and conversion applications. International Journal of Hydrogen Energy, 37(18), 13880-13886. https://doi.org/10.1016/j.ijhydene.2012.05.017

[137] Jiang, F., Yao, Z., Yue, R., Du, Y., Xu, J., Yang, P., and Wang, C. (2012). Electrochemical fabrication of long-term stable Pt-loaded PEDOT/graphene composites for ethanol electrooxidation. International Journal of Hydrogen Energy,37(19), 14085-14093. https://doi.org/10.1016/j.ijhydene.2012.04.084

[138] Choi, K. S., Liu, F., Choi, J. S., and Seo, T. S. (2010). Fabrication of free-standing multilayered graphene and poly (3, 4-ethylenedioxythiophene) composite films with enhanced conductive and mechanical properties. Langmuir, 26(15), 12902-12908. https://doi.org/10.1021/la101698j

[139] Eftekhari, A., and Molaei, F. (2015). Carbon nanotube-assisted electrodeposition. Part II: Superior pseudo-capacitive behavior of manganese oxide film electrodeposited at high current densities. Journal of Power Sources, 274, 1315-1321. https://doi.org/10.1016/j.jpowsour.2013.10.144

[140] Li, X., Wu, Y., Hua, K., Li, S., Fang, D., Luo, Z., Bao, R., Fan, X. and Yi, J. (2018). Vertically aligned polyaniline nanowire arrays for lithium-ion battery. Colloid and Polymer Science, 296(8), 1395-1400.

[141] Khomenko, V., Raymundo-Pinero, E., Frackowiak, E., and Beguin, F. (2006). High-voltage asymmetric supercapacitors operating in aqueous electrolyte. Applied Physics A, 82(4), 567-573.

[142] Majumdar, D. (2018). An Overview on Ruthenium Oxide Composites–Challenging Material for Energy Storage Applications. Material Science Research India, 15(1), 30-40.

[143] Widiastuti, N., and Susanti, I. (2019). Activation of zeolite-Y templated carbon with KOH to enhance the CO2 adsorption capacity. Malaysian Journal of Fundamental and Applied Sciences, 15(2), 249-253.

[144] Luo, J., Yao, X., Yang, L., Han, Y., Chen, L., Geng, X., Vattipalli, V., Dong, Q., Fan, W., Wang, D. and Zhu, H. (2017). Free-standing porous carbon electrodes derived from wood for high-performance Li-O 2 battery applications. Nano Research, 10(12), 4318-4326.

[145] Li, M., Xiang, S., Chang, X., and Chang, C. (2017). Resorcinol-formaldehyde carbon spheres/polyaniline composite with excellent electrochemical performance for supercapacitors. Journal of Solid State Electrochemistry, 21(2), 485-494.

[146] Ofoegbu, S. U., Ferreira, M. G., and Zheludkevich, M. L. (2019). Galvanically stimulated degradation of carbon-fiber reinforced polymer composites: a critical review. Materials, 12(4), 651.

[147] Hellstern, T. R., Kibsgaard, J., Tsai, C., Palm, D. W., King, L. A., Abild-Pedersen, F., and Jaramillo, T. F. (2017). Investigating catalyst–support interactions to improve the hydrogen evolution reaction activity of thiomolybdate [Mo3S13] 2–nanoclusters. ACS Catalysis, 7(10), 7126-7130.

[148] Makgopa, K., Ejikeme, P. M., and Ozoemena, K. I. (2016). Nanostructured manganese oxides in supercapacitors. In Nanomaterials in Advanced Batteries and Supercapacitors (pp. 345-376). Springer, Cham.

[149] Chen, W., Tao, X., Wei, D., Wang, H., Yu, Q., and Li, Y. (2016). High-performance supercapacitor based on actived carbon–MnO 2–polyaniline composite. Journal of Materials Science: Materials in Electronics, 27(2), 1357-1362.

[150] Roldán, S., Blanco, C., Granda, M., Menéndez, R., and Santamaría, R. (2011). Towards a further generation of high-energy carbon-based capacitors by using redox-active electrolytes. Angewandte Chemie International Edition, 50(7), 1699-1701.

[151] Wang, F., Wu, X., Yuan, X., Liu, Z., Zhang, Y., Fu, L., Zhu, Y., Zhou, Q., Wu, Y. and Huang, W. (2017). Latest advances in supercapacitors: from new electrode materials to novel device designs. Chemical Society Reviews, 46(22), 6816-6854.

[152] Shown, I., Ganguly, A., Chen, L. C., and Chen, K. H. (2015). Conducting polymer-based flexible supercapasitor. Energy Sci Eng 3 (1): 2–26.

[153] Gao, H., and Lian, K. (2016). AH 5 BW 12 O 40–polyvinyl alcohol polymer electrolyte and its application in solid supercapacitors. Journal of Materials Chemistry A, 4(24), 9585-9592.

[154] Fang, X., and Yao, D. (2013, November). An overview of solid-like electrolytes for supercapacitors. In ASME International Mechanical Engineering Congress and Exposition (Vol. 56284, p. V06AT07A071). American Society of Mechanical Engineers.

[155] Zhong, C., Deng, Y., Hu, W., Qiao, J., Zhang, L., and Zhang, J. (2015). A review of electrolyte materials and compositions for electrochemical supercapacitors. Chemical Society Reviews, 44(21), 7484-7539.

[156] Sundriyal, S., Kaur, H., Bhardwaj, S. K., Mishra, S., Kim, K. H., and Deep, A. (2018). Metal-organic frameworks and their composites as efficient electrodes for supercapacitor applications. Coordination Chemistry Reviews, 369, 15-38.

[157] Suresh, R., Tamilarasan, K., and Vadivu, D. S. (2018). Electrochemical Features of Symmetric and Asymmetric Supercapacitors Based on Nanostructured Mn-CuO Electrodes. Oriental Journal of Chemistry, 34(6), 3058.

[158] Qian, H., Kucernak, A. R., Greenhalgh, E. S., Bismarck, A., and Shaffer, M. S. (2013). Multifunctional structural supercapacitor composites based on carbon aerogel modified high performance carbon fiber fabric. ACS applied materials and interfaces, 5(13), 6113-6122. https://doi.org/10.1021/am400947j

[159] Bollmann, W. (2012). Crystal defects and crystalline interfaces. Springer Science and Business Media.

[160] Madrid, J. C. M., and Ghuman, K. K. (2021). Disorder in energy materials and strategies to model it. Advances in Physics: X, 6(1), 1848458.

[161] Dornberger, E. (1997). Prediction of OSF ring dynamics and grown-in voids in Czochralski silicon crystals (Doctoral dissertation, UCL-Université Catholique de Louvain).

[162] Peng, S., Fan, L., Wei, C., Bao, H., Zhang, H., Xu, W., and Xu, J. (2016). Polypyrrole/nickel sulfide/bacterial cellulose nanofibrous composite membranes for flexible supercapacitor electrodes. Cellulose, 23(4), 2639-2651.

[163] Shao, H., Li, H. W., Cheng, Y. J., Lin, H., and He, L. (2018). Next-Generation Energy Storage Materials Explored by Advanced Scanning Techniques. Scanning, 2018.

[164] Shan, Y., Tang, J., Wu, L., Lu, S., Dai, X., and Xiang, Y. (2019). Spatial self-phase modulation and all-optical switching of graphene oxide dispersions. *Journal of Alloys and Compounds*, *771*, 900-904.

[165] Men, B., Guo, P., Sun, Y., Tang, Y., Chen, Y., Pan, J., and Wan, P. (2019). High-performance nitrogen-doped hierarchical porous carbon derived from cauliflower for advanced supercapacitors. *Journal of Materials Science*, *54*(3), 2446-2457.

[166] Zhou, H., Zhang, C., Ni, J., and Han, X. (2019). Prevalence of cardiovascular risk factors in non-menopausal and postmenopausal inpatients with type 2 diabetes mellitus in China. *BMC endocrine disorders*, *19*(1), 98.

[167] He, Y., Chen, W., Li, X., Zhang, Z., Fu, J., Zhao, C., and Xie, E. (2013). Freestanding three-dimensional graphene/MnO2 composite networks as ultralight and flexible supercapacitor electrodes. *ACS nano*, *7*(1), 174-182.

[168] Zang, X., Wang, J., Qin, Y., Wang, T., He, C., Shao, Q., and Zhu, H. (2020). Enhancing Capacitance Performance of Ti. sub. 3C. sub. 2T. sub. x MXene as Electrode Materials of Supercapacitor: From Controlled Preparation to Composite Structure Construction. *Nano-Micro Letters*, *12*(1).

[169] Yang, Y. J. (2016). Facile synthesis of poly (Safranine T)/Reduced graphene oxide nanocomposite for supercapacitors with wide potential window in aqueous neutral electrolyte. *Fullerenes, Nanotubes and Carbon Nanostructures*, *24*(4), 243-248.

[170] Zhao, Z., Kong, Y., Liu, C., Liu, J., Wang, Z., Zheng, G., and Mei, Y. (2020). Atomic layer deposition-induced integration of N-doped carbon particles on carbon foam for flexible supercapacitor. Journal of Materiomics, 6(1), 209-215.

[171] Meng, W., Wen, Y., Dai, L., He, Z., and Wang, L. (2018). A novel electrochemical sensor for glucose detection based on Ag@ ZIF-67 nanocomposite. *Sensors and Actuators B: Chemical*, *260*, 852-860.

[172] Xia, K., Wang, G., Zhang, H., Yu, Y., Liu, L., and Chen, A. (2017). Synthesis and characterization of nitrogen-doped graphene hollow spheres as electrode material for supercapacitors. *Journal of Nanoparticle Research*, *19*(7), 254.

[173] Yadav, N., Yadav, N., and Hashmi, S. A. (2020). Ionic liquid incorporated, redox-active blend polymer electrolyte for high energy density quasi-solid-state carbon supercapacitor. *Journal of Power Sources*, *451*, 227771.

[174] Yadav, N., Mishra, K., and Hashmi, S. A. (2017). Optimization of porous polymer electrolyte for quasi-solid-state electrical double layer supercapacitor. *Electrochimica Acta*, *235*, 570-582.

[175] Singh, R., Bhattacharya, B., Gupta, M., Khan, Z. H., Tomar, S. K., Singh, V., and Singh, P. K. (2017). Electrical and structural properties of ionic liquid doped polymer gel electrolyte for dual energy storage devices. *International Journal of Hydrogen Energy*, *42*(21), 14602-14607.

[176] Ouyang, L. Z., Yang, X. S., Zhu, M., Liu, J. W., Dong, H. W., Sun, D. L., Zou, J.and Yao, X. D. (2014). Enhanced hydrogen storage kinetics and stability by synergistic effects of in situ formed CeH2. 73 and Ni in CeH2. 73-MgH2-Ni nanocomposites. *The Journal of Physical Chemistry C*, *118*(15), 7808-7820.

[177] Julien, C. M., and Mauger, A. (2017). Nanostructured MnO2 as electrode materials for energy storage. *Nanomaterials*, *7*(11), 396.

[178] Xu, D., Sun, X. N., Hu, W., and Chen, X. Y. (2017). Carbon nanosheets-based supercapacitors: design of dual redox additives of 1, 4-dihydroxyanthraquinone and hydroquinone for improved performance. *Journal of Power Sources*, *357*, 107-116.

[179] Singh, B. K., Shaikh, A., Dusane, R. O., and Parida, S. (2019). Nanoporous gold–Nitrogen–doped carbon nano-onions all-solid-state micro-supercapacitor. *Nano-Structures and Nano-Objects*, *17*, 239-247.

[180] Zheng, M., Xiao, X., Li, L., Gu, P., Dai, X., Tang, H., and Pang, H. (2018). Hierarchically nanostructured transition metal oxides for supercapacitors. *Science China Materials*, *61*(2), 185-209.

[181] Nguyen, D. N., and Yoon, H. (2016). Recent advances in nanostructured conducting polymers: from synthesis to practical applications. *Polymers*, *8*(4), 118.

[182] Xie, L., Su, F., Xie, L., Guo, X., Kong, Q. Q., Sun, G., and Chen, C. M. (2020). Effect of pore structure and doping species on charge storage mechanisms in porous carbon-based supercapacitor. *Materials Chemistry Frontiers*.

[183] Zhang, L., Yang, S., Chang, J., Zhao, D., Wang, J., Yang, C., and Cao, B. (2020). A Review of Redox Electrolytes for Supercapacitors. *Frontiers in Chemistry*, *8*, 413.

[184] Sun, J., Man, P., Zhang, Q., He, B., Zhou, Z., Li, C. and Li, Q. (2018). Hierarchically-structured Co3O4 nanowire arrays grown on carbon nanotube fibers as novel cathodes for high-performance wearable fiber-shaped asymmetric supercapacitors. *Applied Surface Science*, *447*, 795-801.

[185] Quevedo, M. C., Galicia, G., Mayen-Mondragon, R., and Llongueras, J. G. (2018). Role of turbulent flow seawater in the corrosion enhancement of an Al–Zn–Mg alloy: an electrochemical impedance spectroscopy (EIS) analysis of oxygen reduction reaction (ORR). *Journal of materials research and technology*, *7*(2), 149-157.

[186] Zhao, Y., Li, L., Pan, L., Yu, G., and Shi, Y. (2017). Conducting Polymer Hydrogels and Their Applications as Electrode Materials. *Functional Electrodes For Enzymatic And Microbial Electrochemical Systems*, 291.

[187] Liu, B. T., Shi, X. M., Lang, X. Y., Gu, L., Wen, Z., Zhao, M., and Jiang, Q. (2018). Extraordinary pseudocapacitive energy storage triggered by phase transformation in hierarchical vanadium oxides. *Nature communications*, *9*(1), 1-9.

[188] Dubal, D. P., Nagar, B., Suarez-Guevara, J., Tonti, D., Enciso, E., Palomino, P., and Gomez-Romero, P. (2017). Ultrahigh energy density supercapacitors through a double hybrid strategy. *Materials Today Energy*, *5*, 58-65.

[189] Karuppasamy, M., Muthu, D., Haldorai, Y., and Rajendra Kumar, R. T. (2020). Solvothermal synthesis of Fe 3 S 4@ graphene composite electrode materials for energy storage. *Carbon Letters*, 1-7.

[190] Makgopa, K., Bello, A., Raju, K., Modibane, K. D., and Hato, M. J. (2019). Nanostructured Metal Oxides for Supercapacitor Applications. In *Emerging Nanostructured Materials for Energy and Environmental Science* (pp. 247-303). Springer, Cham.

[191] Li, W., Wang, D., Song, Z., Gong, Z., Guo, X., Liu, J., and Li, G. (2019). Carbon confinement synthesis of interlayer-expanded and sulfur-enriched MoS 2+ x nanocoating on hollow carbon spheres for advanced Li-S batteries. *Nano Research*, *12*(11), 2908-2917.

[192] Yi, C. Q., Zou, J. P., Yang, H. Z., and Xian, L. E. N. G. (2018). Recent advances in pseudocapacitor electrode materials: transition metal oxides and nitrides. *Transactions of Nonferrous Metals Society of China*, *28*(10), 1980-2001.

[193] Mezgebe, M. M., Xu, K., Wei, G., Guang, S., and Xu, H. (2019). Polyaniline wrapped manganese dioxide nanorods: Facile synthesis and as an electrode material for supercapacitors with remarkable electrochemical properties. *Journal of Alloys and Compounds*, *794*, 634-644.

[194] Fang, D. L., Wu, B. C., Mao, A. Q., Yan, Y., and Zheng, C. H. (2010). Supercapacitive properties of ultra-fine MnO2 prepared by a solid-state coordination reaction. *Journal of alloys and compounds*, *507*(2), 526-530.

[195] Cheng, J. H., Shao, G., Yu, H. J., and Xu, J. J. (2010). Excellent catalytic and electrochemical properties of the mesoporous MnO2 nanospheres/nanosheets. *Journal of alloys and compounds*, *505*(1), 163-167.

[196] Maile, N. C., Mahadik, S. B., Takale, M. V., and Fulari, V. J. (2019). Surface deformation studies of MnO2 film by double exposure digital holographic interferometry technique. *Materials Research Express*, *6*(4), 045204.

[197] Ju, J., Zhao, H., Kang, W., Tian, N., Deng, N., and Cheng, B. (2017). Designing MnO2 and carbon composite porous nanofiber structure for supercapacitor applications. *Electrochimica Acta*, *258*, 116-123.

[198] Nasir, F., and Mohammad, M. A. (2020). Investigation of Device Dimensions on Electric Double Layer Microsupercapacitor Performance and Operating Mechanism. *IEEE Access*, *8*, 28367-28374.

[199] Amrouche, S. O., Rekioua, D., Rekioua, T., and Bacha, S. (2016). Overview of energy storage in renewable energy systems. *International Journal of Hydrogen Energy*, *41*(45), 20914-20927.

[200] An, T., and Cheng, W. (2018). Recent progress in stretchable supercapacitors. *Journal of Materials Chemistry A*, *6*(32), 15478-15494.

[201] Lai, Y. C., Deng, J., Zhang, S. L., Niu, S., Guo, H., and Wang, Z. L. (2017). Single-thread-based wearable and highly stretchable triboelectric nanogenerators and their applications in cloth-based self-powered human-interactive and biomedical sensing. *Advanced Functional Materials*, *27*(1), 1604462.

[202] Selivanova, M., Zhang, S., Billet, B., Malik, A., Prine, N., Landry, E., Gu, X., Xiang, P. and Rondeau-Gagné, S. (2019). Branched Polyethylene as a Plasticizing Additive to Modulate the Mechanical Properties of π-Conjugated Polymers. *Macromolecules*, *52*(20), 7870-7877.

[203] Han, S., Kim, M. K., Wang, B., Wie, D. S., Wang, S., and Lee, C. H. (2016). Mechanically reinforced skin-electronics with networked nanocomposite elastomer. *Advanced Materials*, *28*(46), 10257-10265.

[204] Gao, D., Parida, K., and Lee, P. S. (2019). Emerging Soft Conductors for Bioelectronic Interfaces. *Advanced Functional Materials*, 1907184.

[205] Zheng, S., Ma, J., Wu, Z. S., Zhou, F., He, Y. B., Kang, F., and Bao, X. (2018). All-solid-state flexible planar lithium ion micro-capacitors. *Energy and Environmental Science*, *11*(8), 2001-2009.

[206] Borenstein, A., Hanna, O., Attias, R., Luski, S., Brousse, T., and Aurbach, D. (2017). Carbon-based composite materials for supercapacitor electrodes: a review. *Journal of Materials Chemistry A*, *5*(25), 12653-12672.

[207] Han, M., Wang, X., Chen, C., Zou, M., Niu, Z., Yang, Q. H., and Xie, S. (2018). All-solid-state supercapacitors with superior compressive strength and volumetric capacitance. *Energy Storage Materials*, *13*, 119-126.

[208] Yang, J., Hong, T., Deng, J., Wang, Y., Lei, F., Zhang, J., and Guo, C. F. (2019). Stretchable, transparent and imperceptible supercapacitors based on Au@ MnO 2 nanomesh electrodes. *Chemical Communications*, *55*(91), 13737-13740.

[209] Chen, D. Z., Yu, J., Lu, W., Zhao, Y., Yan, Y., and Chou, T. W. (2017). Temperature effects on electrochemical performance of carbon nanotube film based flexible all-solid-state supercapacitors. *Electrochimica Acta*, *233*, 181-189.

[210] Guo, Y., Wang, T., Chen, F., Sun, X., Li, X., Yu, Z.,and Chen, X. (2016). Hierarchical graphene–polyaniline nanocomposite films for high-performance flexible electronic gas sensors. *Nanoscale*, *8*(23), 12073-12080.

[211] Gong, S., Zhao, Y., Shi, Q., Wang, Y., Yap, L. W., and Cheng, W. (2016). Self-assembled Ultrathin Gold Nanowires as Highly Transparent, Conductive and Stretchable Supercapacitor. *Electroanalysis*, *28*(6), 1298-1304.

[212] Cai, G., Park, S., Cheng, X., Eh, A. L. S., and Lee, P. S. (2018). Inkjet-printed metal oxide nanoparticles on elastomer for strain-adaptive transmissive electrochromic energy storage systems. *Science and Technology of Advanced Materials*, *19*(1), 759-770.

[213] Saravanakumara, B., Muralidharanb, G., Vadivel, S., Maruthamani, D., and Kumaravel, M. (2018). Theory, Fundamentals and Application of Supercapacitors. *Electrochemical Capacitors: Theory, Materials and Applications*, *26*, 1.

[214] Yan, J., Wang, S., Chen, Y., Yuan, M., Huang, Y., Lian, J., and Li, H. (2019). Smart in situ construction of NiS/MoS2 composite nanosheets with ultrahigh specific capacity for high-performance asymmetric supercapacitor. *Journal of Alloys and Compounds*, *811*, 151915.

[215] Ma, Y., Hou, C., Zhang, H., Zhang, Q., Liu, H., Wu, S., and Guo, Z. (2019). Three-dimensional core-shell Fe3O4/Polyaniline coaxial heterogeneous nanonets: Preparation and high performance supercapacitor electrodes. *Electrochimica Acta*, *315*, 114-123.

[216] Choudhary, R. B., Ansari, S., and Purty, B. (2020). Robust electrochemical performance of polypyrrole (PPy) and polyindole (PIn) based hybrid electrode materials for supercapacitor application: A review. *Journal of Energy Storage*, *29*, 101302.

[217] Ambade, R. B., Ambade, S. B., Shrestha, N. K., Salunkhe, R. R., Lee, W., Bagde, S. S., ... and Lee, S. H. (2017). Controlled growth of polythiophene nanofibers in TiO 2 nanotube arrays for supercapacitor applications. *Journal of Materials Chemistry A*, *5*(1), 172-180.

[218] Soni, R., Anothumakkool, B., and Kurungot, S. (2016). 1D Alignment of PEDOT in a Buckypaper for High-Performance Solid Supercapacitors. *ChemElectroChem*, *3*(9), 1329-1336.

[219] Kasana, V. K., Kumar, Y., Singh, P., and Dixit, S. (2016). Experimental Studies on Poly (3-Hexylthiophene) Electrode Based Supercapacitors: A Comparison of Electrolytic Species.

[220] Yang, J., Li, X. L., Zhou, J. W., Wang, B., and Cheng, J. L. (2020). Fiber-shaped Supercapacitors: Advanced Strategies toward High-performances and Multi-functions. *Chinese Journal of Polymer Science*, 1-20.

[221] Selvakumar, M. (2018). Multilayered electrode materials based on polyaniline/activated carbon composites for supercapacitor applications. *International Journal of Hydrogen Energy*, *43*(8), 4067-4080.

[222] Liu, Y., and Wang, S. (2017). Polymer/Graphene Composites for Energy Storage. In *Polymer-Engineered Nanostructures for Advanced Energy Applications* (pp. 337-364). Springer, Cham.

[223] Feng, H. P., Tang, L., Zeng, G. M., Tang, J., Deng, Y. C., Yan, M., and Chen, S. (2018). Carbon-based core–shell nanostructured materials for electrochemical energy storage. *Journal of Materials Chemistry A*, *6*(17), 7310-7337.

[224] Harris, K. D., Elias, A. L., and Chung, H. J. (2016). Flexible electronics under strain: a review of mechanical characterization and durability enhancement strategies. *Journal of materials science*, *51*(6), 2771-2805.

[225] Maitra, A., Paria, S., Karan, S. K., Bera, R., Bera, A., Das, A. K., and Khatua, B. B. (2019). Triboelectric nanogenerator driven self-charging and self-healing flexible asymmetric supercapacitor power cell for direct power generation. *ACS applied materials and interfaces*, *11*(5), 5022-5036.

[226] Zhao, S., Wang, J., Du, X., Wang, J., Cao, R., Yin, Y., and Li, C. (2018). All-nanofiber-based ultralight stretchable triboelectric nanogenerator for self-powered wearable electronics. *ACS Applied Energy Materials*, *1*(5), 2326-2332.

[227] Lim, S. (2019). Design of Micro/Nanostructured Materials for Flexible Electronics and Sensing Applications.

[228] Tang, Y., Zhou, H., Sun, X., Feng, T., Zhao, X., Wang, Z., and Mao, Y. (2020). Cotton-based naturally wearable power source for self-powered personal electronics. *Journal of Materials Science*, *55*(6), 2462-2470.

[229] Rodrigue, H., Wang, W., Kim, D. R., and Ahn, S. H. (2017). Curved shape memory alloy-based soft actuators and application to soft gripper. *Composite Structures*, *176*, 398-406.

[230] Liu, L., Niu, Z., and Chen, J. (2016). Unconventional supercapacitors from nanocarbon-based electrode materials to device configurations. *Chemical Society Reviews*, *45*(15), 4340-4363.

[231] Trung, T. Q., and Lee, N. E. (2017). Recent progress on stretchable electronic devices with intrinsically stretchable components. *Advanced Materials*, *29*(3), 1603167.

[232] Wei, Q., Xiong, F., Tan, S., Huang, L., Lan, E. H., Dunn, B., and Mai, L. (2017). Porous one-dimensional nanomaterials: design, fabrication and applications in electrochemical energy storage. *Advanced materials*, *29*(20), 1602300.

[233] Raj, C. J., Rajesh, M., Manikandan, R., Lee, W. G., Yu, K. H., and Kim, B. C. (2018). Direct fabrication of two-dimensional copper sulfide nanoplates on transparent conducting glass for planar supercapacitor. *Journal of Alloys and Compounds*, *735*, 2378-2383.

[234] Wang, Y., Zhang, M., Li, Y., Ma, T., Liu, H., Pan, D., and Wang, A. (2018). Rational design 3D nitrogen doped graphene supported spatial crosslinked Co3O4@ NiCo2O4 on nickel foam for binder-free supercapacitor electrodes. *Electrochimica Acta*, *290*, 12-20.

[235] Cao, C., Chu, Y., Zhou, Y., Zhang, C., and Qu, S. (2018). Recent Advances in Stretchable Supercapacitors Enabled by Low-Dimensional Nanomaterials. *Small*, *14*(52), 1803976.

[236] Choi, C., Park, J. W., Kim, K. J., Lee, D. W., De Andrade, M. J., Kim, S. H., and Kim, S. J. (2018). Weavable asymmetric carbon nanotube yarn supercapacitor for electronic textiles. *RSC advances*, *8*(24), 13112-13120.

[237] Gong, X., Li, S., and Lee, P. S. (2017). A fiber asymmetric supercapacitor based on FeOOH/PPy on carbon fibers as an anode electrode with high volumetric energy density for wearable applications. *Nanoscale*, *9*(30), 10794-10801.

[238] Shi, P., Chen, R., Hua, L., Li, L., Chen, R., Gong, Y., and Huang, W. (2017). Highly concentrated, ultrathin nickel hydroxide nanosheet ink for wearable energy storage devices. *Advanced Materials*, *29*(40), 1703455.

[239] Yu, C., Xu, H., Zhao, X., Sun, Y., Hui, Z., Du, Z., and Huang, W. (2020). Scalable preparation of high performance fibrous electrodes with bio-inspired compact core-fluffy sheath structure for wearable supercapacitors. *Carbon*, *157*, 106-112.

[240] Cai, S., Huang, T., Chen, H., Salman, M., Gopalsamy, K., and Gao, C. (2017). Wet-spinning of ternary synergistic coaxial fibers for high performance yarn supercapacitors. *Journal of Materials Chemistry A*, *5*(43), 22489-22494.

[241] Jiang, W., Zhai, S., Qian, Q., Yuan, Y., Karahan, H. E., Wei, L., and Chen, Y. (2016). Space-confined assembly of all-carbon hybrid fibers for capacitive energy storage: realizing a built-to-order concept for micro-supercapacitors. *Energy and Environmental Science*, *9*(2), 611-622.

[242] Chen, D. Z., Yu, J., Lu, W., Zhao, Y., Yan, Y., and Chou, T. W. (2017). Temperature effects on electrochemical performance of carbon nanotube film based flexible all-solid-state supercapacitors. *Electrochimica Acta*, *233*, 181-189.

[243] Zhang, Q., Wang, X., Pan, Z., Sun, J., Zhao, J., Zhang, J., and Zhang, Z. (2017). Wrapping aligned carbon nanotube composite sheets around vanadium nitride nanowire arrays for asymmetric coaxial fiber-shaped supercapacitors with ultrahigh energy density. *Nano Letters*, *17*(4), 2719-2726.

[244] Li, Q., Zhang, Q., Sun, J., Liu, C., Guo, J., He, B., and Yao, Y. (2019). All Hierarchical Core–Shell Heterostructures as Novel Binder-Free Electrode Materials for Ultrahigh-Energy-Density Wearable Asymmetric Supercapacitors. *Advanced Science*, *6*(2), 1801379.

[245] Choi, C., Lee, J. M., Kim, S. H., Kim, S. J., Di, J., and Baughman, R. H. (2016). Twistable and stretchable sandwich structured fiber for wearable sensors and supercapacitors. *Nano letters*, *16*(12), 7677-7684.

[246] Li, M., Zu, M., Yu, J., Cheng, H., and Li, Q. (2017). Stretchable fiber supercapacitors with high volumetric performance based on buckled MnO2/oxidized carbon nanotube fiber electrodes. *Small*, *13*(12), 1602994.

[247] Guo, F. M., Xu, R. Q., Cui, X., Zhang, L., Wang, K. L., Yao, Y. W., and Wei, J. Q. (2016). High performance of stretchable carbon nanotube–polypyrrole fiber supercapacitors under dynamic deformation and temperature variation. *Journal of Materials Chemistry A*, *4*(23), 9311-9318.

[248] Ren, J., Li, L., Chen, C., Chen, X., Cai, Z., Qiu, L., and Peng, H. (2013). Twisting carbon nanotube fibers for both wire-shaped micro-supercapacitor and micro-battery. *Advanced Materials*, *25*(8), 1155-1159.

[249] Ren, J., Bai, W., Guan, G., Zhang, Y., and Peng, H. (2013). Flexible and weaveable capacitor wire based on a carbon nanocomposite fiber. *Advanced Materials*, *25*(41), 5965-5970.

[250] Chen, T., Hao, R., Peng, H., and Dai, L. (2015). High-performance, stretchable, wire-shaped supercapacitors. *Angewandte Chemie International Edition*, *54*(2), 618-622.

[251] Senthilkumar, S. T., and Selvan, R. K. (2015). Flexible fiber supercapacitor using biowaste-derived porous carbon. *ChemElectroChem*, *2*(8), 1111-1116.

[252] Choi, C., Kim, J. H., Sim, H. J., Di, J., Baughman, R. H., and Kim, S. J. (2017). Supercapacitors: Microscopically Buckled and Macroscopically Coiled Fibers for Ultra-Stretchable Supercapacitors (Adv. Energy Mater. 6/2017). *Advanced Energy Materials*, *7*(6).

[253] Zhou, G., Kim, N. R., Chun, S. E., Lee, W., Um, M. K., Chou, T. W., and Oh, Y. (2018). Highly porous and easy shapeable poly-dopamine derived graphene-coated single walled carbon nanotube aerogels for stretchable wire-type supercapacitors. *Carbon*, *130*, 137-144.

[254] Mokhtari, F., Foroughi, J., Zheng, T., Cheng, Z., and Spinks, G. M. (2019). Triaxial braided piezo fiber energy harvesters for self-powered wearable technologies. *Journal of materials chemistry A*, *7*(14), 8245-8257.

[255] Wang, S., Liu, N., Su, J., Li, L., Long, F., Zou, Z., and Gao, Y. (2017). Highly stretchable and self-healable supercapacitor with reduced graphene oxide based fiber springs. *Acs Nano*, *11*(2), 2066-2074.

[256] Lin, Y., Gao, Y., and Fan, Z. (2017). Printable Fabrication of Nanocoral-Structured Electrodes for High-Performance Flexible and Planar Supercapacitor with Artistic Design. *Advanced Materials*, *29*(43), 1701736.

[257] Li, H., Liu, Z., Liang, G., Huang, Y., Huang, Y., Zhu, M., and Li, B. (2018). Waterproof and tailorable elastic rechargeable yarn zinc ion batteries by a cross-linked polyacrylamide electrolyte. *ACS nano*, *12*(4), 3140-3148.

[258] Kim, K. J., Lee, J. A., Lima, M. D., Baughman, R. H., and Kim, S. J. (2016). Highly stretchable hybrid nanomembrane supercapacitors. *RSC advances*, *6*(29), 24756-24759.

[259] Zhang, N., Zhou, W., Zhang, Q., Luan, P., Cai, L., Yang, F., and Gu, X. (2015). Biaxially stretchable supercapacitors based on the buckled hybrid fiber electrode array. *Nanoscale*, *7*(29), 12492-12497.

[260] Zhou, Q., Zhang, M., Chen, J., Hong, J. D., and Shi, G. (2016). Nitrogen-doped holey graphene film-based ultrafast electrochemical capacitors. *ACS applied materials & interfaces*, *8*(32), 20741-20747.

[261] Tang, Q., Chen, M., Wang, G., Bao, H., and Saha, P. (2015). A facile prestrain-stick-release assembly of stretchable supercapacitors based on highly stretchable and sticky hydrogel electrolyte. *Journal of Power Sources*, *284*, 400-408.

[262] Hu, H., Pei, Z., and Ye, C. (2015). Recent advances in designing and fabrication of planar micro-supercapacitors for on-chip energy storage. *Energy Storage Materials*, *1*, 82-102.

[263] Saito, Y., Meguro, M., Ashizawa, M., Waki, K., Yuksel, R., Unalan, H. E., and Matsumoto, H. (2017). Manganese dioxide nanowires on carbon nanofiber frameworks for efficient electrochemical device electrodes. *RSC advances*, *7*(20), 12351-12358.

[264] Wang, C., Zhang, M., Xia, K., Gong, X., Wang, H., Yin, Z., and Zhang, Y. (2017). Intrinsically stretchable and conductive textile by a scalable process for elastic wearable electronics. *ACS Applied Materials & Interfaces*, *9*(15), 13331-13338.

[265] Lamberti, A., Serrapede, M., Ferraro, G., Fontana, M., Perrucci, F., Bianco, S., and Bocchini, S. (2017). All-SPEEK flexible supercapacitor exploiting laser-induced graphenization. *2D Materials*, *4*(3), 035012.

[266] Liu, N., and Gao, Y. (2017). Recent progress in micro-supercapacitors with in-plane interdigital electrode architecture. *Small*, *13*(45), 1701989.

[267] Song, W., Zhu, J., Gan, B., Zhao, S., Wang, H., Li, C., and Wang, J. (2018). Flexible, stretchable, and transparent planar microsupercapacitors based on 3D porous laser-induced graphene. *Small*, *14*(1), 1702249.

[268] Zhang, H., Cao, Y., Chee, M. O. L., Dong, P., Ye, M., and Shen, J. (2019). Recent advances in micro-supercapacitors. *Nanoscale*, *11*(13), 5807-5821.

[269] Hu, P., Chen, T., Yang, Y., Wang, H., Luo, Z., Yang, J., and Guo, L. (2017). Renewable-emodin-based wearable supercapacitors. *Nanoscale*, *9*(4), 1423-1427.

[270] Lv, Z., Luo, Y., Tang, Y., Wei, J., Zhu, Z., Zhou, X., and Qi, D. (2018). Stretchable Supercapacitors: Editable Supercapacitors with Customizable Stretchability Based on Mechanically Strengthened Ultralong MnO2 Nanowire Composite (Adv. Mater. 2/2018). *Advanced Materials*, *30*(2), 1870008.

[271] He, S., Cao, J., Xie, S., Deng, J., Gao, Q., Qiu, L., and Peng, H. (2016). Stretchable supercapacitor based on a cellular structure. *Journal of Materials Chemistry A*, *4*(26), 10124-10129.

[272] Nam, I., Kim, G. P., Park, S., Han, J. W., and Yi, J. (2014). All-solid-state, origami-type foldable supercapacitor chips with integrated series circuit analogues. *Energy & Environmental Science*, *7*(3), 1095-1102.

[273] Tammela, P., Wang, Z., Frykstrand, S., Zhang, P., Sintorn, I. M., Nyholm, L., and Strømme, M. (2015). Asymmetric supercapacitors based on carbon nanofibre and polypyrrole/nanocellulose composite electrodes. *Rsc Advances*, *5*(21), 16405-16413.

[274] Huang, Y. Z., Chen, X. M., and Li, D. X. (2018). Reduced Graphene Oxide/Carbon Nanotube Composites for High Electrochemical Performance Supercapacitors. In *Materials Science Forum* (Vol. 937, pp. 25-29). Trans Tech Publications Ltd.

[275] Cheng, Z., Cai, L., Qiu, Y., Chang, X., Fan, H., and Ren, B. (2017). Synthesis of redox-active dendronized poly (ferrocenylsilane) and application as high-performance supercapacitors. *Journal of Organometallic Chemistry*, *852*, 43-47.

[276] Wolff, C., Jeong, S., Paillard, E., Balducci, A., and Passerini, S. (2015). High power, solvent-free electrochemical double layer capacitors based on pyrrolidinium dicyanamide ionic liquids. *Journal of Power Sources*, *293*, 65-70.

[277] Kong, C., Qian, W., Zheng, C., Yu, Y., Cui, C., and Wei, F. (2013). Raising the performance of a 4 V supercapacitor based on an EMIBF 4–single walled carbon nanotube nanofluid electrolyte. *Chemical Communications*, *49*(91), 10727-10729.

[278] Yang, C., Zhang, L., Hu, N., Yang, Z., Su, Y., Xu, S., and Zhang, Y. (2017). Rational design of sandwiched polyaniline nanotube/layered graphene/polyaniline nanotube papers for high-volumetric supercapacitors. *Chemical Engineering Journal*, *309*, 89-97.

[279] Hung, P. J., Chang, K. H., Lee, Y. F., Hu, C. C., and Lin, K. M. (2010). Ideal asymmetric supercapacitors consisting of polyaniline nanofibers and graphene nanosheets with proper complementary potential windows. *Electrochimica acta*, *55*(20), 6015-6021.

[280] Zhao, Y., Liu, P., Zhuang, X., Wu, D., Zhang, F., and Su, Y. (2017). Ionothermally synthesized hierarchical porous Schiff-base-type polymeric networks with ultrahigh specific surface area for supercapacitors. *RSC advances*, *7*(32), 19934-19939.

[281] Liu, X., Zou, S., Liu, K., Lv, C., Wu, Z., Yin, Y., and Xie, Z. (2018). Highly compressible three-dimensional graphene hydrogel for foldable all-solid-state supercapacitor. *Journal of Power Sources*, *384*, 214-222.

[282] Kuok, F. H., Chien, H. H., Lee, C. C., Hao, Y. C., Yu, S., Hsu, C. C., and Chen, J. Z. (2018). Atmospheric-pressure-plasma-jet processed carbon nanotube (CNT)–reduced graphene oxide (rGO) nanocomposites for gel-electrolyte supercapacitors. *RSC advances*, *8*(6), 2851-2857.

[283] Liu, J., Ye, J., Pan, F., Wang, X., and Zhu, Y. (2019). Solid-state yet flexible supercapacitors made by inkjet-printing hybrid ink of carbon quantum dots/graphene oxide platelets on paper. *Science China Materials*, *62*(4), 545-554.

[284] Yu, W., Zhou, H., Li, B. Q., and Ding, S. (2017). 3D printing of carbon nanotubes-based microsupercapacitors. *ACS applied materials & interfaces*, *9*(5), 4597-4604.

[285] Lota, G., and Frackowiak, E. (2009). Striking capacitance of carbon/iodide interface. *Electrochemistry Communications*, *11*(1), 87-90.

[286] Fic, K., Frackowiak, E., and Béguin, F. (2012). Unusual energy enhancement in carbon-based electrochemical capacitors. *Journal of Materials Chemistry*, *22*(46), 24213-24223.

[287] Ramachandran, R., Xuan, W., Zhao, C., Leng, X., Sun, D., Luo, D., and Wang, F. (2018). Enhanced electrochemical properties of cerium metal–organic framework based composite electrodes for high-performance supercapacitor application. *RSC advances*, *8*(7), 3462-3469.

[288] Yan, L., Huang, J., Dong, X., Guo, Z., Wang, Z., and Wang, Y. (2020). Energizing Hybrid Supercapacitor by Using Mn2+-Based Active Electrolyte. *Journal of Materials Chemistry A*.

[289] Brza, M., Aziz, S. B., Raza Saeed, S., Hamsan, M. H., Majid, S. R., Abdulwahid, R. T., and Abdullah, R. M. (2020). Energy Storage Behavior of Lithium-Ion Conducting poly (vinyl alcohol)(PVA): Chitosan (CS)-Based Polymer Blend Electrolyte Membranes: Preparation, Equivalent Circuit Modeling, Ion Transport Parameters, and Dielectric Properties. Membranes, 10(12), 381.

[290] Wong, J. I. C., Ramesh, S., Jun, H. K., and Liew, C. W. (2021). Development of poly (vinyl alcohol)(PVA)-based sodium ion conductors for electric double-layer capacitors application. Materials Science and Engineering: B, 263, 114804.

[291] Ye, T., Zou, Y., Xu, W., Zhan, T., Sun, J., Xia, Y., and Yang, D. (2020). Poorly-crystallized poly (vinyl alcohol)/carrageenan matrix: Highly ionic conductive and flame-retardant gel polymer electrolytes for safe and flexible solid-state supercapacitors. Journal of Power Sources, 475, 228688.

[292] Gunday, S. T., Cevik, E., Anil, I., Alagha, O., and Bozkurt, A. (2020). High-temperature symmetric supercapacitor applications of anhydrous gel electrolytes including doped triazole terminated flexible spacers. Journal of Molecular Liquids, 301, 112400.

[293] Yang, Y., Zhu, T., Chi, C., Liu, L., Zheng, J., and Gong, X. (2020). All-Solid-State Asymmetric Supercapacitors with Novel Ionic Liquid Gel Electrolytes. ACS Applied Electronic Materials, 2(12), 3906-3914.

[294] Zakariya'u, I., Gultekin, B., Singh, V., and Singh, P. K. (2020). Electrochemical double-layer supercapacitor using poly (methyl methacrylate) solid polymer electrolyte. High Performance Polymers, 32(2), 201-207.

[295] Jeong, J. H., Kim, Y. A., and Kim, B. H. (2020). Electrospun polyacrylonitrile/cyclodextrin-derived hierarchical porous carbon nanofiber/MnO2 composites for supercapacitor applications. Carbon, 164, 296-304.

[296] Mathela, S., Sangwan, B., Dhapola, P. S., Singh, P. K., and Tomar, R. (2021). Ionic liquid incorporated poly (ethylene oxide)(PEO) doped with potassium iodide (KI) solid polymer electrolyte for energy device. Materials Today: Proceedings.

[297] Pazhamalai, P., Krishnamoorthy, K., Mariappan, V. K., Sahoo, S., Manoharan, S., and Kim, S. J. (2018). A High Efficacy Self-Charging MoSe2 Solid-State Supercapacitor Using Electrospun Nanofibrous Piezoelectric Separator with Ionogel Electrolyte. Advanced Materials Interfaces, 5(12), 1800055.

[298] Peng, X., Liu, H., Yin, Q., Wu, J., Chen, P., Zhang, G., and Xie, Y. (2016). A zwitterionic gel electrolyte for efficient solid-state supercapacitors. Nature communications, 7(1), 1-8.

[299] Fard, H. N., Pour, G. B., Sarvi, M. N., and Esmaili, P. (2019). PVA-based supercapacitors. *Ionics*, *25*(7), 2951-2963.

[300] George, S. M. (2010). Atomic layer deposition: an overview. *Chemical reviews*, *110*(1), 111-131.

[301] Dubal, D. P., and Holze, R. (2013). All-solid-state flexible thin film supercapacitor based on Mn3O4 stacked nanosheets with gel electrolyte. *Energy*, *51*, 407-412.

[302] Karaman, B., Çevik, E., and Bozkurt, A. (2019). Novel flexible Li-doped PEO/copolymer electrolytes for supercapacitor application. *Ionics*, *25*(4), 1773-1781.

[303] Zhao, F., Shi, Y., Pan, L., and Yu, G. (2017). Multifunctional nanostructured conductive polymer gels: synthesis, properties, and applications. *Accounts of chemical research*, *50*(7), 1734-1743.

[304] Chen, L., Li, D., Chen, L., Si, P., Feng, J., Zhang, L., and Ci, L. (2018). Core-shell structured carbon nanofibers yarn@ polypyrrole@ graphene for high performance all-solid-state fiber supercapacitors. *Carbon*, *138*, 264-270.

[305] Pu, X., Li, L., Liu, M., Jiang, C., Du, C., Zhao, Z., and Wang, Z. L. (2016). Wearable self-charging power textile based on flexible yarn supercapacitors and fabric nanogenerators. *Advanced Materials*, *28*(1), 98-105.

[306] Zihong, S. U. N., and Anbao, Y. U. A. N. (2009). Electrochemical performance of nickel hydroxide/activated carbon supercapacitors using a modified polyvinyl alcohol based alkaline polymer electrolyte. *Chinese Journal of Chemical Engineering*, *17*(1), 150-155.

[307] Lawrence, C. J. (1988). The mechanics of spin coating of polymer films. *The Physics of fluids*, *31*(10), 2786-2795.

[308] Yilbas, B. S., Al-Sharafi, A., and Ali, H. (2019). *Self-Cleaning of Surfaces and Water Droplet Mobility*. Elsevier.

[309] Brinker, C. J., and Scherer, G. W. (2013). *Sol-gel science: the physics and chemistry of sol-gel processing*. Academic press.

[310] Sahu, N., Parija, B., and Panigrahi, S. (2009). Fundamental understanding and modeling of spin coating process: A review. *Indian Journal of Physics*, *83*(4), 493-502.

[311] Steele, A., Bayer, I., and Loth, E. (2009). Inherently superoleophobic nanocomposite coatings by spray atomization. *Nano letters*, *9*(1), 501-505.

[312] Faure, B., Salazar-Alvarez, G., Ahniyaz, A., Villaluenga, I., Berriozabal, G., De Miguel, Y. R., and Bergström, L. (2013). Dispersion and surface functionalization of oxide nanoparticles for transparent photocatalytic and UV-protecting coatings and sunscreens. *Science and technology of advanced materials*, *14*(2), 023001.

[313] Zhang, H., Kuwata, M., Bilotti, E., and Peijs, T. (2015). Integrated damage sensing in fibre-reinforced composites with extremely low carbon nanotube loadings. *Journal of Nanomaterials*, *2015*.

[314] Philips'Gloeilampenfabrieken, O. (1958). A method of measuring specific resistivity and Hall effect of discs of arbitrary shape. *Philips Res. Rep*, *13*(1), 1-9.

[315] Devi, M., and Kumar, A. (2016). In-situ reduced graphene oxide nanosheets–polypyrrole nanotubes nanocomposites for supercapacitor applications. *Synthetic Metals*, *222*, 318-329.

[316] Allagui, A., Freeborn, T. J., Elwakil, A. S., Fouda, M. E., Maundy, B. J., Radwan, A. G.,and Abdelkareem, M. A. (2018). Review of fractional-order electrical characterization of supercapacitors. *Journal of Power Sources*, *400*, 457-467.

[317] Bhoyate, S., Kahol, P. K., and Gupta, R. K. (2020). Broadening the horizon for supercapacitor research via 2D material systems. In *Nanoscience* (pp. 120-149).

[318] Khan, Z. N., Shuja, A., Ali, M., and Alam, S. (2018). Charge transient behaviour and spectroscopic ellipsometry characteristics of TiN/HfSiO MOS capacitors. The European Physical Journal Applied Physics, 83(1), 10101 https://doi.org/10.1051/epjap/2018180104.

[319] Ali, M., Ahmed, S., Younus, F., and Ali, Z. (2019). Electrical, charge transients and photo response study of as-deposited and phosphorus implanted Cd1-xZnxTe devices for PV applications. Radiation Physics and Chemistry, 108498. https://doi.org/10.1016/j.radphyschem.2019.108498

[320] Rothenberger, J. B., Montenegro, D. E., Prelas, M. A., Ghosh, T. K., Tompson, R. V., and Loyalka, S. K. (2012). A Q-DLTS investigation of aluminum nitride surface termination. Journal of Materials Research, 27(8), 1198-1204.

[321] Lee, C. W., Renaud, C., Le Rendu, P., Nguyen, T. P., Seneclauze, B., Ziessel, R., and Jolinat, P. (2010). Performance and defects in phosphorescent organic light-emitting diodes. Solid state sciences, 12(11), 1873-1876.

[322] Thurzo, I., Kampen, T. U., and Zahn, D. R. (2002). Giant polarization in organic heterostructures. Journal of Vacuum Science and Technology A: Vacuum, Surfaces, and Films, 20(5), 1597-1602.

[323] Wagner, N., and Gülzow, E. (2004). Change of electrochemical impedance spectra (EIS) with time during CO-poisoning of the Pt-anode in a membrane fuel cell. Journal of Power Sources, 127(1-2), 341-347.

[324] Huang, J., Li, Z., Liaw, B. Y., and Zhang, J. (2016). Graphical analysis of electrochemical impedance spectroscopy data in Bode and Nyquist representations. Journal of Power Sources, 309, 82-98.

[325] Allagui, A., Freeborn, T. J., Elwakil, A. S., Fouda, M. E., Maundy, B. J., Radwan, A. G., and Abdelkareem, M. A. (2018). Review of fractional-order electrical characterization of supercapacitors. Journal of Power Sources, 400, 457-467.

[326] Yuan, X. Z. R., Song, C., Wang, H., and Zhang, J. (2009). Electrochemical impedance spectroscopy in PEM fuel cells: fundamentals and applications. Springer Science and Business Media.

[327] Allen, J. B., and Larry, R. F. (2001). Electrochemical methods fundamentals and applications. John Wiley and Sons.

[328] Orazem, M. E., and Tribollet, B. (2008). Electrochemical impedance spectroscopy. New Jersey, 383-389.

[329] Purkait, T., Singh, G., Kumar, D., Singh, M., and Dey, R. S. (2018). High-performance flexible supercapacitors based on electrochemically tailored three-dimensional reduced graphene oxide networks. Scientific reports, 8(1), 1-13

[330] Vallikkodi, M. (2018). Synthesis, growth and characterization of piperazinium P-aminobenzoate and piperazinium P-chlorobenzoate nonlinear optical single crystals. Alagappa University, Karaikudi, India.

[331] Aoki, T. (2002). Photoluminescence spectroscopy. Characterization of Materials, 1-12.

[332] Guidote Jr, A. M., Pacot, G. M. M., and Cabacungan, P. M. (2015). Low-cost magnetic stirrer from recycled computer parts with optional hot plate. Journal of Chemical Education, 92(1), 102-105.

[333] Microscopy, A. (2014). Microanalysis research facility. Scanning Electron Microscope Training module..

[334] Mohammed, A., and Abdullah, A. (2018, November). Scanning electron microscopy (SEM): A review. In Proceedings of the 2018 International Conference on Hydraulics and Pneumatics—HERVEX, Băile Govora, Romania (pp. 7-9).

[335] Blonskaya, I. V., Kristavchuk, O. V., Nechaev, A. N., Orelovich, O. L., Polezhaeva, O. A., and Apel, P. Y. (2021). Observation of latent ion tracks in semicrystalline polymers by scanning electron microscopy. Journal of Applied Polymer Science, 138(8), 49869.

[336] Kwon, S., Kim, Y., and Roh, Y. (2021). Cesium removal using acid-and base-activated biotite and illite. Journal of Hazardous Materials, 401, 123319.

[337] Kanakamedala, K. Fabrication and Analysis of Tin Oxide-Ni (SnO2-Ni) Sensors

[338] Ebnesajjad, S. (2011). Surface and material characterization techniques. In Handbook of Adhesives and Surface Preparation (pp. 31-48). William Andrew Publishing.

[339] Colpan, C. O., Nalbant, Y., and Ercelik, M. (2018). 4.28 Fundamentals of Fuel Cell Technologies

[340] Nasrollahzadeh, M., Atarod, M., Sajjadi, M., Sajadi, S. M., and Issaabadi, Z. (2019). Plant-mediated green synthesis of nanostructures: mechanisms, characterization, and applications. In Interface Science and Technology (Vol. 28, pp. 199-322). Elsevier.

[341] Jalili, N., and Laxminarayana, K. (2004). A review of atomic force microscopy imaging systems: application to molecular metrology and biological sciences. Mechatronics, 14(8), 907-945.

[342] Chen, R., Fan, Y., Dong, X., Ma, X., Feng, Z., Chang, M., and Li, N. (2021). Impact of pH on interaction between the polymeric flocculant and ultrafine coal with atomic force microscopy (AFM). Colloids and Surfaces A: Physicochemical and Engineering Aspects, 126698.

[343] Kodera, N., Noshiro, D., Dora, S. K., Mori, T., Habchi, J., Blocquel, D., and Ando, T. (2021). Structural and dynamics analysis of intrinsically disordered proteins by high-speed atomic force microscopy. Nature Nanotechnology, 16(2), 181-189.

[344] Liu, Y., Murtaza, I., Shuja, A., and Meng, H. (2020). Interfacial modification for heightening the interaction between PEDOT and substrate towards enhanced flexible solid supercapacitor performance. Chemical Engineering Journal, 379, 122326. https://doi.org/10.1016/j.cej.2019.122326

[345] Thiyagu, S., Hsueh, C. C., Liu, C. T., Syu, H. J., Lin, T. C., and Lin, C. F. (2014). Hybrid organic–inorganic heterojunction solar cells with 12% efficiency by utilizing flexible film-silicon with a hierarchical surface. Nanoscale, 6(6), 3361-3366. DOI:10.1039/C3NR06323B

[346] Ali, A., Khan, Z. S., Jamil, M., Khan, Y., Ahmad, N., and Ahmed, S. (2018). Simultaneous reduction and sulfonation of graphene oxide for efficient hole selectivity in polymer solar cells. Current Applied Physics, 18(5), 599-610. https://doi.org/10.1016/j.cap.2018.02.016

[347] Akhmadishina, K. F., Bobrinetskii, I. I., Ibragimov, R. A., Komarov, I. A., Malovichko, A. M., Nevolin, V. K., and Petukhov, V. A. (2014). Fabrication of flexible transparent conductive coatings based on single-walled carbon nanotubes. Inorganic materials, 50(1), 23-28.

[348] Noh, Y. J., Park, S. M., Yeo, J. S., Kim, D. Y., Kim, S. S., and Na, S. I. (2015). Efficient PEDOT: PSS-free polymer solar cells with an easily accessible polyacrylonitrile polymer material as a novel solution-processable anode interfacial layer. ACS applied materials & interfaces, 7(45), 25032-25038.

[349] Alemu, D., Wei, H. Y., Ho, K. C., and Chu, C. W. (2012). Highly conductive PEDOT: PSS electrode by simple film treatment with methanol for ITO-free polymer solar cells. Energy & environmental science, 5(11), 9662-9671.

[350] Kim, Y. H., & Sachse, C. (2011). Ml L. MacHala, C. May, L. Müller-Meskamp and K. Leo,"Highly conductive PEDOT: PSS electrode with optimized solvent and thermal post-treatment for ITO-free organic solar cells. Adv. Funct. Mater., 21(6), 1076-1081.

[351] Hsieh, H. C., Hsiow, C. Y., Lin, K. F., Shih, Y. C., Wang, L., Renaud, C., and Nguyen, T. P. (2018). Analysis of Defects and Traps in N–I–P Layered-Structure of Perovskite Solar Cells by Charge-Based Deep Level Transient Spectroscopy (Q-DLTS). The Journal of Physical Chemistry C, 122(31), 17601-17611. https://doi.org/10.1021/acs.jpcc.8b01949

[352] Nguyen, T. P., Renaud, C., Rendu, P. L., and Yang, S. H. (2009). Investigation of defects in organic semiconductors by charge based Deep Level Transient Spectroscopy (Q-DLTS). physica status solidi c, 6(8), 1856-1861. https://doi.org/10.1002/pssc.200881458

[353] Wang, Y., Li, W., Guo, Y., Cao, J., Murtaza, I., Shuja, A., He, Y. and Meng, H. (2018). Recombination Strategy for Processable Ambipolar Electroactive Polymers in Pseudocapacitors. Macromolecules, 51(18),7350-7359. https://doi.org/10.1021/acs.macromol.8b01688

[354] Lewandowski, A., Jakobczyk, P., Galinski, M., and Biegun, M. (2013). Self-discharge of electrochemical double layer capacitors. *Physical Chemistry Chemical Physics*, *15*(22), 8692-8699. DOI:10.1039/C3CP44612C

[355] Tayel, M. B., Soliman, M. M., Ebrahim, S., and Harb, M. E. (2016). An introduced hybrid graphene/polyaniline composites for improvement of supercapacitor. Journal of Electronic Materials, 45(1), 820-828. DOI: 10.1007/s11664-015-4212-8.

[356] Rehman, H. U., Shuja, A., Ali, M., Murtaza, I., and Meng, H. (2020). Evaluation of defects and current kinetics for aging analysis of PEDOT: PSS based supercapacitors. Journal of Energy Storage, 28, 101243.

[357] Martinović, S., Vlahović, M., Ponomaryova, E., Ryzhkov, I. V., Jovanović, M., Bušatlić, I., Volkov, T and Husović, Z. (2017). Electrochemical Behavior of Supercapacitor Electrodes Based on Activated Carbon and Fly Ash. Int. J. Electrochem. Sci, 12, 7287-7299.

[358] Carter, B., and Mancini, R. (2017). Op Amps for everyone. Newnes.

[359] Poli, F., Seri, J., Santoro, C., and Soavi, F. (2020). Boosting Microbial Fuel Cell Performance by Combining with an External Supercapacitor: An Electrochemical Study. ChemElectroChem, 7(4), 893-903. https://doi.org/10.1002/celc.201901876

[360] Kötz, R., and Carlen, M. J. E. A. (2000). Principles and applications of electrochemical capacitors. Electrochimica acta, 45(15-16), 2483-2498. https://doi.org/10.1016/S0013-4686(00)00354-6

[361] Hamid, E. Y. (2001). Wavelet packet transform for RMS values and power measurements. IEEE Power Engineering Review, 21(9), 49-51. DOI: 10.1109/PESS.2001.970246

[362] Negroiu, R., Svasta, P., Pirvu, C., Vasile, A., and Marghescu, C. (2017, May). Electrochemical impedance spectroscopy for different types of supercapacitors. In 2017 40th International Spring Seminar on Electronics Technology (ISSE) (pp. 1-4). IEEE.

[363] https://www.avrfreaks.net/forum/input-impedance-digital-ios-atmega328p

[364] Poli, F., Seri, J., Santoro, C., and Soavi, F. (2020). Boosting microbial fuel cell performance by combining with an external supercapacitor: an electrochemical study. *ChemElectroChem*, *7*(4), 877-877.

[365] Haider, I., Khan, B., Ali, M., Shuja, A., Qureshi, A. F., and Ali, Z. (2020). Influence of device deposition techniques on the process optimization of CdZnTe thin-film matrix using charge-based analysis. *Materials Science in Semiconductor Processing*, *114*, 105074.

[366] Hussain, K., Shuja, A., Ali, M., and Fahad, S. (2021). Carrier removal and transport in photonic integrated circuit ready InGaAsP/InP substrate: Electrical and transients of charges evaluation. Materials Science in Semiconductor Processing, 121, 105384

[367] Fahad, S., Noman, M., Qureshi, A. F., Ali, M., and Ahmed, S. (2021). Defect mapping of active layer of CdTe solar cells using charge deep level transient spectroscopy (Q-DLTS). Engineering Failure Analysis, 119, 104991

[368] Aziz, S. B. (2016). Modifying poly (vinyl alcohol)(PVA) from insulator to small-bandgap polymer: A novel approach for organic solar cells and optoelectronic devices. Journal of Electronic Materials, 45(1), 736-745.

[369] Qi, G.; Huang, L.; Wang, H. Highly conductive free standing polypyrrole films prepared by freezing interfacial polymerization. Chem. Commun. 2012, 48, 8246.

[370] Rahy, A.; Yang, D.J. Synthesis of highly conductive polyaniline nanofibers. Mater. Lett. 2008, 62, 4311–4314

[371] Chiang, C.K.; Fincher, C.R.; Park, Y.W.; Heeger, A.J.; Shirakawa, H.; Louis, E.J.; Gau, S.C.; MacDiarmid, A.G. Electrical Conductivity in Doped Polyacetylene. Phys. Rev. Lett. 1977, 39, 1098–1101.

[372] Worfolk, B.J.; Andrews, S.C.; Park, S.; Reinspach, J.; Liu, N.; Toney, M.F.; Mannsfeld, S.C.B.; Bao, Z. Ultrahigh electrical conductivity in solution-sheared polymeric transparent films. Proc. Natl. Acad. Sci. 2015, 112, 14138–14143.

[373] Khasim, S., Pasha, A., Badi, N., Lakshmi, M., and Mishra, Y. K. (2020). High performance flexible supercapacitors based on secondary doped PEDOT–PSS–graphene nanocomposite films for large area solid state devices. Rsc Advances, 10(18), 10526-10539

[374] Manjakkal, L., Pullanchiyodan, A., Yogeswaran, N., Hosseini, E. S., and Dahiya, R. (2020). A wearable supercapacitor based on conductive PEDOT: PSS-coated cloth and a sweat electrolyte. Advanced Materials, 32(24), 1907254.

[375] Song, J., Ma, G., Qin, F., Hu, L., Luo, B., Liu, T., Yin, X., Su, Z., Zeng, Z., Jiang, Y. and Li, Z. (2020). High-Conductivity, Flexible and Transparent PEDOT: PSS Electrodes for High Performance Semi-Transparent Supercapacitors. Polymers, 12(2), 450

[376] Pico, F., Pecharroman, C., Ansón, A., Martínez, M. T., and Rojo, J. M. (2007). Understanding carbon–carbon composites as electrodes of supercapacitors: A study by AC and DC measurements. Journal of The Electrochemical Society, 154(6), A579.

[377] Zhao, S., Wu, F., Yang, L., Gao, L., and Burke, A. F. (2010). A measurement method for determination of dc internal resistance of batteries and supercapacitors. Electrochemistry Communications, 12(2), 242-245

[378] Yuan, C., Zhang, X., Wu, Q., and Gao, B. (2006). Effect of temperature on the hybrid supercapacitor based on NiO and activated carbon with alkaline polymer gel electrolyte. Solid State Ionics, 177(13-14), 1237-1242.

[379] Vandana, M., Vijeth, H., Ashokkumar, S. P., and Devendrappa, H. (2020). Effect of different gel electrolytes on conjugated polymer-Graphene quantum dots based electrode for solid state hybrid supercapacitors. Polymer-Plastics Technology and Materials.

[380] Zhang, Q., Yang, F., Zhang, C., Dong, H., Sui, J., Yu, L., Chen, Y., Yu, J. and Dong, L. (2021). A novel wire-shaped supercapacitor based on MnO2 nanoflakes and carbon nanotubes with high performance synthesized by sacrificial template method. Applied Surface Science, 551, 149417.